

Functional analysis of the molecular interactions between ebolaviruses and host proteins

Inauguraldissertation

zur

Erlangung des akademischen Grades eines

Doktors der Naturwissenschaft
(Dr. rer. nat.)

der

Mathematisch-Naturwissenschaftlichen Fakultät

der

Universität Greifswald

vorgelegt von

Janine Brandt

Greifswald, Mai 2021

Dekan: Prof. Dr. Gerald Kerth

1. Gutachter: Prof. Dr. Dr. h.c. Thomas C. Mettenleiter

2. Gutachter: PD Dr. Jens Bohne

Tag der Promotion: 14.10.2021

Table of Content

Table of Content	I
List of abbreviations	VI
1 Introduction	1
1.1 Ebolavirus taxonomy.....	1
1.2 History and epidemiology.....	2
1.3 Virion morphology.....	5
1.4 Genome organization.....	6
1.5 Viral proteins.....	7
1.5.1 Nucleoprotein (NP).....	7
1.5.2 Viral protein 35	8
1.5.3 Viral protein 40	8
1.5.4 Glycoprotein (GP).....	9
1.5.5 Viral protein 30	9
1.5.6 Viral protein 24	10
1.5.7 Viral polymerase (L)	10
1.6 Ebolavirus lifecycle	10
1.7 Clinical manifestation and pathogenesis	13
1.8 Ebolaviruses and host factors	15
1.8.1 Carbamoyl-phosphate synthetase 2, aspartate transcarbamylase, and dihydroorotase (CAD)	16
1.8.2 Nuclear export factor 1 (NXF1).....	17
1.8.3 DEAD box polypeptide 39B (DDX39B; UAP56).....	19
1.9 RNA interference (RNAi).....	20
1.10 Ebolavirus reverse genetic systems	21
1.10.1 Minigenome systems	23
1.10.2 Transcription and replication competent virus like particle (trVLP) system	25
1.11 Objectives of this study.....	26
2 Material and Methods	29
2.1 Material.....	29
2.1.1 Equipment and Devices.....	29
2.1.2 Chemicals and reagents.....	30
2.1.2.1 Buffers, solutions and reagents.....	30
2.1.2.2 Recipes for buffers and solutions	32

2.1.3 Consumables	35
2.1.4 Oligonucleotides.....	36
2.1.5 Vectors and recombinant plasmids.....	39
2.1.6 Enzymes	41
2.1.7 Antibodies	41
2.1.8 siRNAs	42
2.1.9 Kits	42
2.1.10 Cell lines and bacteria	43
2.1.11 Viruses	43
2.1.12 Bacterial and cell culture media	43
2.1.13 Computer software	44
2.2 Methods.....	46
2.2.1 Molecular biology methods.....	46
2.2.1.1 Polymerase chain reaction (PCR).....	46
2.2.1.2 Preparative restriction digest	48
2.2.1.3 Analytical restriction digest	48
2.2.1.4 Agarose gel electrophoresis	49
2.2.1.5 Purification of DNA from agarose gel.....	50
2.2.1.6 Purification of PCR products.....	50
2.2.1.7 Dephosphorylation.....	50
2.2.1.8 Ligation.....	51
2.2.1.9 Phosphorylation of oligonucleotides	51
2.2.1.10 Hybridization of oligonucleotides	52
2.2.1.11 Preparation of chemically competent bacteria	52
2.2.1.12 Transformation of chemically competent bacteria.....	53
2.2.1.13 Preparation of plasmid DNA from bacterial cultures.....	53
2.2.1.14 Determination of DNA concentration	54
2.2.1.15 Sequencing	54
2.2.1.16 Subcloning	55
2.2.1.17 Cloning of PCR fragments	55
2.2.1.18 RNA extraction	55
2.2.1.19 DNase digestion	56
2.2.1.20 Reverse transcription.....	56
2.2.1.21 qPCR.....	57
2.2.2 Tissue culture methods, cell harvest, lysis and trVLP purification	58
2.2.2.1 Cultivation of mammalian cells	58
2.2.2.2 Classical transfection of mammalian cells	58

2.2.2.3	Reverse transfection of mammalian cell lines	59
2.2.2.4	Minigenome system.....	60
2.2.2.5	trVLP assay	61
2.2.2.6	Infection with recombinant EBOV.....	61
2.2.2.7	Cell harvest.....	62
2.2.2.8	Cell lysis with sample loading buffer	62
2.2.2.9	Luciferase measurement	62
2.2.2.10	Purification of trVLPs using a sucrose cushion.....	62
2.2.2.11	Pyrimidine supplementation.....	63
2.2.3	Protein biochemistry methods	64
2.2.3.1	Sodium dodecyl sulfate polyacrylamide gel electrophoresis (SDS-PAGE).....	64
2.2.3.2	Western blotting.....	65
2.2.3.3	Immunofluorescence assay	66
2.2.4	Statistical analysis	68
2.2.5	Sequence alignment.....	68
3	Results.....	69
3.1	Optimization of molecular biological methods	69
3.1.1	Optimization of minigenome assays	69
3.1.1.1	Generation of a replication deficient minigenome with nano luciferase	69
3.1.1.2	Comparison of RdM containing Renilla or nano luciferase	69
3.1.1.3	Generation of a minigenome under control of a Pol-II promoter	70
3.1.1.4	Comparison of T7 and Pol-II-driven replication-deficient minigenomes	71
3.1.2	Establishment and optimization of host factor knockdown	72
3.1.2.1	Generation of amiRNA and shRNA vectors for host cell knockdown.....	72
3.1.2.2	Establishment of a host factor knockdown protocol	73
3.1.3	Optimization of immunofluorescence assay.....	74
3.1.3.1	Testing of different fluorescence proteins for IFA.....	75
3.2	Influence of CAD on the EBOV lifecycle.....	78
3.2.1	Quantification of siRNA knockdown of CAD and EBOV-L.....	78
3.2.2	Role of CAD on total EBOV RNA synthesis.....	80
3.2.3	CAD is important for Ebola virus transcription	82
3.2.4	Influence of CAD knockdown on EBOV genome replication	83
3.2.5	The role of CAD during pyrimidine synthesis is critical for the EBOV lifecycle ...	84
3.2.6	CAD accumulates in NP-induced inclusion bodies	85
3.2.7	CAD is recruited into inclusion bodies during EBOV infection.....	87
3.2.8	The GLN domain of CAD is responsible for accumulation in inclusion bodies ...	88

3.3 Role of NXF1 during the EBOV lifecycle	89
3.3.1 Quantification of NXF1 knockdown.....	89
3.3.2 NXF1 is important for EBOV RNA synthesis.....	90
3.3.3 NXF1 knockdown affects EBOV transcription and/or protein expression	92
3.3.4 Influence of NXF1 knockdown on EBOV genome replication and mRNA transcription.....	93
3.3.5 Establishment of a complementation assay for NXF1 knockdown	93
3.3.5.1 Generation of NXF1 and NXF1 deletion mutants vectors for complementation assay	94
3.3.5.2 The RBD but not RRM domain of NXF1 is important for later steps in EBOV mRNA processing.....	95
3.3.6 NXF1 is recruited into NP-derived inclusion bodies	96
3.3.7 NTF2 and UBA domains of NXF1 are responsible for recruitment into inclusion bodies.....	98
3.3.8 Analysis of the role of nucleoporins on recruitment of NXF1 into inclusion bodies	100
3.3.9 Influence of NXF1 deletion mutants on the intracellular distribution of NXF1 and relocalisation in inclusion bodies	102
3.3.10 RNA binding of both NXF1 and NP is required for exit of NXF1 from inclusion bodies.....	105
3.3.11 The C-terminal domain of NP is responsible for recruitment of NXF1 in inclusion bodies.....	108
3.4 Analysis of the role of UAP56 for the EBOV lifecycle	110
3.4.1 Quantification of siRNA knockdown of UAP56.....	110
3.4.2 Influence of UAP56 on EBOV total RNA synthesis	111
3.4.3 UAP56 knockdown but not overexpression affects EBOV transcription and/or protein expression	113
3.4.4 Influence of UAP56 knockdown and overexpression on EBOV genome replication	114
3.4.5 Establishment of a complementation assay for UAP56 knockdown.....	114
3.4.5.1 Generation of siRNA binding-deficient UAP56 plasmids	116
3.4.5.2 siRNA mediated knockdown of UAP56 can be complemented with a siRNA-resistant UAP56.....	116
3.4.6 Analysis of the cellular localization of UAP56 in presence and absence of EBOV-NP	117
3.4.7 Influence of EBOV infection on the intracellular distribution of UAP56.....	118
3.4.8 Investigation of the cellular distribution of NES-UAP56	119

3.4.8.1	Generation of NES-UAP56 and NES-RRM constructs.....	120
3.4.8.2	NES-RRM does not relocalize in NP-induced inclusion bodies.....	120
3.4.8.3	NES-UAP56 is recruited into inclusion bodies	121
4	Discussion.....	123
4.1	Functional relevance of CAD for the ebolavirus lifecycle.....	124
4.2	Role of NXF1 for the ebolavirus lifecycle.....	126
4.3	Influence of UAP56 on the ebolavirus lifecycle.....	132
4.4	Conclusion.....	133
5	Summary.....	134
6	Zusammenfassung	136
7	References.....	138
8	Appendix.....	162
8.1	Curriculum vitae.....	162
8.2	Publications	164
8.3	Scientific presentations	165
8.4	Acknowledgment	166
8.5	Eigenständigkeitserklärung.....	168

List of abbreviations

Δ -peptide	non-structural polypeptide
A549	adenocarcinomic human alveolar basal epithelial cells
Ago2	argonaute protein 2
Aly	RNA and export factor
amiRNA	artificial micro RNA
anti-L	siRNA against EBOV-L
APS	ammonium persulfate
ATC	aspartate transcarbamylase
ATP	adenosine triphosphate
ATV	alsever's trypsin versene solution
Axl	tyrosine-protein kinase receptor UFO
BAT1	DEAD box polypeptide 39B
BDBV	Bundibugyo virus
BOMV	Bombali virus
BP	branch point
BSC	biosafety cabinet
BSL	biosafety level
CAD	carbamoyl-phosphate synthetase 2, aspartate transcarbamylase, and dihydroorotase
CD	cluster of differentiation
CDC	Centers for Disease Control and Prevention
cDNA	complementary DNA
CFR	case fatality rate
CoIP	Co-Immunoprecipitation
CPS	carbamoyl-phosphate synthetase 2
cRNA	antigenomic viral RNA
CTE	constitutive transport element
ctrl	control
DAPI	4',6'-diamidino-2-phenylindole
DC	dendritic cells
DC-SIGN	dendritic cell-specific intercellular adhesion molecule-3-grabbing non-integrin
DDX39B	DEAD box polypeptide 39B
DEAD	amino acid sequence D-E-A-D (asp-glu-ala-asp)

dH ₂ O	double distilled water
DHO	dihydroorotase
DHODH	dihydroorotate dehydrogenase
DICER	endoribonuclease
DMSO	dimethyl sulfoxide
DNA	desoxyribonucleic acid
dNTP	deoxynucleotide triphosphates
DRC	Democratic Republic of the Congo
dsRNA	double-stranded ribonucleic acid
DTT	dithiothreitol
<i>E. coli</i>	<i>Escherichia coli</i>
EBOV	Ebola virus
EDTA	ethylenediaminetetraacetic acid
eGFP	enhanced GFP
EHF	Ebola hemorrhagic fever
EJC	exon junction complex
ER	endoplasmic reticulum
ESCRT	endosomal sorting complex required for transport
EVD	Ebola virus disease
FCS	fetal calf serum
FDA	U.S. Food and Drug Administration
FG-repeat	repeating sequences of the amino acids phenylalanine and glycine
FLAG	protein tag
FLI	Friedrich-Loeffler-Institut
GAPDH	glyceraldehyde 3-phosphate dehydrogenase
GFP	green fluorescent protein
GLN	glutaminase
GP	viral surface glycoprotein
HA	protein tag
HBc	HBV core protein
HBV	Hepatitis B virus
HCL	sodium chloride
HEK 293	human embryonic kidney cells
HEK 293T	human embryonic kidney cells, which express a SV40 large T antigen
hrLuc	renilla luciferase

Huh7	human liver, tumorigenic cells
IB	inclusion bodies
IFA	immunofluorescence assay
IFN	interferon
IKK	inhibitor of nuclear factor kappa-B kinase
IL	interleukin
IRF	interferon regulatory factor
ISG	interferon-stimulated genes
L	RNA-dependent RNA polymerase
l	liter
LB	lysogeny broth
log	logarithm
L-SIGN	liver/lymph node-specific intracellular adhesion molecules-3 grabbing non-integrin
M	matrix protein
MAP	mitogen-activated protein kinase
MAPKK	mitogen-activated protein kinase kinase
MARV	Marburg virus
MCP	monocyte chemoattractant protein
Mer	receptor tyrosine kinase
MgCL ₂	magnesium chloride
MHC class II	major histocompatibility complex molecule class 2
MIP-1 α	macrophage inflammatory protein 1 alpha
miRNA	micro RNA
MOI	multiplicity of infection
mRNA	messenger RNA
NC	negative control
NEB	New England Biolabs
NES	nuclear export signal
NF- κ B	nuclear factor kappa-light-chain-enhancer of activated B cells
nLuc	nano luciferase
NP	nucleoprotein
NPC	nuclear pore complex
NPC1	Niemann-Pick C1
NS1	nonstructural protein 1
NTE	N-terminal extension
NTF2	nuclear transport factor 2-like domain

NTR	nuclear transport receptor
Nup	nucleoporin
NXF1	nuclear export factor 1
NXF1-10RA	RNA binding deficient NXF1
NXT1	NTF2-related export protein 1
OD	optical density
ORF	open-reading frame
P	phosphoprotein
p0	producer cells
p1	target cells
p15	NTF2-related export protein 1
p38	mitogen-activated protein kinase
PALA	N-phosphonacetyl-L-aspartate
PBS	phosphate buffered saline
pCAGGS	cloning plasmid
PCR	polymerase chain reaction
PEI	polyethylenimine
Pen/Strep	penicillin/streptomycin
PFA	paraformaldehyde
Pol-II	DNA polymerase II
psiRNA	cloning plasmid
pTP	preterminal protein
qPCR	quantitative polymerase chain reaction
RBBP6	retinoblastoma-binding protein 6
RBD	RNA binding domain
RBD	receptor binding domain
RC	Republic of the Congo
RdM	replication-deficient minigenome
rDNase	recombinant deoxyribonuclease
RESTV	Reston virus
rgEBOV	recombinant EBOV
RIG-I	retinoic acid-inducible gene I
RISC	RNA-induced silencing complex
RLU	relative light unit
RNA	ribonucleic acid
RNAi	RNA interference
RNase	ribonuclease

RNP	ribonucleoprotein
RPM	revolutions per minute
RRM	RNA recognition motif
rSAP	recombinant shrimp alkaline phosphatase
RT-qPCR	reverse transcription–qPCR
SARS-CoV 2	severe acute respiratory syndrome coronavirus type 2
SDS	sodium dodecyl sulfate
SDS-PAGE	sodium dodecyl sulfate polyacrylamide gel electrophoresis
Sec61 α	protein transport protein Sec61 subunit alpha
sGP	soluble glycoprotein
shRNA	short hairpin RNA
siRNA	small interfering RNA
SMYD3	SET (suppressor of variegation, enhancer of Zeste, Trithorax) and MYND (myeloid-Nervy-DEAF-1) domain-containing protein 3
snRNP	small nuclear ribonucleoproteins
SOC	super optimal broth
ssGP	small soluble glycoprotein
STAU1	double-stranded RNA-binding protein Staufen homolog 1
SUDV	Sudan virus
T7	T7 polymerase
TAE	tris acetate EDTA
TAFV	Tai Forest virus
TAM	receptor tyrosine kinase
TAP	nuclear export factor 1
TBK1	TANK-binding kinase 1
TCID50	fifty percent tissue culture infective dose
TEMED	tetramethylethylenediamine
Thr	threonine
TIM	T-cell immunoglobulin and mucin-domain 1
TNF- α	tumor necrosis factor alpha
TREX	transcription-export complex
trVLP	transcription and replication competent virus like particles
UAP56	DEAD box polypeptide 39B
UAP56-1c	RNA binding deficient UAP56
UBA	ubiquitin-associated domain
UDG	uracil-DNA glycosylases

UMPS	uridine monophosphate synthetase
USA	United States of America
UV	ultraviolet
VLP	virus-like particle
VP	viral protein
VP24	nucleocapsid-associated protein
VP30	transcriptional activator
VP35	RNA-depend RNA polymerase cofactor
VP40	matrix protein
vRNA	viral RNA
WHO	World Health Organization

1 Introduction

1.1 Ebolavirus taxonomy

Ebolaviruses are members of the genus *Ebolavirus* within the family *Filoviridae*, which is taxonomically classified in the order *Mononegavirales*. Established in 1991 the order *Mononegavirales* includes related virus families, which share genome organization and replicative systems, but differ in their morphologies (Pringle 1991). In contrast to other members of the order *Mononegavirales* the family *Filoviridae* is characterized by the unique morphological, physicochemical, and biological features of its members. Defined in 1982, the *Filoviridae* family is currently classified into six genera: *Marburgvirus*, *Ebolavirus*, *Cuevavirus*, *Dianlovirus*, *Striavirus* and *Thamnovirus* (Figure 1) (Kiley, Bowen et al. 1982, Kuhn, Adkins et al. 2020). While most of the genera comprise just a single species, within the genus *Ebolavirus* six genetically distinct viruses have been characterized so far: Ebola virus (EBOV), Sudan virus (SUDV), Reston virus (RESTV), Tai Forest virus (TAFV), Bundibugyo virus (BDBV) and Bombali virus (BOMV), each representing a distinct virus species: *Zaire ebolavirus*, *Sudan ebolavirus*, *Reston ebolavirus*, *Tai Forest ebolavirus*, *Bundibugyo ebolavirus* and *Bombali ebolavirus* (Kuhn, Adkins et al. 2020). Although not all filoviruses are pathogenic for humans (e.g. RESTV), they are rated as biosafety level (BSL) 4 as well as category A biothreat agents (Borio, Inglesby et al. 2002).

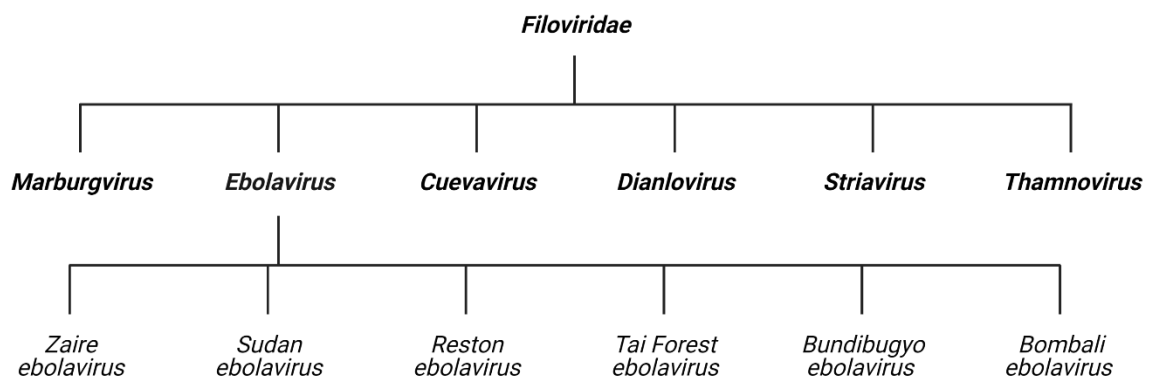


Figure 1. Taxonomy of ebolaviruses. Created with BioRender.com

1.2 History and epidemiology

Of the six described ebolaviruses, four have been identified as etiological agents of human Ebola virus disease (EVD), causing severe symptoms including hemorrhagic fever with case fatality rates between 30 % and 90 % (Feldmann and Geisbert 2011, Burk, Bollinger et al. 2016, Yamaoka and Ebihara 2021).

The first ebolavirus was discovered in 1976, when two consecutive outbreaks of hemorrhagic fever in neighboring areas of the Democratic Republic of Congo (DRC, former Zaire) and South Sudan (former Sudan) occurred (Table 1) (Bowen, Lloyd et al. 1977, Johnson, Lange et al. 1977). Following these events an unknown virus was isolated from infected patients in both outbreaks and named Ebola virus (EBOV) after a small river in northwestern Zaire (Pattyn, van der Groen et al. 1977). Interestingly, years later the causative agents of the two outbreaks were found to be distinct from each other and are now classified as separate viral species within the genus *Ebolavirus*: *Sudan ebolavirus* and *Zaire ebolavirus* (Cox, McCormick et al. 1983). After several years of just sporadic EVD outbreaks in central Africa, a new ebolavirus emerged in 1989 outside of Africa. This new virus, referred to as Reston virus (RESTV), was isolated from *Cynomolgus* monkeys (*Macaca fascicularis*) that were exported from the Philippines to a quarantine facility in Reston (USA). Surprisingly, RESTV, which was assigned to the new ebolavirus species *Reston ebolavirus*, seems to cause asymptomatic human infections and appears to be apathogenic for humans (Miranda, Ksiazek et al. 1999, Miranda, Yoshikawa et al. 2002). In 1994 an ethnologist developed symptoms of EVD after performing a necropsy on a dead chimpanzee in the Taï Forest reserve of the Ivory Coast. However, the isolated virus was distinct from EBOV or SUDV and subsequently designated as Taï Forest virus (TAFV) within the new species *Tai Forest ebolavirus*. TAFV was the first ebolavirus which appeared in West Africa (Le Guenno, Formenty et al. 1995). A fifth ebolavirus was discovered in 2007 during an outbreak of hemorrhagic fever in the Bundibugyo district of western Uganda and named Bundibugyo virus (BDBV) within the species *Bundibugyo ebolavirus* (Towner, Sealy et al. 2008).

Since the first discovery of ebolaviruses in 1976 they have caused sporadic human EVD outbreaks of varying magnitude in Equatorial African regions (Hasan, Ahmad et al. 2019). Because of this, it was believed that EVD represents a zoonotic tropical disease that is mainly limited to central Africa. However, this assumption changed in 2014 when the largest Ebola virus epidemic on record hit the West African region,

causing more than 11.000 fatalities across nine countries worldwide. Lasting over two years, this massive outbreak has shown that ebolaviruses are able to occur in urban regions where they can transmit faster from human-to-human than in rural areas. As a result of this event, researchers have increased efforts to identify the natural reservoir(s) of ebolaviruses, in order to better characterize these viruses. Over the decades, different animal species have been justified as natural reservoirs for ebolaviruses including primates, bats, rodents, arthropods, and plants, but so far the natural reservoir remains unconfirmed (Olival and Hayman 2014). However, since the isolation of Marburg virus (MARV), a virus related to ebolaviruses, from fruit bats of the genus *Rousettus aegyptiacus*, which is believed to represent (at least one of) the primary natural reservoir for this virus (Towner, Amman et al. 2009), fruit bats also seem to be most likely a reservoir species for ebolaviruses. So far, viral RNA and EBOV antibodies have been detected in fruit bats, but no virus was isolated (Pourrut, Delicat et al. 2007, Olival and Hayman 2014, Saez, Weiss et al. 2015, Schuh, Amman et al. 2017). Between 2014 and 2016 researchers set out to identify the source of the devastating EBOV outbreak in Sierra Leone, but against expectations, a new ebolavirus was identified in oral and rectal swab specimens from two free-tailed bat species, *Chaerephon pumilus* (little free-tailed bat) and *Mops condylurus* (Angolan free-tailed bat) (Goldstein, Anthony et al. 2018). RNA of the same virus, now designated as Bombali virus (BOMV), was detected two years later in *Mops condylurus* bats in both Guinea and Kenya, indicating that BOMV is more widely distributed than previously suspected (Forbes, Webala et al. 2019, Karan, Makenov et al. 2019). Although not all ebolaviruses were detected in the same geographic region, all previous human EVD outbreaks can be traced back to an African origin, suggesting, that ebolaviruses are widespread throughout large parts of African.

An interesting feature of ebolavirus outbreaks is that transmission of these viruses occurs either from a single introduction event into the human population followed by persistent human-to-human transmission, or from multiple introduction events followed by lesser human-to-human transmission (Olival and Hayman 2014). Although the introduction event has not always been identified, person-to-person transmission has shown to result from close contact, especially with all kinds of body fluids, from infected patients or animals (gorilla, chimpanzee) (Dowell, Mukunu et al. 1999, Feldmann, Jones et al. 2003). Additionally, sexual transmission and mother-to-child transmission via breast milk were documented (Abbate, Murall et al. 2016).

Table 1. Selected filovirus outbreaks. Adapted from (Feldmann 2013) and expanded by data from the WHO.

Year	Virus	Outbreak location	Human cases	CFR ^a
1976	EBOV	DRC ^b	318	88 %
1976	SUDV	Sudan	284	53 %
1979	SUDV	Sudan	34	65 %
1989	RESTV	USA ^c (origin Philippines)	4 ^d	0 %
1994	TAFV	Ivory Coast	1	0 %
1995	EBOV	DRC ^b	315	81 %
1995	TAFV	Liberia	1	0 %
1996	EBOV	Gabon	60	75 %
2000-2001	SUDV	Uganda	425	53 %
2001-2002	EBOV	Gabon, RC ^e	124	79 %
2003	EBOV	RC ^e	143	89 %
2003	EBOV	RC ^e	35	83 %
2004	SUDV	Sudan	17	41 %
2005	EBOV	RC ^e	12	83 %
2007	EBOV	DRC ^b	264	71 %
2007	BDBV	Uganda	131	32 %
2008	EBOV	DRC ^b	32	47 %
2012	BDBV	DRC ^b	57	51 %
2014	EBOV	DRC ^b	69	71 %
2014-2016	EBOV	primary in Guinea, Sierra Leone and Liberia ^f	28616	39.5 %
2017	EBOV	DRC ^b	8	50 %
2018	EBOV	DRC ^b	54	61 %
2018-2020	EBOV	DRC ^b	3481	66 %
2020	EBOV	DRC ^b	130	42 %
2021	EBOV	DRC ^b	12 (ongoing)	(50 %)
2021	EBOV	Guinea	15 (ongoing)	(60 %)

^a Case fatality rate among human cases

^b Democratic Republic of the Congo

^c United States of America

^d Outbreak among imported Macaques

^e Republic of the Congo

^f Small outbreaks also in Nigeria and Mali, isolated cases in Senegal, the United Kingdom and Italy, imported cases which led to secondary infection of medical workers in the United States and Spain

1.3 Virion morphology

The particles of ebolaviruses form filamentous and pleomorphic structures, which occur as either long filaments or branched, U-shaped, 6-shaped or circular forms (Figure 2) (Feldmann and Geisbert 2011, Leroy, Gonzalez et al. 2011, Majid, Tahir et al. 2016). The uniform diameter of these particles is 80 nm with a density of 1.14 g/ml (Geisbert and Jahrling 1995). Although ebolavirus particles vary considerably in length, reaching up to 14000 nm, the unit length of the virion in association with their peak infectivity is about 970 nm (Kiley, Regnery et al. 1980). The virion is structurally divided into three layers: a surface glycoprotein layer, a lipid membrane envelope unit and an internal tubular helical nucleocapsid (Feldmann and Geisbert 2011). The envelope is studded with trimers of the viral surface protein (glycoprotein, GP), which are separated by distances of about 5 nm to 10 nm, while the surface layer consists of the glycoprotein spikes, which range from 7 nm to 10 nm in length (Feldmann, Will et al. 1991, Feldmann and Klenk 1996). In ebolavirus infection the GP protein is required for the combined functions of attachment to host cells, endosomal entry, and membrane fusion (Takada, Robison et al. 1997, Nanbo, Imai et al. 2010, Saeed, Kolokoltssov et al. 2010, Moller-Tank and Maury 2015). The inner leaflet of the envelope is lined with the viral matrix protein (viral protein 40 (VP40)), which represents the main protein controlling virion morphology (Elliott, Kiley et al. 1985, Beniac, Melito et al. 2012). Surrounded by the lipid membrane, in the center of the virion the tubular helical ribonucleoprotein (RNP) complex is located, which has a diameter of 50 nm and consists of the nucleoprotein (NP), VP35, VP30, the RNA-dependent RNA polymerase (L) and the viral RNA (Figure 2) (Geisbert and Jahrling 1995). The nucleocapsid-associated protein VP24 is bound to the RNP complex in virions in order to facilitate RNP complex assembly (Noda, Halfmann et al. 2007, Hoenen, Jung et al. 2010b, Watt, Moukambi et al. 2014).

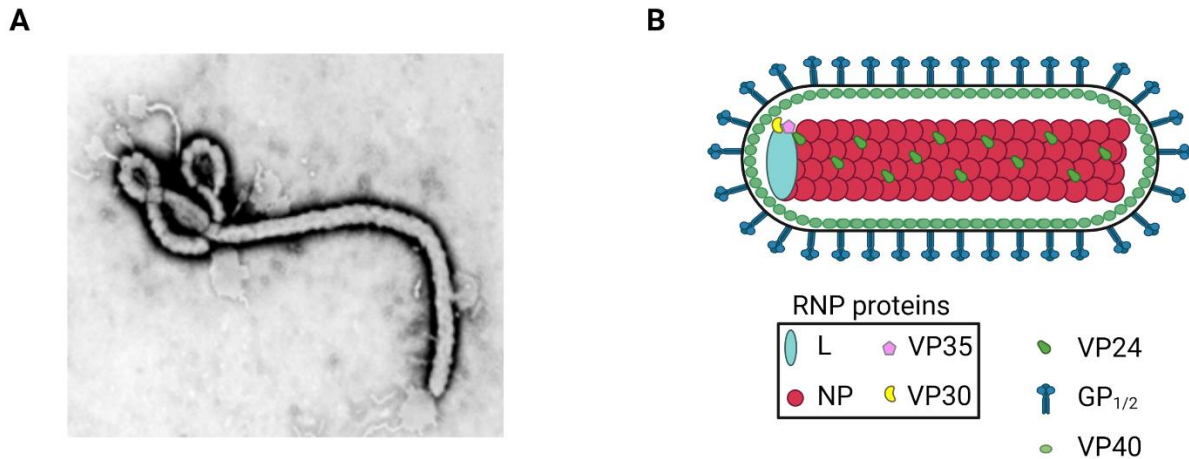


Figure 2. Ebolavirus structure **(A)** Electron micrograph of an EBOV particle by Dr. F.A. Murphy (1976) CDC. **(B)** Schematic drawing of a filovirus particle and its components. The genome consists of a single-stranded RNA that interacts with the RNP proteins to form a helical nucleocapsid. The nucleocapsid is surrounded by a membrane envelope formed by VP40, in which the GP proteins are incorporated. VP40 is located between the nucleocapsid and the envelope, whereas VP24 is bound to the RNP-complex. Created with BioRender.com

1.4 Genome organization

All ebolaviruses share the same genome organization and have a non-segmented single-stranded negative-sense RNA genome with a total length of approximately 19 kb, which represents the largest genome in the order *Mononegavirales*. The RNA is non-infectious and neither polyadenylated nor capped (Kiley, Regnery et al. 1980). The genome contains seven sequentially arranged conserved genes in the order: 3' - leader - NP - VP35 - VP40 - GP - VP30 - VP24 - L - trailer - 5', with non-coding regions (named leader and trailer), which are partially complementary to each other and consists of cis-acting signals required for replication, transcription and encapsidation, at the 3' and 5' ends of the genome (Figure 3) (Muhlberger, Lotfering et al. 1998, Feldmann and Kiley 1999). Interestingly, the length of the 5' trailer region varies among ebolaviruses and ranges from 25 bases for RESTV to 676 bases for EBOV. Each gene is flanked by highly conserved transcriptional start and stop signals with the consensus sequence 3'-CUNCNUNUAAUU-5' and 3'-UAAUUCUUUUU-5', respectively (Sanchez, Kiley et al. 1993). A special feature of filoviruses is that these start and stop signals are overlapping between VP35 and VP40, GP and VP30 (absent in RESTV) and VP24 and L (Bukreyev, Belanov et al. 1995). These overlaps have a length of 18-20 bases (Sanchez, Kiley et al. 1993). The other genes are separated by usually short intergenic regions, spanning 4-7 nonconserved nucleotides, although one large

intergenic region was identified between VP30 and VP24 (Ikegami, Calaor et al. 2001, Towner, Khristova et al. 2006).

While five of the ebolavirus proteins (NP, VP35, VP40, GP and L) are equivalent to proteins found in all negative-sense RNA viruses, VP24 and VP30 appear to be unique to filoviruses, although in case of VP30 a similar protein has been described for pneumoviruses (Biacchesi, Skiadopoulos et al. 2003). Another striking feature of ebolaviruses is that the fourth gene possesses three overlapping open reading frames (ORFs), which encode for at least four different proteins via proteolytic processing and transcriptional polymerase stuttering that results in frame shifts (Clarke, Collar et al. 2017).

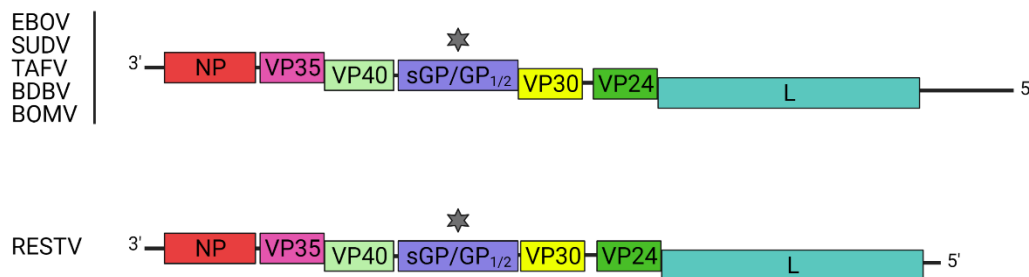


Figure 3. Genome organization of Ebolaviruses. The gene orders of fully sequenced ebolavirus genomes are presented. Intergenic regions are shown as black line between the individual genes. Steps indicate the position of gene overlaps and asterisks indicate the position of the RNA editing site in the ebolavirus genomes. EBOV, SUDV, TAFV, BDBV and RESTV genomes adapted and modified from (Hoenen, Brandt et al. 2017). Created with BioRender.com

1.5 Viral proteins

1.5.1 Nucleoprotein (NP)

The nucleoprotein (NP) is encoded by the first ebolavirus gene and forms long, linear polymers that encapsidates the viral RNA genome, making NP the main nucleocapsid component (Sanchez, Kiley et al. 1993, Watanabe, Noda et al. 2006, Leung, Borek et al. 2015, Baseler, Chertow et al. 2017). Although NP does not interact directly with the viral polymerase L, these NP-RNA complexes serve as the functional templates for L to perform replication and transcription. This indirect interaction of NP and L is bridged by either the polymerase cofactor VP35 or the transcriptional activator VP30, which enables L to switch between replication and transcription (Becker, Rinne et al. 1998, Muhlberger, Lotfering et al. 1998, Groseth, Charton et al. 2009, Cantoni and Rossman 2018). Structural analysis has shown that NP consist of two domains. While the N-

terminal region is required for RNA binding and oligomerization, the C-terminal domain is most important for scaffolding L, VP30 and VP35 in the nucleocapsid complex (Dziubanska, Derewenda et al. 2014, Dong, Yang et al. 2015).

1.5.2 Viral protein 35

The second ebolavirus gene encodes for VP35, which is the equivalent of phosphoproteins (P) found in other negative-sense RNA viruses (Muhlberger, Weik et al. 1999). However, in contrast to other P proteins, VP35 appears not to be strongly phosphorylated, although it shares their essential role in virus replication and transcription (Elliott, Kiley et al. 1985). As cofactor of the RNA-dependent RNA polymerase (L), VP35 is able to interact with both L and NP in order to facilitate viral RNA synthesis (Prins, Binning et al. 2010, Trunschke, Conrad et al. 2013). Additionally, VP35 has shown to work as a virulence factor through its suppression of the host innate immunity by interfering with sensing of double stranded RNA (dsRNA) and by inhibition of the host RNA interference pathway (Leung, Prins et al. 2010a, Leung, Prins et al. 2010b). Furthermore, VP35 has also been shown to suppress the host cell innate immune response by inhibition of the RIG-I-like receptor pathway and activation of the interferon regulatory factor (IRF) 3 and 7, which are required for the anti-viral IFN-response (Basler, Mikulasova et al. 2003, Leung, Prins et al. 2010b, Messaoudi, Amarasinghe et al. 2015, Rojas, Monsalve et al. 2020).

1.5.3 Viral protein 40

VP40, the third protein encoded by the viral genome, represents the most abundant structural protein of ebolaviruses and is the equivalent of the matrix (M) proteins found in other mononegaviruses (Brandt, Wendt et al. 2018). As major structural protein VP40 is able to polymerize underneath the viral membrane, which gives the virion its characteristic shape (Geisbert and Jahrling 1995). During assembly and budding VP40 is required for recruitment of the nucleocapsid into the virion, as well as interaction with GP and the host cell membrane (Hoenen, Biedenkopf et al. 2010a, Bharat, Noda et al. 2012, Pleet, DeMarino et al. 2017). Additionally, VP40 levels have also been shown to be critical for transcriptional control (Hoenen, Jung et al. 2010b). Single expression of VP40 is sufficient to promote the formation of filamentous virus-like particles (VLPs), which resemble virions (Timmins, Scianimanico et al. 2001, Panchal, Ruthel et al. 2003, Johnson, McCarthy et al. 2006). Structural analysis revealed that VP40 consists

of two compact domains which are connected by a flexible linker (Dessen, Volchkov et al. 2000). While the N-terminal domain has been shown to be important for VP40 oligomerization, the C-terminal region is required for membrane interaction (Jasenosky, Neumann et al. 2001, Timmins, Schoehn et al. 2003).

1.5.4 Glycoprotein (GP)

The fourth gene in the genome encodes for the glycoprotein GP, which constitutes the only transmembrane surface protein of ebolaviruses. Embedded as trimer in the viral envelope, GP forms the virion surface peaks, which are required for receptor-mediated viral entry into the host cell (Feldmann, Will et al. 1991, Bukreyev, Volchkov et al. 1993, Feldmann, Nichol et al. 1994, Lee, Fusco et al. 2009). Because GP represents the only surface protein of ebolaviruses, it constitutes the main target for vaccine development (Feldmann, Volchkov et al. 2001). The GP gene encodes for four different proteins, which are produced in course of transcriptional editing mediated by the polymerase L. These proteins are GP, sGP, ssGP and a smaller fragment called Δ -peptide, which is produced by proteolytic cleavage of sGP by Furin (Volchkova, Klenk et al. 1999, Lee, Fusco et al. 2009, Mehedi, Falzarano et al. 2011, Cantoni and Rossman 2018). In recent years many efforts were directed at understanding the function of the non-structural glycoproteins ssGP and sGP, as well as the Δ -peptide. Interestingly, it was shown that the secreted glycoprotein (sGP) has no transmembrane domain and forms dimers, which get abundantly secreted from infected cells (Sanchez, Trappier et al. 1996, Sanchez, Yang et al. 1998). It was also shown that sGP is involved in evading the immune system via antigenic subversion (Mohan, Li et al. 2012). Additionally, recent studies showed that the Δ -peptide induces cellular toxicity through pore formation in the plasma membrane and enhancing ion permeability (He, Melnik et al. 2017, Rojas, Monsalve et al. 2020).

1.5.5 Viral protein 30

The nucleocapsid component VP30 is encoded by the fifth ebolavirus gene and is unique to filoviruses. Due to its function as a transcriptional activator, it is believed that VP30 mediates the switch between replication and transcription via interaction with NP and through the regulation of its phosphorylation state (Biedenkopf, Hartlieb et al. 2013, Ilinykh, Tigabu et al. 2014, Kirchdoerfer, Moyer et al. 2016). Additionally, VP30

is also involved in nucleocapsid assembly (Hartlieb, Muziol et al. 2007, John, Wang et al. 2007).

1.5.6 Viral protein 24

Encoded by the sixth ebolavirus gene, the nucleocapsid-associated protein VP24 is necessary for assembly and function of the RNP complex and plays important roles during inhibition of the host immune response (Noda, Halfmann et al. 2007, Watanabe, Noda et al. 2007, Hoenen, Jung et al. 2010b, Banadyga, Hoenen et al. 2017). VP24 has an interferon antagonizing function by blocking the phosphorylation of p38 mitogen-activated protein kinase and by binding to karyopherin α proteins, which results in an inhibition of their downstream signaling (Mateo, Reid et al. 2010, Halfmann, Neumann et al. 2011). Moreover, VP24 also inhibits IFN production via IRF3 and TNF (early tumor necrosis factor)-induced NF- κ B signaling (Guito, Albarino et al. 2017, Rojas, Monsalve et al. 2020). Similar to VP40, VP24 has also shown to regulate viral genome replication and transcription (Hoenen, Jung et al. 2010b).

1.5.7 Viral polymerase (L)

The last gene of the ebolavirus genome encodes the RNA-dependent RNA polymerase, which is expressed as a single polypeptide. L is a component of the RNP complex and essential for replication and transcription of the viral RNA (Muhlberger, Weik et al. 1999). Recently it was shown that a GDNQ motif, which is believed to be the catalytic center of the polymerase, seems to be crucial for the EBOV lifecycle, providing a promising target for the development of antivirals (Schmidt and Hoenen 2017).

1.6 Ebolavirus lifecycle

The ebolavirus lifecycle is characteristic for cytoplasmically replicating negative-sense RNA viruses and can be divided into three major parts: (1) virus entry, (2) transcription and replication of the genome, and (3) assembly and budding (Figure 4).

Attachment to a host-cell surface receptor is the initial step in the lifecycle of ebolaviruses. This interaction with the cell surface is mediated by various attachment receptors, which reflect the fact that ebolaviruses are able to infect a broad range of different cell types. Interestingly, all attachment factors, which have been identified so far, can be assigned to two different types of alternative cell surface receptors:

carbohydrate-binding receptors or phosphatidylserine receptors (Alvarez, Lasala et al. 2002, Marzi, Gramberg et al. 2004, Ji, Olinger et al. 2005). It was shown that carbohydrate-binding receptors, such as DC-SIGN (dendritic cell-specific intercellular adhesion molecule-3-grabbing non-integrin) or L-SIGN (liver/lymph node-specific ICAM-3 grabbing nonintegrin), interact with N- and O-linked glycans on the receptor binding domain (RBD) of GP, resulting in an enhanced entry of ebolaviruses into the host cell. In contrast, phosphatidylserine receptors, such as TIM-1 and TIM-4 (T-cell immunoglobulin and mucin domain) or members of the TAM family of receptor tyrosine kinases (Axl, Mer), interact with phosphatidylserine that is embedded in the ebolavirus envelope (Moller-Tank and Maury 2015). After binding to the cell surface the virion is internalized into the endosomal compartment primary through macropinocytosis, although other endocytic uptake pathways have been reported (it is believed that the route of ebolavirus uptake differs from cell to cell and is most likely driven by the receptor used) (Kuhn, Radoshitzky et al. 2006, Nanbo, Imai et al. 2010, Aleksandrowicz, Marzi et al. 2011, Moller-Tank and Maury 2015). Uptake through the endosomal pathway allows the virus to penetrate deep into the cytoplasm as well as to evade the host cell immune response and large barriers such as the cytoskeleton (Franco and Shuman 2012). The trafficking of the internalized virus particle through the endosomal pathway facilitates endosomal acidification that leads to proteolytic cleavage of GP by endosomal cysteine proteases like cathepsin B and L, which are most active in acidic pH environments (Weissenhorn, Calder et al. 1998, White, Delos et al. 2008, Misasi, Chandran et al. 2012). In the course of this process the mucin and glycan rich cap domains are removed from the C-terminal region of GP₁, which exposes receptor binding sites and leads to a conformational change in the GP₂ subunit (Chandran, Sullivan et al. 2005, Hood, Abraham et al. 2010). Cleavage and rearrangement enables GP to interact with specific endosome proteins, such as the lysosomal cholesterol transporter Niemann-Pick C1 (NPC1), which mediates fusion of the viral and cellular membranes and release of the viral nucleocapsid into the cytoplasm (Ito, Watanabe et al. 1999, Watanabe, Takada et al. 2000, Chandran, Sullivan et al. 2005, Carette, Raaben et al. 2011, Miller, Obernosterer et al. 2012, Fels, Bortz et al. 2021). After fusion the nucleocapsid serves as template for primary transcription of the ebolavirus genome. It has been suggested that transcription initiation is dependent on dissociation of VP24 from the surface of the nucleocapsid (Watt, Moukambi et al. 2014). During primary transcription capped and polyadenylated

monocistronic RNAs (mRNAs) are synthesized from the viral RNA by NP, VP35, VP30 and L (Muhlberger, Weik et al. 1999, Biedenkopf, Schlereth et al. 2016). Similar to other negative-sense RNA viruses, the ebolavirus polymerase binds at a single polymerase binding site at the 3' end of the genome and synthesizes the viral RNA template by stopping at transcriptional stop signals and reinitiating at the next start signal for each gene (Whelan, Barr et al. 2004). The polymerase is slowed down by each gene junction, and the nascent mRNA gets polyadenylated, which can lead to a disconnection of L from the RNA template. Since the interruption of transcription takes place at the gene junction, this results in a decreasing gradient in transcript abundance with NP being transcribed at the highest level and L at the lowest (Muhlberger, Trommer et al. 1996, Shabman, Hoenen et al. 2013). The produced mRNAs are subsequently translated by the cellular translation machinery into the viral proteins, which are required for secondary transcription and replication. During replication the polymerase synthesizes a full-length positive-sense copy of the viral RNA genome (antigenome). The antigenome in turn is used to synthesize genomic RNA (Muhlberger 2007). After synthesis, both the viral antigenomes and genomes are encapsidated by the nucleocapsid proteins. The accumulation of encapsidated RNA genomes in viral inclusion bodies, which represent the sites of replication and secondary transcription, is believed to be the initial step of viral assembly (Becker, Rinne et al. 1998, Hartlieb and Weissenhorn 2006, Hoenen, Shabman et al. 2012). While VP40 is transported via the vacuolar protein sorting/late endosomal pathway to the plasma membrane, GP precursors are synthesized in the endoplasmic reticulum (ER) and transported to the budding site through the secretory Golgi apparatus (Licata, Simpson-Holley et al. 2003, Yasuda, Nakao et al. 2003, Hartlieb and Weissenhorn 2006). While transport of VP40 and GP is well described, the transport mechanism of nucleocapsids to the budding site still needs to be investigated. Once they have reached the budding sites, nucleocapsids are enveloped by a lipid bilayer and the VP40 matrix, in which GP is inserted, and extrude from the host cell as infectious viral particles (Noda, Ebihara et al. 2006).

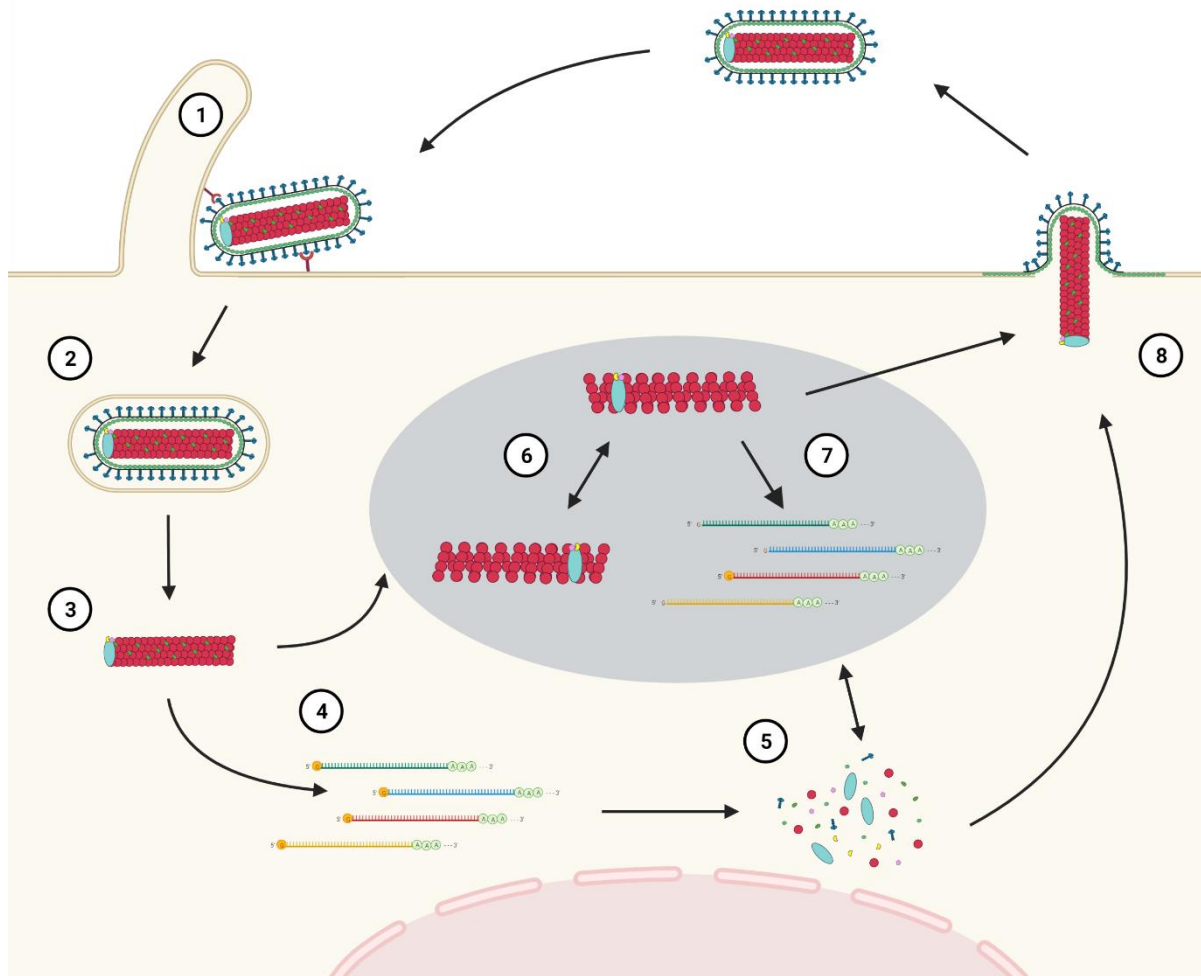


Figure 4. Ebolavirus lifecycle. (1) Entry. (2) Macropinocytosis. (3) Uncoating and release of the nucleocapsid in the cytoplasm. (4) Primary transcription. (5) mRNA translation. (6) Replication. (7) Secondary transcription. (8) Budding. Created with BioRender.com

1.7 Clinical manifestation and pathogenesis

Ebolaviruses cause a severe infection in humans that is known as Ebola hemorrhagic fever (EHF) or Ebola virus disease (EVD). After an incubation period of 2 - 21 days (average 8 – 10 days) EVD develops abruptly. The initial symptoms such as fever, chills, malaise, and myalgia, are unspecific and often mistaken for other infections including malaria, influenza and typhoid fever (Del Rio, Mehta et al. 2014). In the further course of infection, at the end of the first week, initial symptoms are followed by systemic gastrointestinal (anorexia, nausea, vomiting, abdominal pain, diarrhea), respiratory (chest pain, shortness of breath, cough), vascular (conjunctival injection, hypotension, edema), and neurologic (headache, confusion, coma) manifestations, indicating a multisystem involvement (Feldmann and Geisbert 2011). Late in infection a hemorrhagic manifestation develops, which encompasses melena, petechiae,

ecchymoses and bleeding from puncture sites (Sureau 1989, Malvy, McElroy et al. 2019). However, hemorrhagic developments are only observed in ~50 % of the EVD patients and have been linked with an increased mortality (Richards, Murphy et al. 2000). Additionally, fatal cases have been associated with an early onset of clinical signs and the victims die within 6 to 14 days after initial onset of symptom due to hemorrhage, multiorgan failure and shock (Malvy, McElroy et al. 2019). Case fatality rates associated with EVD vary from 30 % to 90 % and are mainly dependent on the virus species (Feldmann and Geisbert 2011, Burk, Bollinger et al. 2016, Yamaoka and Ebihara 2021). Non-fatal cases are characterized with an extended convalescence that is linked to fatigue, musculoskeletal pain, headache and sometimes eye abnormalities (Scott, Sesay et al. 2016). In EVD survivors that developed a Post-Ebola syndrome, virus was still detectable in samples of semen, conjunctival swab and aqueous humor of the eye, indicating that ebolaviruses can persist for long periods in immunologically privileged sites (Rowe, Bertolli et al. 1999).

The high virulence of ebolaviruses is at least in part caused by their ability to interfere with the host cell immune response causing the release of different cytokines and other proinflammatory factors, which results in the impairment of the vascular, coagulation and innate and adaptive immune systems (Feldmann and Geisbert 2011). Although ebolaviruses are able to infect a broad range of different cell types, the initial target cells are macrophages, monocytes and dendritic cells (DC) (Geisbert, Hensley et al. 2003). While it is believed that ebolaviruses use the migratory potential of DC for further dissemination and inhibition of the release of costimulatory molecules like CD40, CD80, CD86 and MHC class II, an infection of monocytes and macrophages triggers the release of proinflammatory cytokines and chemokines, such as interleukin (IL)-1 β , IL-8, IL-15, IL-18, and - β , monocyte chemoattractant protein-1 (MCP-1), tumor necrosis factor α (TNF- α) and macrophage inflammatory protein-1 α (MIP-1 α) (Gupta, Mahanty et al. 2001, Hensley, Young et al. 2002, Geisbert, Hensley et al. 2003, Mahanty, Hutchinson et al. 2003, Bixler and Goff 2015). An increased release of these immunogenic factors leads to the recruitment of additional monocytes, macrophages and neutrophilic granulocytes to the site of infection increasing the availability of target cells (Hensley, Young et al. 2002, Geisbert, Hensley et al. 2003). Additionally, infected macrophages have been shown to secrete abnormal and increased amounts of TNF- α , which leads to an increased vascular permeability and leakage causing vascular dysfunction and intravascular coagulation (Hensley, Young et al. 2002).

To evade the antiviral host cell immune response, ebolaviruses are able to inhibit the production of and cellular response to type I interferon signaling by expression of two immunosuppressive factors: VP35 and VP24. While VP35 suppresses the activation of interferon regulatory factor 3 through interfering with sensing of double stranded RNA (dsRNA), VP24 blocks interferon-mediated signaling by inhibition of the phosphorylation of p38 and binding to karyopherin α (see section 1.5) (Mateo, Reid et al. 2010, Leung, Prins et al. 2010b).

1.8 Ebolaviruses and host factors

While there is detailed knowledge about the role of the viral proteins during the ebolavirus lifecycle, only a few host proteins have been identified that might participate in these processes. However, due to the limited number of viral genes, ebolaviruses are strongly dependent on their host cell and an involvement of host cell factors is required for successful genome replication and transcription. Since genome replication and transcription is taking place in NP-induced or virus-induced inclusion bodies (IB), recruitment of host factors to these sites can be indicative of a functional role of these factors. For instance, SMYD3 is recruited into inclusion bodies by EBOV NP in order to modulate NP-VP30 interaction and enhance mRNA transcription (Chen, He et al. 2019). Similarly, the host protein STAU1 has been shown to redistribute into inclusion bodies upon virus infection or NP expression and to interact not only with NP but also with VP30, VP35 and the viral RNA, suggesting that STAU1 plays a crucial role in EBOV RNA synthesis by coordinating the interactions between the viral genome and the RNP proteins (Fang, Pietzsch et al. 2018). Additionally, in order to promote EBOV replication and transcription, several cellular kinases and phosphatases are known to redistribute into inclusion bodies (Kruse, Biedenkopf et al. 2018, Morwitzer, Tritsch et al. 2019, Takamatsu, Krahling et al. 2020). Furthermore, RBBP6 has been identified to influence EBOV replication through impairing the VP30-NP interface (Batra, Hultquist et al. 2018). Although no colocalization with IBs was observed, the host protein Sec61 α has been shown to interact with VP24, and to be involved in regulation of genome replication and transcription by altering EBOV polymerase activity (Iwasa, Halfmann et al. 2011). Nevertheless, despite this progress in our understanding of the interplay between ebolaviruses and their host cell, the identification and characterization of novel host factors involved in EBOV RNA synthesis remains important in order to detect further targets for antiviral drug development. In order to

address this issue, we recently performed a genome-wide siRNA screen identifying three host factors, the carbamoyl-phosphate synthetase 2, aspartate transcarbamylase, and dihydroorotase (CAD), the nuclear export factor 1 (NXF1) and the DEAD box polypeptide 39B (DDX39B), which seem to be crucial for EBOV genome replication and transcription (Martin, Chiramel et al. 2018).

1.8.1 Carbamoyl-phosphate synthetase 2, aspartate transcarbamylase, and dihydroorotase (CAD)

The trifunctional polypeptide CAD has a size of 243 kDa and represents an important component of the pyrimidine *de novo* synthesis pathway (Figure 5A). Via its four distinct enzymatic domains CAD catalyzes the first steps of the *de novo* biosynthesis of pyrimidine nucleotides, which play a critical role in the cellular metabolism by serving as precursors of RNA and DNA (Figure 5B) (Coleman, Suttle et al. 1977, Jones 1980, Lee, Kelly et al. 1985). The pyrimidine pathway is initiated by the hydrolysis of glutamine into ammonia and glutamate, which is catalyzed by the first domain, glutaminase (GLN), of CAD (Figure 5A (1)). This is followed by the synthesis of carbamoyl phosphate out of bicarbonate, ammonia and two ATP molecules and facilitated by the carbamoyl-phosphate synthetase (CPS) domain (Figure 5A (2)). Next, carbamoyl phosphate serves together with aspartate as substrate for the synthesis of carbamoyl aspartate (Figure 5A (3)). This step is catalyzed by the carbamoyl aspartate (ATC) domain of CAD (Christopherson and Jones 1980, Irvine, Shaw et al. 1997). Finally, carbamoyl aspartate is condensed to dihydroorotate by the Zn metalloenzyme dihydroorotase (DHO) (Figure 5A (4)) (Evans and Guy 2004). Upregulation of CAD in response to cell growth and proliferation is mediated by phosphorylation through MAP kinases at position Thr-456, which has shown to be dephosphorylated in resting cells (Sigoillot, Berkowski et al. 2003). Furthermore, in response to Thr-456 phosphorylation the primarily cytoplasmic CAD is able to translocate into the nuclear compartment, indicating an additional function of CAD in the nucleus (Chaparian and Evans 1988, Sigoillot, Kotsis et al. 2005). However, less is known about the role of CAD during virus infection, and in particular with respect to its role in the EBOV lifecycle, which still needs to be elucidated.

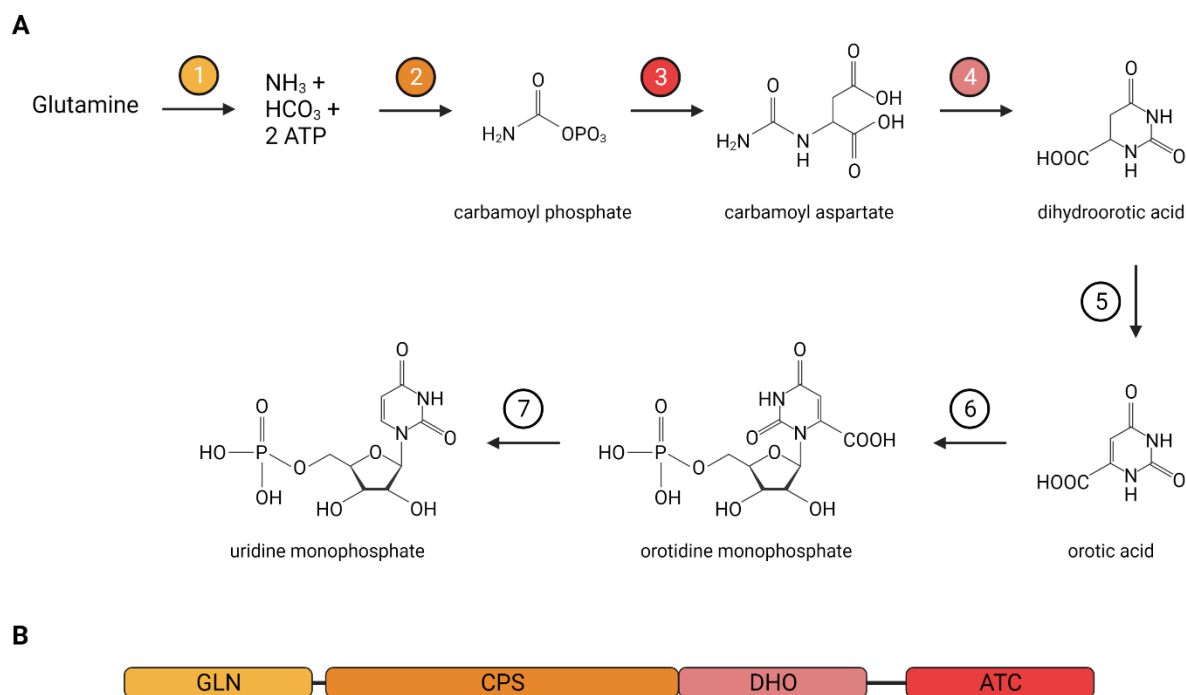


Figure 5. CAD catalyzes the first steps in pyrimidine synthesis. **(A)** Pyrimidine synthesis pathway. (1) Glutaminase (GLN). (2) Carbamoyl-phosphate synthetase (CPS). (3) Aspartate transcarbamylase (ATC). (4) Dihydroorotase (DHO). (5) Dihydroorotate dehydrogenase (DHODH). (6), (7) Uridine monophosphate synthetase (UMPS). **(B)** Molecular arrangement of CAD domains. Created with BioRender.com

1.8.2 Nuclear export factor 1 (NXF1)

NXF1, also known as tip-associated protein (TAP), is an essential component of the nuclear mRNA export machinery and transports mRNA from the nucleus to the cytoplasm via interaction with several nuclear factors (Figure 6A) (Katahira, Strasser et al. 1999, Bachi, Braun et al. 2000, Valkov, Dean et al. 2012). While NXF1 consists of five distinct domains, RNA binding of NXF1 is mainly facilitated through an N-terminal arginine-rich RNA-binding domain (RBD) that has no sequence specificity and binds a variety of RNA substrates (Figure 6B) (Zolotukhin, Tan et al. 2002, Hautbergue, Hung et al. 2008). However, it was shown that besides the RBD two additional domains of NXF1, which are the amino terminal domains pseudo RNA recognition motif (RRM) and a region with leucine rich repeats (LRR), are also important for mRNA binding (Bachi, Braun et al. 2000, Hautbergue, Hung et al. 2008). Once bound to mRNA, NXF1 transports the RNA throughout the nucleus to the nuclear pore complex (NPC), where NXF1 interacts with different nucleoporins (NUPs) via its nuclear-transport factor 2-like (NTF2) and ubiquitin-associated (UBA) domains (Fribourg, Braun et al. 2001). Interaction with nucleoporins also requires the formation of a stable heterodimer

between NXF1 and p15 (also called NXT1), mediated by the NTF2-like domain of NXF1 (Fribourg, Braun et al. 2001, Guzik, Levesque et al. 2001). Co-transcriptional binding of NXF1 to RNA and transport of mRNA throughout the nucleus requires the presence of multiple nuclear adaptors in order to release mature mRNA transcripts into the cytoplasm for translation (Viphakone, Hautbergue et al. 2012, Viphakone, Sudbery et al. 2019). NXF1-mediated nuclear export of mRNA is hijacked by many nuclear replicating viruses, such as influenza viruses and herpesviruses, which usurp this pathway to export their viral RNAs from the nucleus (Satterly, Tsai et al. 2007, Tunncliffe, Hautbergue et al. 2011, Larsen, Bui et al. 2014, Tunncliffe, Hautbergue et al. 2014). Additionally, NXF1 is known to bind and export Hepatitis B virus pregenomic RNA and retroviral RNA containing a constitutive transport element (CTE) (Gruter, Taberero et al. 1998, Yang, Huang et al. 2014). In contrast to these viruses, ebolavirus genome replication and transcription takes place in the cytoplasm and so far, no nuclear factor involved in these processes has been described, indicating that the function of NXF1 during the EBOV lifecycle has to be different from what is yet known about this host factor.

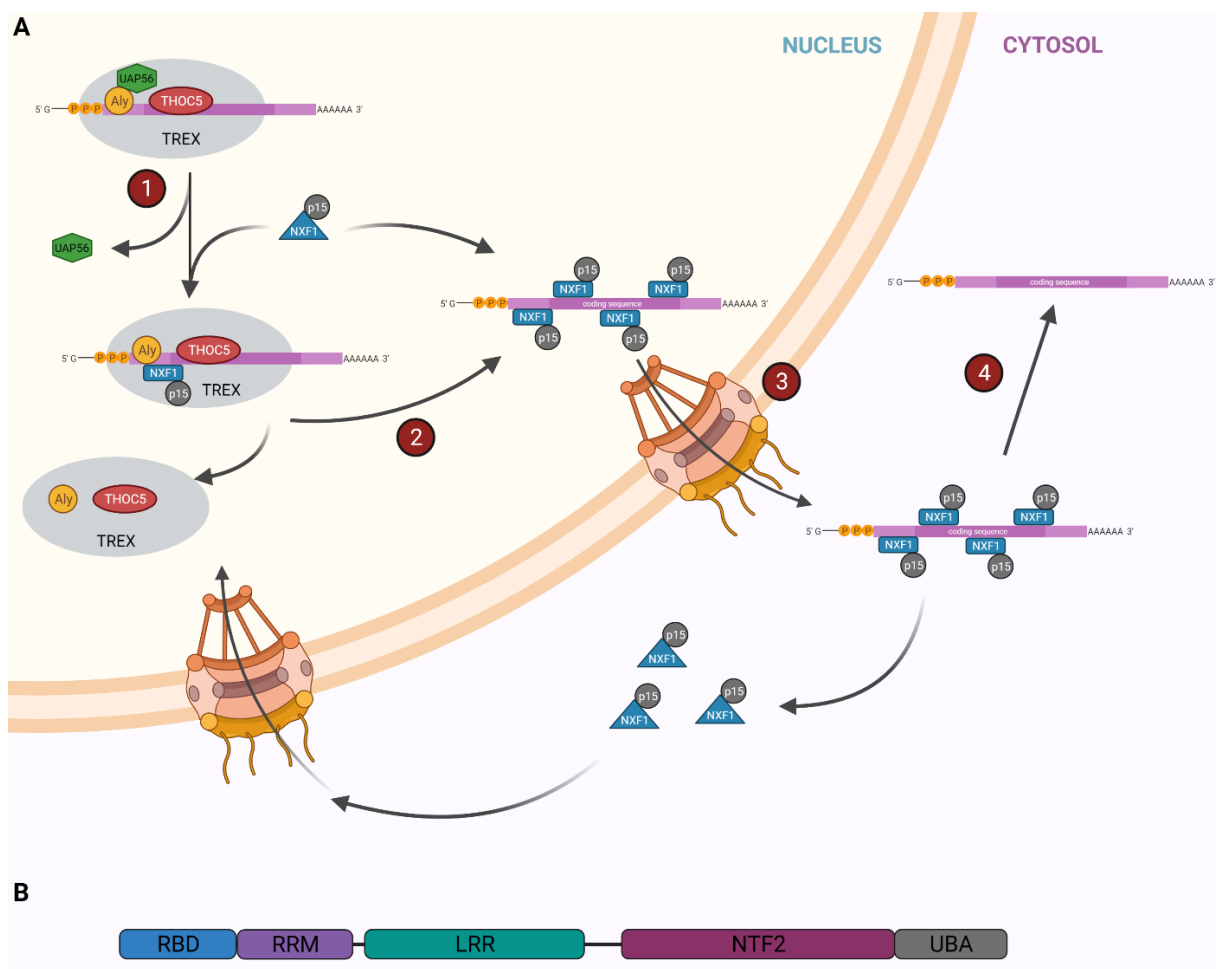


Figure 6. NXF1 mediates the nuclear export of mRNA. **(A)** Nuclear export pathway of cellular mRNA. (1) NXF1 and p15 are recruited to the spliced mRNA by the TREX complex. UAP56 dissociates from the mRNA. (2) The mRNA is packed by NXF1. (3) NXF1 transports the mRNA from the nucleus through the nuclear pore complex into the cytoplasm. (4) NXF1 dissociates from the mRNA and passages back into the nucleus. **(B)** Molecular arrangement of NXF1 domains. Created with BioRender.com

1.8.3 DEAD box polypeptide 39B (DDX39B; UAP56)

UAP56, also known as DDX39B or BAT1, is a member of the ATP-dependent RNA helicases and belongs to the DEAD box family. Besides its essential function in pre-mRNA splicing, UAP56 is also important for nuclear export of mRNA and cytoplasmic mRNA localization (Figure 7) (Fleckner, Zhang et al. 1997, Luo, Zhou et al. 2001, Meignin and Davis 2008, Shen, Zheng et al. 2008). With respect to splicing, UAP56 is required for ATP-dependent RNA unwinding and ATP hydrolysis in order to rearrange specific RNA structures during spliceosome assembly (Fleckner, Zhang et al. 1997, Kistler and Guthrie 2001). While ATP hydrolysis facilitates the stable interaction of the U2 small nuclear ribonucleoprotein (snRNP) at the pre-mRNA branch point, ATP-dependent RNA unwinding is essential to promote the unwinding of the U4/U6 snRNP duplex to mediate assembly of mature spliceosomes (Fleckner, Zhang et al. 1997, Shen, Zheng et al. 2008). However, during mRNA export UAP56 interacts with the exon junction complex (EJC) and recruits the nuclear export factor Aly to the spliced mRNA (Luo, Zhou et al. 2001, Reichert, Le Hir et al. 2002). Because of this function, UAP56 is known to belong to the TREX (Transcription-export) complex, which is a multiprotein complex that plays a major role during mRNA transcription, processing, decay, and nuclear export (Reed and Cheng 2005, Kohler and Hurt 2007, Katahira and Yoneda 2009). It has been shown that UAP56 is involved in influenza virus infection by facilitating viral RNP loading by promoting the interaction between NP and the viral RNA (Momose, Basler et al. 2001, Hu, Gor et al. 2017). However, UAP56 represents, similar to NXF1, a nuclear factor that is so far not linked to the lifecycle of cytoplasmically replicating viruses.

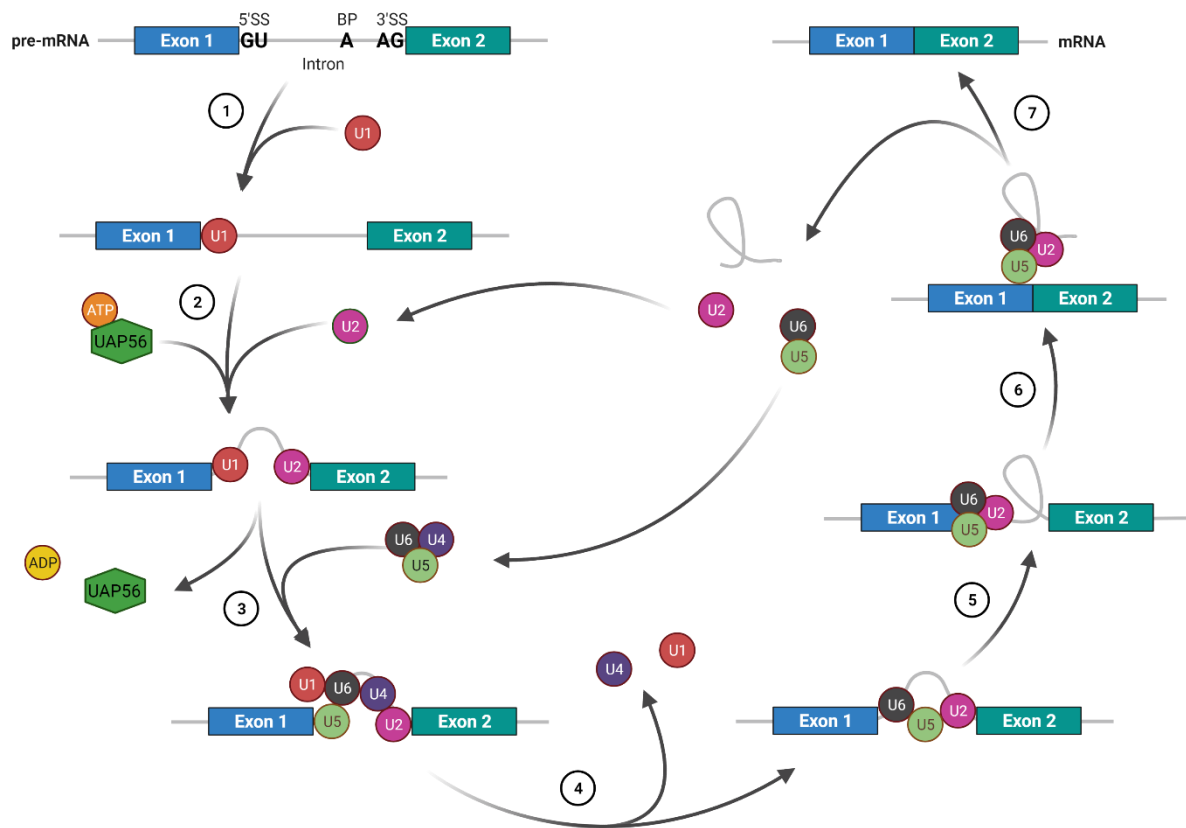


Figure 7. The mRNA splicing process. (1) The U1 snRNP binds to the GU sequence at the 5' splice site (5'SS) of an intron. (2) The U2 snRNP binds to the branch point (BP) sequence. For this ATP hydrolysis, which is mediated by UAP56, is required. Binding of U1 and U2 snRNP to the pre-mRNA leads to the formation of the pre-spliceosome complex (complex A). (3) The U5/U4/U6 snRNP trimer is recruited and binds to the pre-mRNA, which leads to the formation of the pre-catalytic spliceosome (complex B) (4) The U1 and U4 snRNPs are released from complex B, U5 shifts from exon to intron, and the U6 binds at the 5' splice site of the intron. This complex is described as the activated spliceosome (complex B*) (5) The U6 and U2 snRNPs catalyze transesterification, which leads to the ligation of the 5' end of the intron to the branch point. Simultaneously, U5 binds to exon 1 at the 3' end, while the 5' site of the intron is cleaved, resulting in the formation of a lariat. After lariat formation the complex is described as catalytic spliceosome (complex C). (6) The U2, U5 and U6 snRNPs remain bound to the lariat, while the 3' site of the intron is cleaved and the exons are ligated, which is facilitated by ATP hydrolysis. Ligation of the exons leads to the formation of the post spliceosomal complex (complex C*). (7) The spliced RNA is released from the spliceosome complex. The lariat dissociates from the snRNPs and is degraded, while the snRNPs are recycled. Created with BioRender.com

1.9 RNA interference (RNAi)

RNAi is a natural cellular process that regulates protein expression by activation of an mRNA degradation process and was first described by Fire and Mello in 1998 (Fire, Xu et al. 1998). This pathway of gene silencing plays an important role in gene regulation and the innate defense against invading viruses by using non-coding double-stranded RNA (dsRNA) that can target cellular and viral mRNAs (Agrawal, Dasaradhi et al. 2003). Because of this, RNAi is used in molecular biology as a tool to

study the influence of cellular gene silencing on various processes (e.g. their impact on virus infection). In course of the cellular RNAi pathway dsRNA, which is either transcribed from cellular or viral genes or artificially introduced into the cell, is cleaved in the cytoplasm by a ribonuclease (RNase) III-like enzyme called Dicer. This results in the production of short dsRNA fragments that have a length of 19 - 25 nucleotides and 3' two-nucleotide overhangs (Vermeulen, Behlen et al. 2005, Merritt, Bar-Eli et al. 2010). Accumulation of short dsRNA fragments in the cytoplasm of cells leads to the activation of the RNA-induced silencing complex (RISC). Next, the endonuclease argonaute 2 (AGO2), a component of RISC, cleaves the passenger (sense) strand of the dsRNA. The guide (antisense) strand, which remains associated with RISC, then scans the cellular mRNA for its target sequence. Once bound to the target site, gene silencing occurs via translational repression, degradation or cleavage of the mRNA by AGO2 (Kim and Rossi 2007, Pecot, Calin et al. 2011, Lam, Chow et al. 2015). In order to perform gene silencing three classes of non-coding dsRNAs are described: siRNA (small interfering RNA), miRNA (micro RNA) and shRNA (short hairpin RNA). In contrast to miRNA, siRNA and shRNA need to be fully complementary to their target mRNA to enable gene silencing. However, in order to avoid off-target effects and increase mRNA target specificity, artificial miRNAs (amiRNA) were designed, which also require a fully complementary to their target mRNA (Figure 8) (Eamens, McHale et al. 2014).

1.10 Ebolavirus reverse genetic systems

Reverse genetics describes a method used in the field of molecular biology in order to analyze the effect of modified genome sequences on the phenotype of an organism. In contrast to “forward” or “regular” genetics the research is directed from genotype to phenotype rather than from phenotype to genotype. When it comes to reverse genetics a fundamental knowledge of the desired gene sequence as well as a suitable model system for expression of the target gene is required. With respect to viruses, reverse genetics refers to the generation, and subsequent replication and transcription of viral genomes or genome analogues from cDNA plasmids (Hoenen, Groseth et al. 2011, Hoenen and Feldmann 2014). While for positive-sense RNA viruses their genomic RNA serves as mRNA, so that a cDNA copy of the virus genome cloned into an expression plasmid is sufficient for the establishment of a reverse genetic system, for negative-sense RNA viruses the development of such systems is more challenging, as

here the viral proteins required for replication and transcription have to be provided in addition to the genomic (or antigenomic) viral RNA.

With respect to ebolaviruses, reverse genetic systems encompass full length clone systems, which allow the generation of recombinant, infectious ebolaviruses, as well as lifecycle modelling systems, which utilize a shortened version of the viral genome (i.e. a minigenome) and permit to study the ebolavirus lifecycle under low containment condition (biosafety level (BSL) 1 or 2) (Muhlberger, Weik et al. 1999, Neumann, Feldmann et al. 2002, Hoenen and Feldmann 2014). Lifecycle modelling systems for ebolaviruses can be further divided into classical minigenome systems, which allow to study viral RNA synthesis, and transcription- and replication-competent virus like particle (trVLP) systems, which model almost all aspects of the virus lifecycle.

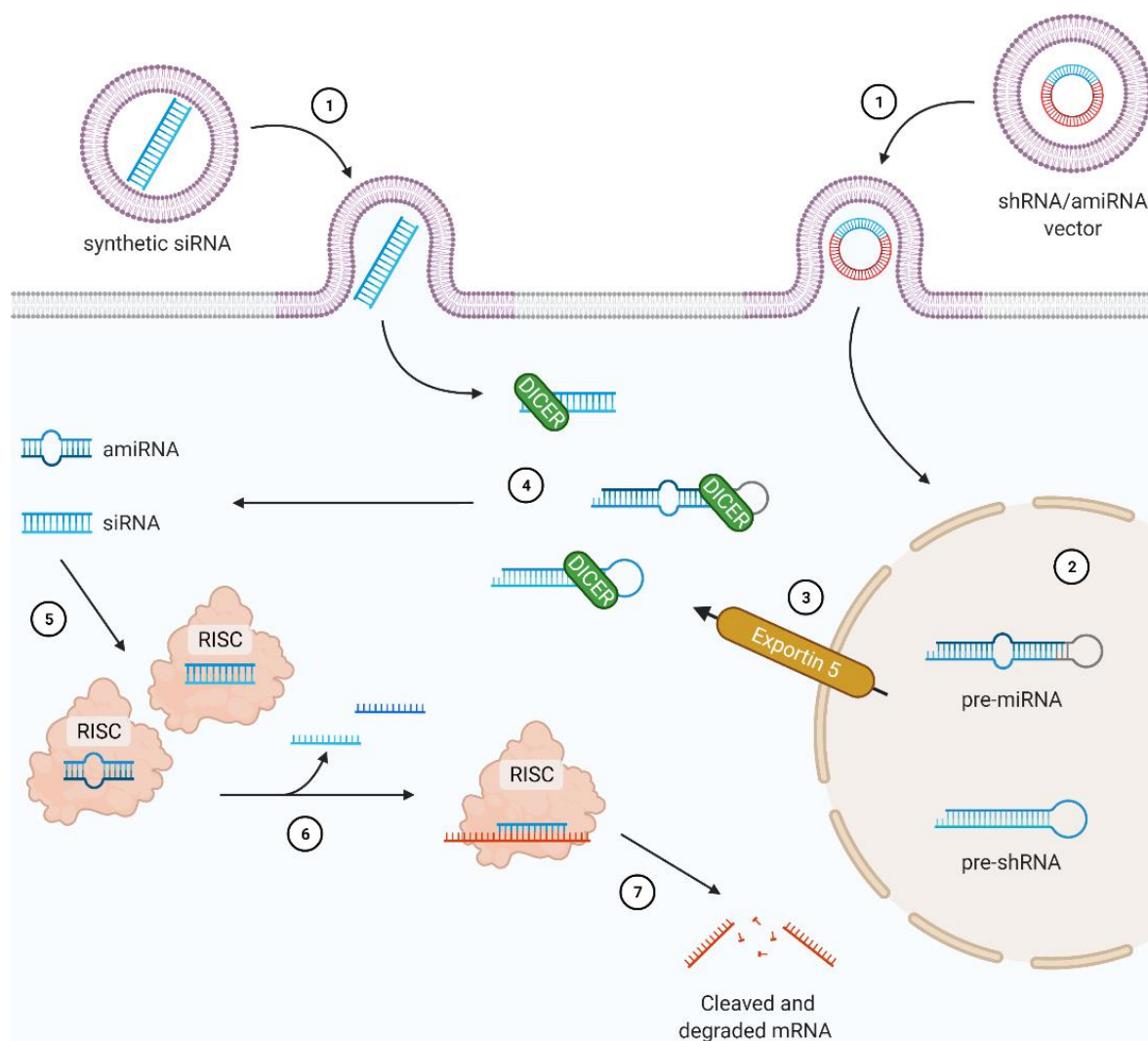


Figure 8. RNA interference pathways. (1) Transfection of synthetic siRNAs or vectors encoding for shRNA or amiRNA. (2) Transcription of the shRNA or amiRNA in the nucleus of target cells. (3) Pre-shRNA or pre-amiRNA are transported into the cytoplasm via exportin 5. (4) The ribonuclease DICER

is recruited to the RNAs and cleaves pre-siRNA or pre-shRNA into functional siRNAs and pre-amiRNA into functional amiRNA. (5) Accumulation of cytoplasmic siRNAs or amiRNAs activate the RNA-induced silencing complex (RISC). (6) siRNA/amiRNA duplex get unwound and passenger strand is released. (7) siRNA or amiRNA guide the RISC complex to the target mRNA. Fully complementary binding of the target RNA leads to cleavage and/or degradation of the mRNA, which results in gene silencing. Created with BioRender.com

1.10.1 Minigenome systems

In contrast to full-length clone systems minigenome systems consist of a minimal version of the ebolavirus genome in which all viral genes are removed and replaced by a reporter gene encoding e. g. luciferase or a fluorescent protein (Figure 9) (Muhlberger, Weik et al. 1999). The reporter protein is flanked by the viral non-coding terminal leader and trailer regions as well as the 3' untranslated region of the NP gene and the 5' non-coding region of the L gene, ensuring that the minigenome is recognized as an authentic template by the viral polymerase complex. In order to initially express the minigenome in mammalian cells most of the existing minigenome systems use a T7 RNA polymerase (T7) promoter, which requires cotransfection of a T7 polymerase expressing plasmid to provide T7 polymerase expression in the cells (Muhlberger, Weik et al. 1999, Uebelhoer, Albarino et al. 2014). However, cellular polymerases including RNA polymerase II (Pol-II) have been recently described to be more efficient in the initial transcription of the minigenome in contrast to the T7 polymerase (Nelson, Pacheco et al. 2017), although this effect was not observed in all cell types. A further advantage of a minigenome under control of a Pol-II promoter is that one plasmid less has to be cotransfected, as Pol-II already exists in mammalian cells. In difference to the T7 polymerase, where transcription leads to a 3' -polyadenylated transcript, which requires the addition of a hepatitis delta virus ribozyme at the 3' end of the minigenome to generate authentic genome ends, but an authentic 5' genome end, Pol-II transcription leads to a 5' -capped and 3' -polyadenylated transcript, which requires another hammerhead ribozyme at the 5' end of the minigenome. After initial transcription the minigenome is artificially encapsidated by the RNP proteins, which are expressed from plasmids that are cotransfected with the plasmids encoding for the minigenome and, if needed, the T7 polymerase. The encapsidated minigenome is then recognized as authentic template by the viral polymerase and serves as template for replication and transcription, leading to production of mRNAs, which results in the expression of the reporter protein. As transcription depends on the amount of vRNA produced by genome replication, reporter activity reflects both replication and

transcription (Figure 9). In order to distinguish between replication and transcription, a replication-deficient minigenome has been developed, which, in contrast to the classical minigenome, has a 55 nucleotide deletion in the antigenomic promoter that is located in the trailer region of the minigenome (Figure 9) (Hoenen, Jung et al. 2010b). While cRNA is still synthesized, no vRNA is generated from the cRNA in this system, which leads to a block of genome replication. Therefore, reporter activity reflects only genome transcription, but not genome replication (Figure 9).

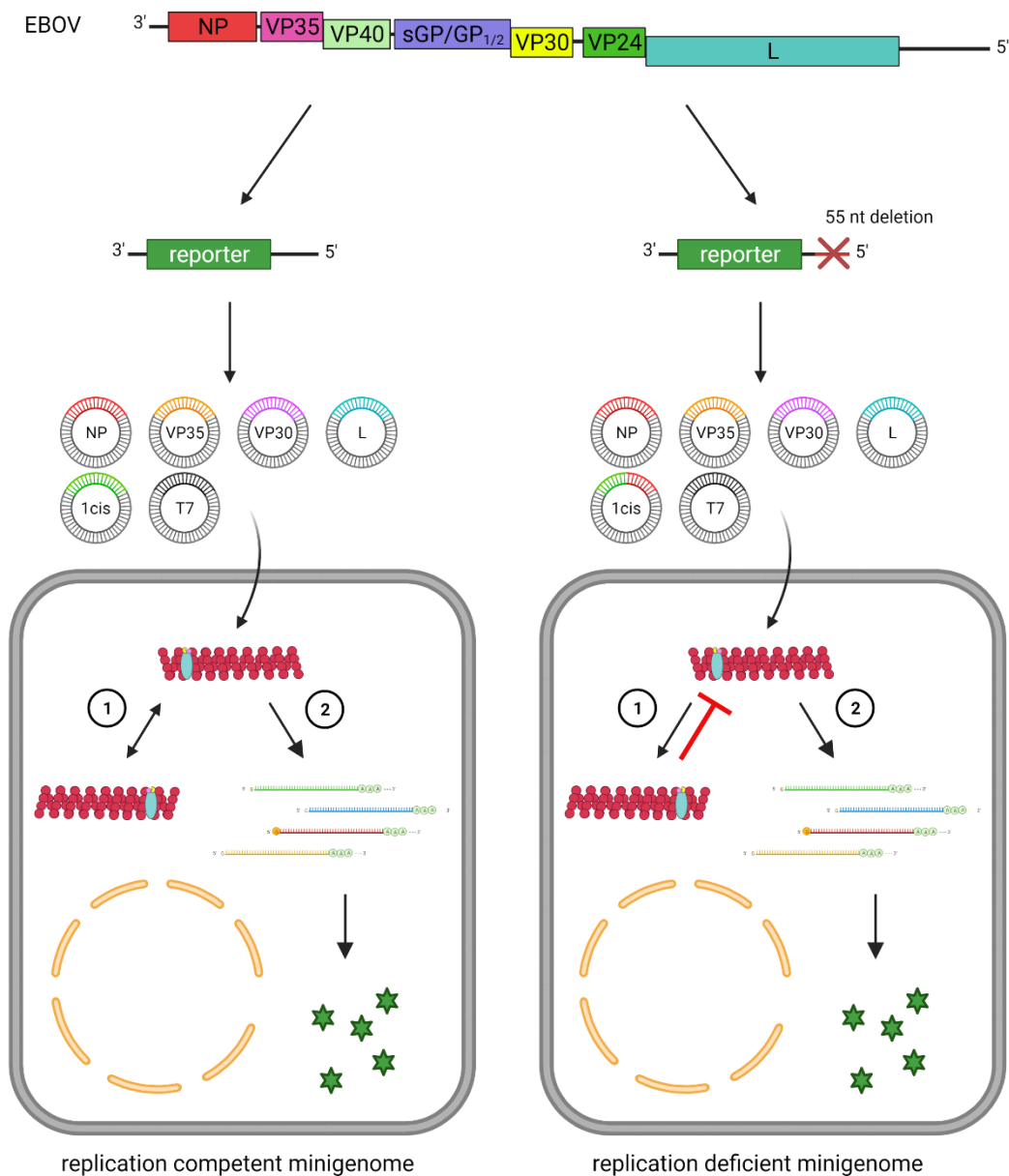


Figure 9. Replication competent and replication deficient monocistronic minigenome system. The full-length genome structure of EBOV, as well as replication-competent and -deficient minigenomes derived

from this full-length genome, are shown. (1) Replication. (2) Secondary transcription. Figure modified from Schmidt et al. 2017 under CC BY 4.0 license (Schmidt and Hoenen 2017). Created with BioRender.com

1.10.2 Transcription and replication competent virus like particle (trVLP) system

Despite their advantages, minigenome systems also have disadvantages, in particular some artificial aspects, including initial transcription of the minigenome by T7 or Pol-II polymerase or illegitimate encapsidation of the minigenome, which can have an influence on reporter activity. Additionally, minigenome systems are limited to modelling replication and transcription, whereas the ebolavirus lifecycle further consists of entry and budding of virus particles. In order to model all aspects of the ebolavirus lifecycle and to get rid of the artificial aspects present in minigenome systems, trVLP systems have been developed (Watanabe, Watanabe et al. 2004, Hoenen, Groseth et al. 2006). In contrast to a classical minigenome system, the trVLP systems consist of a tetracistronic minigenome that contains, in addition to the reporter gene, the genes for the viral structural proteins VP40, GP and VP24 (Figure 10A). Therefore, when producer cells (also called p0 cells) are transfected with all components required for a minigenome assay, expression of the viral structural proteins, which form virus like particles (VLPs) that are coated with GP and harbor nucleocapsid containing the minigenome. VLPs containing nucleocapsids with minigenomes (called trVLPs) are released into the cytoplasm and are able to infect target cells (also called p1 cells). Infection of naive target cells leads to the generation of mRNAs exclusively out of primary transcription resulting in reporter activity that reflects genome replication in and budding from p0 cells as well as entry of trVLPs into and primary transcription in p1 cells. However, when p1 cells are pretransfected with plasmids encoding the RNP proteins, after infection with trVLPs a full ebolavirus lifecycle takes place. Therefore, reporter activity reflects genome replication in and budding from p0 cells as well as entry of trVLPs into p1 cells and genome replication and secondary transcription in p1 cells (Figure 10B) (Watt, Moukambi et al. 2014).

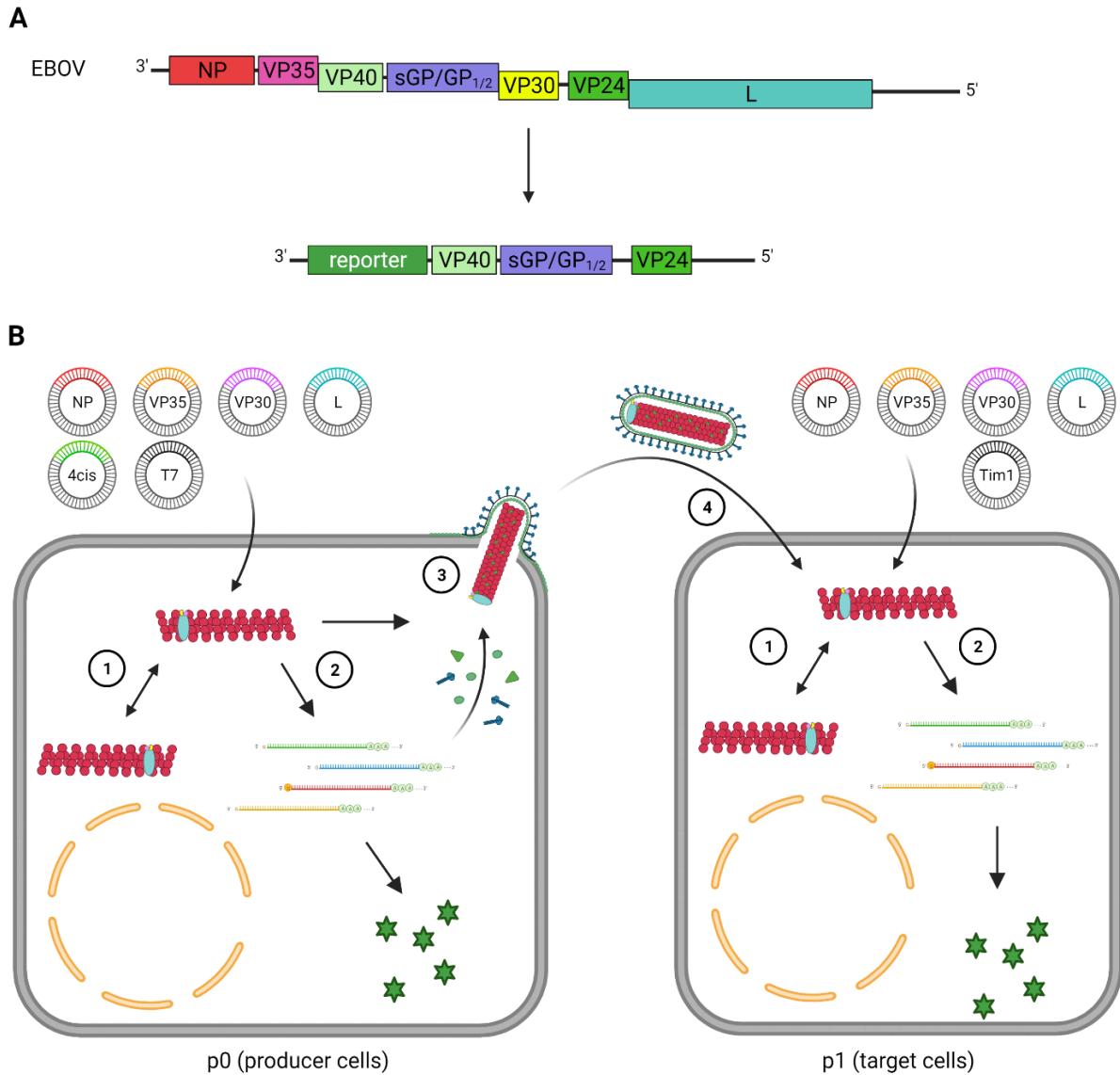


Figure 10. EBOV trVLP system. **(A)** Tetracistronic minigenome. The full-length genome structure of EBOV, as well as the tetracistronic minigenome derived from this full-length genome, is shown. **(B)** trVLP assay. (1) Replication. (2) Transcription. (3) Assembly and budding. (4) Entry. Created with BioRender .com

1.11 Objectives of this study

Host factors have been shown to play an important role in the EBOV lifecycle, but so far host proteins that are involved in replication, transcription and protein expression as well as their role during these processes and the mechanism how they are involved still remains largely unknown. However, recently a genome wide siRNA screen was performed to identify new host factors that are potential host-directed targets (Martin, Chiramel et al. 2018). Out of 37 genes that seem to be highly important for the EBOV lifecycle, the three best hits were CAD, NXF1 and UAP56. The overall goal of this

thesis was, therefore, to investigate the functional role of these three host factors during the EBOV lifecycle, with the following three specific aims:

- **Influence of CAD, NXF1 and UAP56 on the EBOV lifecycle.** It has been previously shown that knockdown of CAD, NXF1 and UAP56 leads to a reduced reporter activity in a classical minigenome assay. However, it was unknown precisely at which step of the viral lifecycle modelled by the minigenome system (i.e. viral genome replication, transcription, or protein expression) CAD, NXF1 and UAP56 are involved. To address this question, classical minigenome systems, replication deficient minigenome assays and trVLP systems as well as RT-qPCR (to check on viral replication) were used in combination with siRNA knockdown of these host factors. In addition, in order to obtain further information with respect to a potential mechanism of the analyzed factors, I also assessed which effect overexpression of these factors had on these processes.
- **Recruitment of CAD, NXF1 and UAP56 into EBOV inclusion bodies.** Recently it was shown that EBOV recruits various host factors into inclusion bodies in order to facilitate genome replication and transcription. Although CAD, NXF1 and UAP56 are known to be important for EBOV RNA synthesis, it is not known whether these host factors are also recruited into inclusion bodies in order to fulfill their function in the EBOV lifecycle. To analyze this, immunofluorescence assays with commercially available antibodies against CAD, NXF1, UAP56 and EBOV proteins, which are involved in inclusion body formation, were performed. Additionally, to examine whether one or more EBOV proteins are required for uptake of these host factors in inclusion bodies, I also performed immunofluorescence analyses in course of an EBOV infection.
- **Influence of CAD, NXF1 and UAP56 single domain or deletion mutants on the EBOV lifecycle and recruitment into inclusion bodies.** With respect to the molecular structure of CAD, NXF1, UAP56, it was shown that they exhibit different domains which are required for their specific function in cells. However, so far it is not known whether all domains or just single domains of

these host factors are important for the EBOV lifecycle. To investigate this complementation assays were used in combination with siRNA knockdown of NXF1 and UAP56. Furthermore, in order to analyze the influence of these domains on recruitment into inclusion bodies I coexpressed EBOV NP together with single domains or domain deletion mutants of CAD and NXF1 and performed immunofluorescence assays.

2 Material and Methods

2.1 Material

2.1.1 Equipment and Devices

Device	Company
96-Well Fast Reaction Module	BioRad
AriaMx Real-time PCR System	Agilent
C1000 Touch Thermal Cycler	BioRad
CO ₂ Incubator	Sayo
Confocal microscope Leica SP5	Leica
Dual 48/48 Fast Reaction Module	BioRad
Inverted research microscope Eclipse Ti-S	Nikon
Laboratory hot water bath	GFL
Lightning plate	Carl Roth
Magnet stirrer MR Hei-Standard	MR Hei-Standard
Microbiological incubators	Heraeus
Microscope TS 100	Nikon
Microwave	Siemens
Mini-PROTEAN® Tetra Cell Systems	BioRad
Mini-Sub Cell GT	BioRad
NanoPhotometer	Implen
Odyssey CLx	LI-COR
Platform shaker Duomax 1030	Heidolph
Power Supply MP-3AP	Major Science
PowerPac	BioRad
Precision balance AZ3102	Sartorius
S1000 Thermal Cycler	BioRad
Semi-Dry Blotter V20-SDB	Biostep
Stackable Shakers with incubation function	Thermo Fisher
Sub Cell GT	BioRad
Thermomixer comfort	Eppendorf
Universal Hood II Gel Doc System	BIO-RAD
Vortex genie 2	Scientific Industries

Centrifuges

Centrifuge 5430R	Eppendorf
Centrifuge 5810R	Eppendorf
Heraeus Pico 17 Centrifuge	Thermo Fisher
Mini Centrifuge	LMS
Optima LE-80K Ultracentrifuge	Beckmann Coulter
PerfectSpin Mini Centrifuge	Peqlab
SW 40 Ti Swinging-Bucket rotor for UZ	Beckmann Coulter

Pipettes

Eppendorf Easypet	Eppendorf
Eppendorf research plus (0.5 µl - 10 µl)	Eppendorf
Eppendorf research plus (10 µl -100 µl)	Eppendorf
Eppendorf research plus (100 µl - 1000 µl)	Eppendorf
Eppendorf research plus (2 µl - 20 µl)	Eppendorf
Eppendorf research plus (50 µl - 200 µl)	Eppendorf
peqMATE electronic pipette controller	peqlab

2.1.2 Chemicals and reagents**2.1.2.1 Buffers, solutions and reagents**

Buffers/ Solutions/ Reagents	Company
10x buffer Tango	Thermo Fisher
10x Cut Smart buffer	NEB
10x T4 DNA Ligase buffer	NEB
2 log Ladder	NEB
2-Mercaptoethanol	MP Biomedicals
2x Lysis Juice	PJK
5x HF iProof™ buffer	BioRad
5x T4 DNA Ligase buffer	Invitrogen
6x Gel loading dye	NEB
Acrylamide 40 %	Carl Roth
Agar bacteriological grade	MP Biomedicals
Agarose	Biozym
Alsever's Trypsin Versene Solution (ATV)	Friedrich-Loeffler-Institut
Ammonium peroxodisulfate (APS)	Carl Roth

Ampicillin	Carl Roth
Beetle-Juice Luciferase assay Firefly	PJK
Bromophenol blue	Carl Roth
Color protein standard, broad range marker	NEB
Cytidine	Sigma-Aldrich
Denatured Ethanol 96 %	Carl Roth
Deoxynucleotides solution mix dNTP	NEB
Dextrose	Sigma Aldrich
dH ₂ O (Aqua bidest.)	Friedrich-Loeffler-Institut
Dimethyl sulfoxide (DMSO)	BioRad
Disodium hydrogen phosphate (Na ₂ HPO ₄)	Carl Roth
Dithiothreitol (DTT)	Carl Roth
Ethidium bromide (1 %)	Carl Roth
Ethylenediaminetetraacetic acid (EDTA)	Carl Roth
Fast blast™ DNA strain (500x)	BioRad
Fetal calf serum (FCS)	Friedrich-Loeffler-Institut
Formalin solution, neutral buffered (10 %)	Sigma Aldrich
GlutaMax Supplement	Thermo Fisher Scientific
Glycerol	Carl Roth
Glycine	Carl Roth
Hydrogen chloride (HCl)	Carl Roth
Isopropanol	Carl Roth
Lipofectamine RNAiMax Transfection Reagent	Thermo Fisher Scientific
Mounting Medium with DAPI	ibidi
NanoLuc-Serum	Promega
NanoLuc-Substrate	Promega
NEBuffer 3.1 (10x)	NEB
Paraformaldehyde	Carl Roth
Penicillin	Thermo Fisher
Polyethylenimine (PEI)	Friedrich-Loeffler-Institut
Potassium chloride (KCl)	Carl Roth
Potassium dihydrogen phosphate (KH ₂ PO ₄)	Carl Roth
PowerUp™ SYBR™ Green Master Mix	Thermo Fisher Scientific
ProLong™ Diamond Antifade Mountant with 4',6-diamidino-2-phenylindole (DAPI)	Thermo Fisher
Renilla Juice	PJK
Rotiphorese 50x Tris-acetat-EDTA (TAE) buffer	Carl Roth

Skim milk powder	Hobbybaecker
Sodium chloride (NaCl)	Carl Roth
Sodium dodecyl sulfate (SDS) pellets	Carl Roth
Sodium hydroxide (NaOH)	Carl Roth
Streptomycin	Thermo Fisher
Sucrose	Carl Roth
Tetramethylethylenediamine (TEMED)	Carl Roth
TransIT [®] -LT1	Mirus
Triton X [®] 100	Carl Roth
Trypsine	Invitrogen
Trypton	Carl Roth
Tween [®] 20	AppliChem
UltraPure [™] tris(hydroxymethyl) aminomethane (Tris)	Invitrogen
Uridine	Sigma-Aldrich
Yeast Extract powder	MP Biomedicals
ZB 10 medium	Friedrich-Loeffler-Institut
ZB 28 medium	Friedrich-Loeffler-Institut
ZB 30 (Optimem)	Thermo Fisher

2.1.2.2 Recipes for buffers and solutions

Buffer	Recipe
0.1 % Triton X100	0.1 ml 100 % Triton X 100 1x PBS ad 100 ml
0.1 M Glycine solution	5 ml 1 M Glycine solution dH ₂ O ad 45 ml
0.1 M NaOH	4 g NaOH dH ₂ O ad 1 l
0.5 M Tris-HCl pH 6.8; 0.4 % SDS (Stacking gel buffer)	60.6 g Tris 4 g SDS dH ₂ O ad 1 l
0.8 % agarose in 1x TAE buffer	0.8 g Agarose 1x TAE ad 100 ml
1 M Glycine solution	7.5 g Glycine

	dH ₂ O ad 100 ml
1 M Tris-HCl pH 6.8	121.14 g Tris 500 ml dH ₂ O ad HCL until pH 6.8 add dH ₂ O ad 1 l
1.5 M Tris-HCl pH 8.8; 0.4 % SDS (Resolving gel buffer)	181.8 g Tris 4 g SDS, dH ₂ O ad 1 l
10 % APS	1 g APS dH ₂ O ad 10 ml
10 % FCS	10 ml 100 % FCS 1x PBS ad 100 ml
100 mM Cytidine solution	0.1 g Cytidine DMSO ad 4.1 ml
100 mM Uridine solution	0.1 g Uridine DMSO ad 4.1 ml
100x Fast Blast	20 ml 500x Fast blast DNA strain dH ₂ O ad 100 ml
10x Phosphate buffered saline (PBS)	80 g NaCl 2 g KCl 11.5 g Na ₂ HPO ₄ 2 g KH ₂ PO ₄ ; pH 7.3, dH ₂ O ad 1 l
10x SDS-PAGE buffer	30 g Tris 10 g SDS 144 g Glycine dH ₂ O ad 1 l
1x Lysis Juice	25 ml 2x Lysis-Juice dH ₂ O ad 25 ml

1x PBS + 0.1 % Tween	2 ml 100 % Tween 1x PBS ad 2l
1x PBS buffer	100 ml 10x PBS dH ₂ O ad 1l
1x Sample buffer	100 ml 4x Sample buffer dH ₂ O ad 400 ml
1x SDS-PAGE buffer	100 ml 10x SDS-PAGE buffer dH ₂ O ad 1000 ml
1x TAE buffer	100 ml 50x TAE buffer dH ₂ O ad 1000 ml
2 log DNA Ladder	500 µl 2 log Ladder 4.5 ml dH ₂ O 1 ml 6x loading dye (from NEB)
20 % Sucrose solution	20 g Sucrose dH ₂ O ad 100 ml
4 % PFA	2 g PFA ZB10 (5 % FCS) ad 50 ml
4x Sample buffer	20 ml Glycerol 1 ml 2-Mercaptoethanol 4 g SDS 6.25 ml 1 M Tris-HCl, pH 6.8 0.5 g Bromphenol blue add dH ₂ O ad 50 ml
5 % Triton X 100	5 ml 100% Triton X 100 1x PBS ad 100 ml
7 % milk powder solution	7 g Milk powder 1x PBS + 0.1 % Tween ad 100 ml
70 % Ethanol	729 ml 96 % Ethanol dH ₂ O ad 1000 ml

Ampicillin stock solution	5 g Ampicillin dH ₂ O ad 100 ml
Ethidium bromide solution	12 µl Ethidium bromide dH ₂ O ad 250 µl
Glucose solution (1 M)	3.6 g Glucose dH ₂ O ad 20 ml
KCl solution (1 M)	7.46 g KCl dH ₂ O ad 100 ml
SOC-Medium	20 g Trypton 5 g yeast extract 0.5 g NaCl 2.5 ml 1 M KCl pH 7.5, dH ₂ O ad 1 l add 20 ml 1 M glucose after autoclaving
Western Blot transfer buffer	5.8 g Tris 2.9 g Glycine 200 ml Ethanol dH ₂ O ad 1 l

2.1.3 Consumables

Material

µ-slide 8 well: IbiTreat: 1.5 polymer coverslip
 96 well microplate (black)
 Cell culture bottles with filter (25 cm, 75 cm)
 Cell culture plate (6 well, 12 well)
 Costar® Stripette (serological pipet) 10 ml
 Costar® Stripette (serological pipet) 2 ml
 Costar® Stripette (serological pipet) 25 ml
 Costar® Stripette (serological pipet) 5 ml
 Cover slip (∅ 15 mm)
 DNA LoBind Tubes, DNA LoBind, 1.5 mL
 Eppendorf tube (1 ml)

Company

ibidi
 Greiner Bio-One
 Sarstedt
 Corning Incorporated
 Corning Incorporated
 Corning Incorporated
 Corning Incorporated
 Corning Incorporated
 Carl Roth
 Eppendorf
 Sarstedt

Eppendorf tube (2 ml)	Starlab
Extra Thick Western Blotting Filter Paper	Thermo Fisher
Falcon tube (15 ml; 50 ml)	Sarstedt
Microscope slide	Heinz Herenz Hamburg
Nitrocellulose Blotting Membrane	GE Healthcare Life Science
Parafilm® M Laboratory Film	Bemis flexible packaging
PCR Bio-Rad 8-Tube-Strips Low Profile	Bio-Rad
PCR Soft Tubes 0.2 ml	Biozym Scientific
Petri dish	Sarstedt
Pipette tip boxes	Nerbe plus
Pipette tip filtered (1000 µl, 200 µl, 100 µl, 20 µl, 10 µl)	Nerbe plus
Pipette tip unfiltered (1 – 10 µl)	Starlab
Pipette tip unfiltered (100 - 1000 µl)	Greiner
Pipette tip unfiltered (20 – 200 µl)	Starlab
Ultra-Clear Tube, 50 Stk, 14 x 95 mm for SW40	Beckman Coulter
Tweezers	Dumont

2.1.4 Oligonucleotides

Primers were ordered from Eurofins Scientific.

The following primers were used:

Primer	Sequence (5'→ 3')	Name
<i>Sequencing primers</i>		
#0030	TCTTTTCTACGGGGTCTGAC	siRNA_OL178
#0040	GAACTGGGCGGAGTTAGG	psiRNA-rev
#1233	CCTTCTTCTTTTTCTACAG	pCAGGS_fw
#1234	CCTTTATTAGCCAGAAGTCAG	pCAGGS_rev
#3185	CGGACACACAAAAAGAAAGAAG	rgZ_seq_23f
#3240	CAGGGAGAGAGGCTAAATATAG	rgZ_seq_18366r
#3544	CCG TTCAGACCCAGATTTGGTG	TH_NXF1-seq-696-fwd
#3547	AGACAGCCAAGAGTATGAGGG	TH_CAD-seq-627-fwd

#3548	TGGCCAAGCTGGAGAATTTGAC	TH_CAD-seq-1218-fwd
#3549	ACTGTGTCACGGTGTGTAACATGG	TH_CAD-seq-1832-fwd
#3550	CCAGTCAGCGATATGGAGTTGG	TH_CAD-seq-2386-fwd
#3551	CTGAAGGTGTGATCCTATCCATGG	TH_CAD-seq-3023-fwd
#3553	CAGCTAGCTGAGAAAACTTTGAG	TH_CAD-seq-4147-fwd
#3555	TGGACAGGATGTACGGAAGTGG	TH_CAD-seq-5415-fwd
#4003	CCAACGAAATCTTCGAGTGTGA	CK_nluc_seq_fwd2
#4004	TCACACTCGAAGATTTTCGTTGG	CK_nluc_seq_rev2

Cloning primers

#3514	GATCCTCGAGAAGACAACATGGCAGAGAACGATG TGGAC	BAT1-fwd
#3515	GATCGCTAGCGAAGACGTTCTACCGTGTCTGTTC AATGTAGG	BAT1-rev
#4143	CTCCGCTACTAGCGGAAAAGAACATTTAATGTCAT ACAATGTTCTGCTCCTCTAGTAGCT	anti-UAP56-miRNA3-fwd
#4144	TCTTAGCTACTAGTGGAGCAGAACATTGTATGACA TTAAATGTTCTTTTCCGCTAGTAGC	anti-UAP56-miRNA3-rev
#4145	CTCCAAGGATATATACTCATCATTTAATGTCATA CAATGATGATGATAGATATCCTTC	anti-NXF1-miRNA3-fwd
#4146	TCTTGAAGGATATCTATCATCATCATTGTATGACAT TAAATGATGAGTATATATATCCTT	anti-NXF1-miRNA3-rev
#4147	CTCCAAGTGCAGAATAACACTAGATTTAATGTCAT ACAATCTAGTAGTATGCTGCACTTC	UAP56-scr-miRNA-fwd
#4148	TCTTGAAGTGCAGCATACTACTAGATTGTATGACA TTAAATCTAGTGTTATTCTGCACTT	UAP56-scr-miRNA-rev
#4149	CTCCACTCTTCACACACAACACTACATTTAATGTCATA CAATGTAGTGTTGTTTGAAGAGTC	CAD-scr-miRNA2-fwd
#4150	TCTTGACTCTTCAAACAACACTACATTGTATGACAT TAAATGTAGTTGTGTGTGAAGAGT	CAD-scr-miRNA2-rev
#4200	GTACCTCATTTATATACAGCTTCGTAAGACG TACGAAGCTGTATATAAATTTTTTGAAA	anti_EBOV_L_shR_fwd

#4201	AGCTTTTCCAAAAAATTTATATACAGCTTCGTACGT CTTCAGTACGAAGCTGTATATAAATGAG	anti_EBOV_L_shR_rev
#4390	TTTTCCAGGAATCCTTTTTGCAAC	1cis_dtrl_rev
#4391	ACTATAGTGAGTCGTATTAACCCG	1cis_dtrl_fwd
#4408	CCTTGGTTTTGAACTTGAACACTTAG	1cis_ldr_fwd
#4409	AAGTTCAAACCAAGGTTAATTCTCAATC	1cis_ldr_rev
#4571	CATGCTCGAGCGTCTCAAATTACACTGCCTGGTG TGTGGC	HDV_rev
#4572	GACCGGTAGAAAAGTATGAGTCCGTGAGGACGA AACGGAGTCTAGACTCCGTCTTTTCCAGGAATCCT TTTTGCAACGTTTATTCTG	RdM_POLII_fwd
#4585	TCCATTATTATCAACTCTTCTGCTCCACCC	NXF1_dsiRNA2_fwd
#4586	GATTCTCCGGTTCTCCCGATCCAAAATC	NXF1_dsiRNA2_rev
#4911	TTGCCTTGGCCCAACTGCTGGTGAACAAAATT CCCAGCCA	UAP56_dsiRNA2_fwd
#4912	TGGCTGGGAAGTTTTGTTGACCAGCAGTTGGGC CAAGGCAA	UAP56_dsiRNA2_rev
#4922	GTCGGAATTCGGTCTCGCATGAACCTCGTCGATC TCCAGAA	NES-RRM_fwd
#4923	TATACTCGAGCGTCTCTAGTCGTGGGGTGGAGCA GAAGAGTTG	RRM_del-TAG_rev
#4924	GCCGGAATTCGGTCTCGCATGTGGTTCAAGATTA CAATTCCTTATGG	RRM_fwd
#4925	GATCACCGGTACCTGCATATCATGGCGGACGAGG GGAAGT	NXF1_fwd
#4926	GGATCCCAGCTGTCCGGAACCGTTCTTTGAGGTC CCATCCTGGC	NXF1-Linker_rev
#4927	GGTTCGGACAGCTGGGATCCACTATACTGAATG AACTGAAGCC	NXF1-Linker_fwd
#4928	TATAGCGGCCGCACCTGCTATATCTACTTCATGAA TGCCACTTCT	NXF1_rev
#4966	CCAGCAGATCTGCATCTCAATTAGT	dBamHI-fwd

#4967	TGCAGCAGATCTAGACATGATAAGATAC	dBamHI-rev
-------	------------------------------	------------

cDNA synthesis primer

#4389	AGTGTGAGCTTCTAAAGCAACC	nLuc-RT
-------	------------------------	---------

#4428	TTTTTTTTTTTTTTTTTTTTTTT	Oligo(dT)
-------	-------------------------	-----------

q-PCR primer

#3610	CGACAACCACTACCTGAGCAC	pCA-GFP-seq-fwd-2331
-------	-----------------------	----------------------

#3707	CTTGTACAGCTCGTCCATGC	Seq-GFP_698-rev
-------	----------------------	-----------------

#4387	TTCAGAATCTCGGGGTGTCC	nLuc_fwd
-------	----------------------	----------

#4388	CGTAACCCCGTCGATTACCA	nLuc_rev
-------	----------------------	----------

2.1.5 Vectors and recombinant plasmids

For this PhD thesis, the following plasmids and vectors were used for molecular cloning and transfection. The accuracy of the plasmids was confirmed by Sanger sequencing. Sanger sequencing was done by the company GATC Biotech and Microsynth SeqLab.

Number	Designation
AB151	pCAGGS-ZsGreen
AB154	pCAGGS-mWasabi
AB155	pCAGGS-tagRFP
pTH4481	pCAGGS-FLAG-HA-iBsmBI
pTH4507	pCAGGS-UAP56
pTH4559	pCAGGS-FLAG-HA-UAP56
pTH4670	pCAGGS-NXF1
pTH4684	pCAGGS-FLAG-HA-NXF1
pTH4743	pCAGGS- miRNA124v11-anti-NXF1.1
pTH4749	pCAGGS- miRNA124v11-anti-BAT1.1
pTH4755	pCAGGS- miRNA124v11-anti-BAT1.2
pTH4860	pCAGGS-miRNA124
pTH4885	pCAGGS-miRNA124v11-anti-CAD.1
pTH4891	pCAGGS-miRNA124v11-anti-NXF1.2

pTH4897	pCAGGS-miRNA124v11-anti-CAD.2
pTH4913	pCAGGS-CAD
pTH5438	pmScarlet-i_C1
pTH5782	pCAGGS-NES
pTH5908	pCAGGS-FLAG-HA-CAD
pTH6023	pCAGGS_FLAG-HA-NXF1-10RA
pTH6024	pCAGGS-FLAG-HA-NXF1- Δ RBD
pTH6025	pCAGGS-FLAG-HA-NXF1- Δ RRM
pTH6026	pCAGGS-FLAG-HA-NXF1- Δ LRR
pTH6028	pCAGGS-FLAG-HA-NXF1- Δ UBA
pTH6029	pCAGGS-flag-HA-CAD- Δ ATC
pTH6060	psiRNA-hH1neo-G2
pTH6087	pT7-4cis-EBOV-vRNA-nluc-dBsmBI-GP.dBsmBI
pTH6141	pCAGGS-mCherry
pTH6211	pCAGGS-flag-HA-CAD- Δ GLN
pTH6216	pCAGGS-NXF1-RRM
pTH6233	pCAGGS-flag-HA-CAD- Δ CPS
pTH6253	pCAGGS-FLAG-HA-NXF1-RBD
pTH6254	pCAGGS-FLAG-HA-NXF1-RRM
pTH6284	pCAGGS-EBOV-VP35-v1.1
pTH6286	pT7-EBOV-1cis-vRNA-nluc
pTH6287	pCAGGS-EBOV-L-v1.1
pTH6288	pCAGGS-EBOV-VP30-v1.1
pTH6289	pCAGGS-EBOV-NP-v1.1
pTH6292	pCAGGS_Luc2
pTH6293	pT7-EBOV-1cis-vRNA-nluc-dtrl1-56
pTH6300	pCAGGS_Tim1-opt-v1.2
pTH6301	pCAGGS-T7-opt
pTH6302	pCAGGS-eGFP
pTH6303	pCAGGS-p15
pTH6343	pCAGGS-FLAG-HA-NXF1- Δ NTF2-structure
pTH6373	pCAGGS-myc-EBOV-VP35
pTH6443	pCAGGS-FLAG-HA-NXF1-NTF2-structure
pTH6459	pCAGGS-EBOV-NP-myc
pTH6463	pCAGGS-EBOV-NP-dC-tail
pTH6584	pCAGGS-FLAG-HA-NXF1-UBA-structure
pTH6594	pCAGGS_NXF1-LRR_structure-flag-HA

pTH6637	pCAGGS-flag-HA-UAP56-Ic_RNA
pTH6680	pCAGGS-EBOV-NP-K160A.K171A.R174A
pTH6718	pCAGGS-UAP56-D199A
pTH6758	pCAGGS-UAP56-E197A
pTH6807	pCAGGS-v1.0

2.1.6 Enzymes

Enzyme	Company
<i>General enzymes</i>	
I-Proof high fidelity Polymerase	BioRad
KAPA HiFi Hot Start DNA-Polymerase	Roche
RevertAid Reverse Transcriptase (200 U/μL)	Thermo Scientific
rSap Phosphatase	NEB
T4 DNA Ligase	Invitrogen
T4 Polynucleotide	NEB
Turbo DNase	Thermo Scientific

Restriction endonucleases

Agel	NEB
BbsI	Thermo Scientific
BsmBI (Esp3I)	Thermo Scientific
ClaI	NEB
DpnI	NEB
EcoRI	NEB
EcoRV	NEB
NotI	NEB
RsrII	NEB
XhoI	NEB

2.1.7 Antibodies

Antibody	Company	Order number
Anti-mCherry	GeneTex (Biozol)	GT857
Monoclonal Anti-CAD	Abcam	ab40800
Monoclonal Anti-NPC	BioLegend	902907
Monoclonal Anti-NXF1	Abcam	ab50609
Monoclonal Anti-UAP56	Abcam	ab181061

Polyclonal Alexa Fluor 488 anti-mouse	Thermo-Fisher	A-11029
Polyclonal Alexa Fluor 488 anti-rabbit	Abcam	ab150077
Polyclonal Alexa Fluor 568 anti-mouse	Thermo Fisher	A-11031
Polyclonal Alexa Fluor 568 anti-rabbit	Thermo Fisher	A-11036
Polyclonal Alexa Fluor 647 anti-chicken	Thermo Fisher	A-21449
Polyclonal Anti-c-myc	Thermo Fisher	A-21281
Polyclonal Anti-flag	Sigma-Aldrich	F7425
Polyclonal ANTI-FLAG® M2	Sigma-Aldrich	F1804-200 ug
Polyclonal Anti-Mouse IgG (IRDye® 680RD)	Li-cor	926-68070
Polyclonal Anti-Mouse IgG (IRDye® 800CW)	Li-cor	926-32210
Polyclonal Anti-NP (EBOV)	Gentaur	0301-012
Polyclonal Anti-Rabbit IgG (IRDye® 680RD)	Li-cor	926-68071
Polyclonal Anti-Rabbit IgG (IRDye® 800CW)	Li-cor	926-32211
Polyclonal GAPDH Antibody (0411)	Santa Cruz	sc47724

2.1.8 siRNAs

siRNA	Company	Order number
Anti-Bat1	Thermo-Fisher	s15474
Anti-CAD#1	Thermo-Fisher	s2320
Anti-CAD#2	Thermo-Fisher	117891
Anti-EBOV-L ¹	Eurofins genomics	-
Anti-NXF1#1	Thermo-Fisher	s20532
Anti-NXF1#2	Thermo-Fisher	s20533
Silencer™ Select Negative Control No. 2 siRNA	Thermo-Fisher	-

2.1.9 Kits

Kit	Company
Mix & Go <i>E. coli</i> Transformation Kit & Buffer Set	Zymo Research
NucleoBond Xtra Midi Plus	Macherey-Nagel
NucleoSpin Gel and PCR clean-up	Macherey-Nagel
NucleoSpin Plasmid EasyPure	Macherey-Nagel
NucleoSpin RNA kit	Macherey-Nagel
TURBO DNA-free Kit	Thermo Scientific

¹ Sequence: UUUUAUACAGCUUCGUActt

2.1.10 Cell lines and bacteria

Cell line	Description	Origin
Escherichia Coli K12 XL1-blue	Competent E.coli cells for transformation	
A549	Adenocarcinomic human alveolar basal epithelial cells	Cell line collection Friedrich-Loeffler-Institut
HEK 293	Human embryonic kidney cells	Cell line collection Friedrich-Loeffler-Institut
HEK 293T	Human embryonic kidney cells, which express a SV40 large T antigen	Cell line collection Friedrich-Loeffler-Institut
Huh 7	Human liver, epithelial-like, carcinoma cells	Cell line collection Friedrich-Loeffler-Institut

2.1.11 Viruses

Recombinant virus	Strain	GeneBank number
Zaire ebolavirus rec/COD/1976/Mayinga-rgEBOV	EBOV Mayinga	KF827427.1

2.1.12 Bacterial and cell culture media

Media	Composition
LB (lysogeny broth)-Miller agar + 0.1 % Ampicillin	15 g agar 1 ml Ampicillin ad 1 l LB-Miller medium 20-25 ml of LB agar per 10 cm petri dish
LB-Miller media + 0.1 % Ampicillin	10 g Trypton 5 g Yeast Extract 10 g NaCl, pH 7.5 1 ml Ampicillin stock solution ad 1 l dH ₂ O
ZB10 media	ZB10 medium:
+ 1 % Penicillin/Streptomycin	9.9 g/l DEMEM (Dulbecco's Modified Eagle Medium)
+ 1 % GlutaMAX	4.5 g/l Glucose
+ 10 % FCS	3.7 g/l NaHCO ₃

	0.12 g/l Natriumpyruvate
	5 ml Penicillin/Streptomycin
	5 ml GlutaMax
	add FCS for a final volume of 10 %
ZB10 media	ZB10 medium:
+ 1 % Penicillin/Streptomycin	9.9 g/l DEMEM (Dulbecco's Modified Eagle Medium)
+ 1 % GlutaMAX	4.5 g/l Glucose
+ 5 % FCS	3.7 g/l NaHCO ₃
	0.12 g/l Natriumpyruvate
	5 ml Penicillin/Streptomycin
	5 ml GlutaMax
	add FCS for a final volume of 5 %
ZB10 media	ZB10 medium:
+ 1 % GlutaMAX	9.9 g/l DEMEM (Dulbecco's Modified Eagle Medium)
+ 5 % FCS	4.5 g/l Glucose
	3.7 g/l NaHCO ₃
	0.12 g/l Natriumpyruvate
	5 ml GlutaMax
	add FCS for a final volume of 5 %
Alsever's Trypsin Versene Solution (ATV)	8 g NaCl
	0.4 g KCl
	1 g Dextrose
	0.58 g NaHCO ₃
	0.5 g Trypsine
	0.2 g EDTA
	ad 1l dH ₂ O

2.1.13 Computer software

Software	Company
Adobe Acrobat Reader	Adobe Systems
AriaMx	Agilent
BioRender	bioRender
Clone Manager	Sci-Ed Software

EndNote	Clarivate Analytics
Geneious	Biomatters Limited
GloMax Discover	Promega
Image Studios	LI-COR
ImageJ	NIH
InkScape 1.1.0	InkScape Community
MEGA X	MEGA
Microsoft Offices	Microsoft Corporation
Prism 8.1.0	GraphPad
siRNA wizard	InvivoGen

2.2 Methods

2.2.1 Molecular biology methods

2.2.1.1 Polymerase chain reaction (PCR)

The polymerase chain reaction (PCR), which was developed in 1983, is one of the most common methods used in molecular biology and allows the in vitro amplification of a particular DNA sequence (Mullis 1990). In addition to a template DNA, two specific primers, nucleotides and a thermostable DNA polymerase are required for PCR amplification. During a PCR run the DNA polymerase synthesizes a new strand of DNA that is complementary to the existing template strand. To this end three different repeating steps are necessary, starting with a denaturation step with high temperature (95 - 98 °C) that leads to a denaturation of the template DNA into separated DNA strands. This is followed by annealing of the primers to the complementary target region on the template DNA. The annealing temperature is typically 5 °C below the melting temperature of the used primers and depends on the GC content of the primers as well as on the number of nucleotides. In a last step (elongation) the polymerase binds to the annealed primers and extends them at the 3'OH end, which results in a double stranded DNA fragment that is identical to the template DNA. The temperature during elongation is adjusted to the optimal reaction temperature of the polymerase in order to guarantee best possible results. Under ideal conditions, for each PCR cycle the quantity of the DNA doubles.

Touchdown PCR:

To reduce background and unspecific binding of primers a touchdown PCR was performed. In contrast to a classical PCR protocol the initial annealing temperature is 5 °C above the melting temperature of the used primers and decreases with every cycle 0.5 °C to a lower, more permissive annealing temperature until the optimal annealing temperature of the primers is reached (Don, Cox et al. 1991, Korbie and Mattick 2008).

setup:	1 µl	template DNA (20 ng)
	10 µl	5x HF buffer
	1 µl	dNTPs (10 mM each)
	2.5 µl	forward primer (10 µM)

2.5 µl	reverse primer (10 µM)
1.5 µl	DMSO
0.5 µl	MgCl ₂
0.5 µl	IProof high fidelity polymerase
30.5 µl	dH ₂ O

Cycle conditions:

1x	denaturation	98°C	60 seconds
	/	denaturation	98°C
			10 seconds
10 x	annealing	T _m + 5 °C – 0.5 °C per cycle	20 seconds
	\	elongation	72°C
			20 seconds per KB
	/	denaturation	98°C
			10 seconds
30 x	annealing	T _m	20 seconds
	\	elongation	72°C
			20 seconds per KB
1x	elongation	72°C	3 minutes
1x	store at	4 °C	∞

Kappa polymerase:

In order to avoid issues with possible secondary structures and for more complex templates, a KAPA HiFi Hot Start DNA-Polymerase was used.

setup:	1 µl	template DNA (50 ng)
	2.5 µl	forward primer (10 µM)
	2.5 µl	reverse primer (10 µM)
	25 µl	KAPA HotStart ready Mix (2x)
	19 µl	dH ₂ O

Cycle conditions:

1x	denaturation	95°C	3 minutes
	/	denaturation	98°C
			20 seconds
35 x	annealing	65°C	15 seconds
	\	elongation	72°C
			30 seconds per KB
1x	elongation	72°C	3 minutes
1x	store at	4 °C	∞

2.2.1.2 Preparative restriction digest

To modify DNA for further use, the DNA fragments were digested by restriction endonucleases (Danna and Nathans 1999). These endonucleases are bacterial enzymes that cleave double stranded DNA at specific recognition sites, which are 4 - 8 base pairs in length, and often generate single-stranded DNA overhangs. Therefore, they are used in molecular biology as a common tool prior to ligation of DNA fragments (see chapter 2.2.1.8) and for subcloning of DNA fragments from vectors (see chapter 2.2.1.11). Restriction enzymes are classified into several types and subtypes with different properties (Smith 1993). While type II restriction endonucleases recognize palindromic sequences and cleave the DNA within these motifs, type IIS restriction enzymes have asymmetric recognition sites and cleave the DNA at a defined distance outside of their recognition motif, usually within 1 - 20 nucleotides.

In this project enzymes from New England Biolabs (NEB) and Thermo Fisher (enzyme: BsmBI/Esp3I) were used for preparative restriction digest.

setup:	NEB digest	BsmBI/Esp31 digest
	3 µg DNA	3 µg DNA
	5 µl 10x restriction buffer	2 µl 10x Tango buffer
		1 µl DTT
	1 µl restriction enzyme(s)	1 µl BsmBI/Esp31
	ad 50 µl dH ₂ O	ad 20 µl dH ₂ O

All samples were incubated for 16 hours at 37 °C and stored afterwards at 4 °C until further use.

2.2.1.3 Analytical restriction digest

Analytical restriction digest was performed to control whether the desired insert is present in the cloned construct. In order to confirm the right size of the digestion products, the obtained fragments were analyzed via agarose gel electrophoresis (see chapter 2.2.1.4.) Enzymes from NEB and Thermo Fisher were used for analytical digestion.

setup:	NEB digest		BsmBI/Esp31 digest	
	200 ng	DNA	200 ng	DNA
	1 µl	10x restriction buffer	1 µl	10x Tango buffer
			1 µl	DTT
	0.5 µl	restriction enzyme(s)	0.5 µl	BsmBI/Esp31
	ad 10 µl	dH ₂ O	ad 10 µl	dH ₂ O

All samples were incubated for 30 minutes at 37 °C and the products were afterwards analyzed via agarose gel electrophoresis (see chapter 2.2.1.4).

2.2.1.4 Agarose gel electrophoresis

Agarose gel electrophoresis is a standard method used in molecular biology to separate and visualize DNA fragments. Due to the negative charged phosphate backbone, nucleic acid molecules are able to migrate through an agarose matrix within an electric field. However, the degree of separation depends strongly on the pore size of the agarose gel, which is influenced by the agarose concentration. The migration velocity of nucleic acids through the agarose pores is inversely proportional to their length, so that larger DNA fragments move slower than shorter fragments.

For agarose gel electrophoresis the agarose was first dissolved in 1x Tris acetate EDTA (TAE) buffer by heating and subsequently poured into a casting tray. Next a comb was inserted in the hot agarose solution to generate wells for sample loading. After the gel has hardened, samples were mixed with 6x gel loading dye (final concentration 1x) (NEB) to increase the density of the sample, and loaded (10 - 20 µl) onto the 0.8 % agarose gel. Electrophoresis was performed at a constant voltage of 100 V for 50 minutes. A standardized marker (1 kb 2 log DNA Ladder) was used to determine the size of the DNA fragments.

Analytic agarose gel electrophoresis:

To determine the size of DNA fragments analytic agarose gel electrophoresis was performed. Agarose gel was prepared, and electrophoresis was carried out, as described above. After electrophoresis the gel was incubated for at least 20 minutes in an ethidium bromide solution. Ethidium bromide intercalates with the nucleobases of the DNA and leads to orange fluorescence under UV radiation. Subsequently, the DNA was visualized under UV light and the bands were documented.

Preparative agarose gel electrophoresis:

To isolate and purify specific DNA fragments, preparative agarose gel electrophoresis was performed. An agarose gel was prepared and electrophoresis was carried out, as described above. After electrophoresis the gel was incubated for 3 minutes under gentle rocking in 100x fast blast solution, which binds to the negatively charged phosphate groups of the DNA. The gel was subsequently washed with warm water until the DNA bands were clearly visible and the DNA fragment of the desired size was excised from the gel with a scalpel and transferred into a 2 ml reaction tube. DNA was purified using the NucleoSpin Gel and PCR clean-up Kit from Macherey Nagel (see chapter 2.2.1.5).

2.2.1.5 Purification of DNA from agarose gel

For purification of DNA fragments from preparative agarose gels the NucleoSpin Gel and PCR clean-up Kit from Macherey Nagel was used accordingly to the manufacturer's instructions. For each 100 mg of gel containing the desired DNA fragment 200 µl NTI buffer was added. The mixture was then incubated at 55 °C for 10 minutes on a thermo shaker, loaded onto a DNA binding column, which contains a silica gel membrane that binds DNA in the presence of chaotropic salts, and washed with ethanolic NT3 buffer to remove agarose, salt and contaminations. Finally, DNA was eluted under low salt conditions with 30 µl elution buffer NE.

2.2.1.6 Purification of PCR products

After restriction digest DNA was purified using the NucleoSpin Gel and PCR clean-up Kit from Macherey Nagel according to the manufacturer's instructions. The sample was mixed with 2x its volume of NTI buffer, loaded onto a DNA binding column, and washed with NT3 buffer. Finally, DNA was eluted under low salt conditions with 30 µl elution buffer NE (see chapter 2.2.1.5).

2.2.1.7 Dephosphorylation

Restriction digestion of the vector with one (or more) endonucleases results in compatible 5' and 3' ends, which are able to be joined during ligation (see chapter 2.2.1.8). To minimize religation, shrimp alkaline phosphatase (rSAP) was used, which removes the free 5' phosphate groups from DNA by hydrolytic cleavage. 2 µl of rSAP was added directly to the unpurified digest product and incubated for one to six hours

at 37 °C. No additional buffer was added, because alkaline phosphatase is active in many restriction buffers. However, if purified DNA was dephosphorylated, a suitable amount of 10x restriction buffer Cut Smart was additionally added to the sample. After dephosphorylation the sample was purified by PCR purification (see chapter 2.2.1.6).

2.2.1.8 Ligation

Ligation was performed to insert a foreign DNA fragment into a digested vector. Therefore, the DNA samples were incubated with the *E. coli* bacteriophage T4 DNA ligase, which catalyzes the formation of a phosphodiester bond between the 3' hydroxyl group of one nucleotide and the 5' phosphate group of another nucleotide in the presence of ATP (Weiss and Richardson 1967). A phosphorylation of the 5' ends of at least one DNA fragment is, therefore, required to enable the enzyme-catalyzed linking of the DNA segments. To minimize religation an excess of insert was used for ligation. For this, dephosphorylated vector and insert were mixed at a molar ratio of 1:4. To determine the amount of religated vector a religation control was additionally performed for every ligation, in which the insert was exchanged against dH₂O.

setup: 9 µl insert
 2 µl vector
 3 µl 5x T4 ligase buffer
 1 µl T4 DNA ligase

The samples were incubated at 14 °C for 16 hours, and then stored at 4 °C until transformation (see chapter 2.2.1.14).

2.2.1.9 Phosphorylation of oligonucleotides

To produce oligonucleotides with phosphorylated ends, which can afterwards be hybridized and ligated into digested vectors, a phosphorylation step was performed by using the T4 polynucleotide kinase. Each oligonucleotide was phosphorylated separately.

setup: 1 µl oligonucleotide (100 µM)
 2 µl 10x T4 ligase buffer
 1 µl T4 polynucleotide kinase

16 μ l dH₂O

The samples were incubated for one hour at 37 °C, and then hybridized (see chapter 2.2.1.10).

2.2.1.10 Hybridization of oligonucleotides

Hybridization was used to generate short double stranded DNA out of two complementary single stranded phosphorylated oligonucleotides. The hybridization process is based on the property of double stranded DNA to separate into single strands under high temperature. By lowering the temperature the complementary single stranded oligonucleotides are able to hybridize with each other and form double stranded DNA.

setup: 1 μ l phosphorylated oligonucleotide 1
 1 μ l phosphorylated oligonucleotide 2
 18 μ l dH₂O

Cycle conditions:

1 x	99°C	5 minutes
73 x	98°C -1 °C per cycle	1 minute
1 x	4 °C	∞

The samples were stored at 4 °C until ligation. Ligation was performed without further purification of the hybridized oligonucleotides (insert) and as described in chapter 2.2.1.8.

2.2.1.11 Preparation of chemically competent bacteria

Chemically competent *E. coli* (strain XL1-Blue) for efficient DNA transformation were prepared using the *E. coli* Transformation Buffer Set from Zymo Research. To this end, 100 μ l of *E. coli* XL1-Blue suspension was transferred into 5 ml LB medium (without antibiotics) and incubated overnight at 37 °C under constant shaking. After incubation, 1 ml of the *E. coli* culture was added into 100 ml SOC medium and cultivated at 27 °C in a shaker until an OD₆₀₀ (optical density) between 0.4 and 0.6 was achieved. The cells were then placed on ice for 10 minutes and pelleted by centrifugation at 2500x g for 10 minutes at 4 °C. After removing of the supernatant, the cell pellet was gently

resuspended in 5 ml ice cold 1x wash buffer and, under the same conditions as before, centrifuged. The obtained pellet was then gently resuspended in 5 ml ice cold 1x competent buffer and the cell suspension was aliquoted in 100 µl aliquots into Eppendorf tubes. Immediately afterwards, the competent bacteria were frozen in liquid nitrogen and stored at -80 °C until further use. 1x wash buffer and 1x competent buffer were prepared according to the manufacturer's instructions.

2.2.1.12 Transformation of chemically competent bacteria

Transformation describes the internalization of exogenous DNA through competent bacterial cells and was first discovered in 1928 (Griffith 1928). For transformation, competent *E. coli* cells were first thawed on ice and 50 µl *E. coli* suspension was then gently mixed with 10 µl of the ligation product, without up and down pipetting due to the labile condition of the cells. Subsequently the mix was incubated for 1 hour on ice and plated on LB agar plates containing the appropriate antibiotic (Ampicillin 0.1 %) for selection. Incubation was done overnight at 37 °C.

2.2.1.13 Preparation of plasmid DNA from bacterial cultures

Isolation of plasmid DNA from transformed *E. coli* was done using the NucleoSpin Plasmid EasyPure Kit for small cultures, or the NucleoBond Xtra Midi Plus Kit (Macherey-Nagel) for large scale preparations. For mini preparations 5 ml of LB medium with appropriate antibiotics (Ampicillin) was inoculated with a colony of the transformed bacteria and incubated overnight at 37 °C shaking at 220 RPM. In contrast, for midi preparation 100 ml of LB medium with appropriate antibiotics was inoculated with 1 ml of the mini preparation culture and incubated overnight at 37 °C under constant shaking. Extraction of plasmid DNA was performed according to the manufacturer's instructions. To this end, 1.5 ml (mini) or 100 ml (midi) overnight culture was pelleted by centrifugation and resuspended in an RNase containing buffer. Subsequently plasmid DNA was isolated from the bacteria cells by adding a lysis buffer containing SDS and NaOH. To precipitate the denatured genomic DNA a neutralization buffer containing potassium acetate and glacial acetic acid was added afterwards. In contrast to the genomic DNA, the plasmid DNA renatures because of its characteristics during the neutralization step and can, therefore, be separated from the cell compartments. This method is based on the NaOH/SDS lysis method of Birnboim and Doly (Birnboim and Doly 1979). To clear the lysate from precipitated genomic

DNA, SDS and cell debris a centrifugation (mini) or filtration (midi) step was performed. The plasmid DNA was purified using spin columns (mini) or gravity flow columns (midi), both containing a silica gel membrane. After loading of the supernatant and binding of the DNA under high salt conditions, the DNA was washed and eluted with 50 μ l of a low salt elution buffer (mini) or with 5 ml of a high salt elution buffer (midi). The eluate of the midiprep was then desalted using isopropanol precipitation and DNA was pelleted by centrifugation at 3200 g for 45 minutes. After washing with ethanol (70 %), the DNA pellet was dried and resuspended with 400 μ l dH₂O.

2.2.1.14 Determination of DNA concentration

To determine the concentration of the eluted plasmid DNA, the optical density (OD) was measured at 260 nm and calculated using a NanoPhotometer. Furthermore, the degree of purity was determined by the ratio of maximal absorbance of DNA and proteins. In contrast to DNA, proteins have a maximal absorbance at 280 nm, which is influenced by the aromatic amino acids tryptophan, tyrosine and phenylalanine. Therefore, pure DNA shows a ratio of the two absorbance maxima E₂₆₀/E₂₈₀ between 1.8 and 2.0.

2.2.1.15 Sequencing

Sequencing was performed to confirm the exact order of nucleotides and absence of unwelcome mutations within the produced DNA constructs. Therefore, the constructs were sent to GATC Biotech or SeqLab where sequencing was accomplished. GATC Biotech and SeqLab offer sequencing based on the Sanger method (Sanger and Coulson 1975).

setup GATC: 5 μ l DNA (90 ng/ μ l)
 5 μ l forward or reverse Primer (5 μ M)

setup SeqLab: 12 μ l DNA (90 ng/ μ l)
 3 μ l forward or reverse Primer (10 μ M)

2.2.1.16 Subcloning

Subcloning is used to move a DNA fragment (insert) from an original vector to a destination vector in order to further study the functionality of the moved fragment. To this end the source plasmid was first digested with endonucleases that were flanking the desired DNA fragment (see chapter 2.2.1.2). The DNA fragment was then isolated by agarose gel electrophoresis and purified using the NucleoSpin Gel and PCR clean-up Kit (see chapter 2.2.1.4 and 2.2.1.5). Before ligation was accomplished, the target vector was digested with, if possible, the same restriction enzymes that were used for the digestion of the insert, or with endonucleases that have different recognition sites, but produce compatible overhangs. The digested vector was dephosphorylated and purified by PCR or gel purification (see chapter 2.2.1.7 and 2.2.1.6 or 2.2.1.5). After ligation of the insert with the destination vector the sample was transformed into competent *E. coli* bacteria and plated onto agarose plates (see chapter 2.2.1.8 and 2.2.1.12). All plates were incubated overnight and colonies were picked and incubated in a miniprep culture. After overnight incubation the cells were harvested and the vector DNA was purified and analyzed by analytical restriction digest (see chapter 2.2.1.13 and 2.2.1.3). A positive clone was transferred from the miniprep culture to a midiprep culture and incubated overnight. DNA was then isolated, sequenced and stored at -20 °C until further use (see chapter 2.2.1.13 and 2.2.1.15).

2.2.1.17 Cloning of PCR fragments

Cloning of foreign DNA fragments allows the introduction of additional sequences (e.g. restriction or recognition sites) into target vectors or sequences. Therefore, the DNA fragments were first amplified by touchdown or Kappa PCR and afterwards either directly purified via PCR purification/gel extraction or, in case of DNA amplification from a vector, treated with 2 µl DpnI to eliminate methylated plasmid residues (see chapter 2.2.1.1; 2.2.1.5 and 2.2.1.6). To generate DNA overhangs the fragments were digested with endonucleases and subsequently PCR purified (see chapter 2.2.1.2 and 2.2.1.5). Digestion of the destination vector, ligation, transformation, mini- and maxiprep was performed as described in chapter 2.2.1.16.

2.2.1.18 RNA extraction

For extraction of RNA from mammalian cells the NucleoSpin RNA kit from Macherey-Nagel was used following the manufacturer's instructions. To this end, cells were lysed

by incubation in 350 μ l of lysis buffer containing 2-Mercaptoethanol. This lysis buffer contains large amount of chaotropic ions, which inactivates RNases. In order to reduce viscosity and to get rid of cell debris, the sample was transferred to a filter column and centrifuged. The supernatant was then mixed with 70 % Ethanol and loaded onto a silica membrane, which leads to the binding of RNA and DNA to the membrane. After desalting and drying of the membrane, contaminating DNA was removed by incubation with a DNase solution. To clear the sample from salts, metabolites and macromolecular cellular components, the membrane was washed several times after DNase digestion. Pure RNA was finally eluted under low ionic conditions with RNase free dH₂O.

2.2.1.19 DNase digestion

Since the efficiency of the DNase digestion during RNA extraction was not sufficiently high, an additional DNase digestion was performed after RNA purification using the TURBO DNA-free kit from Thermo Fisher.

setup: 50 μ l RNA eluate
 5 μ l 10x Turbo DNase buffer
 1 μ l Turbo DNase

The samples were incubated for 30 min at 37 °C and subsequently mixed with 5 μ l of 10x DNase inactivation buffer. During a 5 minute incubation step at room temperature the tubes were flicked several times in order to mix all components. Finally, the samples were centrifuged at 10.000x g for 1.5 minutes and the supernatant was transferred in a new RNase free reaction tube. The samples were then stored at -80 °C until reverse transcription.

2.2.1.20 Reverse transcription

For cDNA synthesis, DNA free RNA samples were incubated with an oligo(dT)-primer for mRNA quantification or with a strand-specific primer for vRNA quantification using the RevertAid Reverse Transcriptase following the manufacturer's instructions. For this a first annealing step was performed.

setup: 10 μ l RNase free dH₂O
 1 μ l template RNA

2 μ l Primer (10 μ M)

After an incubation of 5 minutes at 65 °C the samples were subsequently placed on ice for 1 minute. Following this, all additional components required for cDNA synthesis were added successively to the reaction mixture.

setup: 13 μ l reaction mixture (from above)
 4 μ l 5x reaction buffer
 2 μ l dNTPs (10 mM)
 1 μ l RevertAid Reverse Transcriptase

The samples were incubated for 60 min at 42 °C and the enzyme was inactivated by a following incubation at 70 °C for 10 minutes. All samples were either stored at -80 °C or on ice until qPCR.

2.2.1.21 qPCR

To quantify vRNA and mRNA amounts, qPCR was performed using the PowerUp SYBR Green Master Mix with primers targeting either the reporter gene or GFP as a control. Values for vRNA and mRNA levels were normalized to control GFP mRNA levels. qPCR was evaluated by using the AriaMx software.

setup: 3 μ l dH₂O
 1 μ l cDNA
 0.5 μ l forward primer (10 μ M)
 0.5 μ l reverse primer (10 μ M)
 5 μ l PowerUp SYBR Green Master Mix

Cycle conditions:

1x	UDG ² activation	50°C	2 minutes
1x	Dual-Lock DNA poly.	95°C	2 minutes
/	denaturation	95°C	15 seconds
40 x	annealing	54°C	15 seconds

² Uracil-DNA glycosylases (UDG)

\	elongation	72°C	1 minute
1x	melt curve stage	95°C	15 seconds
1x	melt curve stage	60°C	1 minute
1x	melt curve stage	99°C	15 seconds

2.2.2 Tissue culture methods, cell harvest, lysis and trVLP purification

2.2.2.1 Cultivation of mammalian cells

Mammalian cells were maintained and cultured in a T75 flask with 15 ml medium at 37 °C and at an atmosphere of 5 % CO₂. For cultivation of cells the provided ZB 10 medium was supplemented with 10 % fetal calf serum (FCS), 1 % GlutaMax and 1 % Penicillin/Streptomycin (Pen/Strep). Cells were passaged when they reached a confluent state of about 90 %. For this, the culture medium was removed and the cells were washed once with 2 ml ATV and then incubated in 2 ml ATV until the cells were detached from the culture vessel (incubation time depends on the cell line). ATV contains the serine protease trypsin, which catalyze the hydrolytic degradation of adhesion proteins and leads to detachment of the cells. The enzymatic reaction was stopped and the cells were washed off by the addition of 8 ml medium. After resuspension of the cells an appropriate amount was transferred into a new flask. HUH 7 and A549 cells were usually split 1:10 to 1:15, and HEK 293T/HEK293 cells 1:20 to 1:30 every 3 to 4 days.

2.2.2.2 Classical transfection of mammalian cells

Transfection was performed to introduce plasmid DNA into eukaryotic cells and to analyze the expression of foreign proteins in specific cell lines.

Transfection with TransIT-LT1

For transfection of minigenome components and host cell factors, the transfection reagent TransIT-LT1 from Mirus, which contains polyamines and cationic lipids that transports DNA efficiently into cells in the presence of serum, was used. Usually HEK 293T cells (or A549, HEK 293 or Huh7 cells in case of miRNA/shRNA transfection) were seeded at 12 well plates at a ratio of 1:8 and transfection was performed when the cells reached a confluency of around 50 %. Appropriate amounts of plasmid DNA were transferred in a 1.5 ml Eppendorf tube outside of a biosafety

cabinet (BSC). 55 µl Optimem per well was added to the vector DNA and the mix was vortexed and spun down. The sample was then mixed with an appropriate amount of TransIT-LT1 and briefly vortexed. After an incubation of 15 minutes 55 µl medium, supplemented with 5 % FCS, 1 % GlutaMax and 1 % Pen/Strep was added and the sample was mixed by up and down pipetting. The mixture was afterwards given dropwise onto the cells and the 12 well plates were rocked back and forth and side by side to ensure a uniform distribution. After an incubation of 24 hours at 37 °C and 5 % CO₂ the medium was exchanged against 1 ml fresh medium supplemented with 5 % FCS, 1 % GlutaMax and 1 % Pen/Strep. Cells were harvested two days post transfection.

Transfection with PEI

For transfection of Huh7 cells the transfection reagent Polyethylenimine (PEI), was used. Huh7 cells were seeded at 12 well plates in a dilution of 1:15 (in order to separate the cells) and transfection was performed when the cells reached a confluency of around 20 %. 500 ng of plasmid DNA was transferred into a 1.5 ml Eppendorf tube outside of a BSC. 200 µl OptiMem per well was added to the plasmid DNA and the sample was mixed with an appropriate amount of PEI (usually in a ratio 1 µg DNA: 1 µl PEI). After vortexing, the sample was incubated for 15 minutes at room temperature. During this, the cell media was exchanged against 1 ml per well fresh medium supplemented with 5 % FCS, 1 % GlutaMax and 1 % Pen/Strep. After incubation the mixture was given dropwise onto the cells and the 12 well plates were rocked back and forth and side by side to ensure a uniform distribution. The transfected cells were used for immunofluorescence analysis after an incubation period of 48 hours by 37 °C and 5 % CO₂ (see section 2.2.3.3).

2.2.2.3 Reverse transfection of mammalian cell lines

Reverse Transfection of siRNAs

For siRNA knockdown of endogenous host factors, HEK 293T cells were reverse transfected with 12 pmol pre-designed silencer select siRNAs or a self-designed anti-EBOV-L siRNA. To this end 1.2 µl of siRNA were transferred in one well of a 12 well plate and mixed with 200 µl Optimem. Subsequently 2 µl Lipofectamine RNAiMax (Thermo Fisher Scientific) transfection reagent was added and the sample was mixed by pipetting up and down. After an incubation period of 15 minutes at room temperature, 1 ml HEK 293T cells were seeded at a ratio of 1:17 and mixed with the

transfection mixture, which was already present in the well. Then, the 12 well plates were rocked back and forth and side by side to ensure a uniform distribution. Since antibiotics are known to interfere with the transfection agent Lipofectamine RNAiMax, the cells were diluted with fresh media containing 5 % FCS and 1 % GlutaMax only. 48 hours after siRNA transfection, the cells were transfected with all components required for a minigenome system, as well as plasmids containing modified host factors (complementation assay) (section 2.2.2.4). In order to measure siRNA knockdown efficiency, cells were incubated for five days without media change and harvested as described in section 2.2.2.6.

2.2.2.4 Minigenome system

In order to investigate the influence of host factors on the EBOV lifecycle, a minigenome and replication deficient minigenome assays, which reflect either total viral RNA synthesis or protein expression, was performed. To analyze the effect of host factor overexpression on EBOV RNA synthesis or protein expression HEK cells were seeded in a dilution of 1:8 on 12 well plates. In contrast, for investigation of the influence of knockdown of endogenous host factors, cells were first reverse transfected with siRNAs (see section 2.2.2.3). In either case, after reaching a confluency of around 50 % (for overexpression experiment after one day, for knockdown experiment after two days) the cells were transfected with all components required for a minigenome system, including pCAGGS-based expression plasmids for NP (62.5 ng), VP35 (62.5 ng), VP30 (37.5 ng), L (500 ng), codon-optimized T7-polymerase (125 ng), firefly luciferase (as a transfection control, 125 ng), and a T7-driven monocistronic minigenome (pT7-EBOV-1cis-vRNA-nLuc; 125 ng) or Pol-II-driven replication-deficient minigenome (pCAGGS-EBOV-1cis-vRNA-nLuc-RdM; 125 ng). In case of host factor overexpression and for complementation experiments plasmids coding for the host factors in question were additionally added. For analyses of vRNA and mRNA levels the control firefly luciferase was replaced with GFP (200 ng). Transfections were performed using Transit LT1 as described in 2.2.2.2. All samples were harvested 48 h post-transfection for either determination of reporter activity (see section 2.2.2.9) or RNA isolation (see section 2.2.1.18).

2.2.2.5 trVLP assay

To perform a trVLP assay, first a plasmid encoding a tetracistronic minigenome and necessary support plasmids were transfected into mammalian cells as described above (2.2.2.4). After transfection of all minigenome components and 48 h incubation, supernatant containing trVLPs was harvested and purified via a sucrose cushion (see section 2.2.2.10). Next p1 cells were seeded at 12 well plates at a ratio of 1:8. In course of host factor knockdown, p1 cells were first reverse transfected with siRNAs as described in section 2.2.2.3 and subsequently seeded at 12 well plates at a ratio of 1:17. Once cells reached a confluency of around 50 %, they were transfected with pCAGGS-based expression plasmids for NP (62.5 ng), VP35 (62.5 ng), VP30 (37.5 ng), L (500 ng), firefly luciferase (as a transfection control, 125 ng), the adhesion factor Tim1 (125 ng) and, in case of overexpression experiments, plasmids encoding for the host factors. For analyses of vRNA levels the control firefly luciferase was replaced with GFP (200 ng). Transfection was performed using Transit LT1 as described in 2.2.2.2. 6 h (in course of host factor knockdown) or 24 h post transfection cells were infected with purified trVLPs. To this end, the media was first removed from the cells and 1 ml trVLP suspension was added per well. After centrifugation of the plate with 1000 g for 10 minutes the cells were incubated for 1 hour by 37 °C and 5 % CO₂. Subsequently the medium was exchanged against 1 ml fresh medium supplemented with 5 % FCS, 1 % GlutaMax and 1 % Pen/Strep. All samples were harvested 48 h post-infection for either determination of reporter activity (see section 2.2.2.9) or RNA isolation (see section 2.2.1.18).

2.2.2.6 Infection with recombinant EBOV

To investigate the localization of host factors during EBOV infection, Huh7 cells were seeded in 8-well chambered slides (Ibidi) in a dilution of 1:15 and transfected as described in section 2.2.2.2. At 48 h post-transfection, the transfected cells were infected with EBOV at a MOI of 1, and the samples were fixed 16 h post-infection in 10 % formalin twice overnight prior to removal from the BSL4 facility and immunofluorescence analysis (section 2.2.3.3). For infection, Zaire ebolavirus rec/COD/1976/Mayinga-rgEBOV (GenBank accession number KF827427.1), which is identical in sequence to the EBOV Mayinga isolate with the exception of four silent mutations as genetic markers (Shabman, Hoenen et al. 2013) was used. rgEBOV was propagated in VeroE6 cells and virus titers were determined by 50 % tissue culture

infectious dose (TCID₅₀) assay. All work with infectious virus was performed by Dr. Thomas Hoenen or Dr. Bianca Bodmer under BSL-4 conditions at the Friedrich-Loeffler-Institut (Federal Research Institute of Animal Health) following approved standard operating procedures.

2.2.2.7 Cell harvest

For cell harvest supernatant was removed and cells were detached by washing with 1 ml PBS (1x) and transferred into a 1.5 ml Eppendorf tube. After centrifugation at 800 g for 5 minutes, the supernatant was discarded and the pellet was resuspended in 75 µl PBS (1x). Subsequently cells were lysed with 4x sample buffer according to section 2.2.2.8.

2.2.2.8 Cell lysis with sample loading buffer

Cell suspensions from cell harvest were mixed with 4x sample buffer supplemented with 2 % SDS for a final volume of 1x sample loading buffer. After vortexing, the sample was boiled for 5 minutes at 95 °C and either placed on ice or stored at -20 °C until further use in Western Blot (section 2.2.3.1; 2.2.3.2).

2.2.2.9 Luciferase measurement

For measuring the luciferase activity, cells were lysed 48 hours after transfection for 10 min in 1x Lysis Juice (PJK) at room temperature and lysates were cleared of cell debris by centrifugation for 3 min at 10000 g. Then, 40 µL of the cleared lysates were added to either 40 µL of Beetle Juice (PJK), Renilla juice or NanoGlo Luciferase Assay Reagent (Promega) in opaque 96-well plates and luminescence was measured using a Glomax Multi (Promega) microplate reader. NanoLuc luciferase activities were normalized to firefly luciferase activities.

2.2.2.10 Purification of trVLPs using a sucrose cushion

In order to purify trVLPs from the supernatant of p0 cells, an ultracentrifugation over a 20 % sucrose cushion was performed. To this end, supernatant from p0 cells was harvested 48 hours post minigenome transfection and centrifuged two times at 800 g for 5 minutes with 4 °C to get rid of cells and cell debris. For trVLP purification ultracentrifugation tubes suitable for a SW 40 Ti Swinging-Bucket rotor from Beckmann Coulter were used. SW40 tubes were filled with 5 ml of the supernatant and carefully

underlaid with 2 ml of the 20 % sucrose solution, which leads, due to the different density of the two solutions, to the formation of two phases. Next, the remaining supernatant was carefully (in order to retain the two phases) added to the tubes and all tubes were filled to the brim with 1x PBS. After exact taring, the samples were centrifuged at 22500 rpm for 2 hours and 4 °C. During ultracentrifugation, the particles contained in the supernatant are separated based on their density. While particles with lower density such as soluble proteins remain in the media, components with higher density, such as trVLPs, accumulate at the bottom of the ultracentrifuge tube. After centrifugation, the supernatant was discarded and the tubes were dried carefully with a fine cloth in order not to lose the pellet. The pellet was resuspended in 75 µl 1x PBS and transferred to a 15 ml falcon containing 8 ml ZB10 medium supplemented with 5 % FCS, 1 % GlutaMax and 1 % Pen/Strep. The trVLP suspensions were stored at -80 °C until infection of p1 cells (see section 2.2.2.5).

2.2.2.11 Pyrimidine supplementation

For pyrimidine complementation, HEK 293T cells were reverse transfected with either anti-CAD siRNAs, a self-designed anti-EBOV-L siRNA or a negative control siRNA with no cellular target and seeded onto 12 well plates. After an incubation of 48 hours at 37 °C and 5 % CO₂ the medium was exchanged against 1 ml fresh medium supplemented with 5 % FCS and 1 % GlutaMax. Next, the cells were transfected with all components required for a minigenome system, including pCAGGS-based expression plasmids for NP (62.5 ng), VP35 (62.5 ng), VP30 (37.5 ng), L (500 ng), codon-optimized T7-polymerase (125 ng), firefly luciferase (as a transfection control, 125 ng), and the T7-driven monocistronic minigenome (pT7-EBOV-1cis-vRNA-nLuc; 125 ng). In order to investigate whether pyrimidine supplementation has a positive effect on reporter activity after knockdown of CAD, 10 µl of 100 mM pyrimidines (either uridine or cytidine) were added directly after transfection, which lead to a final concentration of 1 mM pyrimidines per well. All controls were supplemented with an equal volume of DMSO. 24 h post-transfection the medium was again exchanged against 1 ml fresh ZB10 medium supplemented with 5 % FCS and 1 % GlutaMax. Additionally, fresh pyrimidines or DMSO (for the negative controls) were added as described above. All samples were harvested 24 h after media change for determination of reporter activity (see section 2.2.2.9).

2.2.3 Protein biochemistry methods

2.2.3.1 Sodium dodecyl sulfate polyacrylamide gel electrophoresis (SDS-PAGE)

Sodium dodecyl sulfate polyacrylamide gel electrophoresis (SDS-PAGE) was developed in 1970 by Laemmli and is used to analyze mixtures of proteins (Laemmli 1970). The procedure is based at the reaction of proteins with the anionic detergent SDS, which results in the formation of a negative charged SDS-protein complex. SDS together with heat denatures the proteins, which leads to their linearization, and prevents protein-protein interaction. Treatment with SDS also results in a negative charge of the proteins, which is proportional to their molecular weight. Due to these characteristics it is possible to separate proteins just based on their molecular mass by electrophoresis through a polyacrylamide gel.

In order to separate proteins SDS-PAGE was performed using the Mini-PROTEAN Tetra Cell system. Polyacrylamide gels were prepared according to the following recipes:

	10 ml resolving gel			5 ml stacking gel
	8 %	10 %	12 %	4 %
dH ₂ O	5.3 ml	4.8 ml	4.3 ml	3.1 ml
Acrylamide 40 %	2.0 ml	2.5 ml	3.0 ml	0.5 ml
1.5M Tris-HCl pH 8.8 0.4 % SDS	2.6 ml	2.6 ml	2.6 ml	-
0.5M Tris-HCl pH 6.8 0.4 % SDS	-	-	-	1.3 ml
APS (10 %)	80 µl	80 µl	80 µl	40 µl
TEMED	20 µl	20 µl	20 µl	10 µl

To catalyze polymerization Tetramethylethylenediamine (TEMED) was added directly before the gel was poured. The resolving gel mixture was then poured into a glass sandwich, leaving about 2 cm free from the top, and directly overlaid with isopropanol to generate a straight gel boundary. After polymerization isopropanol was discarded and a stacking gel mixture was poured into the glass sandwich onto the top of the resolving gel. Then a comb was put in and the gel was led to polymerize. Subsequently the gels were placed in a Mini-PROTEAN Tetra Cell for electrophoresis and 1x SDS-PAGE buffer was added, depending on the number of gels. Samples were

thawed on ice and then boiled for 5 minutes at 95 °C. 25 µl of each sample as well as 1 µl colored protein marker were loaded onto the gel. Electrophoresis was performed at 120 V and 20 mA per gel until the bromophenol blue dye front from the sample buffer had reached the bottom of the gel.

2.2.3.2 Western blotting

Developed in 1979 western blot is one of the main techniques used to detect specific proteins after SDS-PAGE (Towbin, Staehelin et al. 1979). During the blotting process, the proteins are electrophoretically transferred from an SDS gel to an absorbent membrane. Once bound to the membrane the proteins can be detected by using specific antibodies.

For transfer of the proteins from the SDS gel to the membrane a Semi-Dry blotter was used. At first 2 pieces (for each gel) of extra thick western blotting filter paper and the nitrocellulose blotting membrane were soaked in transfer buffer. Then the stacking gel was removed from the resolving gel using a scraper and the nitrocellulose membrane was placed on the remaining gel. Next the blotting paper was laid on the membrane and they were assembled as followed on the Semi-Dry blotter: anode (+) (bottom), filter paper, membrane, gel, filter paper, and cathode (-) (top). Blotting was performed at 25 V and 40 mA per gel for 90 minutes. In case of larger proteins blotting was extended to 120 minutes. After blotting the membrane was blocked for at least one hour in PBS with 7 % skim milk powder at room temperature on a rocker. Subsequently the membrane was incubated with the primary antibody, which was diluted in PBS with 7 % skim milk powder in a final volume of 1 ml per membrane. Incubation was performed in a wet chamber on a glass plate from the Mini-PROTEAN Tetra Cell system that was covered with parafilm. Then the blocked membrane was put onto the spacer plate with the protein side facing up, and the antibody dilution was evenly added onto the membrane. For western blot the following primary antibodies and dilutions were used in this project:

Antibody	Specificity	Dilution	Species	Type
Anti-flag	flag	1:1000	rabbit	polyclonal
Anti-UAP56	UAP56	1:5000	rabbit	monoclonal
Anti-NXF1	NXF1	1:250	mouse	monoclonal
Anti-CAD	CAD	1:250	rabbit	monoclonal
Anti-mCherry	mCherry	1:1000	mouse	-
Anti-GAPDH	Glycerinaldehyd-3-phosphat-Dehydrogenase	1:1000	mouse	polyclonal

After a second piece of parafilm was placed on the membrane the wet chamber was closed and the blots were incubated overnight at 4 °C. Next, the membrane was washed three times with PBS_{0.1 % Tween} for 10 minutes each and incubated with the secondary antibody for one hour at room temperature on a rocking platform. The antibodies were diluted in PBS with 7 % skim milk powder in a final volume of 7 ml. A dilution of 1:14.000 of the secondary antibodies (680RD-coupled goat-anti-mouse or 680RD-coupled goat anti-rabbit and 800CW-coupled goat-anti-rabbit or 800CW-coupled goat anti-mouse antibodies) were used. After incubation the membrane was washed three times with PBS_{0.1 % Tween} for 10 minutes and two times with 1x PBS for 10 minutes each. Fluorescent signals were detected and quantified using an Odyssey CLx infrared imaging system (Li-Cor). For knockdown quantification, host factor signals were normalized to GAPDH signals.

2.2.3.3 Immunofluorescence assay

For immunofluorescence Huh7 cells were seeded (see chapter 2.2.2.1) on coverslips (ø 15 mm) and transfected as described in chapter 2.2.2.2. Two days post transfection the media was removed from the cells and they were gently washed three times with 1x PBS. Cells were then fixed on the coverslips by incubation in 1 ml 4 % Paraformaldehyde/ ZB10 (5 % FCS) for 25 minutes at room temperature. Subsequently the coverslips were gently washed with 1x PBS and the fixation was stop by a 10 minute incubation with 1 ml 0.1 M glycine solution. Next cells were washed with PBS and permeabilized for exactly 10 minutes in 1 ml 0.1 % Triton X-100/PBS. The coverslips were then washed again with 1x PBS, and blocked for 45 minutes in 10 % FCS/PBS to reduce unspecific staining. After another washing step with 1x PBS, the coverslips were placed upside down onto a drop of primary antibody solution.

Incubation was performed in a wet chamber on a glass plate from the Mini-PROTEAN Tetra Cell system that was covered with parafilm. Primary antibodies were diluted in PBS with 10 % FCS and cells were incubated for 1 h at room temperature with the prepared antibody solutions. For IFA the following primary antibodies and dilutions were used in this project:

Antibody	Specificity	Dilution	Species	Type
Anti-UAP56	UAP56	1:100	rabbit	monoclonal
Anti-flag	Flag-tag	1:2000	mouse	polyclonal
Anti-EBOV-NP	EBOV-NP	1:500	rabbit	polyclonal
Anti-myc	Myc-tag	1:1500	chicken	polyclonal
Anti-NPC	Nuclear pore complex	1:2500	mouse	monoclonal

After incubation, the coverslips were washed with PBS and incubated with the secondary antibody for 45 minutes in the dark. Secondary antibodies were prepared and incubated as described for the primary antibodies. The following secondary antibodies were used for IFA:

Antibody	Specificity	Dilution	Species	Type
Alexa Fluor 488 anti-mouse	mouse	1:1200	goat	polyclonal
Alexa Fluor 488 anti-rabbit	rabbit	1:1000	goat	polyclonal
Alexa Fluor 568 anti-mouse	mouse	1:500	goat	polyclonal
Alexa Fluor 568 anti-rabbit	rabbit	1:500	goat	polyclonal
Alexa Fluor 647 anti-chicken	chicken	1:1200	goat	polyclonal

After staining, coverslips were washed with PBS and subsequently dipped in dH₂O to wash them briefly. In order to remove excess water, the coverslip was next tapped on a piece of tissue until the water had run down from the coverslip. For mounting DAPI mounting solution was dropped at a microscope slide and the coverslip was placed face-down onto the drop of mounting medium using a tweezer. The arrangement was dried overnight and immunofluorescence was visualized using confocal laser scanning microscopy.

2.2.4 Statistical analysis

In order to calculate statistical significance, One-way ANOVA with a Dunnett's multiple comparisons test was performed using the GraphPad Prism 8.1.0 software.

2.2.5 Sequence alignment

To analyze the evolutionary distance between different proteins, first a sequence alignment (ClustalW) was conducted by using the Geneious software. Subsequently, the evolutionary analyses were performed in MEGA X and the evolutionary history was inferred using the Neighbor-Joining method in combination with a bootstrap test.

3 Results

3.1 Optimization of molecular biological methods

To analyze the functional relevance of host factors during the EBOV lifecycle, different methods had to be established and optimized. This included optimization of minigenome assays, establishment of a suitable knockdown protocol and testing of multiple tag variants and antibodies for immunofluorescence analysis (IFA).

3.1.1 Optimization of minigenome assays

Since minigenome systems are important tools for studying the EBOV lifecycle under low containment conditions and represent a key method of this thesis, optimization of these assays was undertaken in order to generate robust results.

3.1.1.1 Generation of a replication deficient minigenome with nano luciferase

Monocistronic minigenome systems are based on a reporter open reading frame (ORF) flanked by the 3'- and 5'-untranslated regions (leader and trailer) of the EBOV genome. While different reporters exist, the most suitable reporter strongly depends on the experimental setup. To measure reporter activity, which reflects replication and transcription of the minigenome, and to validate the influence of host factors at these processes, minigenomes containing a luciferase as reporter gene were used in this thesis. In contrast to the replication-competent minigenome, of which multiple variants with different luciferases already existed, only one replication-deficient minigenome (RdM) containing Renilla luciferase was available. In order to increase reporter activity of the RdM, an RdM containing nano luciferase (nLuc) was generated. To this end, the RdM was amplified by PCR using a replication competent minigenome as template and omitting the last 55 nt of the trailer region. The PCR product was then digested with Type IIS restriction endonucleases and religated to yield the vector pT7-EBOV-1cis-vRNA-nluc-dtrl1-56.

3.1.1.2 Comparison of RdM containing Renilla or nano luciferase

To analyse the functionality of the generated minigenome and to validate reporter activity, a minigenome assay was performed. For this, HEK 293T cells were transfected with an RdM containing either Renilla or nLuc as reporter gene and all

other components required for a minigenome system. The obtained reporter activity from both minigenomes was compared to assess whether reporter activity is higher for the nLuc RdM. As a control, minigenome assays without the L polymerase were performed (referred to as -L control).

As expected, the nLuc RdM showed increased reporter activity compared to the Renilla RdM, which corresponds to previous studies using replication-competent minigenomes. However, an increased reporter activity was also observed for the -L control, which results in no increase of the dynamic range of the RdM assay (Figure 11).

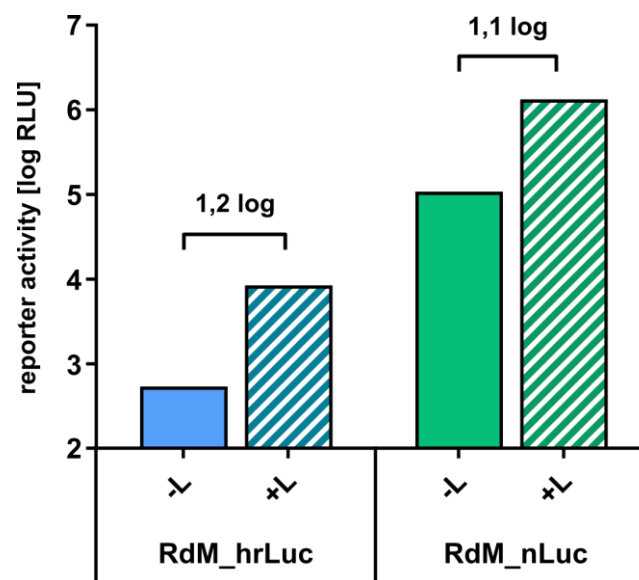


Figure 11. Comparison of Renilla (hrLuc) and nanoLuc (nLuc) monocistronic Minigenomes. 293T cells were transfected with all components required for a replication-deficient minigenome assay and either an RdM containing Renilla or nano Luciferase. 48 h post transfection, cells were harvested and reporter activity was measured. As negative control, the plasmid encoding for the viral polymerase was omitted.

3.1.1.3 Generation of a minigenome under control of a Pol-II promoter

A high dynamic range of the minigenome assays is necessary to evaluate a possible influence of host factors on EBOV transcription and/or protein expression. Therefore, in order to increase the dynamic range of the RdM system, the T7 promoter of the RdM was exchanged against a polymerase II (Pol-II) promoter. For this, the RdM was amplified by PCR using the generated construct from 3.1.1.1. After restriction digest of the PCR product, the RdM was integrated into a pCAGGS vector, which contains a Pol-II promoter, to yield pCAGGS_v1.0_1cis-EBOV-vRNA-nLuc_dtrl1-56. To generate authentic genome ends, the RdM was flanked not only by a hepatitis delta virus ribozyme at the 3' end but also by a hammerhead ribozyme at the 5' end of the

minigenome. Sequences for both ribozymes were added to the primers used for PCR amplification of the RdM.

3.1.1.4 Comparison of T7 and Pol-II-driven replication-deficient minigenomes

To test whether the generated Pol-II-driven RdM shows a higher dynamic range than the T7-driven RdM, HEK 293T cells were transfected with a plasmid encoding either of those minigenomes and all other components required for a minigenome assay. As control, minigenome assays without the L polymerase were performed (-L). The obtained reporter activity of all samples was measured and compared with each other. Using the Pol-II-driven RdM resulted in even higher reporter activity as well as in a ~25-fold bigger difference between the negative (-L) and positive (+L) control compared to the T7-driven RdM, suggesting that initial transcription of the minigenome is more efficient when using a Pol-II polymerase (Figure 12).

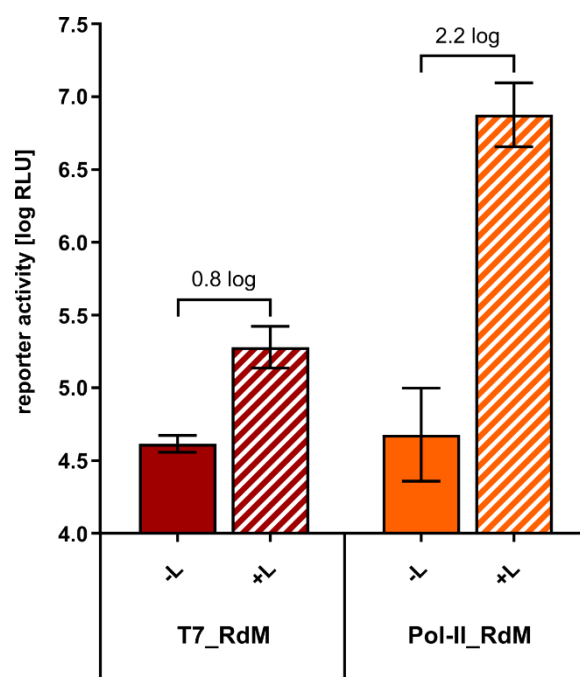


Figure 12. Comparison of T7 and pol-II-driven replication deficient minigenomes. 293T cells were transfected with plasmids encoding for all minigenome components (NP, VP35, VP30, polymerase L, T7) as well as either a T7-driven or pol-II-driven monocistronic minigenome. After 48 hours, cells were harvested and reporter activity was measured. As negative control, the plasmid encoding for the viral polymerase was omitted. Means and standard deviations for two independent experiments are shown. Figure modified from [Brandt 2020] under CC BY 4.0 license. Copyright © 2020 Janine Brandt, Lisa Wendt, Bianca Bodmer, Thomas C Mettenleiter, Thomas Hoenen. <https://doi.org/10.3390/cells9010187>.

3.1.2 Establishment and optimization of host factor knockdown

In order to investigate the role of host factors in the EBOV lifecycle, the influence of knockdown and overexpression of CAD, NXF1 and UAP56 on minigenome systems was compared. Since CAD and NXF1 are indispensable for the cellular lifecycle, a knockout of this factors would lead to cell death. Therefore, the establishment of a knockdown protocol was required to analyse the effect of these host factors of interest on different aspects of the EBOV lifecycle.

3.1.2.1 Generation of amiRNA and shRNA vectors for host cell knockdown

As a first step prior to optimization of the knockdown protocols expression constructs for artificial micro RNA (amiRNA) and short hairpin RNA (shRNA) were generated by molecular cloning. To this end, potential target sequences as well as scrambled sequences (used as negative control) for amiRNA and shRNA were determined using the siRNA wizard software from InvivoGen. Additionally, amiRNA and shRNA vectors against the EBOV polymerase L were generated for use as controls. Oligonucleotides corresponding to the desired amiRNAs/shRNAs were designed, phosphorylated, hybridized and inserted into a suitable vector, either pCAGGS-miRNA124 or psiRNA (Figure 13) (Table 2). Additional shRNA/amiRNA expression vectors were already available in the laboratory.

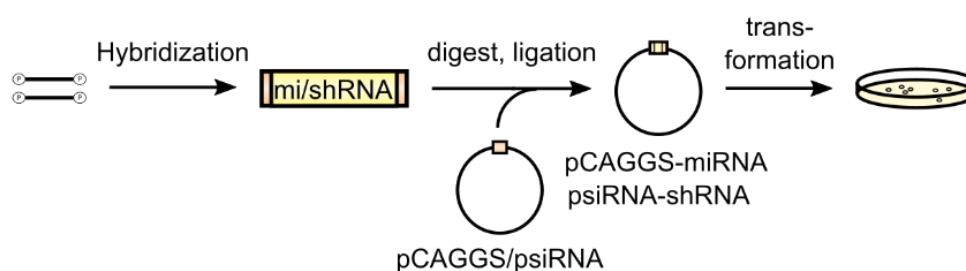


Figure 13. Scheme of the cloning strategy. Primers containing sequences for miRNA or shRNA were hybridized and then cloned into the vector pCAGGS or psiRNA.

Table 2. List of shRNA and amiRNA plasmids generated by molecular cloning.

shRNA Plasmids	amiRNA Plasmid
psiRNA_anti-EBOV-L	pCAGGS_miRNA_anti-NXF1.3 pCAGGS_miRNA_anti-UAP56.3 pCAGGS_miRNA_anti-CAD-scrambled pCAGGS_miRNA_anti-UAP56-scrambled pCAGGS_miRNA_anti-EBOV-L

3.1.2.2 Establishment of a host factor knockdown protocol

After generation of all required knockdown plasmids, a replication-competent minigenome assay in connection with a shRNA knockdown was performed. To this end HEK 293T cells were transfected with all minigenome components as well as different amounts of a shRNA vector against the EBOV polymerase (referred to as anti-L) or a scrambled psiRNA plasmid (NC). As control, minigenome assays without the L polymerase were performed (-L). 48 h post transfection cells were harvested and reporter activity was measured.

shRNA knockdown of EBOV-L resulted in no reduction in reporter activity compared to the negative control (NC), indicating that shRNA knockdown under the chosen conditions was not efficient (Figure 14A). Indeed, even after increasing plasmid amounts, changing of the cell line used (HEK 293, Huh7, A549) or when using different media supplementation for the cells, no reduction in reporter activity was observed in presence of the anti-L shRNA expression plasmid compared to the negative control, so that it was decided that this knockdown protocol is not suitable for our purpose.

As an alternative, amiRNA knockdown was attempted in HEK 293T cells in the context of a monocistronic minigenome system. Again, an amiRNA plasmid against the viral polymerase was used as anti-L knockdown control. 48 h post transfection cells were harvested and reporter activity was measured.

When using this approach, amiRNA knockdown resulted in a clear reduction in reporter activity for the anti-L control compared to the two negative controls (ctrl amiRNA 1 and 2) (Figure 14B). However, again no reduction in reporter activity was observed for the amiRNA plasmids used for knockdown of CAD, NXF1 and UAP56. Also, after optimization of the assay by using different amiRNA plasmid amounts, cells lines and media supplements, a decrease of reporter activity was only observed for anti-L, in contrast to previous results obtained in a high throughput siRNA screening assay.

Since CAD, NXF1 and UAP56 were identified to be important for the EBOV lifecycle by using a genome-wide siRNA screen, the same siRNAs used in the siRNA screen were ordered (Martin, Chiramel et al. 2018). To establish a siRNA knockdown protocol, HEK 293T cells were transfected with siRNAs targeting the host factors. For control, a siRNA with no specific target sequence was used as negative control (ctrl). 48 hours post minigenome transfection, the cells were harvested and reporter activity was measured.

All samples transfected with siRNAs targeting CAD, UAP56 and NXF1 showed a reduction in reporter activity compared to the negative control, demonstrating that under the experimental conditions employed by us, siRNA knockdown of the target host factors was the most suitable protocol (Figure 14C).

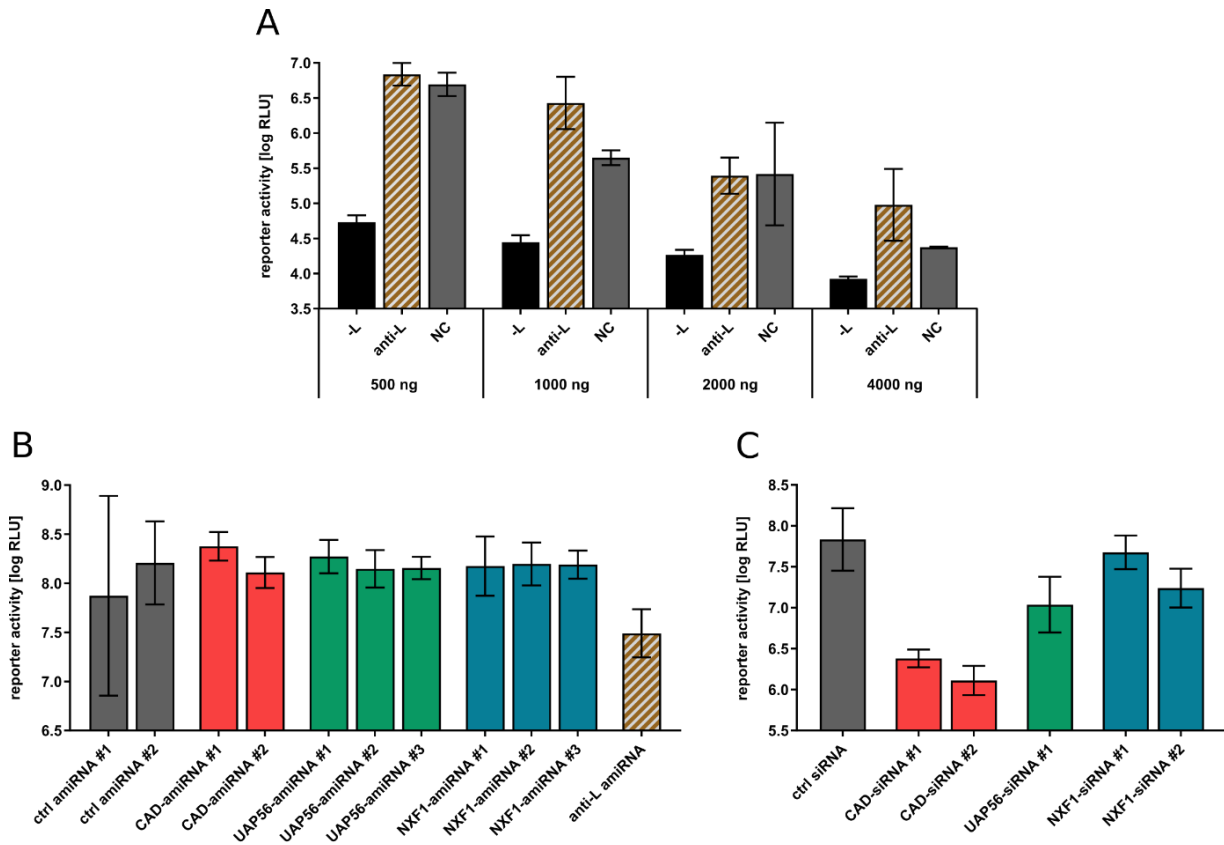


Figure 14. Establishment of a host factor knockdown protocol. **(A)** shRNA knockdown. 293T cells were transfected with plasmids encoding for all minigenome components (NP, VP35, VP30, polymerase L, T7, T7-driven minigenome) as well as a shRNA plasmid against EBOV-L (anti-L) or scrambled psiRNA vector (NC). After 48 hours, cells were harvested and reporter activity was measured. As negative control, the plasmid encoding for the viral polymerase was omitted. **(B)** amiRNA knockdown. 293T cells were transfected with plasmids encoding for all minigenome components (NP, VP35, VP30, polymerase L, T7, T7-driven minigenome) as well as amiRNA plasmids against CAD, UAP56, NXF1, EBOV-L (anti-L) or scrambled amiRNA vectors (ctrl amiRNA). After 48 hours, cells were harvested and reporter activity was measured. **(C)** siRNA knockdown. 293T cells were reverse transfected with siRNAs targeting either CAD (CAD-siRNA), UAP56 (UAP56-siRNA), NXF1 (NXF1-siRNA) or a negative control (ctrl siRNA). 48 h post-transfection, cells were transfected with all the components required for a replication-competent minigenome assay. Another 48 h later, cells were harvested and the reporter activity was measured. The means and standard deviations for three independent experiments are shown for each panel.

3.1.3 Optimization of immunofluorescence assay

Immunofluorescence analyses (IFA) are key to investigate the cellular localization of proteins. In this thesis IFA was used to study the cellular localization of CAD, UAP56, NXF1 and Ebola virus proteins, such as NP, VP35 and VP30, as well as possible

colocalization between host and viral proteins. As a first step, I assessed the possibility to use fluorescently tagged host proteins for this purpose.

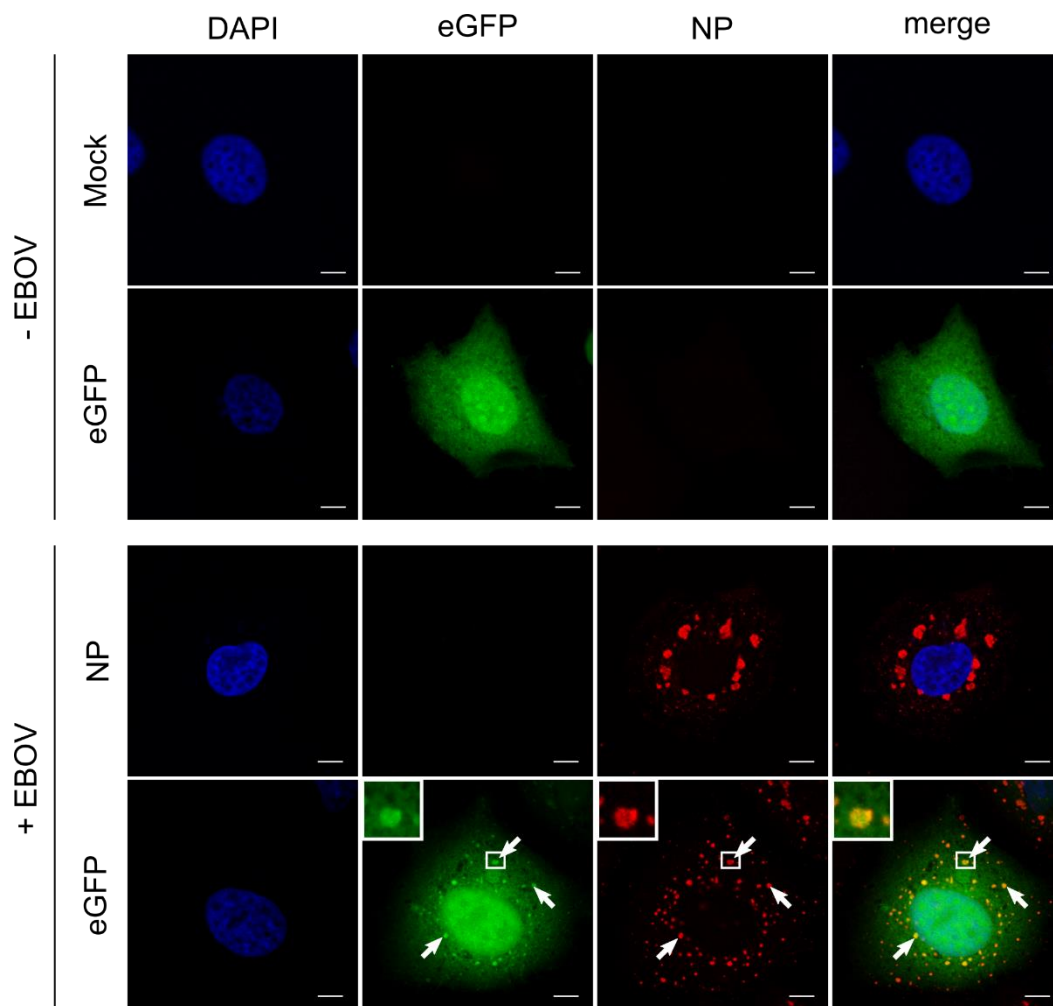


Figure 15. eGFP localizes into EBOV inclusion bodies. Huh7 cells were transfected with plasmids encoding eGFP (shown in green). 48 h post-transfection, the cells were infected with rgEBOV at an MOI of 1. After incubation for 16 h, the cells were fixed with 10 % formalin and permeabilized with Triton X-100. NP (shown in red) was stained with an anti-EBOV-NP antibody. All nuclei were stained with DAPI (shown in blue), and the cells were visualized by confocal laser scanning microscopy. The scale bars indicate 10 μ m. The arrows point out colocalization, and the insets show magnifications of the indicated areas. Merge shows an overlay of all three channels.

3.1.3.1 Testing of different fluorescence proteins for IFA

As endogenous protein levels of CAD, UAP56 and NXF1 were too low for clear detection in IFA (data not shown), enhanced green fluorescent protein (eGFP) tagged versions of these host proteins overexpressed from plasmids were considered to be used. However, Schmidt et al. have previously shown that eGFP by itself accumulates in NP-driven inclusion bodies (IB) of Marburg virus (Schmidt, Schumann et al. 2011). Independent relocalization of eGFP in the IBs could lead to misinterpretation of the

actual cellular localization of the host proteins in presence of viral proteins and IB formation, as eGFP might drag CAD, UAP56 and NXF1 into inclusion bodies. Therefore, in order to check whether eGFP is recruited into NP-induced IBs of EBOV, Huh7 cells were transfected with plasmids containing eGFP. 48 h post transfection cells were infected with recombinant infectious EBOV and IFA was performed 16 h after infection. All samples were stained for NP as an inclusion body marker.

Similar to the results of Schmidt et al. eGFP strongly accumulated in EBOV-induced inclusion bodies, while eGFP inclusions were not detected in absence of EBOV (Figure 15). This result indicates that eGFP is not suitable as a tag for CAD, NXF1 and UAP56 as it might modify their cellular localization.

To find a fluorescence protein which does not accumulate in inclusion bodies, I wanted to test a range of phylogenetically unrelated reporter proteins. To guide my selection, I therefore performed a protein alignment of the sequences of 14 fluorescence proteins available in our laboratory and inferred the evolutionary history using the Neighbor-Joining method (Figure 16). Based on the resulting phylogenetic tree, I selected a range of fluorescent proteins (marked in red in Figure 16) and performed IFA as described above.

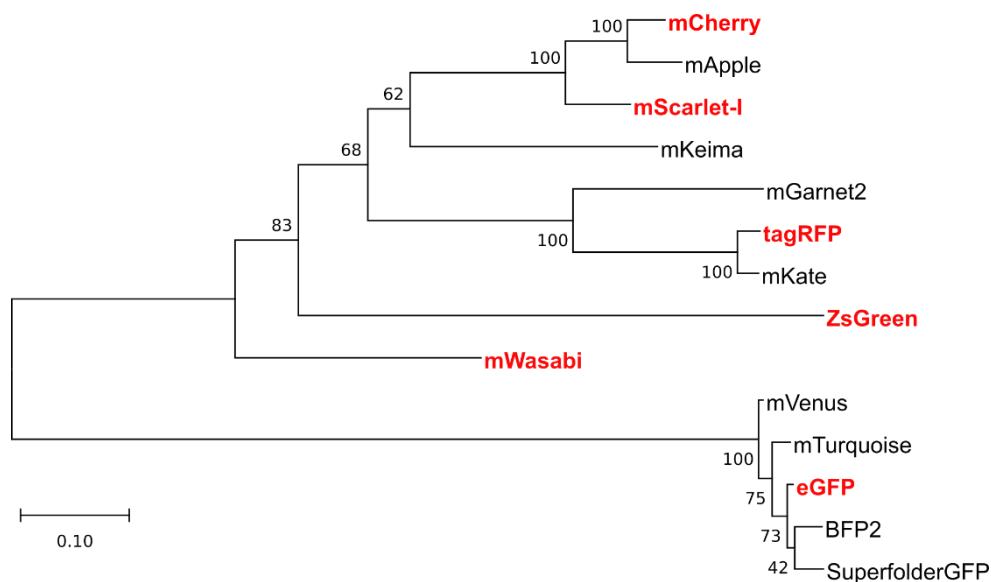


Figure 16. Alignment of different fluorescence proteins. The evolutionary history was inferred using the Neighbor-Joining method. The optimal tree with the sum of branch length = 2.99641115 is shown. The percentage of replicate trees in which the associated taxa clustered together in the bootstrap test (100 replicates) are shown next to the branches. The tree is drawn to scale, with branch lengths in the same units as those of the evolutionary distances used to infer the phylogenetic tree. The evolutionary distances were computed using the Poisson correction method and are in the units of the number of amino acid substitutions per site. Evolutionary analyses were conducted in MEGA X.

Surprisingly, all fluorescence proteins used showed a strong accumulation in NP-induced inclusion bodies during coexpression with EBOV-NP, concluding that none of the fluorescent proteins available to us is suitable to function as a fluorescent tag for the investigation of the cellular distribution of CAD, NXF1 and UAP56 (Figure 17 and 18). Therefore, the cellular localization of the three host factors was instead investigated by using flag-HA-tagged versions of these proteins in combination with an anti-flag antibody.

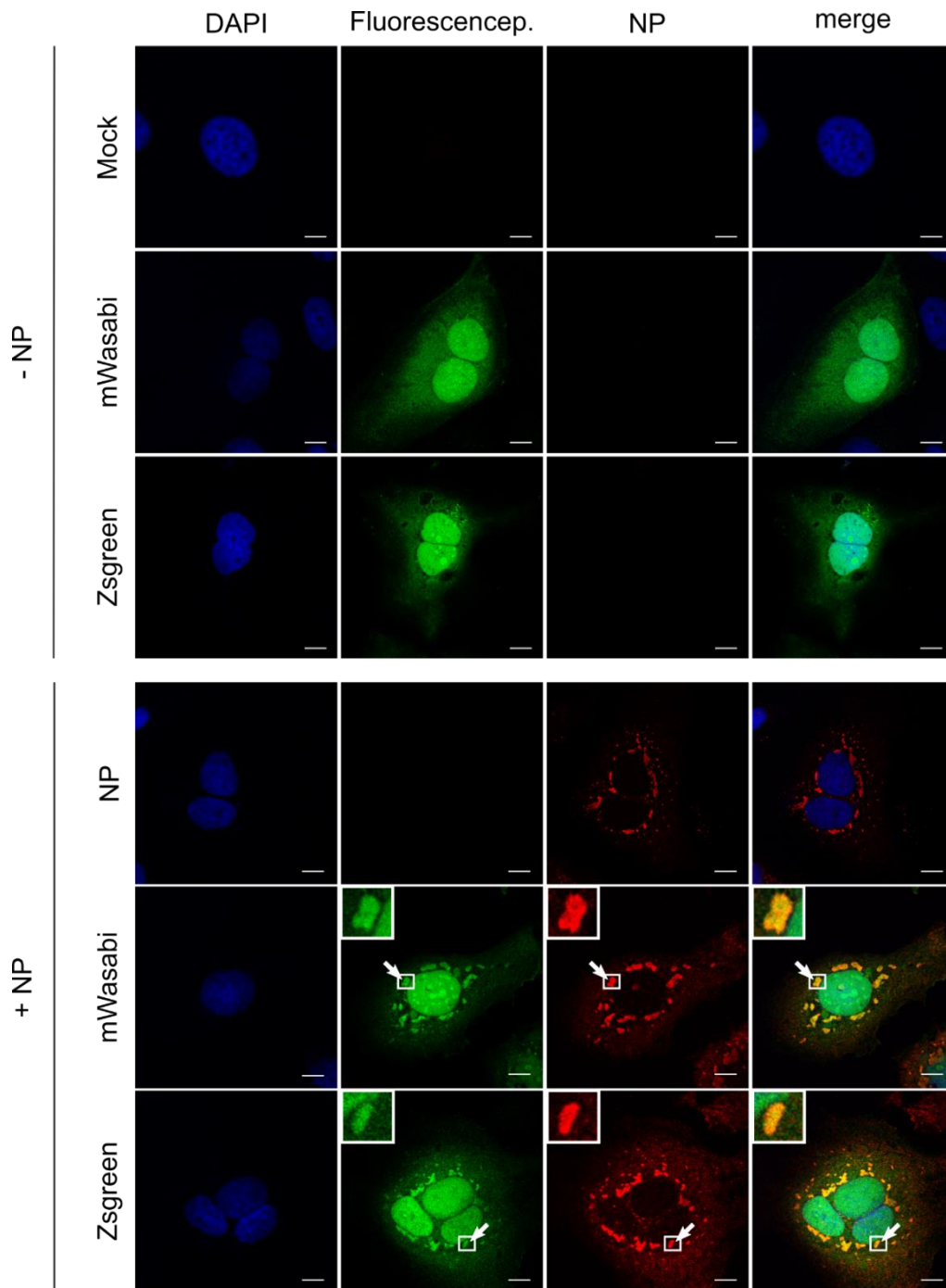


Figure 17. Cellular localization of two green fluorescence proteins. Huh7 cells were transfected with plasmids encoding mWasabi or Zsgreen (shown in green) and EBOV-NP as indicated. 48 h post-

transfection, the cells were fixed with 4 % paraformaldehyde and permeabilized with 0.1 % Triton X-100. NP (shown in red) was stained with an anti EBOV-NP antibody and an Alexa Fluor 568 anti-rabbit secondary antibody. All nuclei were stained with DAPI (shown in blue), and the cells were visualized by confocal laser scanning microscopy. The scale bars indicate 10 μ m. The arrows point out colocalization, and the insets show magnifications of the indicated areas. Merge shows an overlay of all three channels.

3.2 Influence of CAD on the EBOV lifecycle

CAD was previously identified to be important for the EBOV RNA synthesis and/or viral protein expression by using a genome-wide siRNA screen (Martin, Chiramel et al. 2018). However, so far only the effect of CAD knockdown on the sum of these processes had been tested. In order to analyze the role of CAD knockdown and overexpression on individual aspects of the EBOV lifecycle and its cellular distribution during EBOV infection, optimized minigenome systems and IFA was used.

3.2.1 Quantification of siRNA knockdown of CAD and EBOV-L

Before the role of CAD knockdown on different aspects of the EBOV lifecycle was investigated, the efficiency of endogenous CAD and EBOV-L (positive control) siRNA knockdown had first to be assessed in order to ensure that changes in minigenome reporter activity results from knockdown of CAD or L. For CAD knockdown, HEK 293T cells were reverse transfected with two different siRNAs against endogenous CAD (CAD-siRNA #1, CAD-siRNA #2) or a ctrl siRNA and CAD expression levels were detected by quantitative Western blotting. In contrast, for EBOV-L knockdown, 293T cells were reverse transfected with either an anti-L siRNA or ctrl siRNA.

CAD knockdown resulted in a 60 % to 80 % reduction in endogenous CAD expression levels for the two different siRNAs compared to the ctrl siRNA (Figure 19A and 19B). Additionally, siRNA knockdown of L-mCherry resulted in an 80 % reduction in L-mCherry expression levels compared to the ctrl siRNA, indicating that siRNA knockdown of both CAD and EBOV-L is highly efficient (Figure 19C and 19D).

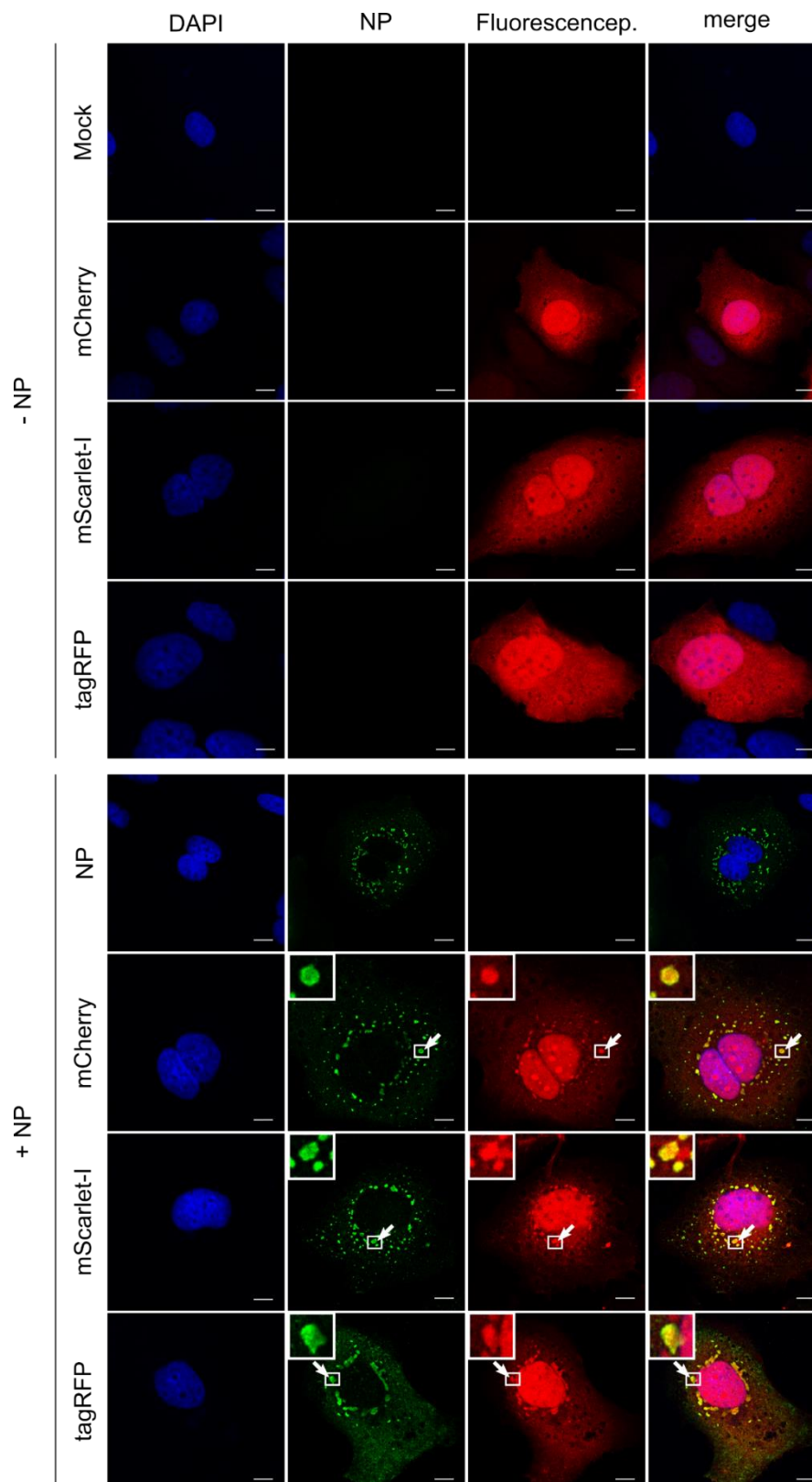


Figure 18. Cellular localization of different red fluorescence proteins. Huh7 cells were transfected with plasmids encoding mCherry, tagRFP or mScarlet-I (shown in red) and EBOV-NP as indicated. 48 h post-transfection, the cells fixed with 4 % paraformaldehyde and permeabilized with 0.1 % Triton X-100. NP (shown in green) was stained with an anti EBOV-NP antibody and an Alexa Fluor 488 anti-rabbit secondary antibody. All nuclei were stained with DAPI (shown in blue), and the cells were visualized by confocal laser scanning microscopy. The scale bars indicate 10 μ m. The arrows point out colocalization, and the insets show magnifications of the indicated areas. Merge shows an overlay of all three channels.

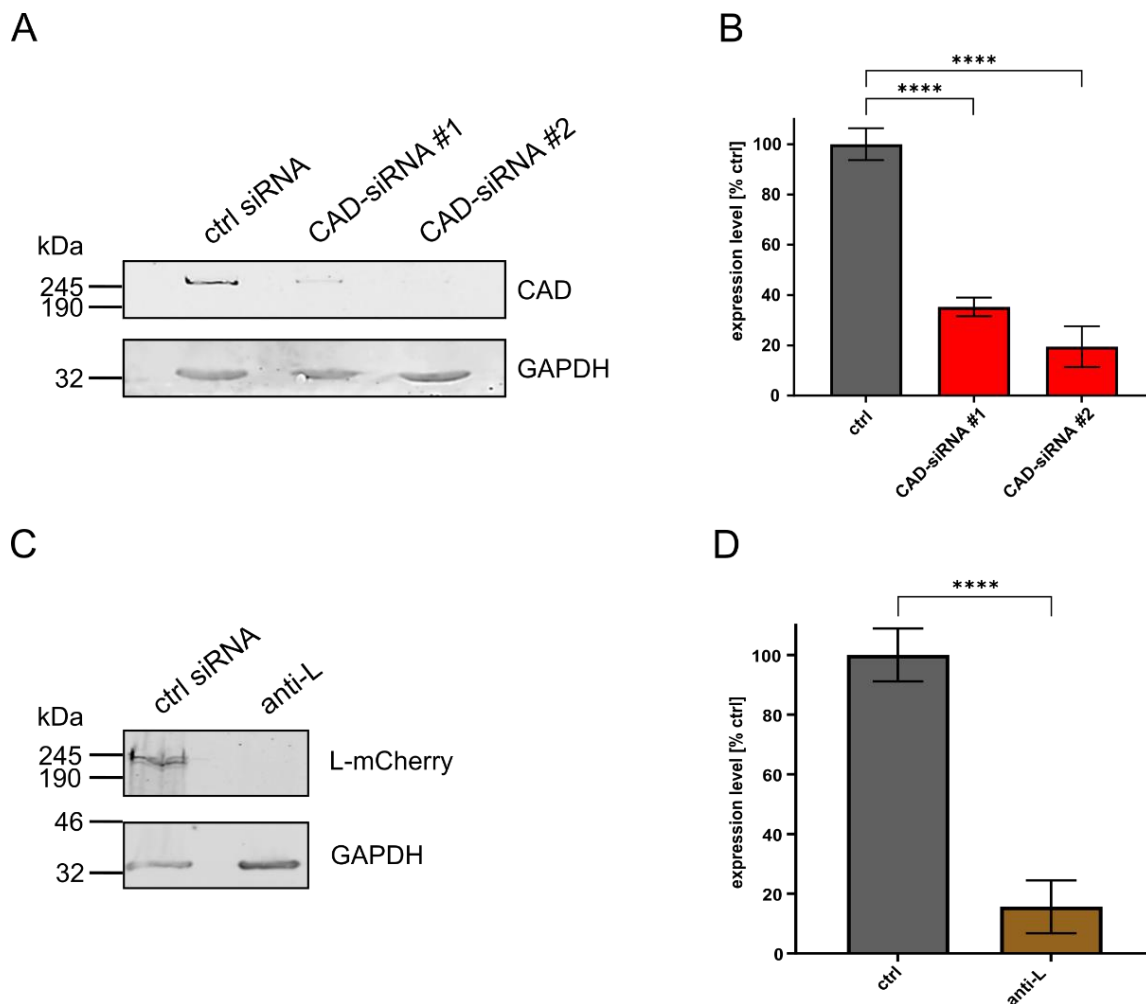


Figure 19. Quantification of siRNA knockdown. **(A)** Analysis of CAD knockdown. 293T cells were transfected with siRNAs targeting CAD (CAD-siRNA), or a negative control (ctrl siRNA). The cells were harvested 48 h post-transfection and the lysates were subjected to SDS-PAGE and Western blotting. **(B)** Quantification of CAD knockdown. The Western blot signals for CAD knockdown (as shown in Figure 19A) were measured and normalized to the GAPDH signals. The negative control (ctrl siRNA) was set to 100 % and the efficiency of CAD knockdown was calculated (**** $p \leq 0.0001$). **(C)** Analysis of L knockdown. 293T cells were transfected with siRNAs targeting EBOV-L (anti-L), or a negative control (ctrl siRNA). 48 h post transfection cells were transfected with L-mCherry and the cells were harvested after an additional incubation period of 48 h. The lysates were subjected to SDS-PAGE and Western blotting. **(D)** Quantification of L knockdown. The Western blot signals for L knockdown (as shown in Figure 19C) were measured and normalized to the GAPDH signals. The negative control (ctrl siRNA) was set to 100 % and the efficiency of L knockdown was calculated. The means and standard deviations of 3 [(A), (B)] or 4 [(C), (D)] independent experiments are shown for each panel. Asterisks indicate p-values from a one-way ANOVA (**** $p \leq 0.0001$). Figure modified from [Brandt 2020] under CC BY 4.0 license. Copyright © 2020 Janine Brandt, Lisa Wendt, Bianca Bodmer, Thomas C Mettenleiter, Thomas Hoenen. <https://doi.org/10.3390/cells9010187>.

3.2.2 Role of CAD on total EBOV RNA synthesis

In order to confirm the results from the genome-wide siRNA screen with the optimized knockdown protocol and to analyze the influence of CAD overexpression on EBOV RNA synthesis a classical minigenome assay in connection with an siRNA knockdown

or an overexpression of CAD was performed. For CAD knockdown, HEK 293T cells were reverse transfected with different siRNAs against endogenous CAD (CAD-siRNA #1, CAD-siRNA #2), EBOV-L (anti-L) or a ctrl siRNA. In course of CAD overexpression, 293T cells were transfected with all components required for a replication-competent minigenome system as well as different amounts (62.5 ng, 250 ng and 1000 ng) of a vector encoding for CAD wildtype or the empty vector pCAGGS.

As previously shown, knockdown of CAD led to a 40 to 53-fold reduction in reporter activity, confirming an influence of CAD on EBOV viral RNA synthesis and protein expression (Figure 20A) (Martin, Chiramel et al. 2018). In contrast, CAD overexpression had no influence on reporter activity, demonstrating that increased amounts of CAD in the cell are not relevant for the Ebola virus lifecycle (Figure 20B). In order to avoid artificial effects present in the monocistronic minigenome system and to validate the results obtained from CAD overexpression, a trVLP assay was performed. However, due to detachment of cells during trVLP infection after CAD knockdown, a trVLP assay was only performed for CAD overexpression. To this end, p1 293T cells were transfected with plasmids encoding for the EBOV RNP proteins and the attachment factor Tim 1 as well as different amounts (62.5 ng, 250 ng and 1000 ng) of a vector encoding for CAD wildtype or the empty vector pCAGGS. As observed for the replication competent minigenome system, CAD overexpression had no influence on reporter activity compared to the pCAGGS control, indicating that increased amounts of CAD indeed have no relevance for total EBOV RNA synthesis (Figure 20C).

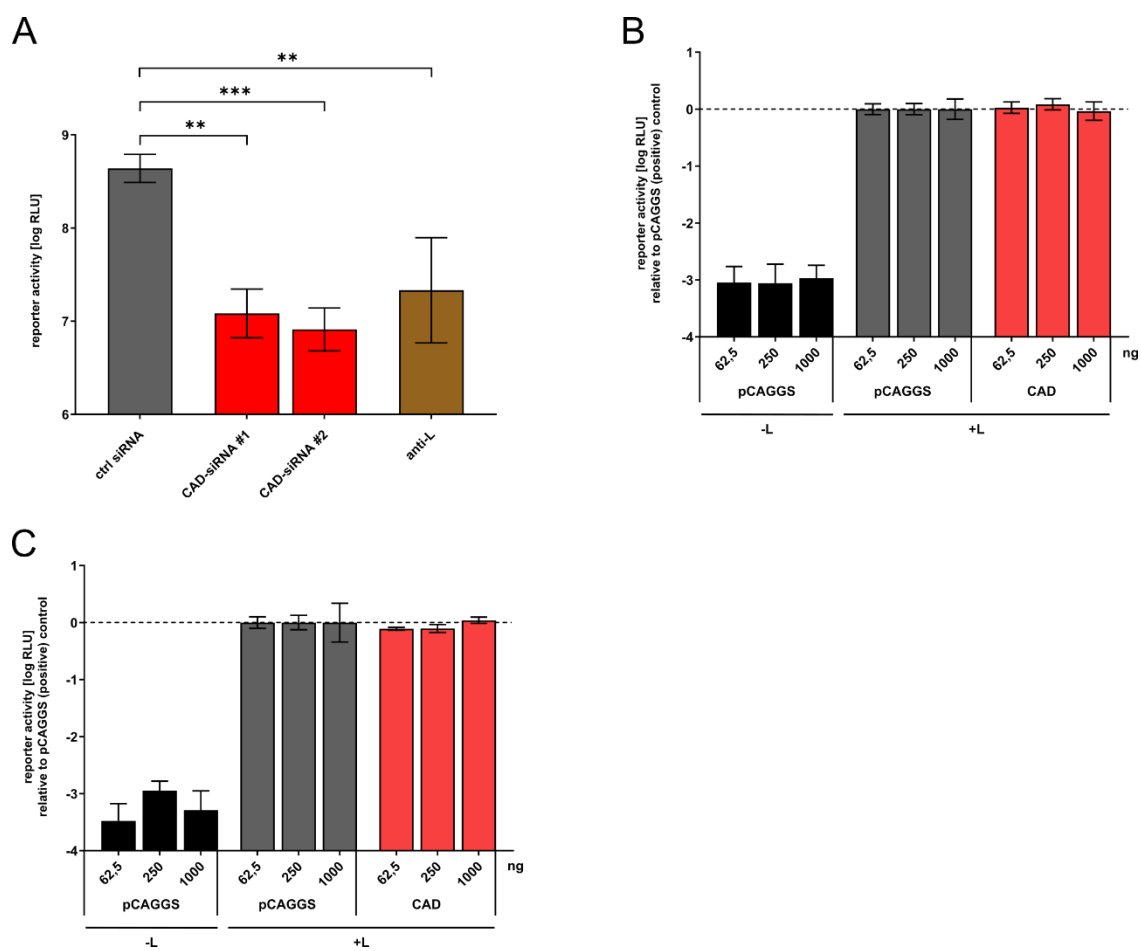


Figure 20. Influence of CAD knockdown and overexpression on the Ebola virus life cycle. **(A)** Influence of CAD knockdown on EBOV RNA synthesis. 293T cells were transfected with siRNAs targeting either CAD (CAD-siRNA), EBOV-L (anti-L), or a negative control (ctrl siRNA). 48 h post-transfection, cells were transfected with all the components required for a replication-competent minigenome assay. Another 48 h later, cells were harvested and the reporter activity was measured. **(B)** Influence of CAD overexpression on EBOV RNA synthesis. 293T cells were transfected with all components required for a replication-competent minigenome assay, as well as different amounts (62.5 ng, 250 ng and 1000 ng) of a vector encoding for CAD wildtype or the empty vector pCAGGS. Cells were harvested and reporter activity was measured 48 h post transfection. **(C)** Role of CAD overexpression for EBOV RNA synthesis in trVLP assay. p1 293T cells were transfected with plasmids encoding for the EBOV RNP proteins and the attachment factor Tim 1 as well as different amounts (62.5 ng, 250 ng and 1000 ng) of a vector encoding for CAD wildtype or the empty vector pCAGGS. 24 h post transfection, cells were infected with trVLPs containing a tetracistronic minigenome and cells were harvested 48 h post infection. The means and standard deviations of 3 [(A), (C)] or 5 (B) independent experiments are shown for each panel. Asterisks indicate p-values from a one-way ANOVA (* $p \leq 0.05$; ** $p \leq 0.01$; *** $p \leq 0.001$; **** $p \leq 0.0001$; ns: $p > 0.05$). Figure modified from [Brandt 2020] under CC BY 4.0 license. Copyright © 2020 Janine Brandt, Lisa Wendt, Bianca Bodmer, Thomas C Mettenleiter, Thomas Hoenen. <https://doi.org/10.3390/cells9010187>.

3.2.3 CAD is important for Ebola virus transcription

To analyze the function of CAD for EBOV transcription and/or protein expression independent of genome replication, a replication-deficient minigenome system was performed. In contrast to a replication-competent minigenome, the replication-deficient

minigenome lacks 55 nt in the antigenomic replication promoter leading to a block of minigenome vRNA replication, while minigenome transcription still takes place (Hoenen, Jung et al. 2010b). As CAD overexpression had no effect on total viral RNA synthesis, only the influence of CAD knockdown on EBOV transcription and/or protein expression was investigated.

By using this system, CAD knockdown resulted in a clear reduction in reporter activity, indicating that CAD is important for EBOV transcription and/or protein expression independent of viral genome replication (Figure 21).

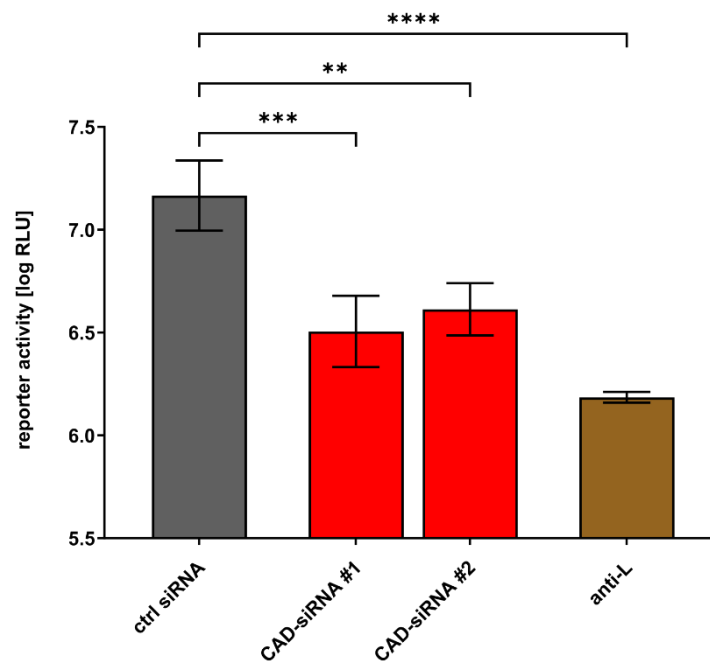


Figure 21. Analysis of CAD knockdown on EBOV transcription and protein expression. 293T cells were transfected with siRNAs targeting either CAD (CAD-siRNA), EBOV-L (anti-L), or a negative control (ctrl siRNA). 48 h post-transfection, cells were transfected with all the components required for a replication-deficient minigenome assay (repl.def.). Another 48 h later, cells were harvested and the reporter activity was measured. The means and standard deviations of 3 independent experiments are shown. Asterisks indicate p-values from a one-way ANOVA (* $p \leq 0.05$; ** $p \leq 0.01$; *** $p \leq 0.001$; **** $p \leq 0.0001$; ns: $p > 0.05$). Figure modified from [Brandt 2020] under CC BY 4.0 license. Copyright © 2020 Janine Brandt, Lisa Wendt, Bianca Bodmer, Thomas C Mettenleiter, Thomas Hoenen. <https://doi.org/10.3390/cells9010187>.

3.2.4 Influence of CAD knockdown on EBOV genome replication

To further dissect the influences of CAD on viral genome replication, mRNA transcription, and later steps of viral protein expression, a classical minigenome assay in connection with a siRNA knockdown of CAD was performed and vRNA and mRNA levels were determined by RT-qPCR

Cells treated with CAD siRNA showed a strong reduction in both vRNA and mRNA levels in comparison to the control cells, demonstrating that CAD is important for both EBOV transcription and viral genome replication (Figure 22A and 22B).

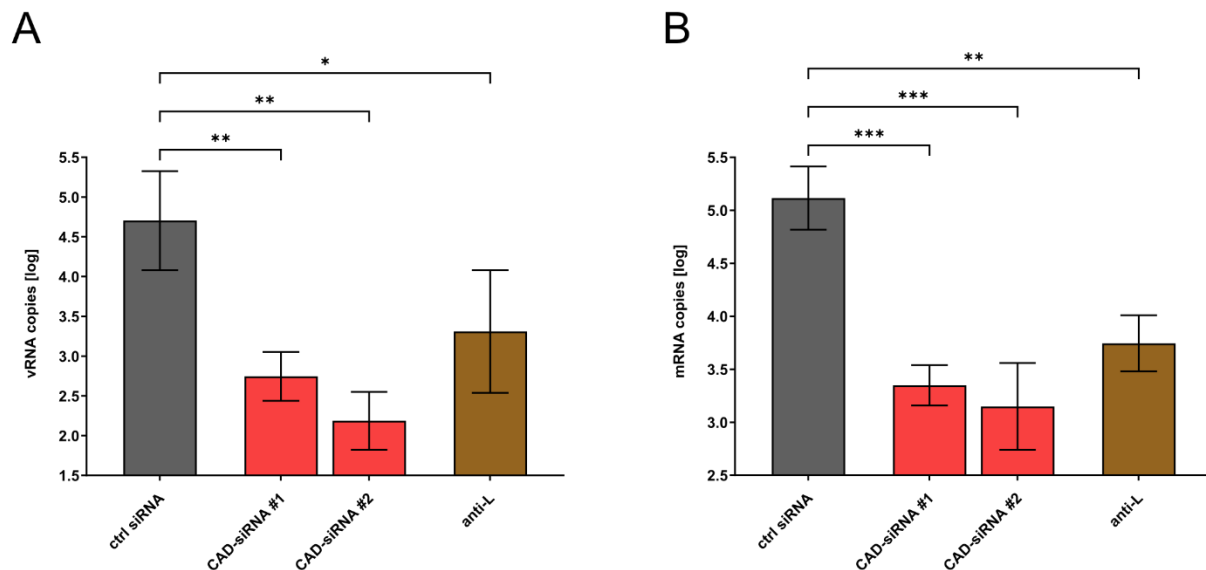


Figure 22. Influence of CAD knockdown on viral genome replication and mRNA transcription **(A)** Impact of CAD knockdown on EBOV replication. 293T cells were transfected with siRNAs targeting either CAD (CAD-siRNA), EBOV-L (anti-L), or a negative control (ctrl siRNA). 48 h post-transfection, cells were transfected with all the components required for a replication-competent minigenome assay. After cell harvesting, RNA was extracted from the cell lysates and RT-qPCR for vRNA was performed. **(B)** Influence of CAD knockdown on EBOV mRNA levels. Cells were treated as described above. After cell harvesting, RNA was extracted from cell lysates and RT-qPCR for mRNA was performed. The means and standard deviations of 3 independent experiments are shown for each panel. Asterisks indicate p-values from a one-way ANOVA (* p ≤ 0.05; ** p ≤ 0.01; *** p ≤ 0.001; **** p ≤ 0.0001; ns: p > 0.05). Figure modified from [Brandt 2020] under CC BY 4.0 license. Copyright © 2020 Janine Brandt, Lisa Wendt, Bianca Bodmer, Thomas C Mettenleiter, Thomas Hoenen. <https://doi.org/10.3390/cells9010187>.

3.2.5 The role of CAD during pyrimidine synthesis is critical for the EBOV lifecycle

CAD represents an important component of pyrimidine synthesis, and inhibition of this pathway has been shown to have a negative influence on the EBOV lifecycle (Martin, Chiramel et al. 2018). However, whether the effect of CAD knockdown on EBOV replication and transcription indeed results from a lack of pyrimidines still needed to be investigated. In order to examine this negative effect on EBOV replication and transcription, a minigenome assay in connection with a siRNA knockdown of CAD was performed as described in 3.2.2. Supplementation of 1 mM of exogenous pyrimidines, either uridine or cytidine, was performed right after minigenome transfection.

Provision of uridine resulted in reporter activities similar to the positive controls, concluding that the effect of CAD knockdown on EBOV genome replication and

transcription is due to a lack of pyrimidines (Figure 23). When complementing cytidine, a similar rescue effect was seen, albeit less pronounced, possibly because cytidine is not metabolized into uridine, whereas exogenous uridine can be metabolized into cytidine during the natural pyrimidine synthesis.

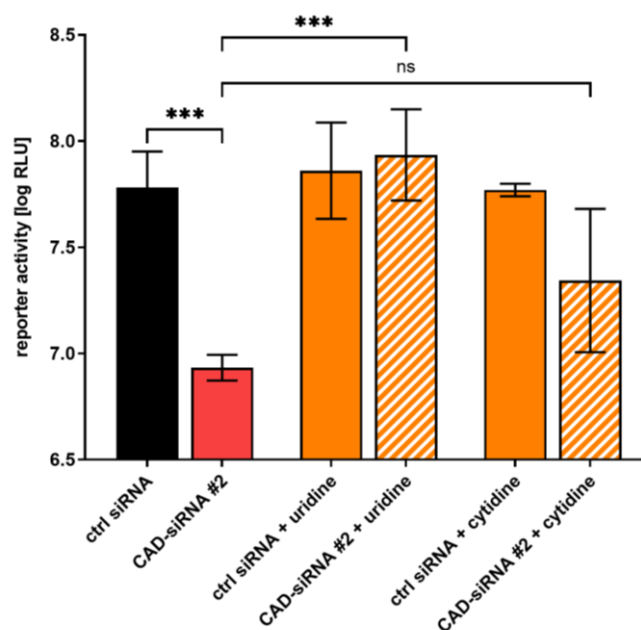


Figure 23. Supplementation of pyrimidines compensates for the effect of CAD knockdown. 293T cells were transfected with siRNAs targeting CAD (CAD-siRNA #2) or a negative control (ctrl siRNA). 48 h post-transfection, the cells were transfected with all components required for a replication-competent minigenome assay and treated with 1 mM pyrimidines, either uridine or cytidine. Another 48 h later, the cells were harvested and the reporter activity was measured. The means and standard deviations of 3 independent experiments are shown. Asterisks indicate p-values from a one-way ANOVA (***) $0.0001 < p \leq 0.001$; ns: $p > 0.05$). Figure modified from [Brandt 2020] under CC BY 4.0 license. Copyright © 2020 Janine Brandt, Lisa Wendt, Bianca Bodmer, Thomas C Mettenleiter, Thomas Hoenen. <https://doi.org/10.3390/cells9010187>.

3.2.6 CAD accumulates in NP-induced inclusion bodies

An important characteristic of negative-sense RNA viruses is the formation of inclusion bodies in the cytoplasm of infected cells (Hoenen, Shabman et al. 2012, Lier, Becker et al. 2017). These viral inclusions are important sites for replication and transcription and protect the viral RNA from the cellular degradation machinery. While in case of most negative-sense RNA viruses the expression of two viral proteins is required for inclusion body formation, for EBOV the sole expression of NP is apparently sufficient (Becker, Rinne et al. 1998, Boehmann, Enterlein et al. 2005, Groseth, Charton et al. 2009). Since CAD is important for EBOV replication and transcription, an immunofluorescence assay was performed to analyze whether the presence of

inclusion bodies has an influence on the intracellular distribution of CAD, and whether recruitment of CAD into NP-induced inclusion bodies can be detected.

As previously described, single expression of NP resulted in the formation of perinuclear inclusion bodies with a globular shape (Figure 24). In contrast, the sole expression of CAD led to an even distribution throughout the cytoplasm, with small amounts of CAD present in the nuclear region. Interestingly, coexpression of NP and CAD led to a relocalization of CAD into NP-induced inclusion bodies, demonstrating that CAD supports the EBOV lifecycle directly at the site of replication and transcription.

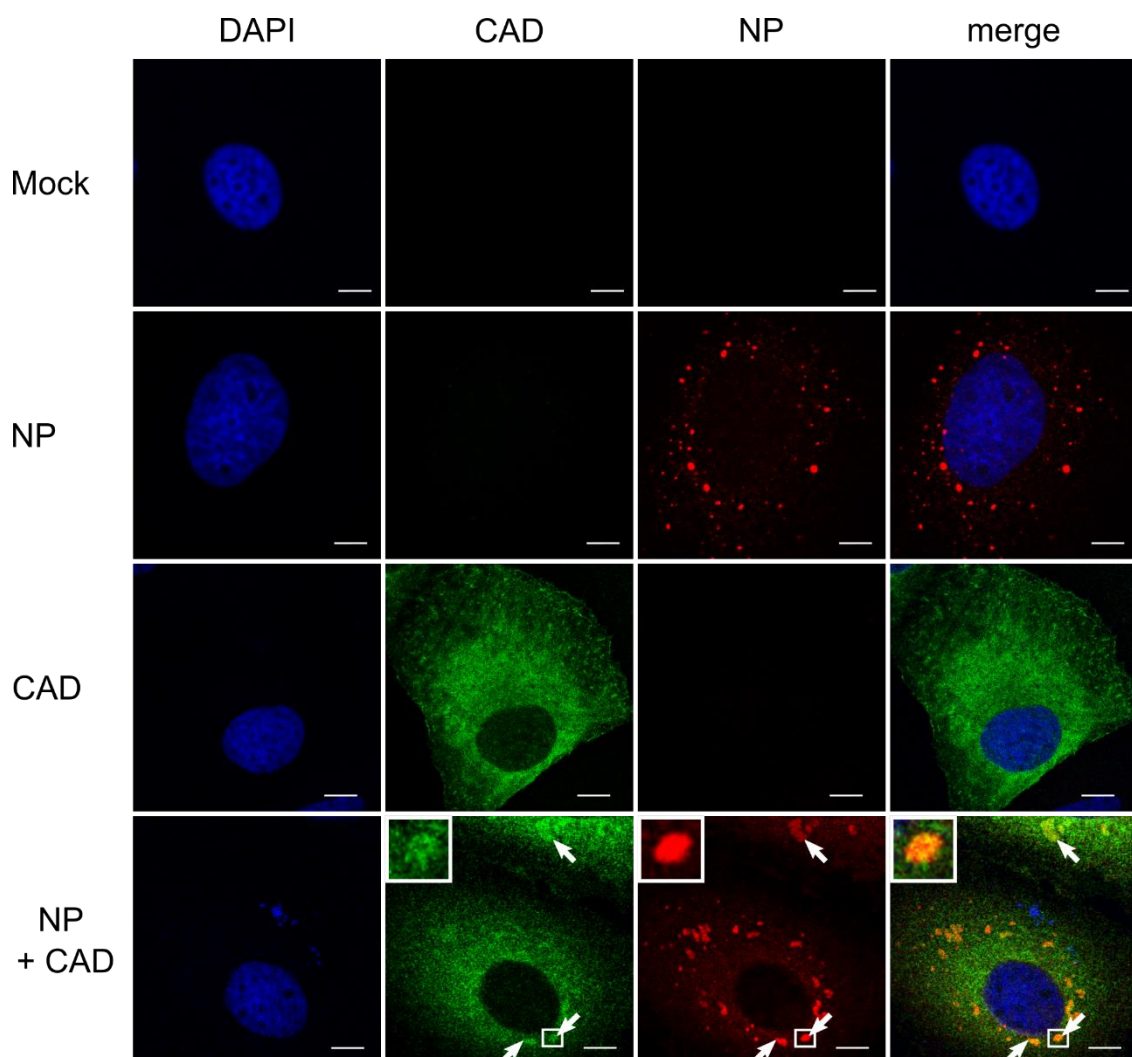


Figure 24. Recruitment of CAD into NP-induced inclusion bodies. Huh7 cells were transfected with plasmids encoding FLAG/HA-CAD and EBOV-NP as indicated. 48 h post-transfection, the cells were fixed with 4 % paraformaldehyde and permeabilized with 0.1 % Triton X-100. FLAG-tagged CAD (shown in green) was detected using an anti-FLAG antibody and NP (shown in red) was stained with anti-EBOV NP antibodies. The nuclei were stained with DAPI (shown in blue). The scale bars indicate 10 μ m. The arrows point out colocalization, and the insets show magnifications of the indicated areas. Merge shows an overlay of all channels. Figure modified from [Brandt 2020] under CC BY 4.0 license. Copyright © 2020 Janine Brandt, Lisa Wendt, Bianca Bodmer, Thomas C Mettenleiter, Thomas Hoenen. <https://doi.org/10.3390/cells9010187>.

3.2.7 CAD is recruited into inclusion bodies during EBOV infection

In order to analyze the influence of EBOV infection on the cellular distribution of CAD and to confirm the results obtained from the colocalization analysis with NP, immunofluorescence analysis in connection with an EBOV infection was performed. As expected, colocalization of CAD and inclusion bodies was still detectable, albeit not as apparent as under conditions of recombinant overexpression of NP, suggesting that CAD is recruited into viral inclusion bodies to provide sufficient amounts of pyrimidines for EBOV genome replication and transcription (Figure 25).

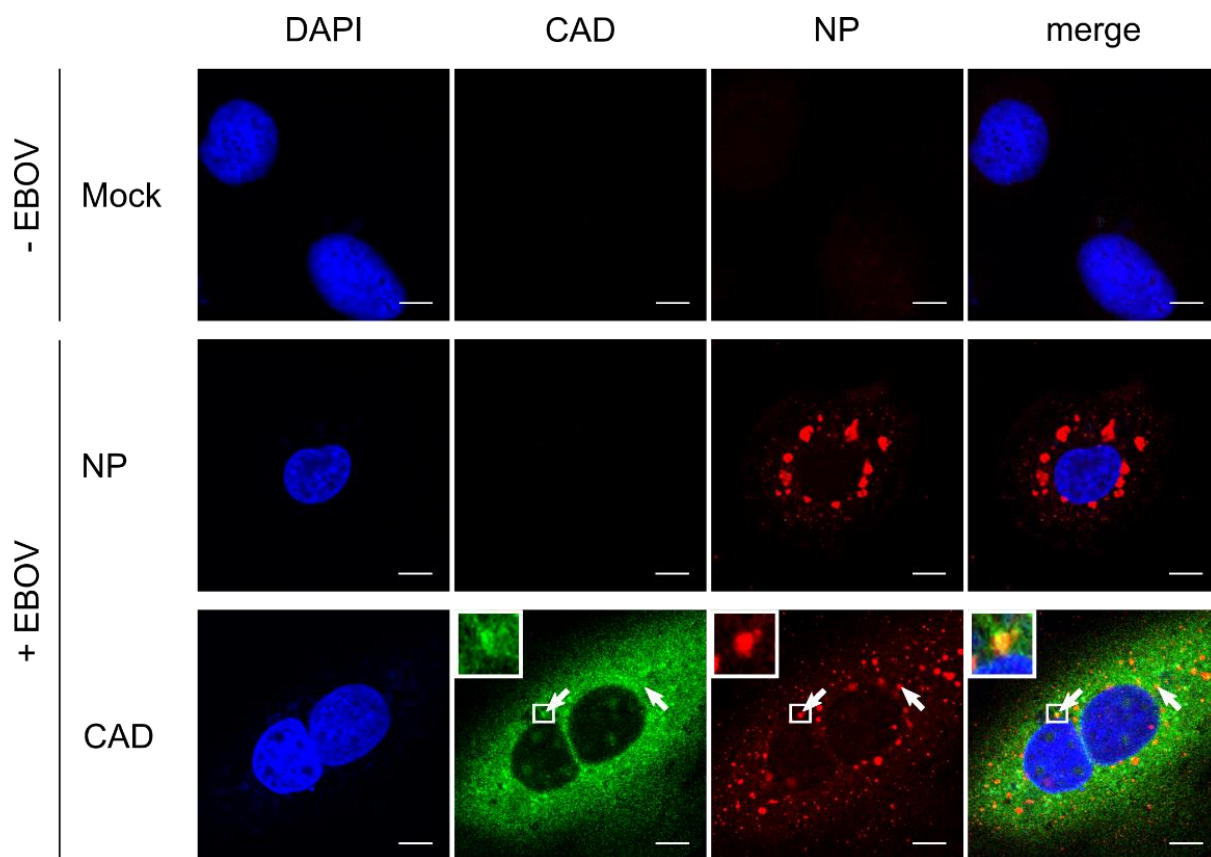


Figure 25. CAD localizes in EBOV inclusion bodies. Huh7 cells were transfected with a plasmid encoding FLAG/HA-CAD. 48 h post-transfection, the cells were infected with rgEBOV at an MOI of 1. After incubation for 16 h, the cells were fixed with 10 % formalin and permeabilized with Triton X-100. CAD (shown in green) was detected with an anti-FLAG antibody and NP (shown in red) with an anti-NP antibody. The nuclei were stained with DAPI (shown in blue), and the cells were visualized by confocal laser scanning microscopy. Scale bars indicate 10 μm. The arrows point out colocalization and the insets show magnifications of the indicated areas. Merge shows an overlay of all three channels. Figure modified from [Brandt 2020] under CC BY 4.0 license. Copyright © 2020 Janine Brandt, Lisa Wendt, Bianca Bodmer, Thomas C Mettenleiter, Thomas Hoenen. <https://doi.org/10.3390/cells9010187>.

3.2.8 The GLN domain of CAD is responsible for accumulation in inclusion bodies

To assess the role of individual CAD domains on its localization in inclusion bodies, I studied CAD deletion mutants, focusing on the GLN and CPS domain by performing IFA using CAD domain deletion mutants.

The single expression of CAD deletion mutants showed a similar intracellular distribution and protein expression compared to wildtype CAD (Figure 26). Interestingly, recruitment into NP-induced inclusion bodies was still observed during coexpression of NP and CAD- Δ CPS, indication that the CPS domain of CAD is dispensable for relocalization into inclusion bodies. In contrast, no colocalization with inclusion bodies was detected when NP was expressed together with CAD- Δ GLN, concluding that the GLN domain is required for recruitment and accumulation in NP-induced inclusion bodies.

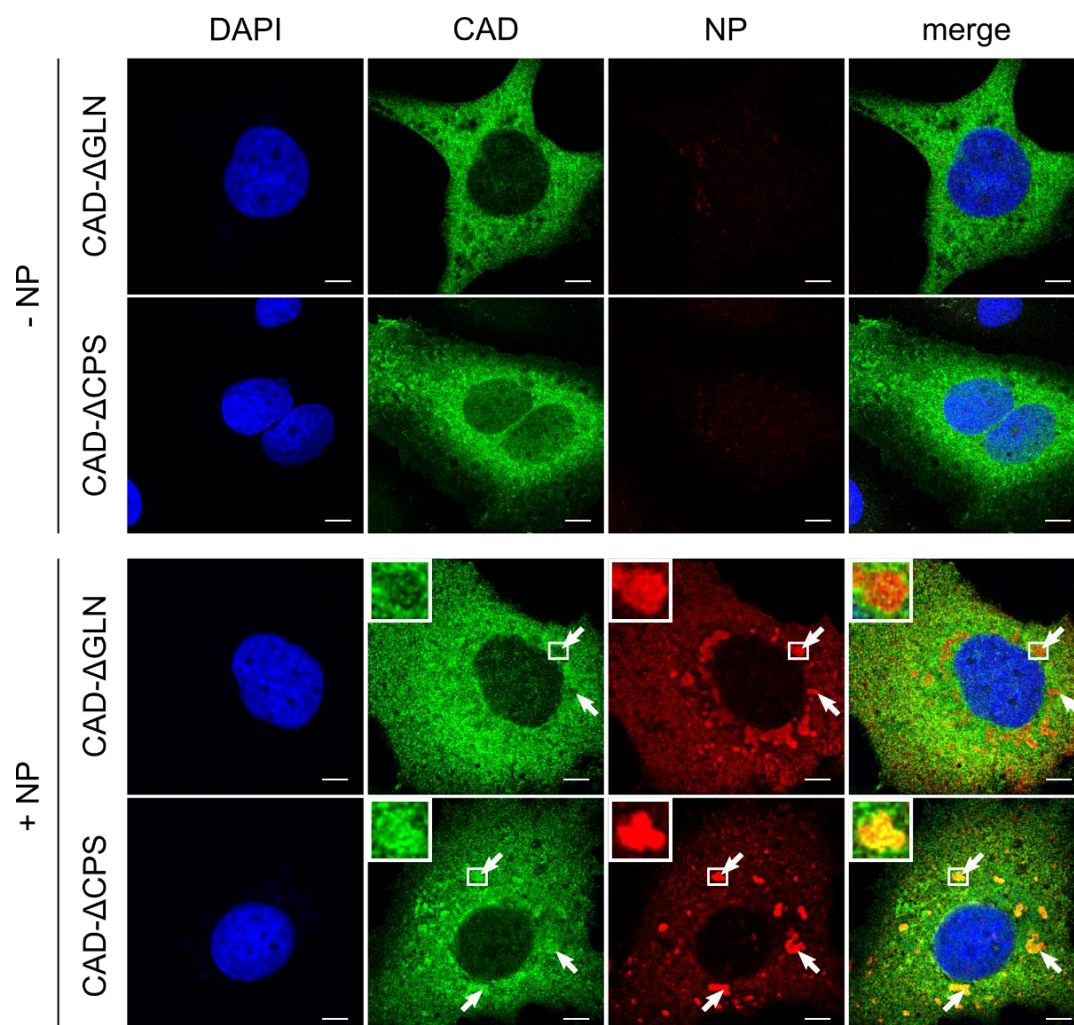


Figure 26. Recruitment of CAD deletion mutants into inclusion bodies. Huh7 cells overexpressing FLAG/HA-CAD- Δ GLN, FLAG/HA-CAD- Δ CPS and EBOV-NP, as indicated, were fixed with 4 % PFA and

permeabilized with 0.1 % Triton X-100 48 h post-transfection. FLAG-tagged CAD (shown in green) was detected using an anti-FLAG antibody and NP (shown in red) was stained with EBOV anti-NP antibodies. The nuclei were stained with DAPI (shown in blue), and the cells were visualized by confocal laser scanning microscopy. Scale bars indicate 10 μ m. The arrows point out inclusion bodies, and the insets show magnifications of the indicated areas. Merge shows an overlay of all three channels. Figure modified from [Brandt 2020] under CC BY 4.0 license. Copyright © 2020 Janine Brandt, Lisa Wendt, Bianca Bodmer, Thomas C Mettenleiter, Thomas Hoenen. <https://doi.org/10.3390/cells9010187>.

Overall, it was shown that CAD is recruited into NP-induced and EBOV-induced inclusion bodies to provide sufficient amounts of pyrimidines for viral genome replication and transcription. Furthermore, it was demonstrated that the GLN domain of CAD is required for recruitment into inclusion bodies, but that the CPS domain is not necessary for this.

3.3 Role of NXF1 during the EBOV lifecycle

Besides CAD, the nuclear export factor 1 (NXF1) has been identified to be important for EBOV RNA synthesis and/or viral protein expression during a genome-wide siRNA screen (Martin, Chiramel et al. 2018). NXF1 is important for export of mRNA from the nucleus into the cytoplasm and therefore crucial by connecting DNA transcription and mRNA translation. Although it was shown that NXF1 is important for the lifecycle of EBOV in the context of infectious virus, EBOV replication and transcription takes place in cytoplasmic inclusion bodies and has no connection with the nuclear compartment of the cell. Therefore, the function of NXF1 during an EBOV infection has to be different from what has been previously described. In order to analyze the functional interaction between NXF1 and EBOV, NXF1 knockdown and overexpression in connection with different minigenome systems as well as IFA was used.

3.3.1 Quantification of NXF1 knockdown

Before the role of NXF1 knockdown on different aspects of the EBOV lifecycle was investigated, the efficiency of endogenous NXF1 siRNA knockdown was assessed. To this end, HEK 293T cells were reverse transfected with two different siRNAs against endogenous NXF1 (NXF1-siRNA #1, NXF1-siRNA #2) or a ctrl siRNA and NXF1 expression levels were detected by quantitative Western blotting.

NXF1 knockdown resulted in a 70 % to 90 % reduction in endogenous NXF1 expression levels for the two different siRNAs compared to the ctrl siRNA (Figure 27A and 27B), indicating that siRNA knockdown of NXF1 is highly efficient.

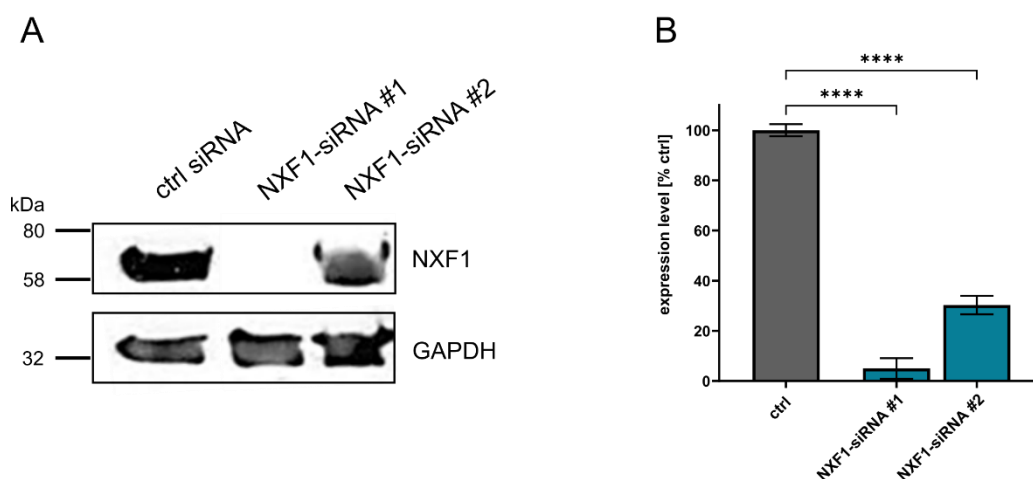


Figure 27. Quantification of siRNA knockdown. **(A)** Analysis of NXF1 knockdown. 293T cells were transfected with siRNAs targeting NXF1 (NXF1-siRNA #1, NXF1-siRNA #2), or a negative control (ctrl siRNA). The cells were harvested 48 h post-transfection and the lysates were subjected to SDS-PAGE and Western blotting. **(B)** Quantification of NXF1 knockdown. The Western blot signals for NXF1 knockdown (as shown in Figure 27A) were measured and normalized to the GAPDH signals. The negative control (ctrl siRNA) was set to 100 % and the efficiency of NXF1 knockdown was calculated. The means and standard deviations of 3 independent experiments are shown for each panel. Asterisks indicate p-values from a one-way ANOVA (**** $p \leq 0.0001$).

3.3.2 NXF1 is important for EBOV RNA synthesis

In order to confirm the results from the genome-wide siRNA screen with the optimized knockdown protocol and to analyze the influence of NXF1 overexpression on EBOV RNA synthesis, a classical minigenome assay in the context of a siRNA-mediated knockdown or an overexpression of NXF1 was performed.

As shown before, knockdown of NXF1 led to a strong reduction in reporter activity, confirming a role of NXF1 in viral RNA synthesis and/or protein expression (Figure 28A). In contrast, NXF1 overexpression had no effect on reporter activity, suggesting that endogenous levels of NXF1 are sufficient for its function during the EBOV lifecycle (Figure 28B) and that excess amounts of NXF1 do not negatively affect viral RNA synthesis and protein expression.

To avoid artificial aspects from the monocistronic minigenome system and to further confirm these results, a trVLP assay was performed. Unfortunately, in case of NXF1 knockdown in target cells I observed strong cytotoxicity and detachment of these cells, so that I only could reliably evaluate results from NXF1 overexpression in this experimental context.

As expected, overexpression of NXF1 had no influence on reporter activity compared to the pCAGGS control, indicating that endogenous levels of NXF1 are indeed sufficient for EBOV RNA synthesis and protein expression (Figure 28C).

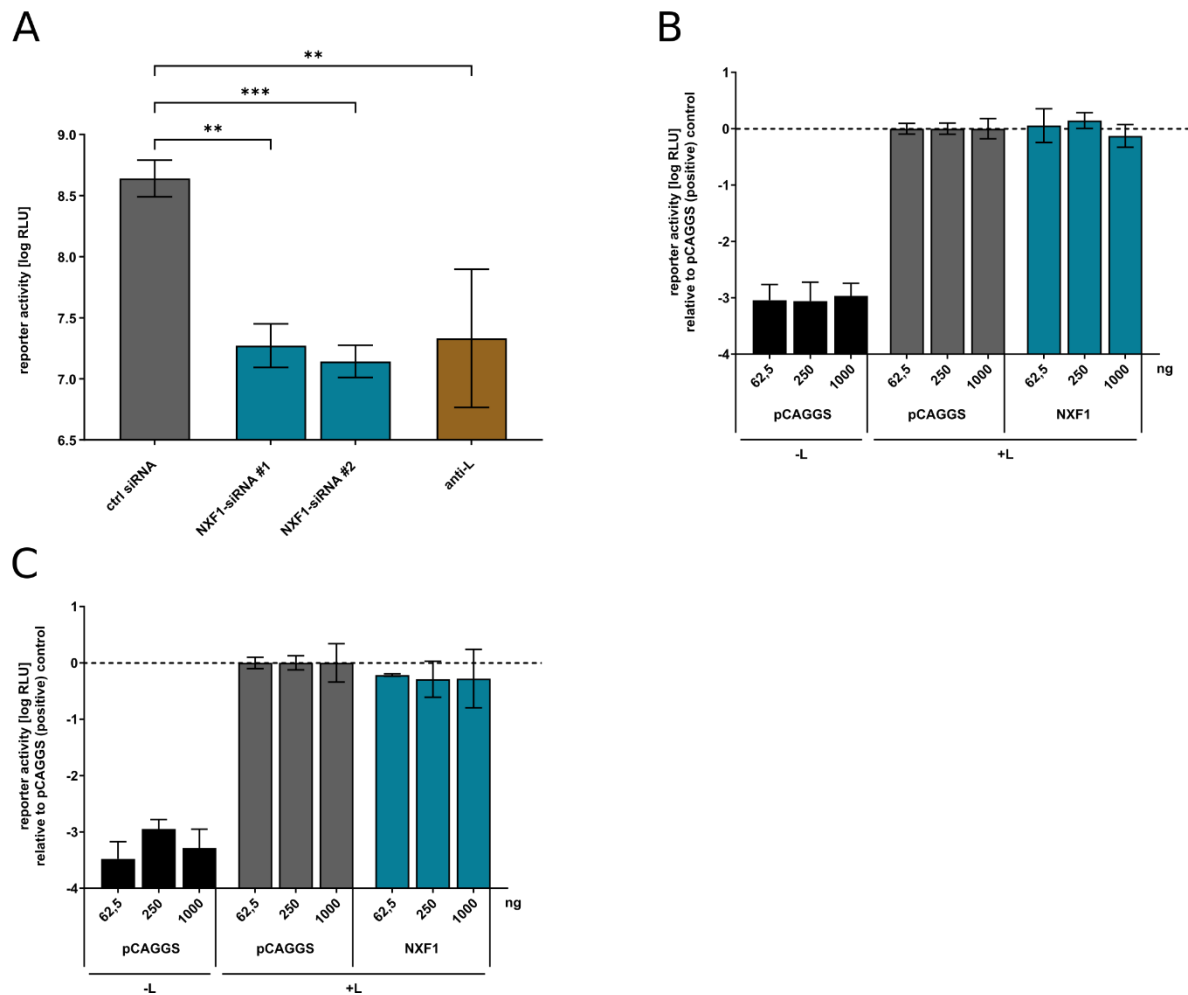


Figure 28. Influence of NXF1 knockdown and overexpression on the Ebola virus life cycle. **(A)** Analysis of NXF1 knockdown on EBOV total RNA synthesis. 293T cells were transfected with siRNAs targeting either NXF1 (NXF1-siRNA #1, NXF1-siRNA #2), EBOV-L (anti-L), or a negative control (ctrl siRNA). 48 h post-transfection, cells were transfected with all the components required for a replication-competent minigenome assay. Another 48 h later, cells were harvested and the reporter activity was measured. **(B)** Influence of NXF1 overexpression on EBOV total RNA synthesis. HEK 293T cells were transfected with all components required for a replication-competent minigenome assay, as well as different amounts (62.5 ng, 250 ng and 1000 ng) of a vector encoding for NXF1 wildtype or the empty vector pCAGGS. Cells were harvested and reporter activity was measured 48 h post transfection. **(C)** Role of NXF1 overexpression for EBOV RNA synthesis in trVLP assay. p1 293T cells were transfected with plasmids encoding for the EBOV RNP proteins and the attachment factor Tim 1 as well as different amounts (62.5 ng, 250 ng and 1000 ng) of a vector encoding for NXF1 wildtype or the empty vector pCAGGS. 24 h post transfection, cells were infected with trVLPs containing a tetracistronic minigenome and cells were harvested 48 h post infection. The means and standard deviations of 3 [(A), (C)] or 5

(B) independent experiments are shown for each panel. Asterisks indicate p-values from a one-way ANOVA (* $p \leq 0.05$; ** $p \leq 0.01$; *** $p \leq 0.001$; **** $p \leq 0.0001$; ns: $p > 0.05$). Figure modified from [Wendt 2020] under CC BY 4.0 license. Copyright © 2020 Lisa Wendt, Janine Brandt, Bianca Bodmer, Sven Reiche, Marie-Luisa Schmidt, Shelby Traeger, Thomas Hoenen. <https://doi.org/10.3390/cells9010187>.

3.3.3 NXF1 knockdown affects EBOV transcription and/or protein expression

To distinguish between a role of NXF1 in viral replication on the one hand and viral transcription and/or protein expression on the other hand, a replication-deficient minigenome system was performed as previous described. As NXF1 overexpression had no effect on total viral RNA synthesis and protein expression, only the influence of NXF1 knockdown on EBOV transcription and/or protein expression was investigated. By using this minigenome system, NXF1 knockdown resulted in an 11.2 to 33.5-fold reduction in reporter activity, indicating that NXF1 is important for either EBOV transcription or protein expression independent of viral genome replication (Figure 29).

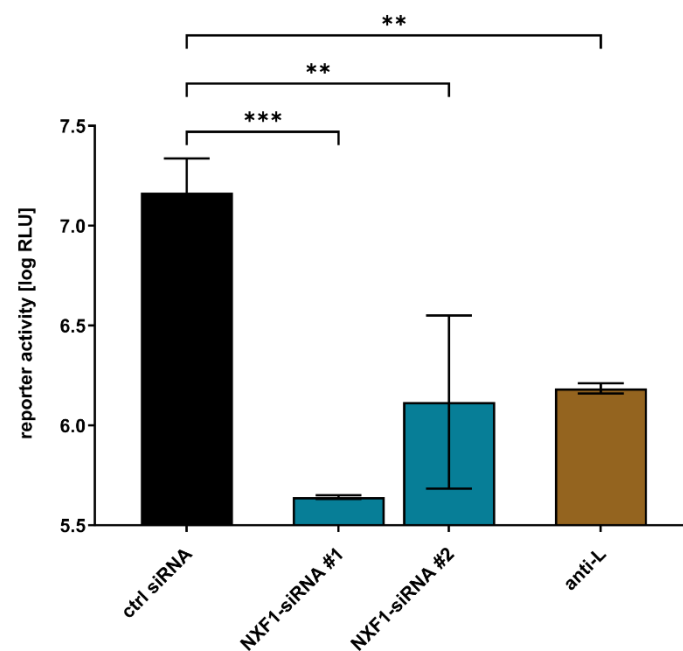


Figure 29. Analysis of viral RNA transcription and protein expression in NXF1 knockdown cells. 293T cells were transfected with siRNAs targeting either NXF1 (NXF1-siRNA #1, NXF1-siRNA #2), EBOV-L (anti-L), or a negative control (ctrl siRNA). 48 h post-transfection, cells were transfected with all the components required for a replication-deficient minigenome assay. Another 48 h later, cells were harvested and the reporter activity was measured. The means and standard deviations of 3 independent experiments are shown. Asterisks indicate p-values from a one-way ANOVA (* $p \leq 0.05$; ** $p \leq 0.01$; *** $p \leq 0.001$; **** $p \leq 0.0001$; ns: $p > 0.05$). Figure modified from [Wendt 2020] under CC BY 4.0 license. Copyright © 2020 Lisa Wendt, Janine Brandt, Bianca Bodmer, Sven Reiche, Marie-Luisa Schmidt, Shelby Traeger, Thomas Hoenen. <https://doi.org/10.3390/cells9010187>.

3.3.4 Influence of NXF1 knockdown on EBOV genome replication and mRNA transcription

In order to discriminate an effect of NXF1 knockdown on EBOV genome replication, mRNA transcription and later steps of viral protein expression such as mRNA transport from inclusion bodies or mRNA translation, a classical minigenome assay in connection with a siRNA knockdown of NXF1 was performed and minigenome-derived viral RNA and mRNA levels were measured using RT-qPCR.

NXF1 siRNA-treated cells showed a slight reduction in vRNA levels, while mRNA levels remained at a similar level compared to the control cells (Figure 30A and 30B). This observation indicates that NXF1 seems not to be important for mRNA transcription, but rather later steps in mRNA processing.

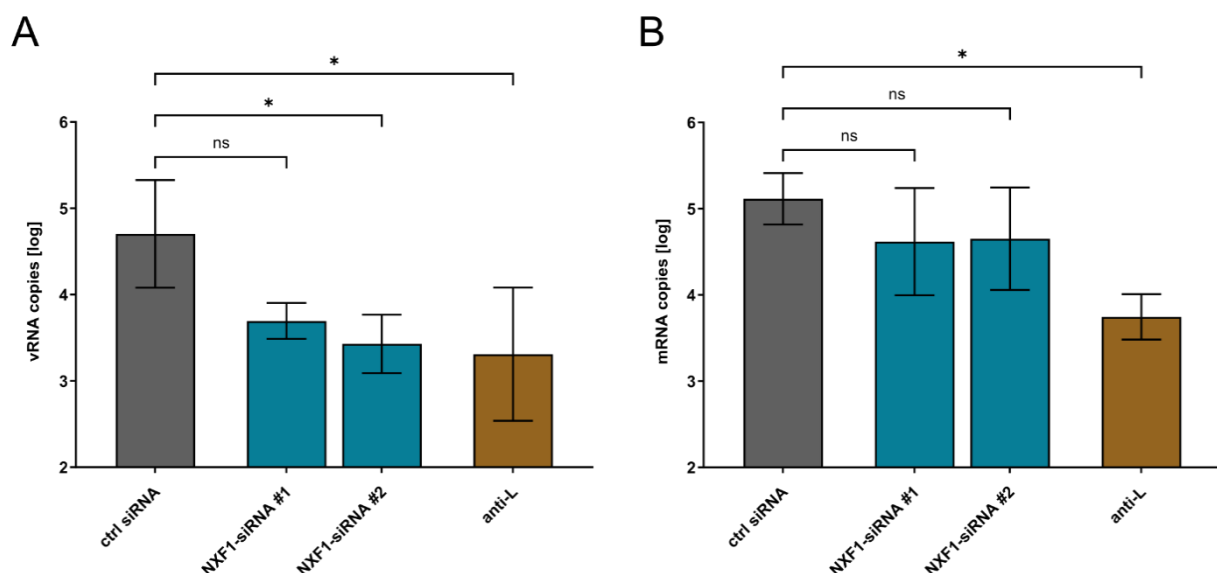


Figure 30. Analysis of viral RNA and mRNA levels in NXF1 knockdown cells. **(A)** Impact of NXF1 knockdown on EBOV replication. 293T cells were transfected with siRNAs targeting either NXF1 (NXF1-siRNA), EBOV-L (anti-L), or a negative control (ctrl siRNA). 48 h post-transfection, cells were transfected with all the components required for a replication-competent minigenome assay. After cell harvesting, RNA was extracted from the cell lysates and RT-qPCR for vRNA was performed. **(B)** Influence of NXF1 knockdown on EBOV mRNA levels. Cells were treated as described above. After cell harvesting, RNA was extracted from cell lysates and RT-qPCR for mRNA was performed. The means and standard deviations of 3 independent experiments are shown for each panel. Asterisks indicate p-values from a one-way ANOVA (* $p \leq 0.05$; ** $p \leq 0.01$; *** $p \leq 0.001$; **** $p \leq 0.0001$; ns: $p > 0.05$). Figure modified from [Wendt 2020] under CC BY 4.0 license. Copyright © 2020 Lisa Wendt, Janine Brandt, Bianca Bodmer, Sven Reiche, Marie-Luisa Schmidt, Shelby Traeger, Thomas Hoenen. <https://doi.org/10.3390/cells9010187>.

3.3.5 Establishment of a complementation assay for NXF1 knockdown

The function of NXF1 is facilitated by its five distinct domains, each contributing to a specific role during nuclear export of RNA. In order to analyze which domain of NXF1

is required for the EBOV lifecycle, a complementation assay, in which NXF1 siRNA-knockdown cells are transfected with vectors encoding for siRNA-resistant NXF1 wildtype or NXF1 deletion mutants, was established.

3.3.5.1 Generation of NXF1 and NXF1 deletion mutant vectors for complementation assay

To investigate the role of each NXF1 domain for EBOV RNA synthesis, plasmids containing a knockout of the siRNA binding site for every NXF1 mutant were first generated. Because of its lower cell toxicity, the NXF1-siRNA #2 was chosen, out of the two NXF1-siRNAs available, as the most suitable for this assay.

The binding site for this siRNA is located in the RRM domain of NXF1 and has the following sequence: CGA AGG ATA TCT ATC ATC. Since siRNAs require matching sequences to target mRNAs, forward and reverse Primers were designed each containing three modified codons of the siRNA binding sequence. To avoid a disruption of the amino acid sequence, only every third nucleotide was exchanged, using the next frequently used codon for each encoded amino acid, resulting in the following altered sequence of the siRNA binding site: CGG AGA ATC TCC ATT ATT (nucleotides that differ from the original sequence are marked in red). Cloning was performed by PCR amplification using plasmids encoding for NXF1 or NXF1 mutants (except of NXF1- Δ RRM) as templates and the two designed primers. The PCR products were afterwards digested with restriction endonucleases and cloned into pCAGGS (Table 3). Additionally, NXF1 double deletion mutants as well as an NXF1- Δ RRM- Δ LRR mutant containing a long linker sequence between the RBD and NTF2 domain to facilitate correct folding of NXF1 were generated by molecular cloning (Table 3).

Table 3. List of plasmids generated by molecular cloning

Plasmids
pCAGGS-flag-HA-NXF1- Δ siRNA
pCAGGS-flag-HA-NXF1- Δ RBD- Δ siRNA
pCAGGS-flag-HA-NXF1- Δ LRR- Δ siRNA
pCAGGS-flag-HA-NXF1- Δ NTF2- Δ siRNA
pCAGGS-flag-HA-NXF1- Δ UBA- Δ siRNA
pCAGGS-flag-HA-NXF1- Δ RRM- Δ LRR
pCAGGS-flag-HA-NXF1- Δ RRM- Δ LRR-long-Linker

3.3.5.2 The RBD but not RRM domain of NXF1 is important for later steps in EBOV mRNA processing

After generation of all NXF1 vectors needed, expression levels of every construct was quantified by Western blotting and adjusted to NXF1 wildtype. Next, a complementation assay was performed using a replication-deficient minigenome system in presence of NXF1-siRNA #2 as well as overexpressed siRNA-resistant NXF1 or NXF1 deletion mutants.

As previously shown, treatment of NXF1 knockdown cells with the empty vector pCAGGS resulted in a strong reduction in reporter activity, confirming a role of NXF1 in later steps of EBOV mRNA processing (Figure 31). In strong contrast, addition of a vector encoding for NXF1 wildtype led to an increase in reporter activity, concluding that siRNA knockdown of NXF1 is specific and can be compensated by exogenous NXF1. Similar to that, supplementation of NXF1- Δ RRM to NXF1 siRNA-treated cells showed also an increase in reporter activity, indicating that the RRM domain of NXF1 is not required for EBOV mRNA processing. In contrast, when complementing NXF1 knockdown cells with the NXF1 deletion mutants Δ RBD, Δ LRR, Δ NTF2 and Δ UBA no increase in reporter activity was observed, suggesting that these domains might be important for the EBOV lifecycle. However, in case of NXF1- Δ NTF2 immunofluorescence analysis showed that this mutant is not able to exit the nucleus, so that its functionality in this assay remains questionable (see section 3.3.9). Additionally, for NXF1- Δ LRR and the double deletion mutant Δ RRM- Δ LRR intramolecular interactions between the RBD and NTF2 domain might be disrupted due to the missing domains, so that it is not clear whether this is the cause for lack of complementation or whether the domains themselves are functionally required. However, complementation with Δ RRM- Δ LRR-long-Linker, a mutant where RRM and LRR are replaced by a long flexible linker, did not show an increase in reporter activity. This suggests that the LRR domain itself might indeed be important for EBOV mRNA processing.

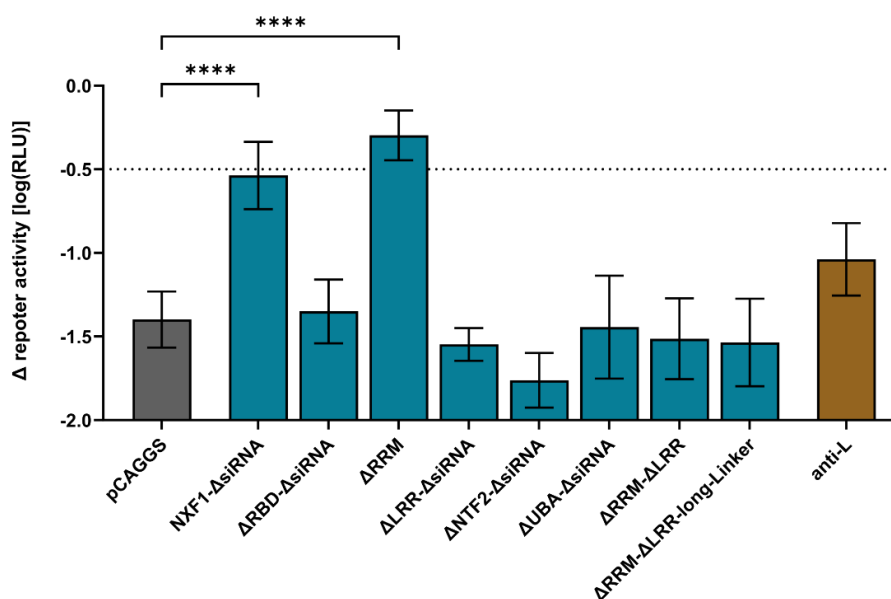


Figure 31. Influence of NXF1 domains on EBOV mRNA processing. HEK 293T cells were transfected with siRNAs targeting either NXF1 (NXF1-siRNA #2), EBOV-L (anti-L), or a negative control (ctrl siRNA). 48 h post-transfection, cells were transfected with all the components required for a replication-deficient minigenome assay as well as NXF1 constructs or pCAGGS as control. The cells were harvested after an additional incubation period of 48 hours and reporter activity was measured. To display reporter activity reduction, a negative influence on reporter activity obtained for NXF1 or NXF1 mutants was subtracted from the reporter activity obtained for each construct in cells transfected with control siRNA. The means and standard deviations of at least 3 independent experiments are shown for each panel. Asterisks indicate p-values from a one-way ANOVA (* $p \leq 0.05$; ** $p \leq 0.01$; *** $p \leq 0.001$; **** $p \leq 0.0001$; ns: $p > 0.05$).

3.3.6 NXF1 is recruited into NP-derived inclusion bodies

Since NXF1 has been shown to be important for EBOV mRNA processing, an immunofluorescence assay was performed to analyze whether an overexpression of EBOV-NP and, inclusion body formation has an influence on the intracellular distribution of NXF1, and whether recruitment of NXF1 into NP-induced inclusion bodies can be observed. To this end, Huh7 cells were transfected with plasmids encoding for either NXF1, NP or both. Additionally, as heterodimerization of NXF1 with p15 is required for NXF1 mediated nuclear RNA export by maintaining the proper folding and function of the NTF2-like domain of NXF1, p15 was always co-expressed with NXF1, NXF1 single domains and NXF1 deletion mutants in this thesis (Braun, Herold et al. 2001, Fribourg, Braun et al. 2001, Guzik, Levesque et al. 2001, Wiegand, Coburn et al. 2002). 48 h post transfection IFA was performed and samples were analyzed using a confocal laser scanning microscope.

As previously described, single expression of NXF1 led to a nuclear distribution and a localization at the nuclear rim, which has been shown to be mediated by the NTF2 and

UBA domain (Figure 32) (Fribourg, Braun et al. 2001). Additionally, overexpression of NXF1 also led to a cytoplasmic localization in globular compartments, which are believed to be stress granules, as has been previously described for NXF1 (Hochberg-Lauer, Schwed-Gross et al. 2019). Interestingly, coexpression of NP and NXF1 led to a slight relocalization of NXF1 into NP-induced inclusion bodies, demonstrating that NXF1 is able to enter inclusion bodies and has the potential to influence EBOV mRNA processing directly at this site.

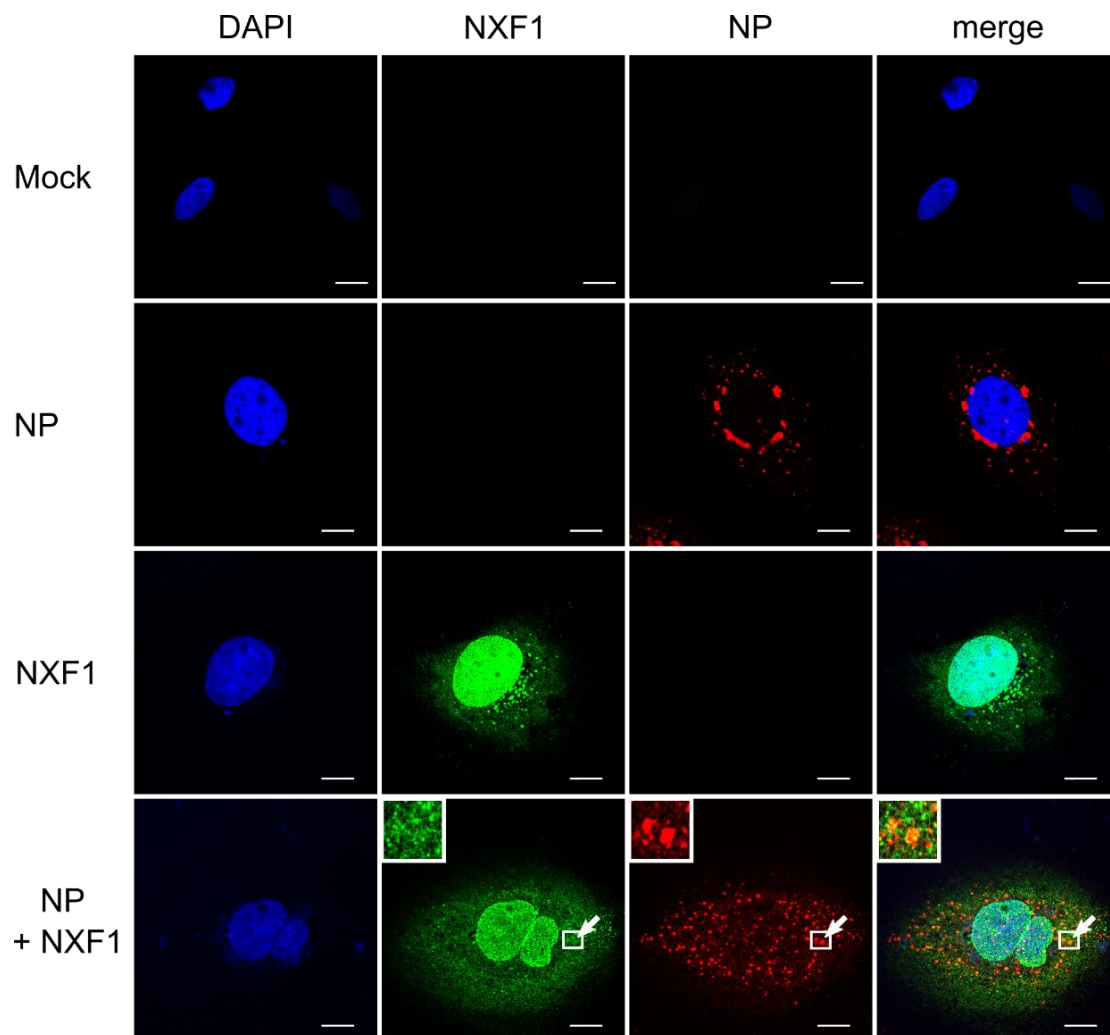


Figure 32. Recruitment of NXF1 into NP-derived inclusion bodies. Huh7 cells were transfected with plasmids encoding flag/HA-NXF1 or EBOV-NP as indicated. 48 h post-transfection, the cells were fixed with 4 % paraformaldehyde and permeabilized with 0.1 % Triton X-100. FLAG-tagged NXF1 (shown in green) was detected using an anti-FLAG antibody and NP (shown in red) was stained with anti-EBOV NP antibodies. Nuclei were stained with DAPI (shown in blue), and cells were visualized by confocal laser scanning microscopy. Scale bars indicate 10 μ m. The arrows point out inclusion bodies, and the insets show magnifications of the indicated areas. Merge shows an overlay of all three channels. Figure modified from [Wendt 2020] under CC BY 4.0 license. Copyright © 2020 Lisa Wendt, Janine Brandt, Bianca Bodmer, Sven Reiche, Marie-Luisa Schmidt, Shelby Traeger, Thomas Hoenen. <https://doi.org/10.3390/cells9010187>.

3.3.7 NTF2 and UBA domains of NXF1 are responsible for recruitment into inclusion bodies

To analyze which domains are important for the recruitment of NXF1 in NP-induced inclusion bodies, Huh7 cells were transfected with NXF1 single domain mutants and/or NP. 48 h post transfection IFA was performed and samples were analyzed using a confocal laser scanning microscope.

Surprisingly, the sole overexpression of each domain led to different cellular distributions (Figure 33). While the LRR, NTF2 and UBA domains showed a localization throughout the cell, including cytoplasmic and nuclear compartments, expression of the RBD domain resulted in a strong nuclear localization, but without nuclear rim staining as it was seen for NXF1 wildtype. In strong contrast to this, the sole expression of the RRM domain led to spatial aggregation in stress granule-like structures within the cytoplasm.

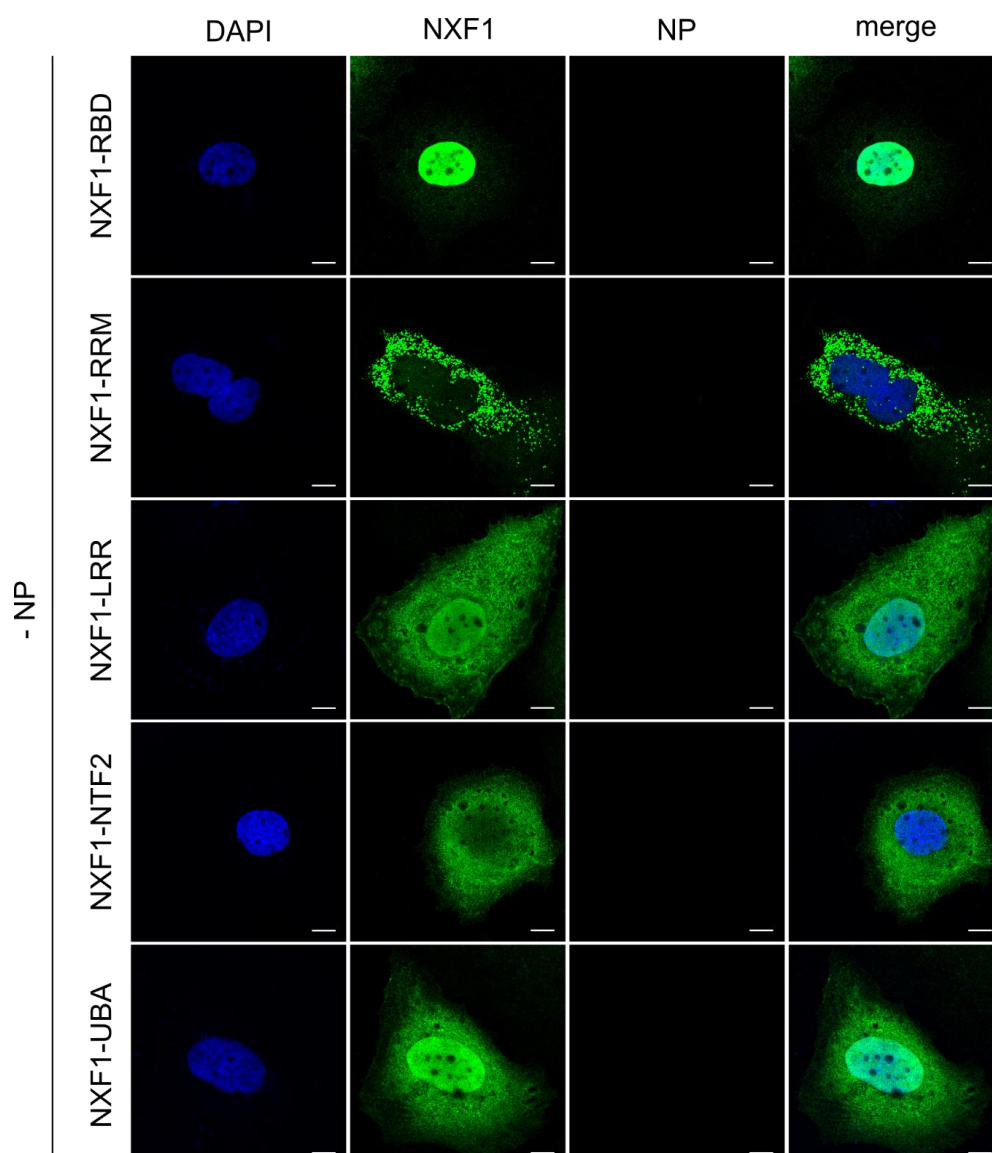


Figure 33. Single expression of NXF1 domain mutants. Huh7 cells were transfected with plasmids encoding flag/HA-NXF1 single domains as indicated. 48 h post-transfection, the cells were fixed with 4 % paraformaldehyde and permeabilized with 0.1 % Triton X-100. FLAG-tagged NXF1 domains (shown in green) were detected using an anti-FLAG antibody. Nuclei were stained with DAPI (shown in blue), and cells were visualized by confocal laser scanning microscopy. Scale bars indicate 10 μ m. Merge shows an overlay of all three channels.

However, during coexpression with NP the NTF2 and UBA domain clearly accumulated in inclusion bodies, while for the RBD, RRM and LRR domain no relocation in NP-derived inclusion bodies was observed, suggesting that the NTF2 and UBA domains of NXF1 could be responsible for recruitment of NXF1 to the sites of EBOV replication and transcription (Figure 34).

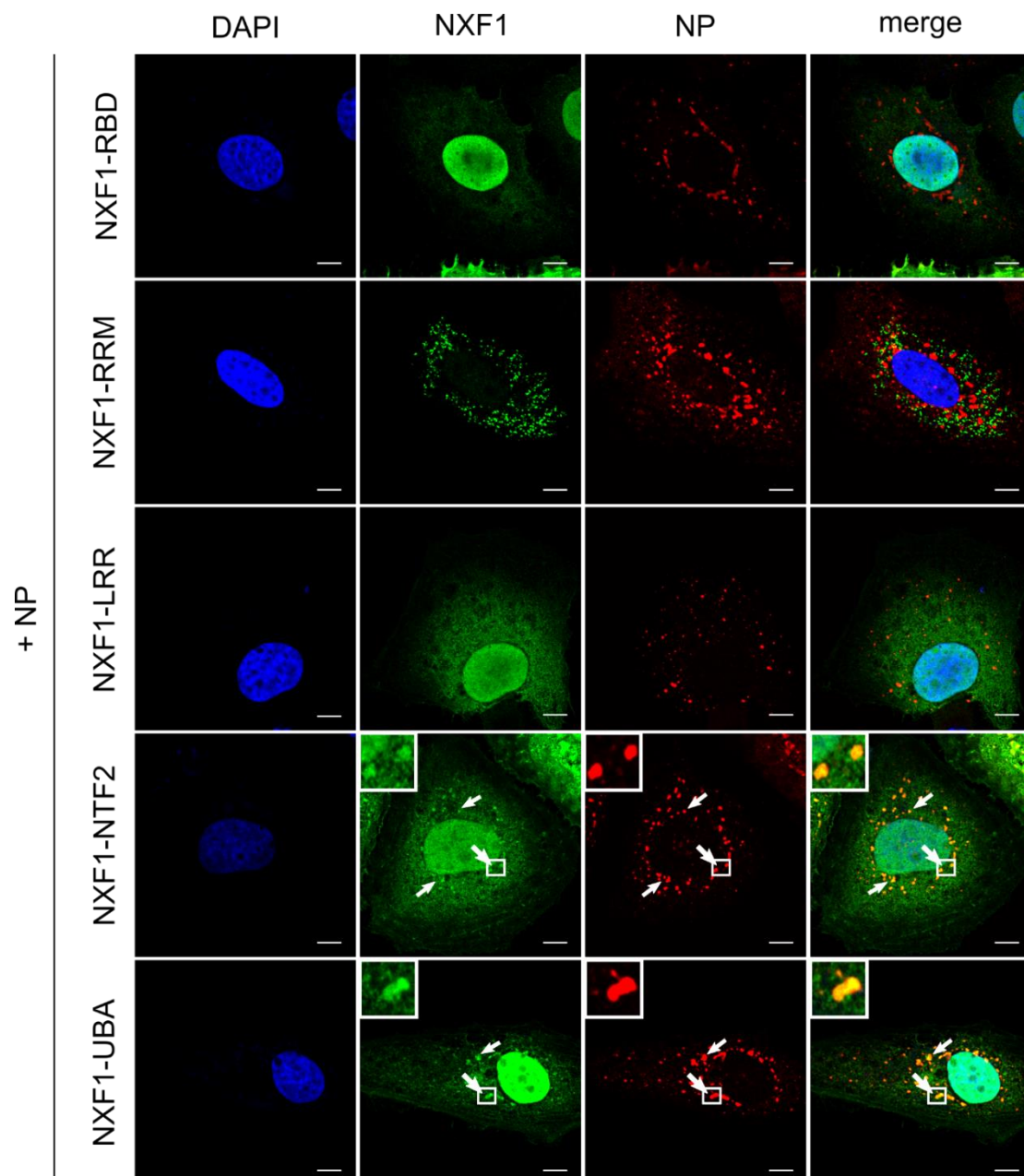


Figure 34. Influence of NXF1 single domains on NXF1 recruitment into NP-induced inclusion bodies. Huh7 cells were transfected with plasmids encoding flag/HA-NXF1 single domains and EBOV-NP as indicated. 48 h post-transfection, the cells were fixed with 4 % paraformaldehyde and permeabilized with 0.1 % Triton X-100. FLAG-tagged NXF1 domains (shown in green) were detected using an anti-FLAG antibody and NP (shown in red) was stained with anti-EBOV NP antibodies. Nuclei were stained with DAPI (shown in blue), and cells were visualized by confocal laser scanning microscopy. Scale bars indicate 10 μ m. The arrows point out inclusion bodies, and the insets show magnifications of the indicated areas. Merge shows an overlay of all three channels.

3.3.8 Analysis of the role of nucleoporins on recruitment of NXF1 into inclusion bodies

While the NTF2 and UBA domain of NXF1 were suggested to be important for localization in NP-induced inclusion bodies, the mechanism of how NXF1 is recruited to inclusion bodies and which interactions are necessary for entering them still remained elusive. However, since both the NTF2 and UBA domain are mainly required for nucleoporin interaction by binding to FG-rich repeats during mRNA export, an involvement of nucleoporins in the recruitment of NXF1 in inclusion bodies was investigated (Fribourg, Braun et al. 2001). To this end, Huh7 cells were transfected with vectors encoding for NXF1 and NP and IFA was performed 48 h post transfection. Alternatively, instead of expressing NP from a plasmid cells were infected with EBOV. For staining of nucleoporins an anti-NPC (nuclear pore complex) antibody was used. As previously described, NPC staining resulted in a characteristic nuclear rim localization and coexpression with NXF1 led to a strong colocalization, confirming that NXF1 is indeed localized at the nuclear pore complex (NPC) (Figure 35A) (Ben-Yishay, Mor et al. 2019). In difference, no colocalization was observed between the NPC and NP- or EBOV-derived inclusion bodies, indicating that nucleoporins are not localized in inclusion bodies and are most likely not involved in recruitment of NXF1 to these sites (Figure 35B).

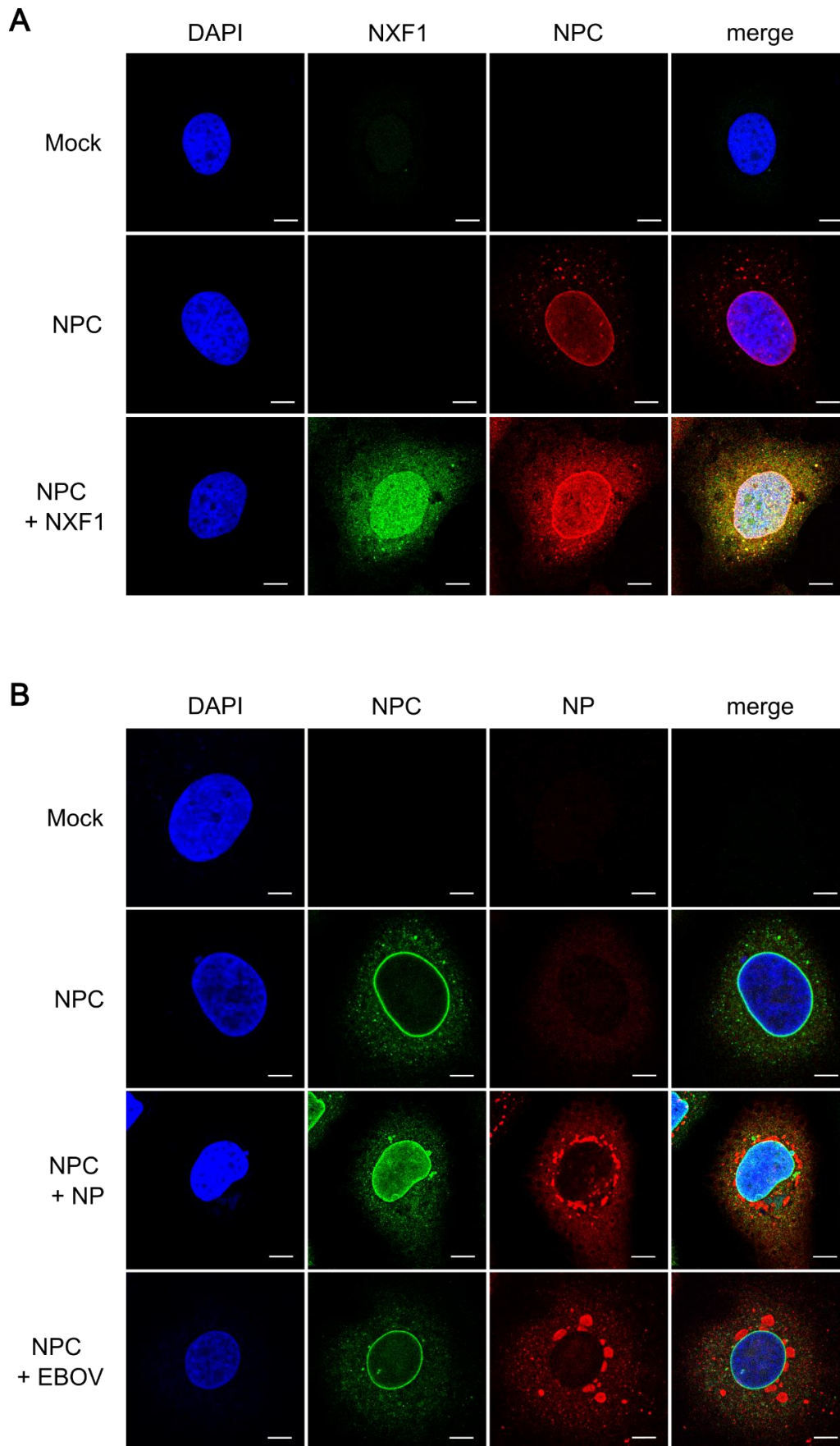


Figure 35. Influence of nucleoporins on NXF1 recruitment into NP-induced inclusion bodies. **(A)** Colocalization analysis between NPC and NXF1. Huh7 cells were transfected with plasmids encoding

flag/HA-NXF1 as indicated. 48 h post-transfection, the cells were fixed with 4 % paraformaldehyde and permeabilized with 0.1 % Triton X-100. FLAG-tagged NXF1 (shown in green) was detected using an anti-FLAG antibody and NPC (shown in red) was stained with anti-NPC antibody. **(B)** Influence of nucleoporins on inclusion body formation. Huh7 cells were transfected with plasmids encoding EBOV-NP or infected with rgEBOV as indicated. 48 h post-transfection/infection, the cells were fixed with 4 % or 10 % paraformaldehyde and permeabilized with 0.1 % Triton X-100. NPC (shown in green) was detected using an anti-NPC antibody and NP (shown in red) was stained with anti-NP antibody. Nuclei were stained with DAPI (shown in blue), and cells were visualized by confocal laser scanning microscopy. Scale bars indicate 10 μ m. The arrows point out inclusion bodies, and the insets show magnifications of the indicated areas. Merge shows an overlay of all three channels.

3.3.9 Influence of NXF1 deletion mutants on the intracellular distribution of NXF1 and relocalization in inclusion bodies

Since the deletion of the RBD, LRR or UBA domain of NXF1 influence the EBOV lifecycle in complementation assay, the intracellular distribution and a possible colocalization with NP-induced inclusion bodies of all NXF1 domain deletion mutants was investigated. For this, Huh7 cells were transfected with NXF1 domain deletion mutants and/or NP.

In contrast to the intracellular localization of NXF1 single domains, the sole expression of NXF1 deletion mutants resulted in a strong nuclear localization comparable to wildtype NXF1 (Figure 36). However, as previously described, expression of NXF1 lacking its NTF2-like domain lead to an almost complete abolishment of nuclear export due to a loss of one nucleoporin-binding site, which resulted in an exclusively nuclear localization of NXF1- Δ NTF2 (Braun, Herold et al. 2002). Therefore, no accumulation of NXF1- Δ NTF2 in inclusion bodies was observed upon co-expression with NP (Figure 37A). In contrast, a clear accumulation in NP-derived inclusion bodies was observed for NXF1- Δ UBA, indicating that a loss of the UBA domain can be compensated by other NXF1 domains, of which in particular the NTF2 domain has also been shown to enter inclusion bodies by itself (see section 3.3.7). However, this phenotype was only observed for samples in which p15 was co-expressed, and omission of p15 resulted in a strong nuclear localization of NXF1- Δ UBA similar to that of NXF1- Δ NTF2 (Figure 37B). Similarly, to NXF1- Δ UBA, NXF1- Δ RBD also accumulated in inclusion bodies, suggesting that the RBD and UBA domain of NXF1 might be required for exit of NXF1 from inclusion bodies. These data are consistent with the results obtained from the complementation assay and confirms an important role of the RBD and UBA domain of NXF1 for the EBOV lifecycle. In contrast, no colocalization was observed for NXF1- Δ RRM and NXF1- Δ LRR with NP-induced inclusion bodies.

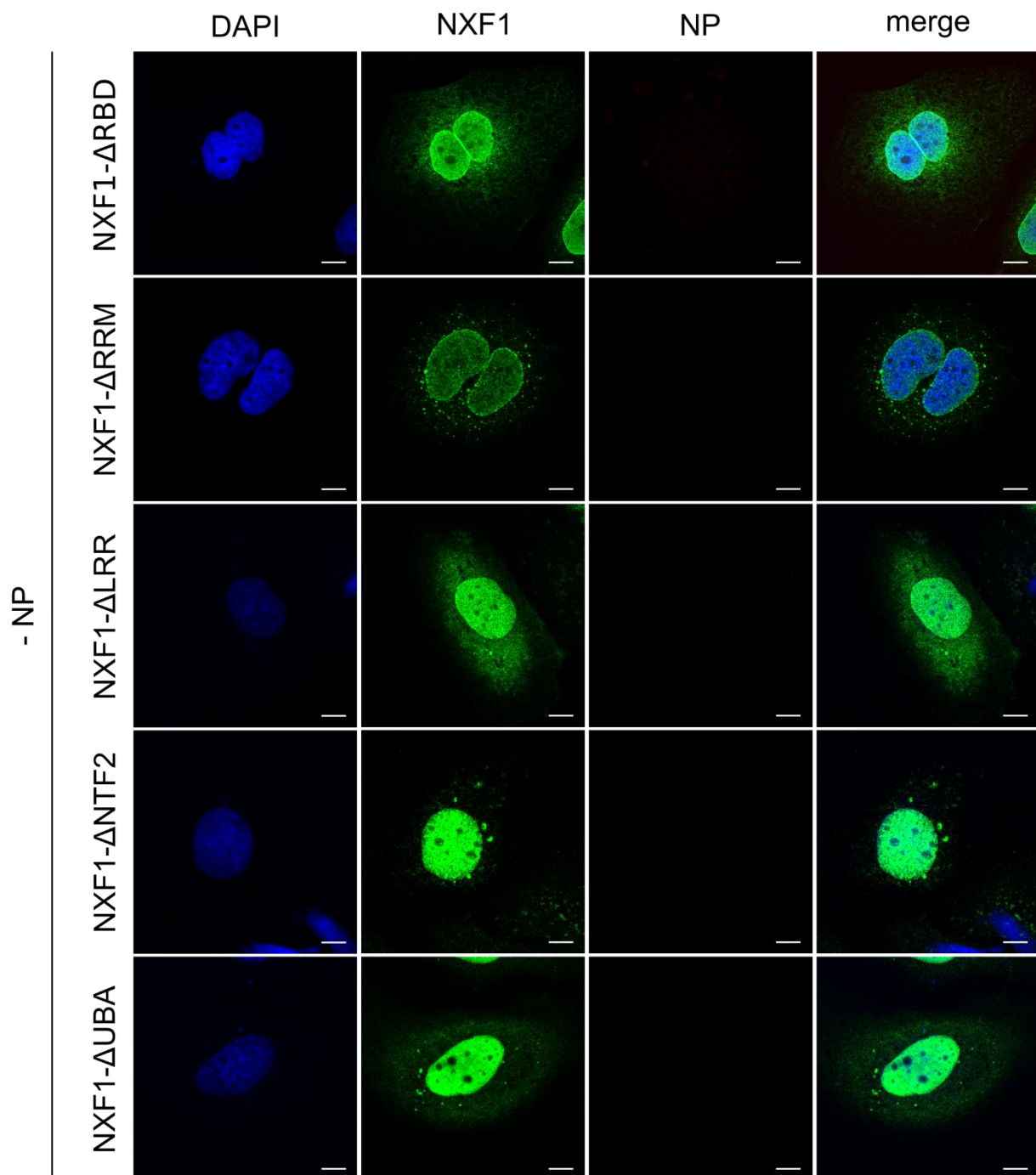


Figure 36. Influence of NXF1 deletion domain mutants on intracellular localisation of NXF1. Huh7 cells were transfected with plasmids encoding flag/HA-NXF1 deletion domain mutants as indicated. 48 h post-transfection, the cells were fixed with 4 % paraformaldehyde and permeabilized with 0.1 % Triton X-100. FLAG-tagged NXF1 deletion mutants (shown in green) were detected using an anti-FLAG antibody. Nuclei were stained with DAPI (shown in blue), and cells were visualized by confocal laser scanning microscopy. Scale bars indicate 10 μ m. Merge shows an overlay of all three channels. Figure modified from [Wendt 2020] under CC BY 4.0 license. Copyright © 2020 Lisa Wendt, Janine Brandt, Bianca Bodmer, Sven Reiche, Marie-Luisa Schmidt, Shelby Traeger, Thomas Hoenen. <https://doi.org/10.3390/cells9010187>.

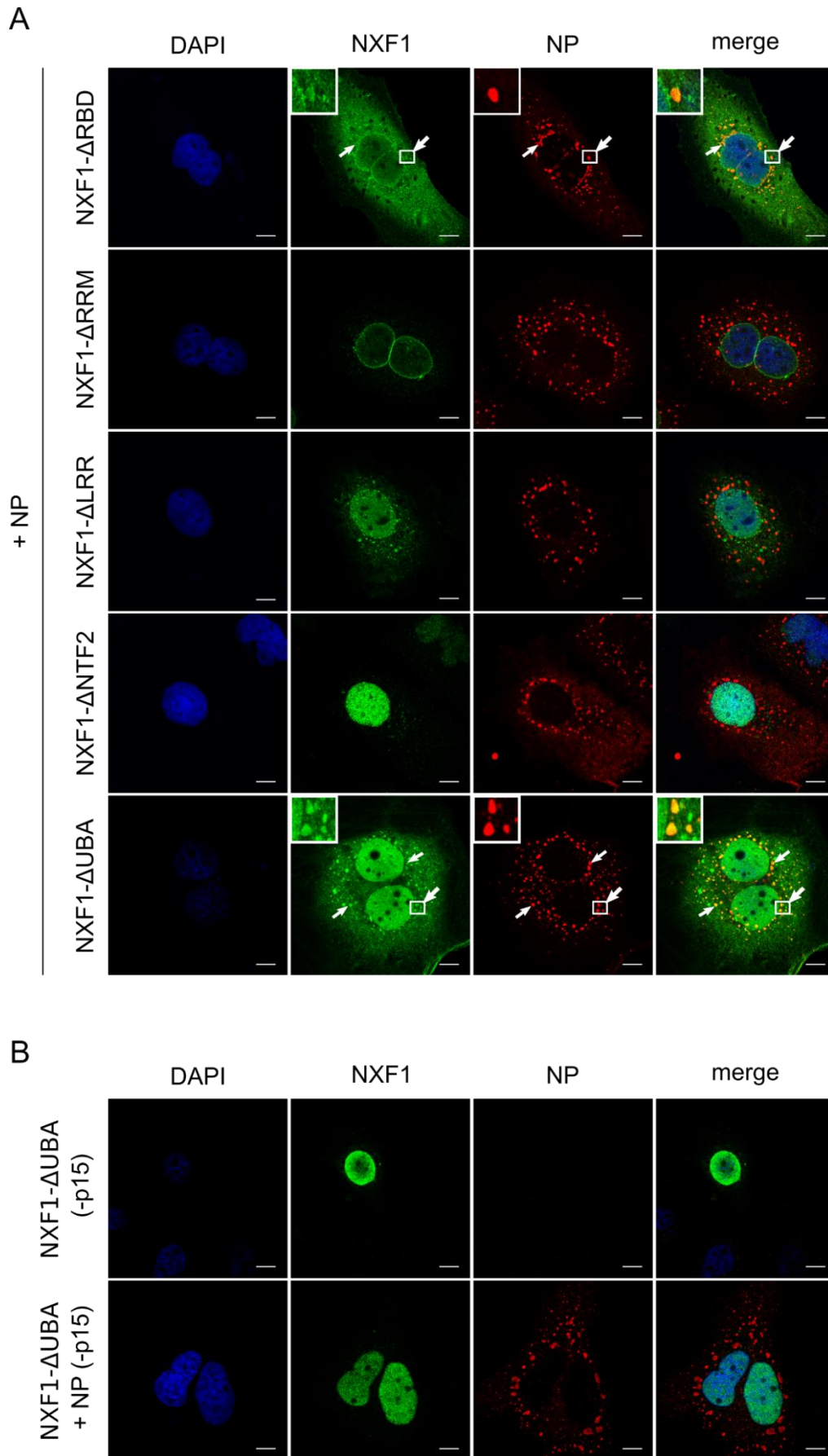


Figure 37. Influence of NXF1 deletion domain mutants on intracellular localisation of NXF1. **(A)** Influence of NXF1 deletion domain mutants on NXF1 recruitment into NP-induced inclusion bodies.

Huh7 cells were transfected with plasmids encoding flag/HA-NXF1 deletion domain mutants and/or EBOV-NP as indicated. 48 h post-transfection, the cells were fixed with 4 % paraformaldehyde and permeabilized with 0.1 % Triton X-100. FLAG-tagged NXF1 deletion mutants (shown in green) were detected using an anti-FLAG antibody and NP (shown in red) was stained with anti-EBOV NP antibodies. Nuclei were stained with DAPI (shown in blue), and cells were visualized by confocal laser scanning microscopy. Scale bars indicate 10 μ m. The arrows point out inclusion bodies, and the insets show magnifications of the indicated areas. Merge shows an overlay of all three channels. Figure modified from [Wendt 2020] under CC BY 4.0 license. Copyright © 2020 Lisa Wendt, Janine Brandt, Bianca Bodmer, Sven Reiche, Marie-Luisa Schmidt, Shelby Traeger, Thomas Hoenen. <https://doi.org/10.3390/cells9010187>. (B) Investigation of the cellular localization of Δ UBA without p15 coexpression. Huh7 cells were transfected with plasmids encoding flag/HA-NXF1- Δ UBA and/or EBOV-NP as indicated. p15 was omitted. 48 h post-transfection, the cells were fixed with 4 % paraformaldehyde and permeabilized with 0.1 % Triton X-100. FLAG-tagged NXF1 (shown in green) was detected using an anti-FLAG antibody and NP (shown in red) was stained with anti-EBOV NP antibodies. Nuclei were stained with DAPI (shown in blue), and cells were visualized by confocal laser scanning microscopy. Scale bars indicate 10 μ m. Merge shows an overlay of all three channels.

3.3.10 RNA binding of both NXF1 and NP is required for exit of NXF1 from inclusion bodies

In the course of this thesis the RBD domain of NXF1 has been shown in the complementation assay and IFA to be important for the function of NXF1 in the EBOV lifecycle and for exit of NXF1 from NP-induced inclusion bodies. As the RBD is mainly necessary for RNA binding of NXF1, IFA was performed using an RNA binding deficient NXF1 mutant, in which 10 arginine residues were replaced by alanine in the RBD domain, to analyze the influence of abolished RNA binding on the cellular distribution of NXF1 (Hautbergue, Hung et al. 2008). For this, Huh7 cells were transfected with RNA binding-deficient NXF1 (NXF1-10RA) and/or NP.

As expected, the single expression of NXF1-10RA resulted in a nuclear localization similar to NXF1 wildtype and NXF1- Δ RBD (Figure 38A). Interestingly, upon co-expression of NXF1-10RA and NP, NXF1-10RA strongly relocalized into NP-induced inclusion bodies, suggesting that the loss of the ability to bind RNA leads to an accumulation of NXF1 in inclusion bodies.

Since RNA binding is also a prominent feature for EBOV-NP, IFA was additionally performed to investigate the influence of an RNA binding-deficient NP on the intracellular localization of NXF1 wildtype. For this, Huh7 cells were first transfected with RNA binding deficient NP (NP- Δ RNA), in which three amino acids K160, K171 and R174 known to be essential for RNA binding were mutated to alanine, in order to compare its cellular localization to wildtype NP.

Comparable to NP wildtype, the single expression of NP- Δ RNA resulted in the formation of inclusion bodies in the perinuclear region of the cell, demonstrating that NP- Δ RNA is still able to form inclusion bodies (Figure 38B).

A key feature of NP is to recruit additional EBOV proteins in inclusion bodies for genome replication and transcription. Since NP- Δ RNA has been shown to form inclusion bodies similar to wildtype NP, the ability of NP- Δ RNA in recruiting other EBOV proteins was also investigated. To this end Huh7 cells were transfected with NP- Δ RNA and EBOV-VP35. Coexpression with VP35 led to a strong relocalization of VP35 to NP- Δ RNA-derived inclusion bodies, indicating that NP- Δ RNA is still functional in recruiting additional EBOV proteins into inclusion bodies (Figure 38B).

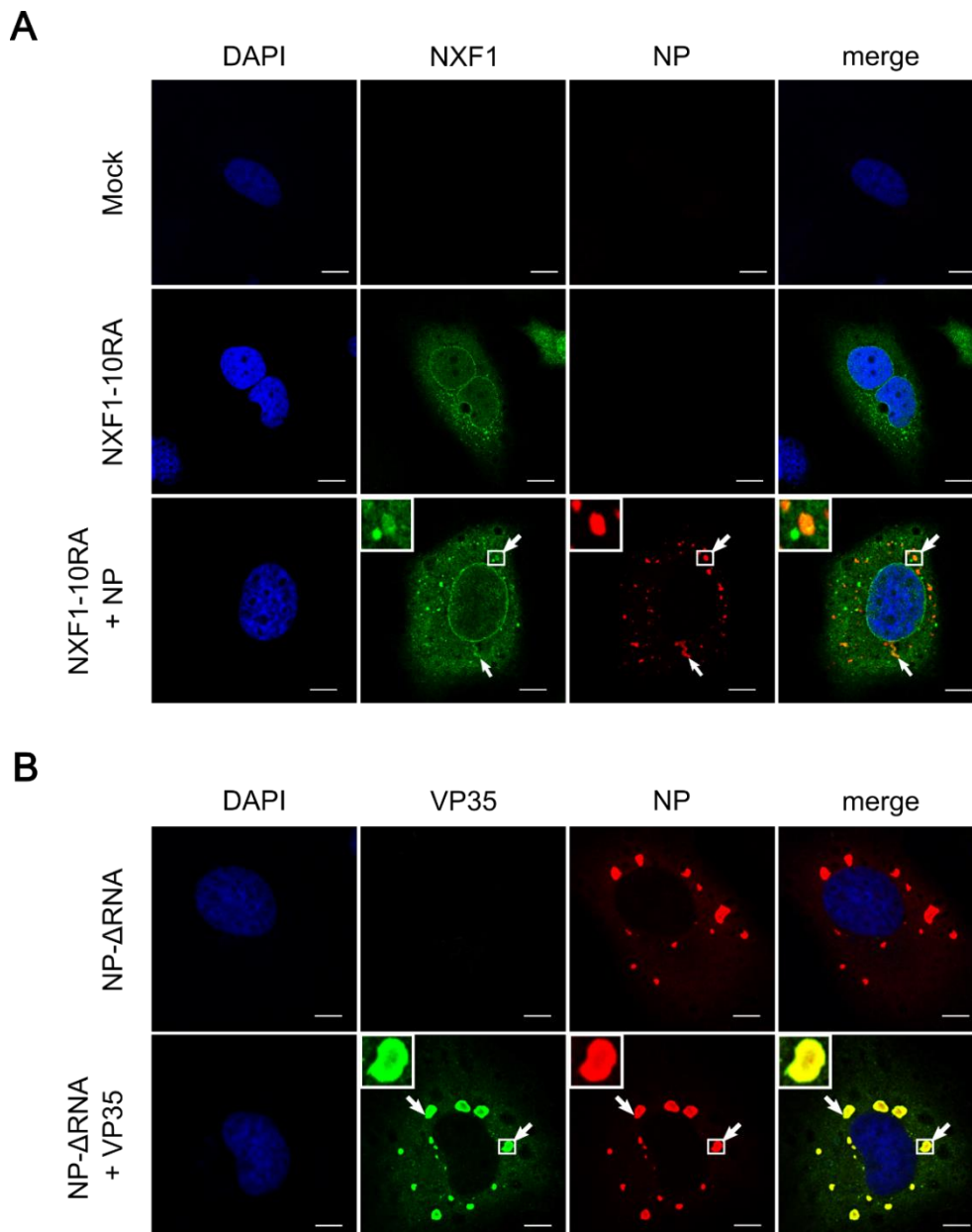


Figure 38. Influence of RNA binding efficiency of NXF1 and NP on their intracellular localisation. **(A)** Cellular distribution of RNA binding deficient NXF1. Huh7 cells were transfected with plasmids encoding flag/HA-NXF1-10RA and/or EBOV-NP as indicated. 48 h post-transfection, the cells were fixed with 4 % paraformaldehyde and permeabilized with 0.1 % Triton X-100. FLAG-tagged NXF1-10RA (shown in green) was detected using an anti-FLAG antibody and NP (shown in red) was stained with anti-EBOV NP antibodies. Figure modified from [Wendt 2020] under CC BY 4.0 license. Copyright © 2020 Lisa Wendt, Janine Brandt, Bianca Bodmer, Sven Reiche, Marie-Luisa Schmidt, Shelby Traeger, Thomas Hoenen. <https://doi.org/10.3390/cells9010187>. **(B)** Cellular distribution and functionality of RNA binding deficient NP. Huh7 cells were transfected with plasmids encoding NP- Δ RNA and/or flag/HA-VP35 as indicated. 48 h post-transfection, the cells were fixed with 4 % paraformaldehyde and permeabilized with 0.1 % Triton X-100. FLAG-tagged VP35 (shown in green) was detected using an anti-FLAG antibody and NP (shown in red) was stained with anti-EBOV NP antibodies. All nuclei were stained with DAPI (shown in blue), and cells were visualized by confocal laser scanning microscopy. Scale bars indicate 10 μ m. The arrows point out inclusion bodies, and the insets show magnifications of the indicated areas. Merge shows an overlay of all three channels.

As NP- Δ RNA is still able to form inclusion bodies and to recruit EBOV proteins to these sites, IFA was performed to investigate the influence of NP- Δ RNA on the cellular localization of NXF1.

Surprisingly, when co-expressed with NP- Δ RNA, NXF1 wildtype strongly accumulated in NP- Δ RNA-induced inclusion bodies, similar to what was observed for NXF1-10RA in NP-derived inclusion bodies, suggesting that RNA binding of both NXF1 and NP is required for exit of NXF1 out of inclusion bodies (Figure 39).

Additionally, to analyze whether NP- Δ RNA also influences the cellular localization and uptake of NXF1-NTF2 or NXF1-UBA in inclusion bodies, Huh7 cells were transfected with the indicated NXF1 single domain mutants and NP- Δ RNA.

Co-expression of NP- Δ RNA with the NTF2 or UBA domain resulted in a clear accumulation of the NXF1 single domains in NP- Δ RNA-derived inclusion bodies, demonstrating that RNA binding of NP is not required for recruitment of NXF1 in inclusion bodies (Figure 39).

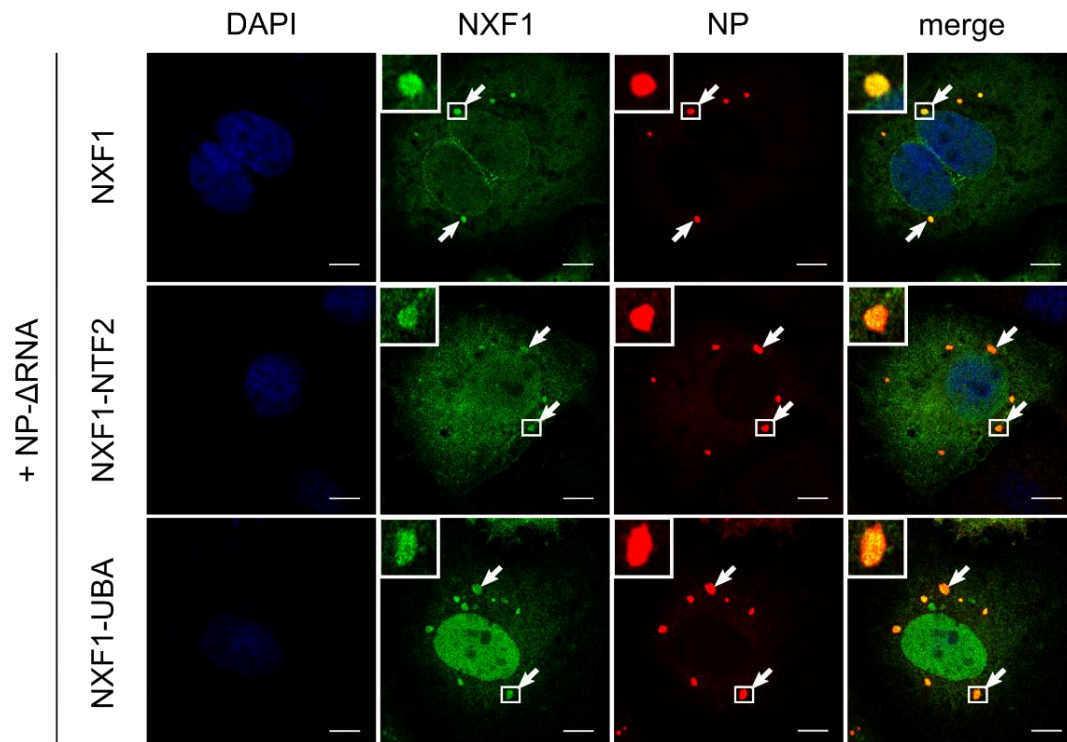


Figure 39. Recruitment of NXF1 into inclusion bodies upon NP- Δ RNA expression. Huh7 cells were transfected with plasmids encoding flag/HA-NXF1 or NXF1 single domain mutants and/or EBOV-NP- Δ RNA as indicated. 48 h post-transfection, the cells were fixed with 4 % paraformaldehyde and permeabilized with 0.1 % Triton X-100. FLAG-tagged NXF1 (shown in green) was detected using an anti-FLAG antibody and NP (shown in red) was stained with anti-EBOV NP antibodies. All nuclei were stained with DAPI (shown in blue), and cells were visualized by confocal laser scanning microscopy. Scale bars indicate 10 μ m. The arrows point out inclusion bodies, and the insets show magnifications of the indicated areas. Merge shows an overlay of all three channels.

3.3.11 The C-terminal domain of NP is responsible for recruitment of NXF1 in inclusion bodies

In order to analyze whether NP is responsible for recruitment of NXF1 into NP-induced inclusion bodies and, if this is the case, which part of NP is involved in this recruitment, IFA was performed using a vector encoding for EBOV-NP in which the C-terminal domain (amino acids 641-739) of NP was deleted.

As previous described, the sole expression of NP- Δ c-tail resulted in an even distribution of NP throughout the cytoplasm and no inclusion body formation was observed (Miyake, Farley et al. 2020) (Figure 40). However, when co-expressing VP35, NP and VP35 clearly localize into inclusion bodies, confirming that VP35 is able to complement a C-terminal deletion of NP (Miyake, Farley et al. 2020). Comparable to the coexpression of NXF1 and NP wildtype, no relocalization of NXF1 in NP- Δ c-tail- and VP35-induced inclusion bodies was observed. Surprisingly, no accumulation of

NXF1-10RA or NXF1-UBA was observed in NP- Δ c-tail- and VP35-derived inclusion bodies either, indicating that the C-terminal domain of NP is required for the recruitment of NXF1 in inclusion bodies.

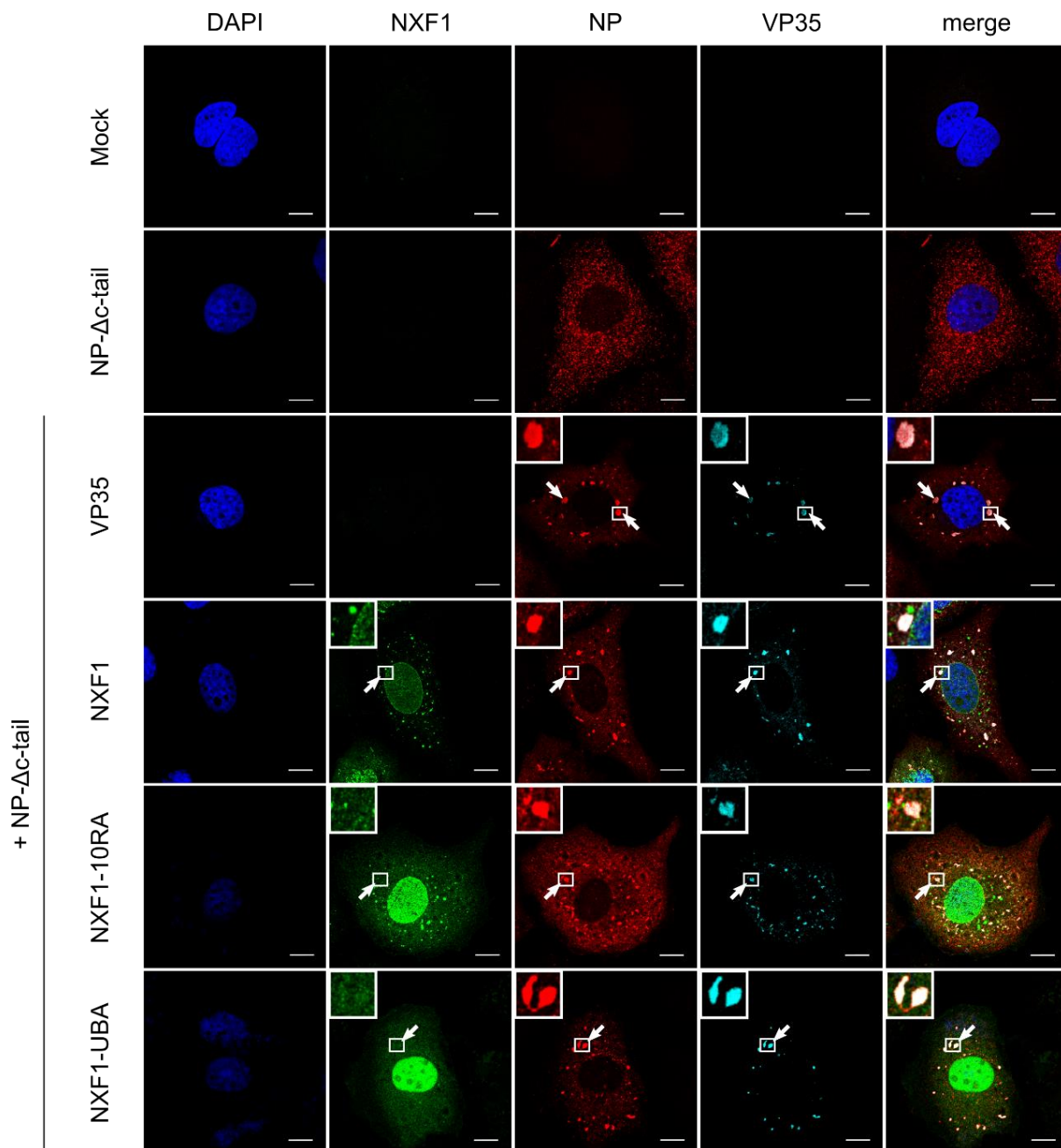


Figure 40. Influence of NP- Δ c-tail on the intracellular localisation of NXF1. Huh7 cells were transfected with plasmids encoding flag/HA-NXF1, 10RA, UBA and/or EBOV-NP- Δ c-tail and myc-VP35 as indicated. 48 h post-transfection, the cells were fixed with 4 % paraformaldehyde and permeabilized with 0.1 % Triton X-100. FLAG-tagged NXF1, 10RA and UBA (shown in green) were detected using an anti-FLAG antibody, NP- Δ c-tail (shown in red) was stained with anti-EBOV NP antibodies and myc-VP35 (shown in cyan) was detected using an anti-myc antibody. All nuclei were stained with DAPI (shown in blue), and cells were visualized by confocal laser scanning microscopy. Scale bars indicate 10 μ m. The arrows point out inclusion bodies, and the insets show magnifications of the indicated areas. Merge shows an overlay of all channels.

Overall, it was shown that NXF1 is recruited into NP-induced inclusion bodies via the FG-repeat interaction domains NTF2 and UBA of NXF1 and the C-terminal domain of NP. Furthermore, it was demonstrated that RNA interaction of NXF1 and NP is not required for this process, but rather important for exit of NXF1 from inclusion bodies.

3.4 Analysis of the role of UAP56 for the EBOV lifecycle

Besides CAD and NXF1, the DEAD box polypeptide 39B (UAP56) was previously identified to be important for Ebola virus RNA synthesis and/or viral protein expression by using a genome-wide siRNA screen (Martin, Chiramel et al. 2018). Comparable to NXF1, UAP56 fulfills its function in the cell nucleus and no connection to EBOV replication has been demonstrated before. Therefore, the function of UAP56 during the EBOV lifecycle has to differ from its cellular function. In order to analyze the precise role of UAP56 on EBOV RNA synthesis and/or viral protein expression, UAP56 knockdown and overexpression in connection with the optimized minigenome systems and IFA was used.

3.4.1 Quantification of siRNA knockdown of UAP56

Before the role of UAP56 knockdown on different aspects of the EBOV lifecycle was investigated, the efficiency of endogenous UAP56 siRNA knockdown had first to be assessed. To this end, HEK 293T cells were reverse transfected with an siRNA against endogenous UAP56 (UAP56-siRNA #1) or a ctrl siRNA and UAP56 expression levels were detected by quantitative Western blotting.

UAP56 knockdown resulted in a 60 % reduction in endogenous UAP56 expression levels when compared to the ctrl siRNA (Figure 41A and 41B).

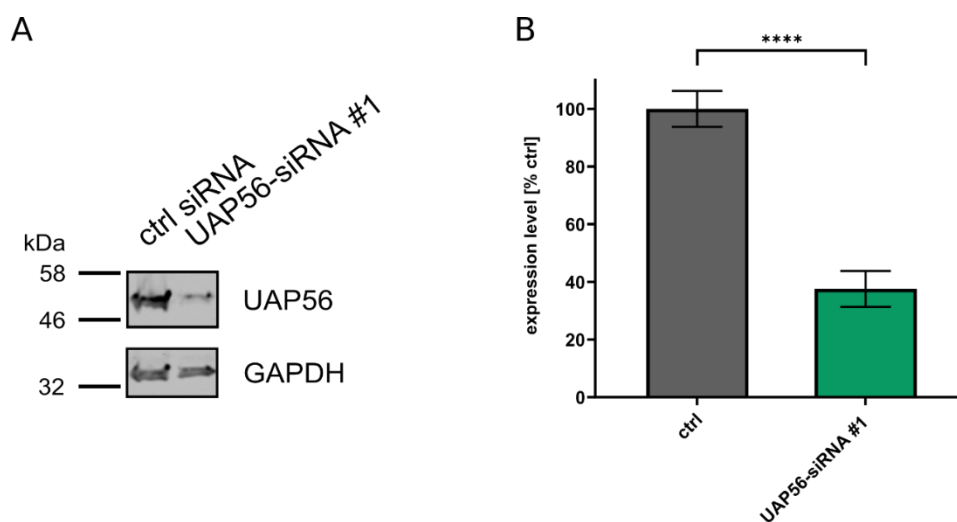


Figure 41. Quantification of UAP56 knockdown. **(A)** Analysis of UAP56 knockdown. 293T cells were transfected with siRNAs targeting UAP56 (UAP56-siRNA #1), or a negative control (ctrl siRNA). The cells were harvested 48 h post-transfection and the lysates were subjected to SDS-PAGE and Western blotting. **(B)** Quantification of UAP56 knockdown. The Western blot signals for UAP56 knockdown (as shown in Figure 41A) were measured and normalized to the GAPDH signals. The negative control (ctrl siRNA) was set to 100 % and the efficiency of UAP56 knockdown was calculated. The means and standard deviations of 3 independent experiments are shown for each panel. Asterisks indicate p-values from a one-way ANOVA (**** $p \leq 0.0001$).

3.4.2 Influence of UAP56 on EBOV total RNA synthesis

In order to confirm the results from the genome-wide siRNA screen with the optimized knockdown protocol and to analyze the influence of UAP56 overexpression on EBOV RNA synthesis, a classical minigenome assay in context of an siRNA-mediated knockdown or an overexpression of UAP56 was performed.

As previously shown, knockdown of UAP56 led to a reduction in reporter activity, confirming a role of UAP56 for EBOV total RNA synthesis or viral protein expression (Figure 42A) (Martin, Chiramel et al. 2018). In contrast to CAD and NXF1, a strong dose-dependent reduction in reporter activity was also observed for UAP56 overexpression, suggesting that the precise level of UAP56 is critical for the EBOV lifecycle (Figure 42B).

In order to avoid artificial aspects present in the monocistronic minigenome system and to validate the results obtained from the classical minigenome experiment, a trVLP assay was performed in presence of UAP56 knockdown or overexpression in p1 cells. Interestingly, UAP56 knockdown resulted in an even stronger reduction in reporter activity compared to the monocistronic minigenome system, confirming a role of UAP56 for EBOV total RNA synthesis (Figure 42C). Similarly, UAP56 overexpression led to a significant dose-dependent reduction in reporter activity, again indicating that

appropriate cellular UAP56 expression levels are important for EBOV RNA synthesis and/or viral protein expression (Figure 42D).

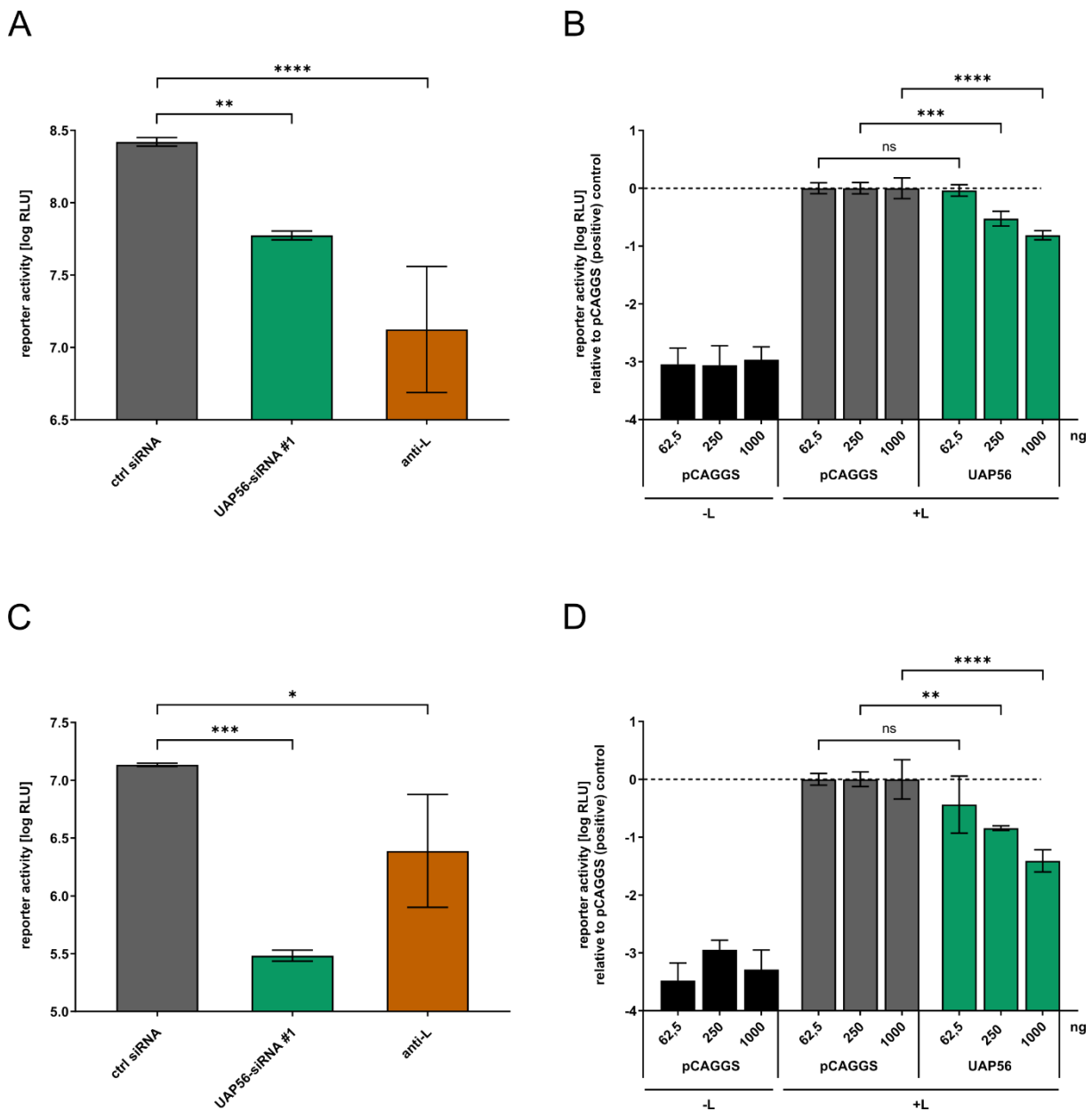


Figure 42. Influence of UAP56 knockdown and overexpression on EBOV total RNA synthesis. **(A)** Influence of UAP56 knockdown on EBOV RNA synthesis. 293T cells were transfected with siRNAs targeting either UAP56 (UAP56-siRNA), EBOV-L (anti-L), or a negative control (ctrl siRNA). 48 h post-transfection, cells were transfected with all the components required for a replication-competent minigenome assay. Another 48 h later, cells were harvested and the reporter activity was measured. **(B)** Influence of UAP56 overexpression on EBOV RNA synthesis. 293T cells were transfected with all components required for a replication-competent minigenome assay, as well as different amounts (62.5 ng, 250 ng and 1000 ng) of a vector encoding for UAP56 wildtype or the empty vector pCAGGS. Cells were harvested and reporter activity was measured 48 h post transfection. **(C)** Analysis of UAP56 knockdown for EBOV RNA synthesis in trVLP assay. p1 293T cells were reverse transfected with siRNAs targeting either UAP56 (UAP56-siRNA), EBOV-L (anti-L), or a negative control (ctrl siRNA). 48 h post-transfection, cells were transfected with plasmids encoding for the EBOV RNP proteins and the

attachment factor Tim 1. 24 h post transfection, cells were infected with trVLPs containing a tetracistronic minigenome and cells were harvested 48 h post infection. **(D)** Role of UAP56 overexpression for EBOV RNA synthesis in trVLP assay. p1 293T cells were transfected with plasmids encoding for the EBOV RNP proteins and the attachment factor Tim 1 as well as different amounts (62.5 ng, 250 ng and 1000 ng) of a vector encoding for UAP56 wildtype or the empty vector pCAGGS. 24 h post transfection, cells were infected with trVLPs containing a tetracistronic minigenome and cells were harvested 48 h post infection. The means and standard deviations of 5 [(A), (B)] or 3 [(C), (D)] independent experiments are shown for each panel. Asterisks indicate p-values from a one-way ANOVA (* $p \leq 0.05$; ** $p \leq 0.01$; *** $p \leq 0.001$; **** $p \leq 0.0001$; ns: $p > 0.05$).

3.4.3 UAP56 knockdown but not overexpression affects EBOV transcription and/or protein expression

In order to distinguish between a role of UAP56 in viral replication on one hand and viral transcription and/or protein expression on the other hand, a replication-deficient minigenome system was used.

In this context, UAP56 knockdown resulted in a clear reduction in reporter activity, indicating that UAP56 is important for either EBOV transcription or protein expression independent of viral genome replication (Figure 43A). Surprisingly, UAP56 overexpression had no effect on reporter activity, suggesting that an increased cellular expression of UAP56 does not affect EBOV transcription, but rather EBOV replication (Figure 43B).

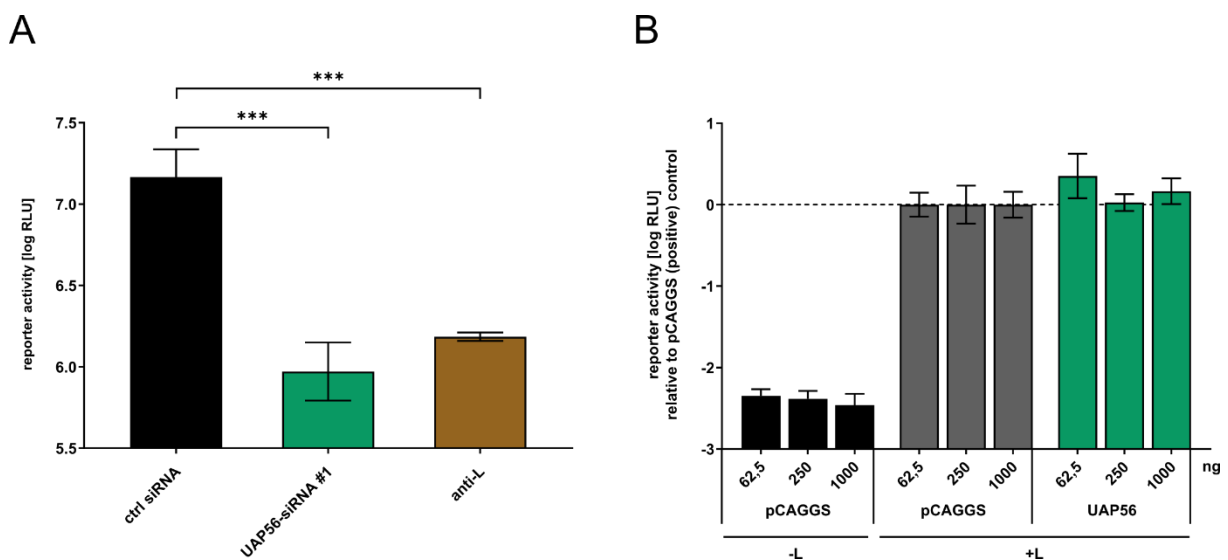


Figure 43. Analysis of UAP56 knockdown and overexpression on EBOV transcription. **(A)** Influence of UAP56 knockdown on EBOV transcription. 293T cells were transfected with siRNAs targeting either UAP56 (UAP56-siRNA #1), EBOV-L (anti-L), or a negative control (ctrl siRNA). 48 h post-transfection, cells were transfected with all the components required for a replication-deficient minigenome assay (repl.def.). Another 48 h later, cells were harvested and the reporter activity was measured. **(B)** Influence of UAP56 overexpression on EBOV transcription. 293T cells were transfected with all components

required for a replication-deficient minigenome assay, as well as different amounts (62.5 ng, 250 ng and 1000 ng) of a vector encoding for UAP56 wildtype or the empty vector pCAGGS. Cells were harvested and reporter activity was measured 48 h post transfection. The means and standard deviations of 3 independent experiments are shown. Asterisks indicate p-values from a one-way ANOVA (* $p \leq 0.05$; ** $p \leq 0.01$; *** $p \leq 0.001$; **** $p \leq 0.0001$; ns: $p > 0.05$).

3.4.4 Influence of UAP56 knockdown and overexpression on EBOV genome replication

To directly investigate the effect of UAP56 on EBOV genome replication, a classical minigenome assay in connection with a siRNA knockdown of UAP56 or a trVLP assay in context of UAP56 overexpression was performed and viral RNA levels were analyzed. Because UAP56 knockdown showed a strong influence on EBOV transcription and/or protein expression, the influence of UAP56 knockdown on EBOV mRNA transcription was additionally investigated.

Cells treated with UAP56 siRNA showed only a slight reduction in both vRNA and mRNA levels, which didn't reach statistical significance, suggesting that, similar to NXF1, UAP56 might be less important for mRNA transcription but rather involved in later steps in mRNA processing or transport (Figure 44A and 44B). UAP56 overexpression resulted in a reduction in vRNA levels by about 9.3-fold, although due to the high standard deviation in these results again no significance was reached (Figure 44C). Nevertheless, these results at least suggest that increasing amounts of UAP56 might directly affect EBOV replication, particularly if also considering the results from the replication-deficient minigenome (Figure 43B).

3.4.5 Establishment of a complementation assay for UAP56 knockdown

UAP56 plays an essential role in mRNA unwinding and ATP hydrolysis during cell growth. In order to analyze whether increased or decreased ATPase activity as well as RNA binding is important for the EBOV lifecycle, a complementation assay, in which UAP56 siRNA-knockdown cells were transfected with siRNA-resistant vectors encoding for UAP56 wildtype or UAP56 mutants, was established.

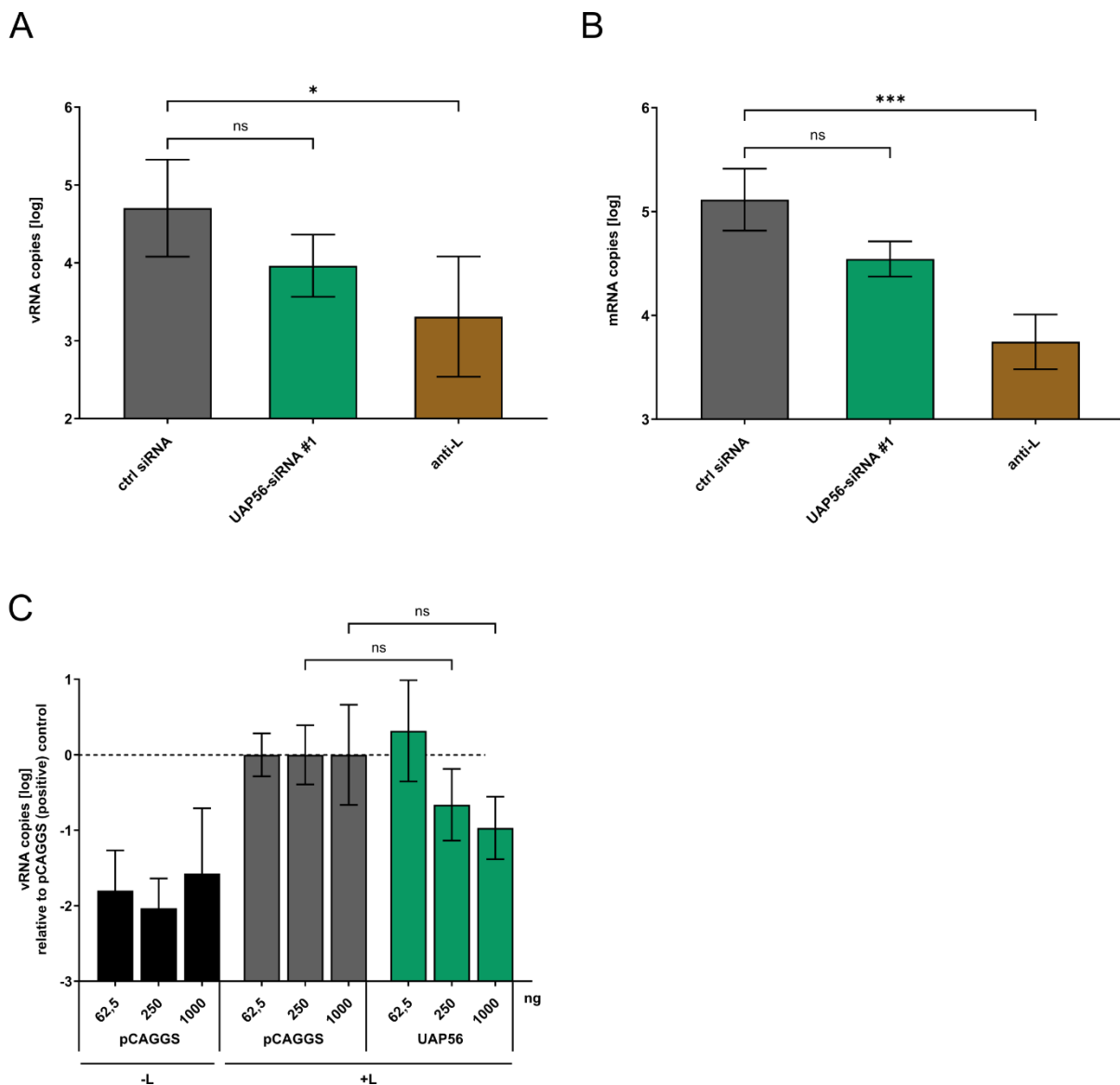


Figure 44. Influence of UAP56 knockdown and overexpression on EBOV genome replication. **(A)** Impact of UAP56 knockdown on EBOV replication. 293T cells were transfected with siRNAs targeting either UAP56 (UAP56-siRNA), EBOV-L (anti-L), or a negative control (ctrl siRNA). 48 h post-transfection, cells were transfected with all the components required for a replication-competent minigenome assay. After cell harvesting, RNA was extracted from the cell lysates and RT-qPCR for vRNA was performed. **(B)** Influence of UAP56 knockdown on EBOV mRNA levels. Cells were treated as described above. After cell harvesting, RNA was extracted from cell lysates and RT-qPCR for mRNA was performed. **(C)** Role of UAP56 overexpression on EBOV replication. p1 293T cells were transfected with plasmids encoding for the EBOV RNP proteins and the attachment factor Tim 1 as well as different amounts (62.5 ng, 250 ng and 1000 ng) of a vector encoding for UAP56 wildtype or the empty vector pCAGGS. 24 h post transfection, cells were infected with trVLPs containing a tetracistronic minigenome and cells were harvested 48 h post infection. After cell harvesting, RNA was extracted from the cell lysates and RT-qPCR for vRNA was performed. The means and standard deviations of 3 [(A), (B)] or 4 [(C)] independent experiments are shown for each panel. Asterisks indicate p-values from a one-way ANOVA (* $p \leq 0.05$; ** $p \leq 0.01$; *** $p \leq 0.001$; **** $p \leq 0.0001$; ns: $p > 0.05$).

3.4.5.1 Generation of siRNA binding-deficient UAP56 plasmids

siRNA-resistant UAP56 expression plasmids were generated analogous to NXF1 (see section 3.3.5.1), mutating the siRNA target sequence CAG CTA CTA GTG GAG CAG to CAA CTG CTG GTC GAA CAA (nucleotides that differ from the original sequence are marked in red). Cloning resulted in the constructs listed in Table 4. RNA binding deficient UAP56 was designated as UAP56-1c, while mutation at position D199 results in an increased and mutation at E197 in a defective ATP hydrolysis of UAP56 (Shen, Zheng et al. 2008).

Table 4. Plasmids generated by molecular cloning.

Plasmids
pCAGGS-flag-HA-UAP56- Δ siRNA
pCAGGS-flag-HA-UAP56-1c- Δ siRNA
pCAGGS-flag-HA-UAP56-E197A- Δ siRNA
pCAGGS-flag-HA-UAP56-D199A- Δ siRNA

3.4.5.2 siRNA mediated knockdown of UAP56 can be complemented with a siRNA-resistant UAP56

After generation of all UAP56- Δ siRNA vectors, a complementation assay was performed using a replication-deficient minigenome system.

As previously shown, transfection of UAP56 siRNA knockdown cells with the empty vector pCAGGS did not result in recovery of reporter activity (Figure 45A). In strong contrast, supplementation of UAP56- Δ siRNA led to a restoration of reporter activity, indicating that siRNA knockdown of UAP56 is specific and can be compensated by supplying exogenous UAP56. However, when cells were transfected with plasmids encoding for UAP56 mutants, this resulted in a reduction in reporter activity already for the control cells, indicating that overexpression of UAP56 mutants exert a dominant negative effect on the cellular function of UAP56 wildtype (Figure 45B), so that it was not possible to perform the complementation assay with these mutants.

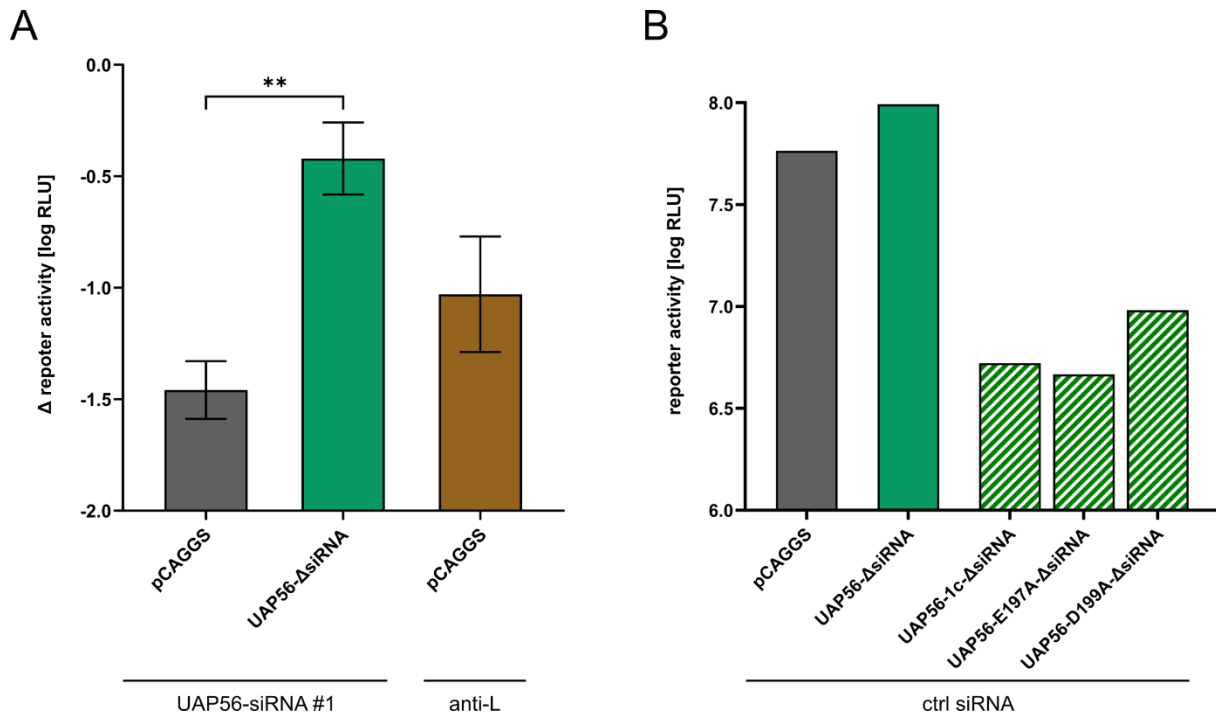


Figure 45. Influence of UAP56 supplementation on EBOV monocistronic minigenome system in course of UAP56 knockdown. **(A)** Effect of UAP56 knockdown can be compensated by supplementation with exogenous UAP56. HEK 293T cells were transfected with siRNAs targeting either UAP56 (UAP56-siRNA #1), EBOV-L (anti-L), or a negative control (ctrl siRNA). 48 h post-transfection, cells were transfected with all the components required for a replication-deficient minigenome assay as well as UAP56-ΔsiRNA construct or pCAGGS as control. The cells were harvested after an additional incubation period of 48 hours and reporter activity was measured. To display reporter activity reduction, a negative influence on reporter activity obtained for UAP56 was subtracted from the reporter activity obtained for each construct in cells transfected with the control siRNA. The means and standard deviations of at least 3 independent experiments are shown. Asterisks indicate p-values from a one-way ANOVA (* $p \leq 0.05$; ** $p \leq 0.01$; *** $p \leq 0.001$; **** $p \leq 0.0001$; ns: $p > 0.05$). **(B)** UAP56 mutants exert a dominant negative effect on the cellular function of UAP56 wildtype. HEK 293T cells were transfected with siRNAs targeting either UAP56 (UAP56-siRNA #1) or a negative control (ctrl siRNA). 48 h post-transfection, cells were transfected with all the components required for a replication-deficient minigenome assay as well as UAP56-ΔsiRNA wildtype and mutants or pCAGGS as control. The cells were harvested after an additional incubation period of 48 hours and reporter activity was measured.

3.4.6 Analysis of the cellular localization of UAP56 in presence and absence of EBOV-NP

Since UAP56 appeared to be important for EBOV RNA synthesis and/or processing, an IFA was performed to analyze whether an overexpression of EBOV-NP and inclusion body formation has an influence on the intracellular distribution of UAP56, and whether recruitment of UAP56 into NP-induced inclusion bodies can be observed. As previously described, single expression of UAP56 led to a predominantly nuclear distribution, although small amounts were also present in the cytoplasm (Figure 46) (Chiba, Hill-Batorski et al. 2018). Interestingly, coexpression of NP and UAP56 led to

no accumulation of UAP56 in inclusion bodies, suggesting that either the amount of UAP56 in the cytoplasm is not sufficient for detection of a colocalization between NP-induced inclusion bodies and UAP56 or that UAP56 is not or only transiently recruited into these structures.

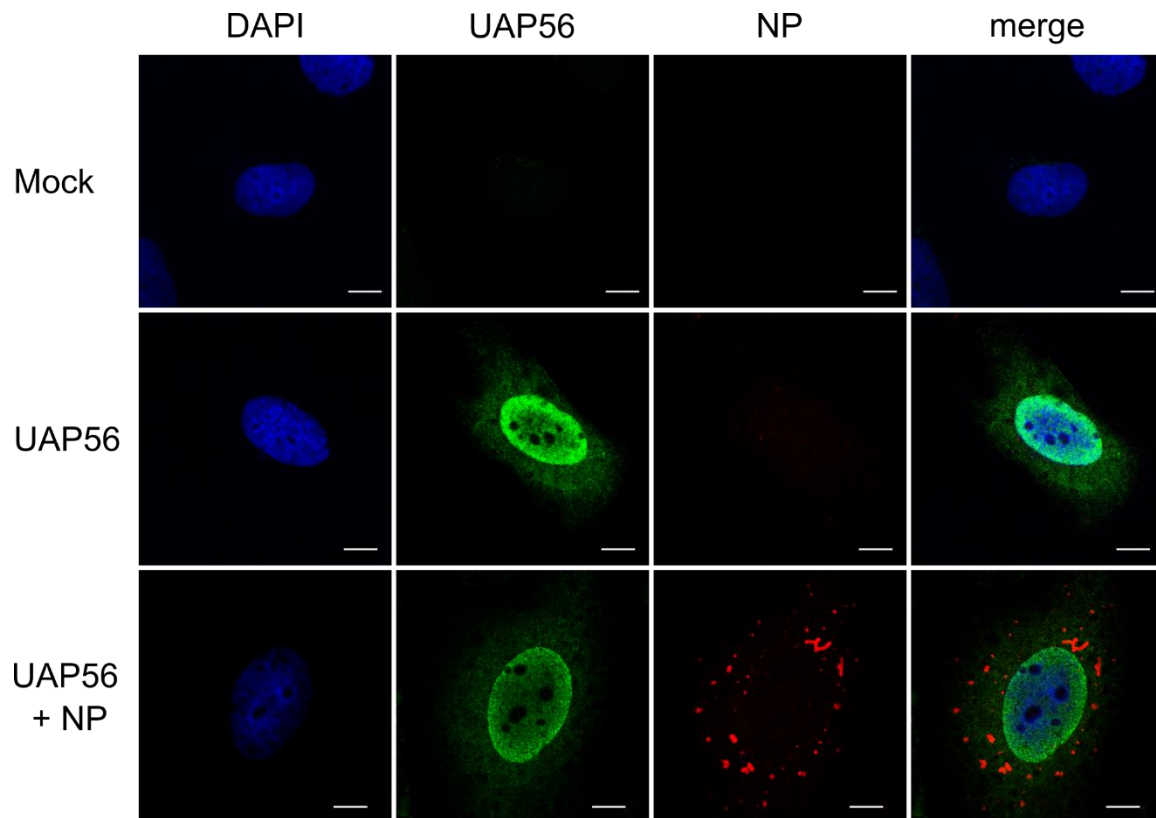


Figure 46. Analysis of the cellular localisation of UAP56 with and without coexpression of EBOV-NP. Huh7 cells were transfected with plasmids encoding flag/HA-UAP56 or EBOV-NP as indicated. 48 h post-transfection, the cells were fixed with 4 % paraformaldehyde and permeabilized with 0.1 % Triton X-100. FLAG-tagged UAP56 (shown in green) was detected using an anti-FLAG antibody and NP (shown in red) was stained with anti-EBOV NP antibodies. Nuclei were stained with DAPI (shown in blue), and cells were visualized by confocal laser scanning microscopy. Scale bars indicate 10 μ m. Merge shows an overlay of all three channels.

3.4.7 Influence of EBOV infection on the intracellular distribution of UAP56

In order to analyze whether additional EBOV proteins are required for recruitment of UAP56 in EBOV inclusion bodies, an immunofluorescence analysis in connection with an EBOV infection was performed. For this, Huh7 cells were first transfected with a vector containing UAP56 or an empty vector for Mock control. 48 h post transfection cells were infected with recombinant infectious EBOV and IFA was performed 16 h after infection. All samples were stained for NP as an inclusion body marker and UAP56.

As observed above, no clear colocalization between inclusion bodies and UAP56 was detected, suggesting that the function of UAP56 for the EBOV lifecycle might take place outside of inclusion bodies, or that the amount of UAP56 was below the detection level (Figure 47).

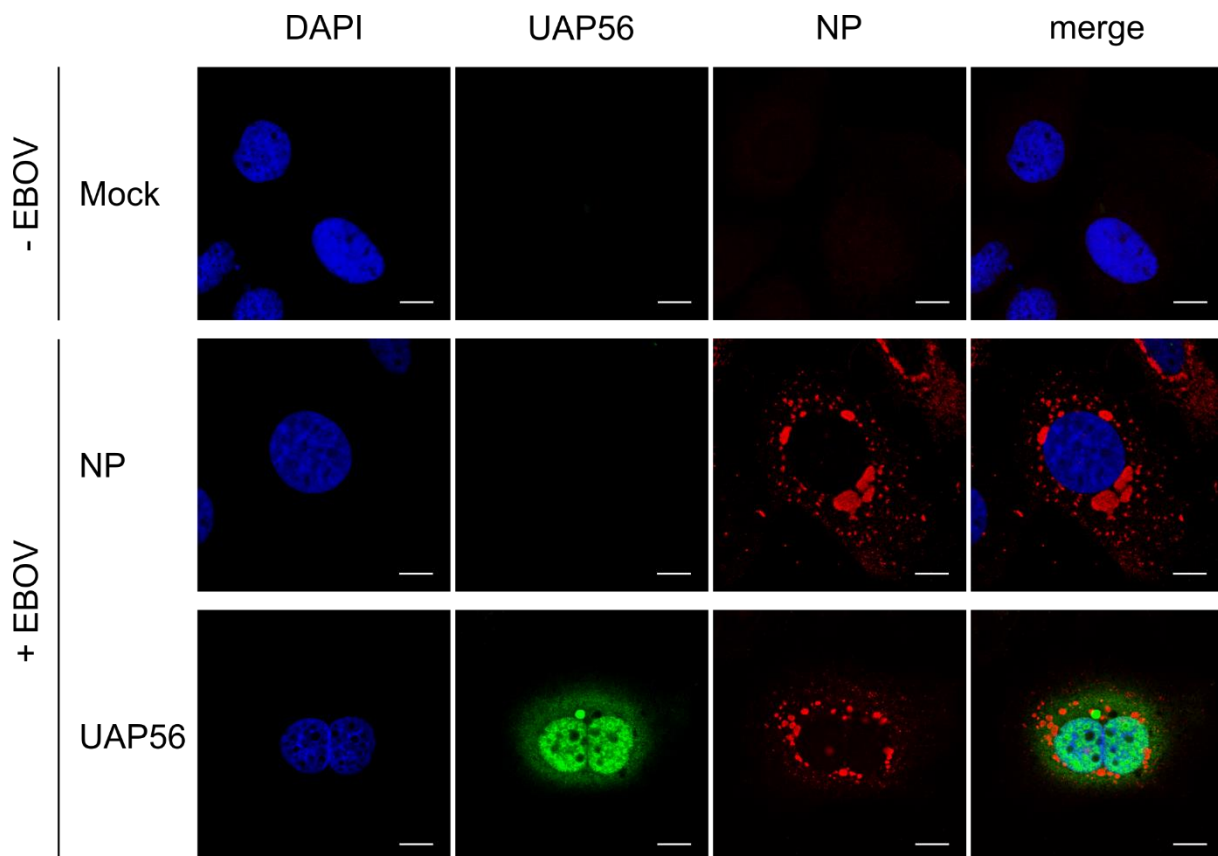


Figure 47. Influence of EBOV infection on the cellular distribution of UAP56. Huh7 cells were transfected with a plasmid encoding FLAG/HA-UAP56. 48 h post-transfection, the cells were infected with rgEBOV at an MOI of 1. After incubation for 16 h, the cells were fixed with 10 % formalin and permeabilized with Triton X-100. UAP56 (shown in green) was detected with an anti-FLAG antibody and NP (shown in red) with an anti-NP antibody. The nuclei were stained with DAPI (shown in blue), and the cells were visualized by confocal laser scanning microscopy. Scale bars indicate 10 μ m. Merge shows an overlay of all three channels.

3.4.8 Investigation of the cellular distribution of NES-UAP56

Because the cellular distribution of UAP56 is mainly restricted to the nuclear compartment, a UAP56 construct containing a nuclear export signal (NES) at its N-terminus was generated to increase the levels of UAP56 present in the cytoplasm, and thus available for a potential recruitment into inclusion bodies.

3.4.8.1 Generation of NES-UAP56 and NES-RRM constructs

As a first step, a NES-UAP56 construct was generated by molecular cloning (Table 5). For this, an artificial NES based on the NES of MAPKK with the following sequence NLVDLQKKLEELDELDEQQ, was used (Zhang, Lohman et al. 2017). Additionally, to exclude that the NES by itself drives relocalization of proteins into inclusion bodies, the NES was cloned in front of NXF1-RRM, as the RRM domain of NXF1 showed a strong cytoplasmic localization but no localization in NP-induced inclusion bodies (Figure 34), and a C-terminal flag tag was added to this construct to allow detection in IFA (Table 5).

Table 5. Plasmids generated by molecular cloning.

Plasmids
pCAGGS-NES-UAP56
pCAGGS-NES-NXF1-RRM
pCAGGS-NES-NXF1-RRM-flag
pCAGGS-NXF1-RRM-flag

3.4.8.2 NES-RRM does not relocalize in NP-induced inclusion bodies

To analyze the cellular distribution of RRM-flag and NES-RRM-flag, IFA was performed by transfection of Huh7 cells with either RRM-flag or NES-RRM-flag and/or NP. 48 h post transfection IFA was performed and samples were analyzed using a confocal laser scanning microscope.

As expected, the sole expression of RRM-flag or NES-RRM-flag showed a similar distribution compared to flag-HA-RRM (shown in Figure 34) (Figure 48). Importantly, no colocalization was observed upon co-expression of RRM-flag or NES-RRM-flag with EBOV-NP, demonstrating that the NES does not trigger relocalization of proteins into NP-derived inclusion bodies.

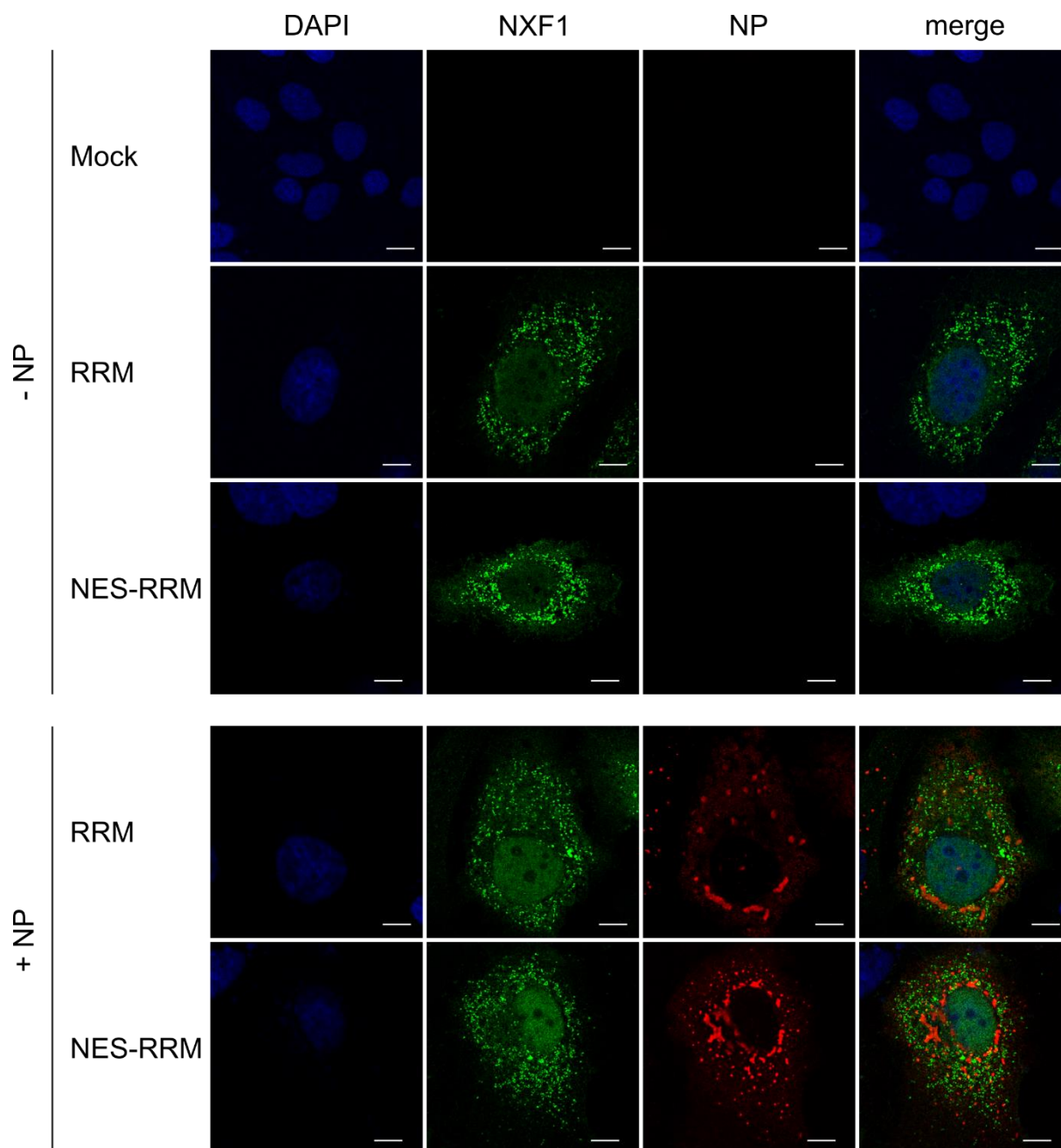


Figure 48. Investigation of the cellular localisation of RRM-flag and NES-RRM-flag. Huh7 cells were transfected with plasmids encoding NXF1-RRM-flag, NES-NXF1-RRM-flag or EBOV-NP as indicated. 48 h post-transfection, the cells were fixed with 4 % paraformaldehyde and permeabilized with 0.1 % Triton X-100. FLAG-tagged NXF1 (shown in green) was detected using an anti-FLAG antibody and NP (shown in red) was stained with anti-EBOV NP antibodies. Nuclei were stained with DAPI (shown in blue), and cells were visualized by confocal laser scanning microscopy. Scale bars indicate 10 μ m. Merge shows an overlay of all three channels.

3.4.8.3 NES-UAP56 is recruited into inclusion bodies

Since the addition of an NES did not alter the cellular distribution of NXF1-RRM with regard to recruitment into inclusion bodies, an IFA was performed using NES-UAP56.

In contrast to UAP56 wildtype, single expression of NES-UAP56 led to a stronger cytoplasmic localization, suggesting that UAP56 is driven out of the nucleus by the attached NES (Figure 49). Surprisingly, upon co-expression of NES-UAP56 and NP, NES-UAP56 localized in NP-induced inclusion bodies, suggesting that UAP56 is able to enter inclusion bodies, and that in the previous experiments the cytoplasmic amount of UAP56 was too low for detection of this colocalization.

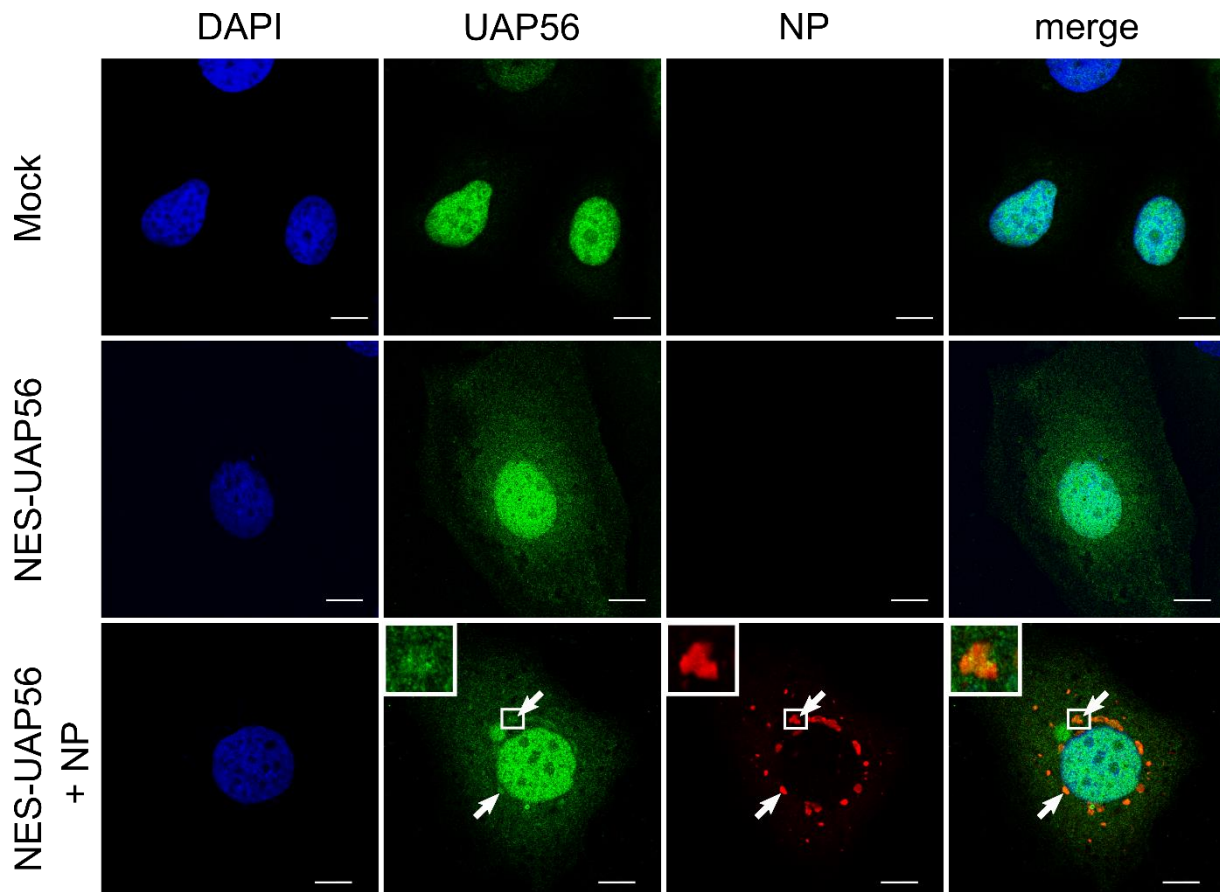


Figure 49. Recruitment of NES-UAP56 in NP-induced inclusion bodies. Huh7 cells were transfected with plasmids encoding NES-UAP56 or myc-EBOV-NP as indicated. 48 h post-transfection, the cells were fixed with 4 % paraformaldehyde and permeabilized with 0.1 % Triton X-100. UAP56 (shown in green) was detected using an anti-UAP56 antibody and NP (shown in red) was stained with anti-myc antibodies. Nuclei were stained with DAPI (shown in blue), and cells were visualized by confocal laser scanning microscopy. Scale bars indicate 10 μ m. The arrows point out inclusion bodies, and the insets show magnifications of the indicated areas. Merge shows an overlay of all three channels.

Overall, it was shown that UAP56 is important for the EBOV lifecycle and that at least when driven out of the nucleus it can be recruited into NP-induced inclusion bodies.

4 Discussion

Ebolaviruses are zoonotic pathogens causing severe infections in humans and non-human primates with high case fatality rates. In recent years, the number and scope of ebolavirus outbreaks has increased, highlighting the importance of a better understanding of the molecular aspects of ebolaviral infections and host cell interactions. The identification of new host cell interaction partners and the characterization of these interactions is of particular importance since they can be used for the development of novel antiviral therapies. To support viral infection, several ebolavirus proteins recruit host proteins for different viral processes. For example, VP35 and VP24 are able to inhibit the innate immune response by targeting several host factors such as IKK (inhibitor of nuclear factor kappa-B kinase), TBK1 (TANK-binding kinase 1), karyopherin α and p38 mitogen-activated protein (MAP) kinase (Basler, Mikulasova et al. 2003, Prins, Cardenas et al. 2009, Mateo, Reid et al. 2010, Halfmann, Neumann et al. 2011, Rojas, Monsalve et al. 2020). Moreover, the matrix protein VP40 interacts with and recruits cellular components of the ESCRT (endosomal sorting complex required for transport) machinery to the sites of viral assembly and budding (Martin-Serrano, Zang et al. 2001). Additionally, various host factors (e.g. SMYD3, STAU1, kinases and phosphatases) are recruited by different viral proteins into NP-induced inclusion bodies, which represent the sites of EBOV RNA synthesis, in order to promote replication and transcription (Fang, Pietzsch et al. 2018, Kruse, Biedenkopf et al. 2018, Chen, He et al. 2019, Morwitzer, Tritsch et al. 2019, Takamatsu, Krahling et al. 2020). However, while ebolavirus genome replication and transcription is well understood, little is known about the mechanism by which host factors are involved in EBOV RNA synthesis. Therefore, a genome-wide siRNA screen was performed to identify new host factors, which contribute to the ebolavirus lifecycle. In this screen, the three host factors CAD, NXF1 and UAP56 were identified to be involved in ebolavirus genome replication and/or transcription and/or protein expression (Martin, Chiramel et al. 2018). However, mechanistical and molecular details of how CAD, NXF1 and UAP56 play a role in the ebolavirus lifecycle were unknown.

4.1 Functional relevance of CAD for the ebolavirus lifecycle

To efficiently perform replication and transcription the EBOV lifecycle requires the provision of pyrimidine bases by the host cell. The *de novo* pyrimidine synthesis represents a complex process, which is mediated by several proteins that possess enzymatic activity. As part of this thesis, I showed that CAD, an essential component of the *de novo* pyrimidine synthesis pathway, is important for both EBOV genome replication and transcription. Furthermore, I was able to demonstrate that the function of CAD in catalyzing the first three steps in pyrimidine synthesis is required for these aspects of the EBOV life cycle. These results are in line with previous studies that investigated the influence of CAD knockdown on replication and transcription of other viruses, e.g., hepatitis C viruses, indicating that CAD plays a crucial role in the lifecycle of different viruses (Borawski, Troke et al. 2009). This role is also supported by the finding that inhibition of CAD by using the antinucleoside compound N-phosphonacetyl-L-aspartate (PALA), which transiently inhibits the aspartate transcarbamylase activity of CAD, showed a strong effect *in vitro* against various viruses, including vaccinia viruses and arenaviruses (Collins and Stark 1971, Katsafanas, Grem et al. 1997, Ortiz-Riano, Ngo et al. 2014). However, although treatment with PALA exhibits antiviral activity against a broad range of viruses, the efficiency of this compound against ebolaviruses still needs to be investigated. Nevertheless, the fact that efficient CAD inhibitors already exist and that CAD knockdown has a strong effect on different viruses, qualifies CAD to be a promising target for antiviral therapy.

The reduction of the cellular pyrimidine pool can not only be achieved via suppression of CAD, but also by several pyrimidine synthesis inhibitors targeting other enzymes in this pathway (Luthra, Naidoo et al. 2018, Martin, Chiramel et al. 2018). Examples are the FDA-approved drug leflunomide and its active metabolite teriflunomide, SW835, as well as S312 and S416. Interestingly, all of these compounds target the *de novo* pyrimidine biosynthesis via inhibition of the dihydroorotate dehydrogenase (DHODH), an enzyme downstream of CAD in the pyrimidine pathway. Interestingly, when using these inhibitors in EBOV minigenome assays, a similar inhibitory effect was observed as for CAD knockdown, although CAD activity was not directly affected (Deans, Morgens et al. 2016, Luthra, Naidoo et al. 2018, Martin, Chiramel et al. 2018, Xiong, Zhang et al. 2020). Additionally, complementation with pyrimidines or upstream metabolites, e.g. orotic acid, reversed the antiviral activity of all pyrimidine pathway

inhibitors. This is consistent with my observation that supplementation with pyrimidines restores EBOV reporter activity after CAD knockdown. Besides their activity against EBOV, pyrimidine pathway inhibitors target a broad-range of viruses, including coronaviruses (e.g. SARS-CoV 2), influenza viruses and Zika virus, demonstrating that these inhibitors are promising compounds for the development of broad-spectrum antivirals (Deans, Morgens et al. 2016, Luthra, Naidoo et al. 2018, Martin, Chiramel et al. 2018, Xiong, Zhang et al. 2020).

To protect the viral RNA from the cellular immune response, EBOV replication and transcription takes place in inclusion bodies, which can be formed by the sole expression of the EBOV nucleoprotein NP (Hoenen, Shabman et al. 2012, Lier, Becker et al. 2017). In this thesis I showed that CAD is recruited to EBOV inclusion bodies and that this recruitment is mediated via an interaction of CAD with NP, as the expression of NP is sufficient for the relocalization of CAD into NP-induced inclusion bodies. This suggestion is supported by observations from CoIP studies that CAD is able to directly interact with NP (Brandt, Wendt et al. 2020). Additionally, experiments with CAD domain deletion mutants showed that redistribution of CAD into NP-derived inclusion bodies is mediated by its GLN domain. So far, direct interactions between CAD and the proteins of other viruses have rarely been described, but Angeletti et al. were able to show that CAD recruits the preterminal protein (pTP) of adenoviruses to the site of adenovirus replication in the nuclear matrix via a direct interaction (Angeletti and Engler 1998). This interaction is believed to be required for anchorage of the adenovirus replication complex at the nuclear matrix in close proximity to the cellular factors required to segregate replicated and genomic viral DNA (Fredman and Engler 1993, Angeletti and Engler 1998).

With respect to its function in pyrimidine synthesis, CAD has been shown to localize primarily in the cytoplasm, but small amounts can also be detected in the nucleus of dividing cells. This nuclear relocalization of CAD during cell growth and proliferation is believed to be a response to phosphorylation by MAP kinases at position Thr-456, which leads to an upregulation of the enzymatic activity of CAD (Sigoillot, Kotsis et al. 2005). To support viral replication and transcription a number of different host factors, including kinases and phosphatases, are recruited by NP into inclusion bodies (Kruse, Biedenkopf et al. 2018, Morwitzer, Tritsch et al. 2019, Takamatsu, Krahling et al. 2020). Therefore, it might be possible that CAD is activated inside inclusion bodies by host

factors already present. Alternatively, CAD could be activated outside in inclusion bodies and only then be imported into inclusion bodies. However, CAD lacking its CPS domain, which contains the phosphorylation site Thr-456, was still recruited into NP-induced inclusion bodies, excluding a selective recruitment of Thr-456-phosphorylated CAD.

4.2 Role of NXF1 for the ebolavirus lifecycle

The nuclear export of cellular mRNAs is a complex process that requires the involvement and interplay of different proteins for successful gene expression. For efficient transport of mRNA through the nuclear pore complex (NPC) into the cytoplasm, nuclear transport receptors (NTRs) are indispensable. In this thesis I was able to show that the nuclear transport receptor NXF1 is recruited into NP-induced inclusion bodies (Wendt, Brandt et al. 2020), which represent the sites of EBOV replication and transcription (Hoenen, Shabman et al. 2012, Lier, Becker et al. 2017). This is in line with findings showing that NXF1 is not only able to enter NP-derived inclusion bodies, but also inclusion bodies during EBOV infection (Wendt, Brandt et al. 2020). Further, this recruitment appears to be mediated by EBOV NP, as the expression of NP is sufficient for the uptake of NXF1 into NP-induced inclusion bodies. However, although our lab could show a direct interaction of NXF1 with NP using CoIP studies (Wendt, Brandt et al. 2020), whether NXF1 is recruited via a direct or an indirect interaction with NP still needs to be investigated. A direct interaction between NXF1 and viral proteins was also previously described for Hepatitis B viruses (HBV), where the HBV core protein (HBc) was shown to interact with NXF1 in order to shuttle between the nucleus and the cytoplasm (Yang, Huang et al. 2014). Additionally, Zhang et al. were able to demonstrate that the NS1 protein of SARS-CoV 2 directly interacts with NXF1, inhibiting NXF1 function, which promotes viral infection via suppression of host gene expression. To this end NS1 inhibits the cellular nuclear export of mRNA by blocking NPC interaction and RNA loading of NXF1 (Zhang, Miorin et al. 2021). However, in contrast to SARS-CoV 2 infection, which leads to a reduced nuclear rim staining of endogenous NXF1, the nuclear localization of endogenous NXF1 was not affected upon EBOV infection, demonstrating that EBOV does not alter the interaction of NXF1 with the NPC (Wendt, Brandt et al. 2020, Zhang, Miorin et al. 2021). Interestingly, Zhang et al. also demonstrated that overexpression of exogenous NXF1 reduces SARS-CoV 2 infection *in vitro*, indicating that NXF1 plays a crucial role in the

lifecycle of these viruses (Zhang, Miorin et al. 2021). In contrast, overexpression of NXF1 had no influence on EBOV RNA synthesis or protein expression as assessed in minigenome systems, indicating that NXF1 has a different role for EBOV compared to its role during the lifecycle of SARS-CoV 2. I could demonstrate that NXF1 seems not to be important for viral transcription, but rather for later steps in mRNA processing, either mRNA transport out of inclusion bodies towards ribosomes or efficient mRNA translation. Similar results were observed for Junín virus, a highly pathogenic arenavirus, where NXF1 knockdown also resulted in reduced viral RNA synthesis and/or protein expression (Martin, Chiramel et al. 2018).

Since RNA binding via its RNA binding domain (RBD) is a key feature of NXF1 to mediate the nuclear export of mRNA, I further analyzed the importance of the RNA binding ability of NXF1 for the EBOV lifecycle. Surprisingly, in contrast to wildtype NXF1, I observed that NXF1 lacking its RBD domain (NXF1- Δ RBD) as well as RNA binding-deficient NXF1 (NXF1-10RA) both strongly accumulated in NP-induced inclusion bodies. Therefore, it can be concluded that RNA binding of NXF1 and its RBD domain are not required for recruitment of NXF1 into inclusion bodies, although interactions of NP with NXF1-10RA and the RBD domain of NXF1 were observed (Wendt, Brandt et al. 2020). However, using complementation assays I was able to show that on a functional level RNA binding seems to be important for the function of NXF1 in the EBOV lifecycle. Taken together the IFA data suggest that the loss of the ability to bind RNA, but not changes in the ability to bind NP, leads to an accumulation of RNA binding-deficient NXF1 in inclusion bodies. Additionally, it can be concluded that the RBD domain of NXF1 is not required for uptake in inclusion bodies, and that NXF1 has to be recruited via another mechanism. This assumption is supported by the fact that I did not observe a colocalization between inclusion bodies and the RBD domain of NXF1.

Interestingly, deletion of the RNA binding site of NP led to a strong accumulation of wildtype NXF1 in inclusion bodies, in contrast to the minute amounts of NXF1 that were observed in inclusion bodies induced by the expression of wildtype NP. These data suggest that RNA binding of both NXF1 and NP is not required for relocalization of NXF1 into inclusion bodies, but rather seems to be important for passage of NXF1 through inclusion bodies. Specifically, these data judicate that in the presence of NP wildtype expression RNA binding-deficient NXF1 is retained and, therefore,

accumulates in inclusion bodies, whereas RNA binding-competent wildtype NXF1 rapidly leaves them again. In contrast to this, upon depletion of the RNA binding ability of NP also wildtype NXF1 is retained and accumulates in inclusion bodies.

NTRs have the ability to interact with nucleoporins in order to promote the translocation of their cargoes across the central channel of the NPC. To this end the phenylalanine-glycine (FG) repeats, which are characteristic for many nucleoporins, function as docking sites for the NTR as it migrates through the pore (Ryan and Wenthe 2000). In case of NXF1, these interactions are mediated by the NTF2 and UBA domains. Surprisingly, upon single expression of these domains I observed a strong accumulation of these domains in NP-derived inclusion bodies, similar to what I observed for NXF1-10RA or NXF1- Δ RBD. I therefore hypothesized that FG repeat interactions via the NTF2 and UBA domain of NXF1 might be involved in the recruitment into EBOV inclusion bodies. However, since it is not described that EBOV NP possesses FG repeat sequences, I investigated whether nucleoporins might be responsible for the relocalization of NXF1 into inclusion bodies. However, endogenous nucleoporins did not colocalize with NP- or EBOV-derived inclusion bodies, which suggests that they are most likely not involved in the recruitment of NXF1 into inclusion bodies. Thus, while I identified the NTF2 and UBA domain as responsible for the recruitment of NXF1 into inclusion bodies, the mechanism of how this takes place and whether it is mediated by a direct or indirect interaction with NP requires further investigation.

Interestingly, NXF1 lacking its UBA domain (NXF1- Δ UBA) accumulated in inclusion bodies, indicating that NXF1 consisting of just one nucleoporin interacting domain is still able to enter but not to exit inclusion bodies. This is in line with my observation that the UBA domain seems to be important for the function of NXF1 in the EBOV lifecycle in the complementation assay, similar to the RBD domain. However, so far, I can not exclude that deletion of the UBA domain changes the overall NXF1 protein structure, and in turn alters its function in the EBOV lifecycle or exit from inclusion bodies. Surprisingly, when omitting the heterodimeric interaction partner of NXF1 p15 (also known as NXT1), colocalization between NXF1- Δ UBA and inclusion bodies was completely abolished and localization of NXF1- Δ UBA was mainly restricted to the nuclear compartment. This is consistent with previous observations that p15 is required for NXF1-mediated nuclear export of mRNA mediating the proper folding and function

of the NTF2 domain (Braun, Herold et al. 2001, Fribourg, Braun et al. 2001, Guzik, Levesque et al. 2001, Braun, Herold et al. 2002). Since p15 is needed to facilitate FG repeat interactions of the NTF2 domain, an absence of p15 leads to a disruption of the NPC passage of NXF1 and results in the phenotype observed for NXF1- Δ UBA localization. In contrast to this, while p15 is required for a proper folding of NXF1, our lab has shown that p15 is dispensable for the interaction between NXF1 and NP, and that the formation of the NXF1-p15 heterodimer is not necessary for the interaction with NP (Wendt, Brandt et al. 2020).

In contrast to NXF1- Δ UBA, which is still able to enter inclusion bodies in the presence of p15, the localization of NXF1- Δ NTF2 is strongly restricted to the nucleus, regardless of whether p15 is present or not. This correlates with the observation that NXF1- Δ NTF2 does not show any effect in EBOV complementation assay, probably because it is not able to leave the nucleus. Similar results were obtained by Braun et al., which were able to show that NXF1 lacking its NTF2 domain only exhibits 5 % of the export activity of the wildtype protein (Braun, Herold et al. 2002). However, when a second UBA domain was inserted in NXF1- Δ NTF2, this restored the export activity of NXF1 to around 55 %, concluding that two NPC-binding sites are required for efficient NXF1-mediated export of cellular mRNA. Therefore, it would be of great interest to analyze whether NXF1- Δ NTF2 containing two UBA domains is able to colocalize with NP-induced inclusion bodies or functional in the complementation assay.

Besides the RBD, UBA and NTF2 domain, NXF1 also contains an RRM and an LRR domain. Interestingly, in contrast to NXF1- Δ RBD or NXF1- Δ UBA, I did not observe an accumulation of NXF1- Δ RRM or NXF1- Δ LRR in inclusion bodies, concluding that they either are not able to enter these structures or are just passing through inclusion bodies like wildtype NXF1. This was also observed for the single expression of these domains. Interestingly, when using the complementation assay, I was able to rescue NXF1 knockdown by supplementation with NXF1- Δ RRM but not with NXF1- Δ LRR. Together these data suggest that in contrast to the RBD, NTF2 and UBA domains of NXF1, which seem to have important functions for the ebolavirus lifecycle, the RRM domain of NXF1 is not required for the function of NXF1 in the EBOV life cycle. This suggestion is supported by the fact that NP does not interact with the RRM domain of NXF1 (Wendt, Brandt et al. 2020). Whether the LRR itself is important for the function of

NXF1, or whether its deletion changes the overall NXF1 protein structure still needs to be further analyzed.

Ebolavirus NP is a multifunctional protein with high RNA binding affinity that is known to recruit viral and cellular proteins into inclusion bodies to facilitate viral RNA synthesis (Leung, Prins et al. 2010b, Kirchdoerfer, Abelson et al. 2015, Fang, Pietzsch et al. 2018, Chen, He et al. 2019). To mediate these functions, NP consists of an N-terminal domain, which is required for RNA binding and NP oligomerization, and a C-terminal domain, which scaffolds L, VP30 and VP35 in the nucleocapsid complex (Dziubanska, Derewenda et al. 2014, Dong, Yang et al. 2015). As part of this thesis I have shown that a loss of the C-terminal domain of NP (NP- Δ c-tail) abolishes the accumulation of NXF1-10RA or NXF1-UBA in inclusion bodies. These findings suggest that the C-terminal region of NP is required for uptake of NXF1 into these structures. However, as NP- Δ c-tail is no longer able to form inclusion bodies on its own (Miyake, Farley et al. 2020), coexpression of VP35 was required to support inclusion body formation. Therefore, it remains to be shown whether inclusion bodies formed under these conditions are functionally equivalent to inclusion bodies produced by wildtype NP, or whether there are differences that are responsible for the inability of NXF1-10RA and NXF1-UBA to accumulate in these structures.

The NXF1-mediated nuclear export of mRNA is used by various nuclear replicating viruses, including retroviruses, Influenza viruses and adenoviruses, to export their mRNA into the cytoplasm to facilitate gene expression (Bachi, Braun et al. 2000, Read and Digard 2010, Yatherajam, Huang et al. 2011, Larsen, Bui et al. 2014, Gales, Kubina et al. 2020). However, since EBOV RNA synthesis occurs in cytoplasmic inclusion bodies, EBOV mRNA does not passage through the nucleus of the host cell but rather needs to be exported from inclusion bodies to reach the ribosomes for translation (Hoenen, Shabman et al. 2012, Zhou, Su et al. 2019). So far it is not clear how naked viral RNAs such as mRNAs would be able to exit inclusion bodies in order to facilitate protein expression. Given the fact that NXF1 is able to bind EBOV mRNA that is produced in inclusion bodies, we propose a model in which NXF1 exports bound mRNA from inclusion bodies into the cytoplasm (Figure 50) (Wendt, Brandt et al. 2020). This is supported by the fact that RNA binding-deficient NXF1 is retained in inclusion bodies while only small quantities of wildtype NXF1 can be detected in these structures. We further propose that the viral mRNA is transferred from NP to NXF1 in

response to an interaction of NXF1 with NP, mediated by the RBD domain of NXF1. This is in line with the fact that wildtype NXF1 is not able to leave inclusion bodies when RNA-binding deficient NP is expressed, indicating that NP has to bind the viral mRNA for proper handover of the RNA to NXF1 and that NXF1 has to bind mRNA to be able to leave inclusion bodies. Furthermore, we propose that NXF1 is recruited into inclusion bodies by the C-terminal domain of NP via direct or indirect interaction with the FG-repeat binding domains of NXF1.

Nevertheless, we cannot fully exclude that NXF1 fulfills another, yet undescribed function in later steps of viral protein expression and further studies are required to address this question. Additionally, the exact mechanism of mRNA export from inclusion bodies by NXF1, as well as the precise localization of NXF1 in inclusion bodies and whether NXF1 is recruited by direct or indirect interaction with NP still needs to be investigated.

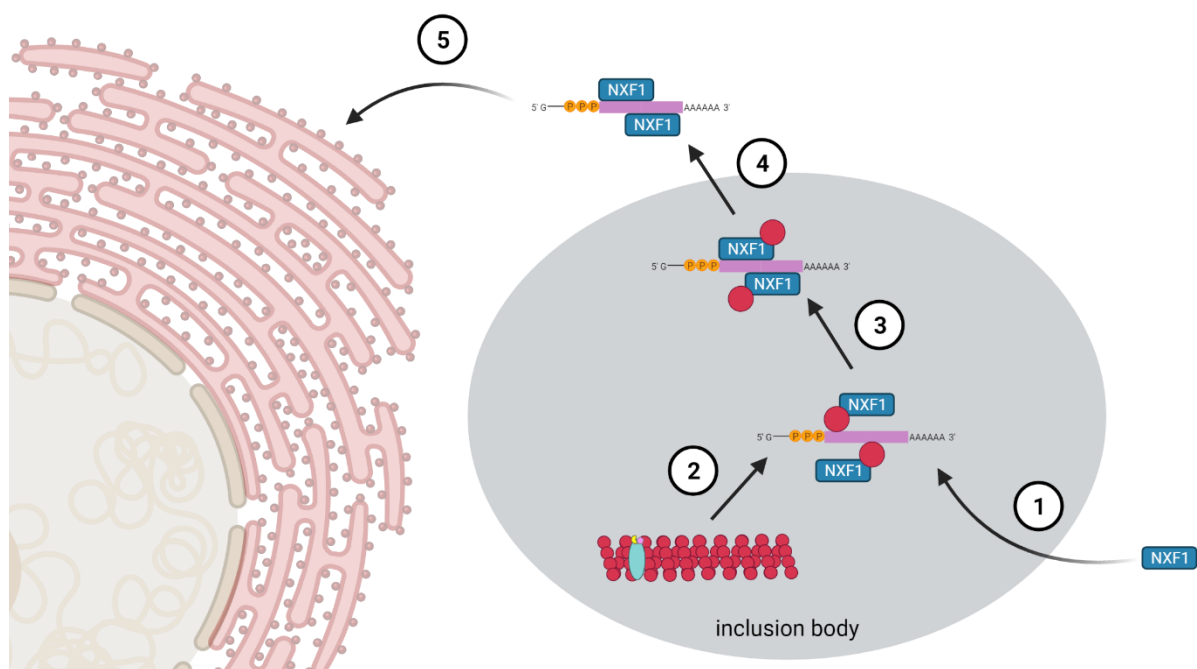


Figure 51. Model of NXF1 mediated export of EBOV mRNA from inclusion bodies. (1) Recruitment of NXF1 via the C-terminal domain of NP and the FG-repeat interaction domains NTF2 and UBA of NXF1. (2) EBOV transcription. (3) Handover of the newly synthesized viral mRNA from NP to NXF1. (4) Dissociation of NP and export of the NXF1 loaded mRNA from inclusion bodies into the cytoplasm. (5) Transport of the viral mRNA to the site of mRNA translation by NXF1. Figure modified from [Wendt 2020] under CC BY 4.0 license. Copyright © 2020 Lisa Wendt, Janine Brandt, Bianca Bodmer, Sven Reiche, Marie-Luisa Schmidt, Shelby Traeger, Thomas Hoenen. <https://doi.org/10.3390/cells9010187>. Created with BioRender.com

4.3 Influence of UAP56 on the ebolavirus lifecycle

During RNA processing the pre-mRNA is successfully spliced into mature mRNA in the nucleus of cells. Besides the removal of introns, splicing also leads to the association of mRNAs with various cellular proteins, and has been shown to greatly improve translation from both cellular and viral mRNAs, independent of any effects on nuclear mRNA export (Nott, Meislin et al. 2003, Nott, Le Hir et al. 2004, Sadek and Read 2016). Although EBOV mRNA does not undergo splicing, work in this thesis demonstrates that the splicing and mRNA export factor UAP56 seems to be important for the ebolavirus lifecycle. These results are in line with previous studies that investigated the influence of UAP56 knockdown on replication and mRNA export of different influenza A viruses, indicating that UAP56 plays a crucial role in the lifecycle of many viruses (Wisskirchen, Ludersdorfer et al. 2011). Interestingly, when overexpressing UAP56, I observed a strong effect on EBOV RNA replication in minigenome systems, indicating that UAP56 is not only important for EBOV transcription but also for EBOV replication.

Since overexpression of UAP56 affects EBOV replication, which takes place in inclusion bodies, I further investigated the cellular localization of UAP56 upon NP expression or EBOV infection. Surprisingly, I did not detect an accumulation or colocalization of wildtype UAP56 with either NP-induced or EBOV-derived inclusion bodies, probably since the localization of UAP56 was strongly restricted to the nuclear compartment. In contrast, expression of NES-UAP56 led to an accumulation of this construct in NP-induced inclusion bodies. Together, this suggests that UAP56 is able to enter inclusion bodies and that small amounts of UAP56 are sufficient for its function in EBOV replication. Since the single expression of NP is sufficient for uptake of UAP56 into NP-induced inclusion bodies, I further propose that this recruitment is mediated by NP. However, whether UAP56 is recruited via a direct or indirect interaction with NP still needs to be investigated. So far, colocalizations between UAP56 and the proteins of other viruses have rarely been described, but Chiba et al. were able to show that UAP56 colocalizes with the influenza A viral NS1 protein in close proximity to the nuclear membrane. Additionally, they were also able to show that this colocalization is mediated via a direct interaction between UAP56 and the NS1 proteins of different influenza A viruses (Chiba, Hill-Batorski et al. 2018). Although NS1 serves as an inhibitor of the host cell innate immune responses, which is stimulated by influenza A virus infection, it was shown that interaction with UAP56 does not contribute to this

function. Therefore, the exact function of this interaction still remains elusive. Interestingly, besides NS1, human and avian influenza A virus NP also directly interacts with UAP56. This interaction prevents the formation of dsRNA during influenza A virus replication (Wisskirchen, Ludersdorfer et al. 2011). Additionally, UAP56 functions as a molecular chaperone for NP and is required for the replication-coupled RNP formation of newly synthesized viral genomes by promoting the assembly of trimeric NP (Momose, Basler et al. 2001, Kawaguchi, Momose et al. 2011, Hu, Gor et al. 2017). Furthermore, UAP56 seems to be required for structural integrity of the NP-RNA complex (Hu, Gor et al. 2017). Recent studies identified the N-terminal extension (NTE) sequence as well as the C-terminal domain of UAP56 as interaction sites with NP, while NP interacts via its N-terminal domain with UAP56 (Momose, Basler et al. 2001, Morris, Wang et al. 2020). Based on these findings it would be of great interest whether UAP56 also directly interacts with EBOV NP and whether this interaction is mediated via the same interaction sites found for influenza A virus NP. Since UAP56 seems to be important for EBOV replication as well as mRNA processing, it is possible that RNP formation is also affected by overexpression or knockdown of UAP56.

UAP56 is known to execute its function in RNA splicing via its RNA and ATP binding domains, which contribute to its RNA helicase activity. However, when analyzing the relevance of these domains for the EBOV lifecycle I observed a strong effect of all mutants on minigenome expression in the control cells, suggesting that the designed constructs have a dominant negative effect on the endogenous wildtype UAP56 levels, so that so far it has not been possible to reliably investigate the functional significance of individual domains of UAP56.

4.4 Conclusion

In this thesis I demonstrated the importance of the host cell factors CAD, NXF1 and UAP56 for the EBOV lifecycle, and provided experimental data helping to elucidate their function. Furthermore, I showed that these host proteins are recruited to the site of EBOV replication and transcription in order to fulfill their respective functions for these processes. These findings increase our understanding of EBOV and its host cell interactions, and provide a basis for future identification of molecular targets for the development of novel therapies against this virus.

5 Summary

Ebolaviruses are zoonotic pathogens causing severe hemorrhagic fevers in humans and non-human primates with high case fatality rates. In recent years, the number and scope of outbreaks has increased, highlighting the importance of better understanding the molecular aspects of ebolaviral infection and host cell interactions in order to be able to better control this virus.

To facilitate virus genome replication, transcription and protein expression, ebolaviruses recruit and interact with specific host factors. These interactions play a key role in viral infection and influence virus survival and disease outcome. Based on a genome-wide siRNA screen, the three host factors CAD, NXF1 and UAP56 were recently identified to be involved in ebolavirus genome replication and/or transcription and/or mRNA-translation. However, mechanistical details of how these host factors affect the ebolavirus lifecycle remained elusive.

In this thesis I analyzed the functional interactions between EBOV and these newly identified host proteins in order to better understand the virus-host interface. To this end I used siRNA knockdown as well as overexpression of these host proteins in combination with different reverse-genetics based lifecycle modelling assays to investigate the influence of CAD, NXF1 and UAP56 on individual aspects of the EBOV lifecycle. Using these systems in relation with a host factor knockdown I was able to show that the provision of pyrimidines by CAD plays an important role for both EBOV genome replication and transcription, whereas NXF1 is predominantly required for mRNA transport. I furthermore used immunofluorescence analysis to examine whether these host factors are recruited by one or more EBOV proteins to inclusion bodies, which represent physical sites of ebolavirus genome replication. During these experiments, I was able to show that CAD and NXF1, and possibly also UAP56, are recruited to EBOV inclusion bodies in order to fulfill their individual function for EBOV RNA synthesis or later steps in protein expression. Additionally, I was able to show that the uptake of NXF1 into NP-induced inclusion bodies is most likely mediated via the C-terminal domain of NP, and that the FG-repeat interaction domains of NXF1 are sufficient for recruitment. Further, my data indicate that RNA interaction of both NXF1 and NP is not required for this process, but rather important for exit of NXF1 from inclusion bodies. I therefore suggest that the viral mRNA is transferred in inclusion

bodies from NP to NXF1, which leads to a rapid export of the NXF1 packed viral mRNA into the cytosol for mRNA translation.

The exact mechanism of how these host factors are recruited into inclusion bodies and whether they have similar functions in the lifecycle of other negative-sense RNA viruses still needs to be investigated. Nevertheless, this study increases our understanding of virus-host interaction of ebolaviruses, and thus helps to identify targets for the development of novel therapeutics against these viruses

6 Zusammenfassung

Ebolaviren sind zoonotische Krankheitserreger, die bei Menschen und Primaten schwere hämorrhagische Fieber mit einer hohen Sterblichkeitsrate verursachen. In den letzten Jahren haben die Anzahl und der Umfang von Ausbrüchen zugenommen. Um diese Infektionen besser bekämpfen zu können, ist es daher von großer Bedeutung, ein besseres Verständnis über die molekularen Aspekte einer ebolaviralen Infektion und Wechselwirkungen von Ebolaviren mit der Wirtszelle zu erlangen.

Um eine effektive Virusreplikation, -transkription und -translation zu gewährleisten, rekrutieren und interagieren Ebolaviren mit verschiedenen Wirtsfaktoren. Diese Wechselwirkungen spielen eine Schlüsselrolle bei der Virusinfektion und haben Einfluss auf das Überleben des Virus und den Krankheitsverlauf. Basierend auf einem genomweiten siRNA-Screening konnten die drei Wirtsfaktoren CAD, NXF1 und UAP56 identifiziert werden, welche an der Replikation und/oder Transkription und/oder mRNA-Translation des Ebolavirus-Genoms beteiligt sind. Mechanistische Details darüber, wie diese Wirtsfaktoren im Ebolavirus-Lebenszyklus eine Rolle spielen, waren jedoch bislang nicht bekannt.

Um die Schnittstelle zwischen Virus und Wirt besser zu verstehen, habe ich in dieser Doktorarbeit die funktionellen Wechselwirkungen zwischen Ebolaviren und diesen drei neu identifizierten Wirtsfaktoren analysiert. Zu diesem Zweck verwendete ich verschiedene auf reverser Genetik basierende Lebenszyklusmodellierungssysteme in Kombination mit siRNA-Knockdown oder Überexpression dieser Wirtsproteine, um den Einfluss von CAD, NXF1 und UAP56 auf einzelne Aspekte des Ebolavirus-Lebenszyklus zu untersuchen. Mittels dieser Modellsysteme und einem Knockdown der Wirtsfaktoren konnte ich zeigen, dass die Bereitstellung von Pyrimidinen durch CAD sowohl für die Replikation als auch für die Transkription des EBOV-Genoms eine wichtige Rolle spielt, während NXF1 vorwiegend für den mRNA-Transport erforderlich ist. Des Weiteren verwendete ich Immunfluoreszenzanalysen, um zu untersuchen, ob diese Wirtsfaktoren von einem oder mehreren Ebolavirus-Proteinen in Einschlusskörperchen, welche Orte der Ebolavirus-Genomreplikation darstellen, rekrutiert werden. Im Verlauf dieser Experimente konnte ich zeigen, dass CAD, NXF1 und möglicherweise auch UAP56 in Ebolavirus-Einschlusskörperchen rekrutiert werden, um ihre individuellen Funktionen in der Ebolavirus-RNA-Synthese oder

Protein-Expression zu erfüllen. Zusätzlich konnten wir zeigen, dass die Aufnahme von NXF1 in NP-induzierte Einschlusskörperchen über die C-terminale Domäne von NP vermittelt wird, und die FG-Repeat-Interaktionsdomänen von NXF1 hierfür hinreichend sind. Obwohl eine RNA-Interaktion von NXF1 oder NP für diese Aufnahme nicht benötigt wird, scheint diese für den Export von NXF1 aus den Einschlusskörpern entscheidend zu sein. Es ist daher zu vermuten, dass die virale mRNA in Einschlusskörpern von NP auf NXF1 übertragen wird. Dies führt wiederum zu einem schnellen Export der NXF1-gebundenen viralen mRNA in das Zytoplasma und zur mRNA Translation.

Unklar bleibt jedoch, wie genau diese Wirtsfaktoren in Einschlusskörper rekrutiert werden, und ob sie ähnliche Funktionen im Lebenszyklus anderer RNA-Viren mit negativer Polarität haben. Dennoch haben diese Untersuchungen unser Verständnis über die Virus-Wirt-Interaktion von Ebolaviren verbessert und dazu beigetragen, Ziele für die Entwicklung neuartiger Therapeutika gegen diese Viren zu identifizieren.

7 References

- Abbate, J. L., C. L. Murall, H. Richner and C. L. Althaus (2016). "Potential Impact of Sexual Transmission on Ebola Virus Epidemiology: Sierra Leone as a Case Study." PLoS Negl Trop Dis **10**(5): e0004676.
- Agrawal, N., P. V. Dasaradhi, A. Mohmmmed, P. Malhotra, R. K. Bhatnagar and S. K. Mukherjee (2003). "RNA interference: biology, mechanism, and applications." Microbiol Mol Biol Rev **67**(4): 657-685.
- Aleksandrowicz, P., A. Marzi, N. Biedenkopf, N. Beimforde, S. Becker, T. Hoenen, H. Feldmann and H. J. Schnittler (2011). "Ebola virus enters host cells by macropinocytosis and clathrin-mediated endocytosis." J Infect Dis **204 Suppl 3**: S957-967.
- Alvarez, C. P., F. Lasala, J. Carrillo, O. Muniz, A. L. Corbi and R. Delgado (2002). "C-type lectins DC-SIGN and L-SIGN mediate cellular entry by Ebola virus in cis and in trans." J Virol **76**(13): 6841-6844.
- Angeletti, P. C. and J. A. Engler (1998). "Adenovirus preterminal protein binds to the CAD enzyme at active sites of viral DNA replication on the nuclear matrix." J Virol **72**(4): 2896-2904.
- Bachi, Braun, J P Rodrigues, N Panté, K Ribbeck, C von Kobbe, U Kutay, M Wilm, D Görlich, M Carmo-Fonseca and E. Izaurralde (2000). "The C-terminal domain of TAP interacts with the nuclear pore complex and promotes export of specific CTE-bearing RNA substrates."
- Bachi, A., I. C. Braun, J. P. Rodrigues, N. Pante, K. Ribbeck, C. von Kobbe, U. Kutay, M. Wilm, D. Gorlich, M. Carmo-Fonseca and E. Izaurralde (2000). "The C-terminal domain of TAP interacts with the nuclear pore complex and promotes export of specific CTE-bearing RNA substrates." RNA **6**(1): 136-158.
- Banadyga, L., T. Hoenen, X. Ambroggio, E. Dunham, A. Groseth and H. Ebihara (2017). "Ebola virus VP24 interacts with NP to facilitate nucleocapsid assembly and genome packaging." Sci Rep **7**(1): 7698.
- Baseler, L., D. S. Chertow, K. M. Johnson, H. Feldmann and D. M. Morens (2017). "The Pathogenesis of Ebola Virus Disease." Annu Rev Pathol **12**: 387-418.
- Basler, C. F., A. Mikulasova, L. Martinez-Sobrido, J. Paragas, E. Muhlberger, M. Bray, H. D. Klenk, P. Palese and A. Garcia-Sastre (2003). "The Ebola virus VP35 protein inhibits activation of interferon regulatory factor 3." J Virol **77**(14): 7945-7956.

- Batra, J., J. F. Hultquist, D. Liu, O. Shtanko, J. Von Dollen, L. Satkamp, G. M. Jang, P. Luthra, T. M. Schwarz, G. I. Small, E. Arnett, M. Anantpadma, A. Reyes, D. W. Leung, R. Kaake, P. Haas, C. B. Schmidt, L. S. Schlesinger, D. J. LaCount, R. A. Davey, G. K. Amarasinghe, C. F. Basler and N. J. Krogan (2018). "Protein Interaction Mapping Identifies RBBP6 as a Negative Regulator of Ebola Virus Replication." *Cell* **175**(7): 1917-1930 e1913.
- Becker, S., C. Rinne, U. Hofsass, H. D. Klenk and E. Muhlberger (1998). "Interactions of Marburg virus nucleocapsid proteins." *Virology* **249**(2): 406-417.
- Ben-Yishay, R., A. Mor, A. Shraga, A. Ashkenazy-Titelman, N. Kinor, A. Schwed-Gross, A. Jacob, N. Kozer, P. Kumar, Y. Garini and Y. Shav-Tal (2019). "Imaging within single NPCs reveals NXF1's role in mRNA export on the cytoplasmic side of the pore." *J Cell Biol* **218**(9): 2962-2981.
- Beniac, D. R., P. L. Melito, S. L. Devarenes, S. L. Hiebert, M. J. Rabb, L. L. Lamboo, S. M. Jones and T. F. Booth (2012). "The organisation of Ebola virus reveals a capacity for extensive, modular polyploidy." *PLoS One* **7**(1): e29608.
- Bharat, T. A., T. Noda, J. D. Riches, V. Kraehling, L. Kolesnikova, S. Becker, Y. Kawaoka and J. A. Briggs (2012). "Structural dissection of Ebola virus and its assembly determinants using cryo-electron tomography." *Proc Natl Acad Sci U S A* **109**(11): 4275-4280.
- Biacchesi, S., M. H. Skiadopoulos, G. Boivin, C. T. Hanson, B. R. Murphy, P. L. Collins and U. J. Buchholz (2003). "Genetic diversity between human metapneumovirus subgroups." *Virology* **315**(1): 1-9.
- Biedenkopf, N., B. Hartlieb, T. Hoenen and S. Becker (2013). "Phosphorylation of Ebola virus VP30 influences the composition of the viral nucleocapsid complex: impact on viral transcription and replication." *J Biol Chem* **288**(16): 11165-11174.
- Biedenkopf, N., J. Schlereth, A. Grunweller, S. Becker and R. K. Hartmann (2016). "RNA Binding of Ebola Virus VP30 Is Essential for Activating Viral Transcription." *J Virol* **90**(16): 7481-7496.
- Birnboim, H. C. and J. Doly (1979). "A rapid alkaline extraction procedure for screening recombinant plasmid DNA." *Nucleic Acids Res* **7**(6): 1513-1523.
- Bixler, S. L. and A. J. Goff (2015). "The Role of Cytokines and Chemokines in Filovirus Infection." *Viruses* **7**(10): 5489-5507.
- Boehmann, Y., S. Enterlein, A. Randolph and E. Muhlberger (2005). "A reconstituted replication and transcription system for Ebola virus Reston and comparison with Ebola virus Zaire." *Virology* **332**(1): 406-417.

- Borawski, J., P. Troke, X. Puyang, V. Gibaja, S. Zhao, C. Mickanin, J. Leighton-Davies, C. J. Wilson, V. Myer, I. Cornellataracido, J. Baryza, J. Tallarico, G. Joberty, M. Bantscheff, M. Schirle, T. Bouwmeester, J. E. Mathy, K. Lin, T. Compton, M. Labow, B. Wiedmann and L. A. Gaither (2009). "Class III phosphatidylinositol 4-kinase alpha and beta are novel host factor regulators of hepatitis C virus replication." *J Virol* **83**(19): 10058-10074.
- Borio, L., T. Inglesby, C. J. Peters, A. L. Schmaljohn, J. M. Hughes, P. B. Jahrling, T. Ksiazek, K. M. Johnson, A. Meyerhoff, T. O'Toole, M. S. Ascher, J. Bartlett, J. G. Breman, E. M. Eitzen, Jr., M. Hamburg, J. Hauer, D. A. Henderson, R. T. Johnson, G. Kwik, M. Layton, S. Lillibridge, G. J. Nabel, M. T. Osterholm, T. M. Perl, P. Russell, K. Tonat and B. Working Group on Civilian (2002). "Hemorrhagic fever viruses as biological weapons: medical and public health management." *JAMA* **287**(18): 2391-2405.
- Bowen, E. T., G. Lloyd, W. J. Harris, G. S. Platt, A. Baskerville and E. E. Vella (1977). "Viral haemorrhagic fever in southern Sudan and northern Zaire. Preliminary studies on the aetiological agent." *Lancet* **1**(8011): 571-573.
- Brandt, J., L. Wendt, B. S. Bodmer, T. C. Mettenleiter and T. Hoenen (2020). "The Cellular Protein CAD is Recruited into Ebola Virus Inclusion Bodies by the Nucleoprotein NP to Facilitate Genome Replication and Transcription." *Cells* **9**(5).
- Brandt, J., L. Wendt and T. Hoenen (2018). "Structure and function of the Ebola virus matrix protein VP40." *future medicine*.
- Braun, I. C., A. Herold, M. Rode, E. Conti and E. Izaurralde (2001). "Overexpression of TAP/p15 heterodimers bypasses nuclear retention and stimulates nuclear mRNA export." *J Biol Chem* **276**(23): 20536-20543.
- Braun, I. C., A. Herold, M. Rode and E. Izaurralde (2002). "Nuclear export of mRNA by TAP/NXF1 requires two nucleoporin-binding sites but not p15." *Mol Cell Biol* **22**(15): 5405-5418.
- Bukreyev, A., V. E. Volchkov, V. M. Blinov and S. V. Netesov (1993). "The GP-protein of Marburg virus contains the region similar to the 'immunosuppressive domain' of oncogenic retrovirus P15E proteins." *FEBS Lett* **323**(1-2): 183-187.
- Bukreyev, A. A., E. F. Belanov, V. M. Blinov and S. V. Netesov (1995). "Complete nucleotide sequences of Marburg virus genes 5 and 6 encoding VP30 and VP24 proteins." *Biochem Mol Biol Int* **35**(3): 605-613.

- Burk, R., L. Bollinger, J. C. Johnson, J. Wada, S. R. Radoshitzky, G. Palacios, S. Bavari, P. B. Jahrling and J. H. Kuhn (2016). "Neglected filoviruses." FEMS Microbiol Rev **40**(4): 494-519.
- Cantoni, D. and J. S. Rossman (2018). "Ebolaviruses: New roles for old proteins." PLoS Negl Trop Dis **12**(5): e0006349.
- Carette, J. E., M. Raaben, A. C. Wong, A. S. Herbert, G. Obernosterer, N. Mulherkar, A. I. Kuehne, P. J. Kranzusch, A. M. Griffin, G. Ruthel, P. Dal Cin, J. M. Dye, S. P. Whelan, K. Chandran and T. R. Brummelkamp (2011). "Ebola virus entry requires the cholesterol transporter Niemann-Pick C1." Nature **477**(7364): 340-343.
- Chandran, K., N. J. Sullivan, U. Felbor, S. P. Whelan and J. M. Cunningham (2005). "Endosomal proteolysis of the Ebola virus glycoprotein is necessary for infection." Science **308**(5728): 1643-1645.
- Chaparian, M. G. and D. R. Evans (1988). "Intracellular location of the multidomain protein CAD in mammalian cells." FASEB J **2**(14): 2982-2989.
- Chen, J., Z. He, Y. Yuan, F. Huang, B. Luo, J. Zhang, T. Pan, H. Zhang and J. Zhang (2019). "Host factor SMYD3 is recruited by Ebola virus nucleoprotein to facilitate viral mRNA transcription." Emerg Microbes Infect **8**(1): 1347-1360.
- Chiba, S., L. Hill-Batorski, G. Neumann and Y. Kawaoka (2018). "The Cellular DExD/H-Box RNA Helicase UAP56 Co-localizes With the Influenza A Virus NS1 Protein." Front Microbiol **9**: 2192.
- Christopherson, R. I. and M. E. Jones (1980). "The overall synthesis of L-5,6-dihydroorotate by multienzymatic protein pyr1-3 from hamster cells. Kinetic studies, substrate channeling, and the effects of inhibitors." J Biol Chem **255**(23): 11381-11395.
- Clarke, E. C., A. L. Collar, C. Ye, Y. Cai, E. Anaya, D. Rinaldi, B. Martinez, S. Yarborough, C. Merle, M. Theisen, J. Wada, J. H. Kuhn and S. B. Bradfute (2017). "Production and Purification of Filovirus Glycoproteins in Insect and Mammalian Cell Lines." Sci Rep **7**(1): 15091.
- Coleman, P. F., D. P. Suttle and G. R. Stark (1977). "Purification from hamster cells of the multifunctional protein that initiates de novo synthesis of pyrimidine nucleotides." J Biol Chem **252**(18): 6379-6385.
- Collins, K. D. and G. R. Stark (1971). "Aspartate transcarbamylase. Interaction with the transition state analogue N-(phosphonacetyl)-L-aspartate." J Biol Chem **246**(21): 6599-6605.

- Cox, N. J., J. B. McCormick, K. M. Johnson and M. P. Kiley (1983). "Evidence for two subtypes of Ebola virus based on oligonucleotide mapping of RNA." *J Infect Dis* **147**(2): 272-275.
- Danna, K. and D. Nathans (1999). "Specific cleavage of simian virus 40 DNA by restriction endonuclease of *Haemophilus influenzae*. 1971." *Rev Med Virol* **9**(2): 75-81.
- Deans, R. M., D. W. Morgens, A. Okesli, S. Pillay, M. A. Horlbeck, M. Kampmann, L. A. Gilbert, A. Li, R. Mateo, M. Smith, J. S. Glenn, J. E. Carette, C. Khosla and M. C. Bassik (2016). "Parallel shRNA and CRISPR-Cas9 screens enable antiviral drug target identification." *Nat Chem Biol* **12**(5): 361-366.
- Del Rio, C., A. K. Mehta, G. M. Lyon, 3rd and J. Guarner (2014). "Ebola hemorrhagic fever in 2014: the tale of an evolving epidemic." *Ann Intern Med* **161**(10): 746-748.
- Dessen, A., V. Volchkov, O. Dolnik, H. D. Klenk and W. Weissenhorn (2000). "Crystal structure of the matrix protein VP40 from Ebola virus." *EMBO J* **19**(16): 4228-4236.
- Don, R. H., P. T. Cox, B. J. Wainwright, K. Baker and J. S. Mattick (1991). "'Touchdown' PCR to circumvent spurious priming during gene amplification." *Nucleic Acids Res* **19**(14): 4008.
- Dong, S., P. Yang, G. Li, B. Liu, W. Wang, X. Liu, B. Xia, C. Yang, Z. Lou, Y. Guo and Z. Rao (2015). "Insight into the Ebola virus nucleocapsid assembly mechanism: crystal structure of Ebola virus nucleoprotein core domain at 1.8 Å resolution." *Protein Cell* **6**(5): 351-362.
- Dowell, S. F., R. Mukunu, T. G. Ksiazek, A. S. Khan, P. E. Rollin and C. J. Peters (1999). "Transmission of Ebola hemorrhagic fever: a study of risk factors in family members, Kikwit, Democratic Republic of the Congo, 1995. Commission de Lutte contre les Epidemies a Kikwit." *J Infect Dis* **179 Suppl 1**: S87-91.
- Dziubanska, P. J., U. Derewenda, J. F. Ellena, D. A. Engel and Z. S. Derewenda (2014). "The structure of the C-terminal domain of the Zaire ebolavirus nucleoprotein." *Acta Crystallogr D Biol Crystallogr* **70**(Pt 9): 2420-2429.
- Eamens, A. L., M. McHale and P. M. Waterhouse (2014). "The use of artificial microRNA technology to control gene expression in *Arabidopsis thaliana*." *Methods Mol Biol* **1062**: 211-224.
- Elliott, L. H., M. P. Kiley and J. B. McCormick (1985). "Descriptive analysis of Ebola virus proteins." *Virology* **147**(1): 169-176.
- Evans, D. R. and H. I. Guy (2004). "Mammalian pyrimidine biosynthesis: fresh insights into an ancient pathway." *J Biol Chem* **279**(32): 33035-33038.

- Fang, J., C. Pietzsch, P. Ramanathan, R. I. Santos, P. A. Ilinykh, M. A. Garcia-Blanco, A. Bukreyev and S. S. Bradrick (2018). "Staufen1 Interacts with Multiple Components of the Ebola Virus Ribonucleoprotein and Enhances Viral RNA Synthesis." *mBio* **9**(5).
- Feldmann, H. and T. W. Geisbert (2011). "Ebola haemorrhagic fever." *Lancet* **377**(9768): 849-862.
- Feldmann, H., S. Jones, H. D. Klenk and H. J. Schnittler (2003). "Ebola virus: from discovery to vaccine." *Nat Rev Immunol* **3**(8): 677-685.
- Feldmann, H. and M. P. Kiley (1999). "Classification, structure, and replication of filoviruses." *Curr Top Microbiol Immunol* **235**: 1-21.
- Feldmann, H. and H. D. Klenk (1996). Filoviruses. *Medical Microbiology*. 4th and S. Baron. Galveston (TX).
- Feldmann, H., S. T. Nichol, H. D. Klenk, C. J. Peters and A. Sanchez (1994). "Characterization of filoviruses based on differences in structure and antigenicity of the virion glycoprotein." *Virology* **199**(2): 469-473.
- Feldmann, H., V. E. Volchkov, V. A. Volchkova, U. Stroher and H. D. Klenk (2001). "Biosynthesis and role of filoviral glycoproteins." *J Gen Virol* **82**(Pt 12): 2839-2848.
- Feldmann, H., C. Will, M. Schikore, W. Slenczka and H. D. Klenk (1991). "Glycosylation and oligomerization of the spike protein of Marburg virus." *Virology* **182**(1): 353-356.
- Fels, J. M., R. H. Bortz, 3rd, T. Alkutar, E. Mittler, R. K. Jangra, J. S. Spence and K. Chandran (2021). "A Glycoprotein Mutation That Emerged during the 2013-2016 Ebola Virus Epidemic Alters Proteolysis and Accelerates Membrane Fusion." *mBio* **12**(1).
- Fire, A., S. Xu, M. K. Montgomery, S. A. Kostas, S. E. Driver and C. C. Mello (1998). "Potent and specific genetic interference by double-stranded RNA in *Caenorhabditis elegans*." *Nature* **391**(6669): 806-811.
- Fleckner, J., M. Zhang, J. Valcarcel and M. R. Green (1997). "U2AF65 recruits a novel human DEAD box protein required for the U2 snRNP-branchpoint interaction." *Genes Dev* **11**(14): 1864-1872.
- Forbes, K. M., P. W. Webala, A. J. Jaaskelainen, S. Abdurahman, J. Ogola, M. M. Masika, I. Kivisto, H. Alburkat, I. Plyusnin, L. Levanov, E. M. Korhonen, E. Huhtamo, D. Mwaengo, T. Smura, A. Mirazimi, O. Anzala, O. Vapalahti and T. Sironen (2019). "Bombali Virus in *Mops condylurus* Bat, Kenya." *Emerg Infect Dis* **25**(5): 955-957.

- Franco, I. S. and H. A. Shuman (2012). "A pathogen's journey in the host cell: Bridges between actin and traffic." Bioarchitecture **2**(2): 38-42.
- Fredman, J. N. and J. A. Engler (1993). "Adenovirus precursor to terminal protein interacts with the nuclear matrix in vivo and in vitro." J Virol **67**(6): 3384-3395.
- Fribourg, S., I. C. Braun, E. Izaurralde and E. Conti (2001). "Structural basis for the recognition of a nucleoporin FG repeat by the NTF2-like domain of the TAP/p15 mRNA nuclear export factor." Mol Cell **8**(3): 645-656.
- Gales, J. P., J. Kubina, A. Geldreich and M. Dimitrova (2020). "Strength in Diversity: Nuclear Export of Viral RNAs." Viruses **12**(9).
- Geisbert, T. W., L. E. Hensley, T. Larsen, H. A. Young, D. S. Reed, J. B. Geisbert, D. P. Scott, E. Kagan, P. B. Jahrling and K. J. Davis (2003). "Pathogenesis of Ebola hemorrhagic fever in cynomolgus macaques: evidence that dendritic cells are early and sustained targets of infection." Am J Pathol **163**(6): 2347-2370.
- Geisbert, T. W. and P. B. Jahrling (1995). "Differentiation of filoviruses by electron microscopy." Virus Res **39**(2-3): 129-150.
- Goldstein, T., S. J. Anthony, A. Gbakima, B. H. Bird, J. Bangura, A. Tremeau-Bravard, M. N. Belaganahalli, H. L. Wells, J. K. Dhanota, E. Liang, M. Grodus, R. K. Jangra, V. A. DeJesus, G. Lasso, B. R. Smith, A. Jambai, B. O. Kamara, S. Kamara, W. Bangura, C. Monagin, S. Shapira, C. K. Johnson, K. Saylor, E. M. Rubin, K. Chandran, W. I. Lipkin and J. A. K. Mazet (2018). "The discovery of Bombali virus adds further support for bats as hosts of ebolaviruses." Nat Microbiol **3**(10): 1084-1089.
- Griffith, F. (1928). "The Significance of Pneumococcal Types." J Hyg (Lond) **27**(2): 113-159.
- Groseth, A., J. E. Charton, M. Sauerborn, F. Feldmann, S. M. Jones, T. Hoenen and H. Feldmann (2009). "The Ebola virus ribonucleoprotein complex: a novel VP30-L interaction identified." Virus Res **140**(1-2): 8-14.
- Gruter, P., C. Taberner, C. von Kobbe, C. Schmitt, C. Saavedra, A. Bachi, M. Wilm, B. K. Felber and E. Izaurralde (1998). "TAP, the human homolog of Mex67p, mediates CTE-dependent RNA export from the nucleus." Mol Cell **1**(5): 649-659.
- Guito, J. C., C. G. Albarino, A. K. Chakrabarti and J. S. Towner (2017). "Novel activities by ebolavirus and marburgvirus interferon antagonists revealed using a standardized in vitro reporter system." Virology **501**: 147-165.

- Gupta, M., S. Mahanty, M. Bray, R. Ahmed and P. E. Rollin (2001). "Passive transfer of antibodies protects immunocompetent and immunodeficient mice against lethal Ebola virus infection without complete inhibition of viral replication." *J Virol* **75**(10): 4649-4654.
- Guzik, B. W., L. Levesque, S. Prasad, Y. C. Bor, B. E. Black, B. M. Paschal, D. Rekosh and M. L. Hammarskjöld (2001). "NXT1 (p15) is a crucial cellular cofactor in TAP-dependent export of intron-containing RNA in mammalian cells." *Mol Cell Biol* **21**(7): 2545-2554.
- Halfmann, P., G. Neumann and Y. Kawaoka (2011). "The Ebolavirus VP24 protein blocks phosphorylation of p38 mitogen-activated protein kinase." *J Infect Dis* **204 Suppl 3**: S953-956.
- Hartlieb, B., T. Muziol, W. Weissenhorn and S. Becker (2007). "Crystal structure of the C-terminal domain of Ebola virus VP30 reveals a role in transcription and nucleocapsid association." *Proc Natl Acad Sci U S A* **104**(2): 624-629.
- Hartlieb, B. and W. Weissenhorn (2006). "Filovirus assembly and budding." *Virology* **344**(1): 64-70.
- Hasan, S., S. A. Ahmad, R. Masood and S. Saeed (2019). "Ebola virus: A global public health menace: A narrative review." *J Family Med Prim Care* **8**(7): 2189-2201.
- Hautbergue, G. M., M. L. Hung, A. P. Golovanov, L. Y. Lian and S. A. Wilson (2008). "Mutually exclusive interactions drive handover of mRNA from export adaptors to TAP." *Proc Natl Acad Sci U S A* **105**(13): 5154-5159.
- He, J., L. I. Melnik, A. Komin, G. Wiedman, T. Fuselier, C. F. Morris, C. G. Starr, P. C. Searson, W. R. Gallaher, K. Hristova, R. F. Garry and W. C. Wimley (2017). "Ebola Virus Delta Peptide Is a Viroporin." *J Virol* **91**(16).
- Hensley, L. E., H. A. Young, P. B. Jahrling and T. W. Geisbert (2002). "Proinflammatory response during Ebola virus infection of primate models: possible involvement of the tumor necrosis factor receptor superfamily." *Immunol Lett* **80**(3): 169-179.
- Hochberg-Laufer, H., A. Schwed-Gross, K. M. Neugebauer and Y. Shav-Tal (2019). "Uncoupling of nucleo-cytoplasmic RNA export and localization during stress." *Nucleic Acids Res* **47**(9): 4778-4797.
- Hoenen, T., N. Biedenkopf, F. Zielecki, S. Jung, A. Groseth, H. Feldmann and S. Becker (2010a). "Oligomerization of Ebola virus VP40 is essential for particle morphogenesis and regulation of viral transcription." *J Virol* **84**(14): 7053-7063.

- Hoenen, T., J. Brandt, Y. Cai, J. H. Kuhn and C. Finch (2017). "Reverse Genetics of Filoviruses." Curr Top Microbiol Immunol **411**: 421-445.
- Hoenen, T. and H. Feldmann (2014). "Reverse genetics systems as tools for the development of novel therapies against filoviruses." Expert Rev Anti Infect Ther **12**(10): 1253-1263.
- Hoenen, T., A. Groseth, F. de Kok-Mercado, J. H. Kuhn and V. Wahl-Jensen (2011). "Minigenomes, transcription and replication competent virus-like particles and beyond: reverse genetics systems for filoviruses and other negative stranded hemorrhagic fever viruses." Antiviral Res **91**(2): 195-208.
- Hoenen, T., A. Groseth, D. Falzarano and H. Feldmann (2006). "Ebola virus: unravelling pathogenesis to combat a deadly disease." Trends Mol Med **12**(5): 206-215.
- Hoenen, T., S. Jung, A. Herwig, A. Groseth and S. Becker (2010b). "Both matrix proteins of Ebola virus contribute to the regulation of viral genome replication and transcription." Virology **403**(1): 56-66.
- Hoenen, T., R. S. Shabman, A. Groseth, A. Herwig, M. Weber, G. Schudt, O. Dolnik, C. F. Basler, S. Becker and H. Feldmann (2012). "Inclusion bodies are a site of ebolavirus replication." J Virol **86**(21): 11779-11788.
- Hood, C. L., J. Abraham, J. C. Boyington, K. Leung, P. D. Kwong and G. J. Nabel (2010). "Biochemical and structural characterization of cathepsin L-processed Ebola virus glycoprotein: implications for viral entry and immunogenicity." J Virol **84**(6): 2972-2982.
- Hu, Y., V. Gor, K. Morikawa, K. Nagata and A. Kawaguchi (2017). "Cellular splicing factor UAP56 stimulates trimeric NP formation for assembly of functional influenza viral ribonucleoprotein complexes." Sci Rep **7**(1): 14053.
- Ikegami, T., A. B. Calaor, M. E. Miranda, M. Niikura, M. Saijo, I. Kurane, Y. Yoshikawa and S. Morikawa (2001). "Genome structure of Ebola virus subtype Reston: differences among Ebola subtypes. Brief report." Arch Virol **146**(10): 2021-2027.
- Ilinykh, P. A., B. Tigabu, A. Ivanov, T. Ammosova, Y. Obukhov, T. Garron, N. Kumari, D. Kovalskyy, M. O. Platonov, V. S. Naumchik, A. N. Freiberg, S. Nekhai and A. Bukreyev (2014). "Role of protein phosphatase 1 in dephosphorylation of Ebola virus VP30 protein and its targeting for the inhibition of viral transcription." J Biol Chem **289**(33): 22723-22738.
- Irvine, H. S., S. M. Shaw, A. Paton and E. A. Carrey (1997). "A reciprocal allosteric mechanism for efficient transfer of labile intermediates between active sites in CAD, the mammalian pyrimidine-biosynthetic multienzyme polypeptide." Eur J Biochem **247**(3): 1063-1073.

- Ito, H., S. Watanabe, A. Sanchez, M. A. Whitt and Y. Kawaoka (1999). "Mutational analysis of the putative fusion domain of Ebola virus glycoprotein." J Virol **73**(10): 8907-8912.
- Iwasa, A., P. Halfmann, T. Noda, M. Oyama, H. Kozuka-Hata, S. Watanabe, M. Shimojima, T. Watanabe and Y. Kawaoka (2011). "Contribution of Sec61alpha to the life cycle of Ebola virus." J Infect Dis **204 Suppl 3**: S919-926.
- Jasenosky, L. D., G. Neumann, I. Lukashevich and Y. Kawaoka (2001). "Ebola virus VP40-induced particle formation and association with the lipid bilayer." J Virol **75**(11): 5205-5214.
- Ji, X., G. G. Olinger, S. Aris, Y. Chen, H. Gewurz and G. T. Spear (2005). "Mannose-binding lectin binds to Ebola and Marburg envelope glycoproteins, resulting in blocking of virus interaction with DC-SIGN and complement-mediated virus neutralization." J Gen Virol **86**(Pt 9): 2535-2542.
- John, S. P., T. Wang, S. Steffen, S. Longhi, C. S. Schmaljohn and C. B. Jonsson (2007). "Ebola virus VP30 is an RNA binding protein." J Virol **81**(17): 8967-8976.
- Johnson, K. M., J. V. Lange, P. A. Webb and F. A. Murphy (1977). "Isolation and partial characterisation of a new virus causing acute haemorrhagic fever in Zaire." Lancet **1**(8011): 569-571.
- Johnson, R. F., S. E. McCarthy, P. J. Godlewski and R. N. Harty (2006). "Ebola virus VP35-VP40 interaction is sufficient for packaging 3E-5E minigenome RNA into virus-like particles." J Virol **80**(11): 5135-5144.
- Jones, M. E. (1980). "Pyrimidine nucleotide biosynthesis in animals: genes, enzymes, and regulation of UMP biosynthesis." Annu Rev Biochem **49**: 253-279.
- Karan, L. S., M. T. Makenov, M. G. Korneev, N. Sacko, S. Boumbaly, S. A. Yakovlev, K. Kourouma, R. B. Bayandin, A. V. Gladysheva, A. V. Shipovalov, I. A. Yurganova, Y. E. Grigorieva, M. V. Fedorova, S. A. Scherbakova, V. V. Kutyrev, A. P. Agafonov, R. A. Maksyutov, G. A. Shipulin, V. V. Maleev, M. Boiro, V. G. Akimkin and A. Y. Popova (2019). "Bombali Virus in Mops condylurus Bats, Guinea." Emerg Infect Dis **25**(9).
- Katahira, J., K. Strasser, A. Podtelejnikov, M. Mann, J. U. Jung and E. Hurt (1999). "The Mex67p-mediated nuclear mRNA export pathway is conserved from yeast to human." EMBO J **18**(9): 2593-2609.
- Katahira, J. and Y. Yoneda (2009). "Roles of the TREX complex in nuclear export of mRNA." RNA Biol **6**(2): 149-152.

- Katsafanas, G. C., J. L. Grem, H. A. Blough and B. Moss (1997). "Inhibition of vaccinia virus replication by N-(phosphonoacetyl)-L-aspartate: differential effects on viral gene expression result from a reduced pyrimidine nucleotide pool." *Virology* **236**(1): 177-187.
- Kawaguchi, A., F. Momose and K. Nagata (2011). "Replication-coupled and host factor-mediated encapsidation of the influenza virus genome by viral nucleoprotein." *J Virol* **85**(13): 6197-6204.
- Kiley, M. P., E. T. Bowen, G. A. Eddy, M. Isaacson, K. M. Johnson, J. B. McCormick, F. A. Murphy, S. R. Pattyn, D. Peters, O. W. Prozesky, R. L. Regnery, D. I. Simpson, W. Slenczka, P. Sureau, G. van der Groen, P. A. Webb and H. Wulff (1982). "Filoviridae: a taxonomic home for Marburg and Ebola viruses?" *Intervirology* **18**(1-2): 24-32.
- Kiley, M. P., R. L. Regnery and K. M. Johnson (1980). "Ebola virus: identification of virion structural proteins." *J Gen Virol* **49**(2): 333-341.
- Kim, D. H. and J. J. Rossi (2007). "Strategies for silencing human disease using RNA interference." *Nat Rev Genet* **8**(3): 173-184.
- Kirchdoerfer, R. N., D. M. Abelson, S. Li, M. R. Wood and E. O. Saphire (2015). "Assembly of the Ebola Virus Nucleoprotein from a Chaperoned VP35 Complex." *Cell Rep* **12**(1): 140-149.
- Kirchdoerfer, R. N., C. L. Moyer, D. M. Abelson and E. O. Saphire (2016). "The Ebola Virus VP30-NP Interaction Is a Regulator of Viral RNA Synthesis." *PLoS Pathog* **12**(10): e1005937.
- Kistler, A. L. and C. Guthrie (2001). "Deletion of MUD2, the yeast homolog of U2AF65, can bypass the requirement for sub2, an essential spliceosomal ATPase." *Genes Dev* **15**(1): 42-49.
- Kohler, A. and E. Hurt (2007). "Exporting RNA from the nucleus to the cytoplasm." *Nat Rev Mol Cell Biol* **8**(10): 761-773.
- Korbie, D. J. and J. S. Mattick (2008). "Touchdown PCR for increased specificity and sensitivity in PCR amplification." *Nat Protoc* **3**(9): 1452-1456.
- Kruse, T., N. Biedenkopf, E. P. T. Hertz, E. Dietzel, G. Stalman, B. Lopez-Mendez, N. E. Davey, J. Nilsson and S. Becker (2018). "The Ebola Virus Nucleoprotein Recruits the Host PP2A-B56 Phosphatase to Activate Transcriptional Support Activity of VP30." *Mol Cell* **69**(1): 136-145 e136.

Kuhn, J. H., S. Adkins, D. Alioto, S. V. Alkhovsky, G. K. Amarasinghe, S. J. Anthony, T. Avsic-Zupanc, M. A. Ayllon, J. Bahl, A. Balkema-Buschmann, M. J. Ballinger, T. Bartonicka, C. Basler, S. Bavari, M. Beer, D. A. Bente, E. Bergeron, B. H. Bird, C. Blair, K. R. Blasdel, S. B. Bradfute, R. Breyta, T. Briese, P. A. Brown, U. J. Buchholz, M. J. Buchmeier, A. Bukreyev, F. Burt, N. Buzkan, C. H. Calisher, M. Cao, I. Casas, J. Chamberlain, K. Chandran, R. N. Charrel, B. Chen, M. Chiumenti, I. R. Choi, J. C. S. Clegg, I. Crozier, J. V. da Graca, E. Dal Bo, A. M. R. Davila, J. C. de la Torre, X. de Lamballerie, R. L. de Swart, P. L. Di Bello, N. Di Paola, F. Di Serio, R. G. Dietzgen, M. Digiario, V. V. Dolja, O. Dolnik, M. A. Drebot, J. F. Drexler, R. Durrwald, L. Dufkova, W. G. Dundon, W. P. Duprex, J. M. Dye, A. J. Easton, H. Ebihara, T. Elbeaino, K. Ergunay, J. Fernandes, A. R. Fooks, P. B. H. Formenty, L. F. Forth, R. A. M. Fouchier, J. Freitas-Astua, S. Gago-Zachert, G. F. Gao, M. L. Garcia, A. Garcia-Sastre, A. R. Garrison, A. Gbakima, T. Goldstein, J. J. Gonzalez, A. Griffiths, M. H. Groschup, S. Gunther, A. Guterres, R. A. Hall, J. Hammond, M. Hassan, J. Hepojoki, S. Hepojoki, U. Hetzel, R. Hewson, B. Hoffmann, S. Hongo, D. Hoper, M. Horie, H. R. Hughes, T. H. Hyndman, A. Jambai, R. Jardim, D. Jiang, Q. Jin, G. B. Jonson, S. Junglen, S. Karadag, K. E. Keller, B. Klempa, J. Klingstrom, G. Kobinger, H. Kondo, E. V. Koonin, M. Krupovic, G. Kurath, I. V. Kuzmin, L. Laenen, R. A. Lamb, A. J. Lambert, S. L. Langevin, B. Lee, E. R. S. Lemos, E. M. Leroy, D. Li, J. Li, M. Liang, W. Liu, Y. Liu, I. S. Lukashevich, P. Maes, W. Marciel de Souza, M. Marklewitz, S. H. Marshall, G. P. Martelli, R. R. Martin, S. L. Marzano, S. Massart, J. W. McCauley, N. Mielke-Ehret, A. Minafra, M. Minutolo, A. Mirazimi, H. P. Muhlbach, E. Muhlberger, R. Naidu, T. Natsuaki, B. Navarro, J. A. Navarro, S. V. Netesov, G. Neumann, N. Nowotny, M. R. T. Nunes, A. Nylund, A. L. Okland, R. C. Oliveira, G. Palacios, V. Pallas, B. Palyi, A. Papa, C. R. Parrish, A. Pauvolid-Correa, J. T. Paweska, S. Payne, D. R. Perez, F. Pfaff, S. R. Radoshitzky, A. U. Rahman, P. L. Ramos-Gonzalez, R. O. Resende, C. A. Reyes, B. K. Rima, V. Romanowski, G. Robles Luna, P. Rota, D. Rubbenstroth, J. A. Runstadler, D. Ruzek, S. Sabanadzovic, J. Salat, A. A. Sall, M. S. Salvato, K. Sarpkaya, T. Sasaya, M. Schwemmler, M. Z. Shabbir, X. Shi, Z. Shi, Y. Shirako, P. Simmonds, J. Sirmarova, M. Sironi, S. Smither, T. Smura, J. W. Song, K. M. Spann, J. R. Spengler, M. D. Stenglein, D. M. Stone, P. Strakova, A. Takada, R. B. Tesh, N. J. Thornburg, K. Tomonaga, N. Tordo, J. S. Towner, M. Turina, I. Tzanetakis, R. G. Ulrich, A. M. Vaira, B. van den Hoogen, A. Varsani, N. Vasilakis, M. Verbeek, V. Wahl, P. J. Walker, H. Wang, J. Wang, X. Wang, L. F. Wang, T. Wei, H. Wells, A. E. Whitfield, J. V. Williams, Y. I. Wolf, Z. Wu, X. Yang, X. Yang, X. Yu, N. Yutin, F. M. Zerbini, T. Zhang, Y. Z. Zhang, G. Zhou and X. Zhou (2020). "2020 taxonomic update for phylum Negarnaviricota (Riboviria: Orthornavirae), including the large orders Bunyavirales and Mononegavirales." *Arch Virol* **165**(12): 3023-3072.

- Kuhn, J. H., S. R. Radoshitzky, A. C. Guth, K. L. Warfield, W. Li, M. J. Vincent, J. S. Towner, S. T. Nichol, S. Bavari, H. Choe, M. J. Aman and M. Farzan (2006). "Conserved receptor-binding domains of Lake Victoria marburgvirus and Zaire ebolavirus bind a common receptor." *J Biol Chem* **281**(23): 15951-15958.
- Laemmli, U. K. (1970). "Cleavage of structural proteins during the assembly of the head of bacteriophage T4." *Nature* **227**(5259): 680-685.
- Lam, J. K., M. Y. Chow, Y. Zhang and S. W. Leung (2015). "siRNA Versus miRNA as Therapeutics for Gene Silencing." *Mol Ther Nucleic Acids* **4**: e252.
- Larsen, S., S. Bui, V. Perez, A. Mohammad, H. Medina-Ramirez and L. L. Newcomb (2014). "Influenza polymerase encoding mRNAs utilize atypical mRNA nuclear export." *Virology* **11**: 154.
- Le Guenno, B., P. Formenty, M. Wyers, P. Gounon, F. Walker and C. Boesch (1995). "Isolation and partial characterisation of a new strain of Ebola virus." *Lancet* **345**(8960): 1271-1274.
- Lee, J. E., M. L. Fusco, D. M. Abelson, A. J. Hessel, D. R. Burton and E. O. Saphire (2009). "Techniques and tactics used in determining the structure of the trimeric ebolavirus glycoprotein." *Acta Crystallogr D Biol Crystallogr* **65**(Pt 11): 1162-1180.
- Lee, L., R. E. Kelly, S. C. Pastra-Landis and D. R. Evans (1985). "Oligomeric structure of the multifunctional protein CAD that initiates pyrimidine biosynthesis in mammalian cells." *Proc Natl Acad Sci U S A* **82**(20): 6802-6806.
- Leroy, E. M., J. P. Gonzalez and S. Baize (2011). "Ebola and Marburg haemorrhagic fever viruses: major scientific advances, but a relatively minor public health threat for Africa." *Clin Microbiol Infect* **17**(7): 964-976.
- Leung, D. W., D. Borek, P. Luthra, J. M. Binning, M. Anantpadma, G. Liu, I. B. Harvey, Z. Su, A. Endlich-Frazier, J. Pan, R. S. Shabman, W. Chiu, R. A. Davey, Z. Otwinowski, C. F. Basler and G. K. Amarasinghe (2015). "An Intrinsically Disordered Peptide from Ebola Virus VP35 Controls Viral RNA Synthesis by Modulating Nucleoprotein-RNA Interactions." *Cell Rep* **11**(3): 376-389.
- Leung, D. W., K. C. Prins, C. F. Basler and G. K. Amarasinghe (2010b). "Ebola virus VP35 is a multifunctional virulence factor." *Virulence* **1**(6): 526-531.
- Leung, D. W., K. C. Prins, D. M. Borek, M. Farahbakhsh, J. M. Tufariello, P. Ramanan, J. C. Nix, L. A. Helgeson, Z. Otwinowski, R. B. Honzatko, C. F. Basler and G. K. Amarasinghe (2010a). "Structural basis for dsRNA recognition and interferon antagonism by Ebola VP35." *Nat Struct Mol Biol* **17**(2): 165-172.

- Licata, J. M., M. Simpson-Holley, N. T. Wright, Z. Han, J. Paragas and R. N. Harty (2003). "Overlapping motifs (PTAP and PPEY) within the Ebola virus VP40 protein function independently as late budding domains: involvement of host proteins TSG101 and VPS-4." *J Virol* **77**(3): 1812-1819.
- Lier, C., S. Becker and N. Biedenkopf (2017). "Dynamic phosphorylation of Ebola virus VP30 in NP-induced inclusion bodies." *Virology* **512**: 39-47.
- Luo, M. L., Z. Zhou, K. Magni, C. Christoforides, J. Rappsilber, M. Mann and R. Reed (2001). "Pre-mRNA splicing and mRNA export linked by direct interactions between UAP56 and Aly." *Nature* **413**(6856): 644-647.
- Luthra, P., J. Naidoo, C. A. Pietzsch, S. De, S. Khadka, M. Anantpadma, C. G. Williams, M. R. Edwards, R. A. Davey, A. Bukreyev, J. M. Ready and C. F. Basler (2018). "Inhibiting pyrimidine biosynthesis impairs Ebola virus replication through depletion of nucleoside pools and activation of innate immune responses." *Antiviral Res* **158**: 288-302.
- Mahanty, S., K. Hutchinson, S. Agarwal, M. McRae, P. E. Rollin and B. Pulendran (2003). "Cutting edge: impairment of dendritic cells and adaptive immunity by Ebola and Lassa viruses." *J Immunol* **170**(6): 2797-2801.
- Majid, M. U., M. S. Tahir, Q. Ali, A. Q. Rao, B. Rashid, A. Ali, I. A. Nasir and T. Husnain (2016). "Nature and History of Ebola Virus: An Overview." *Arch Neurosci*.
- Malvy, D., A. K. McElroy, H. de Clerck, S. Gunther and J. van Griensven (2019). "Ebola virus disease." *Lancet* **393**(10174): 936-948.
- Martin-Serrano, J., T. Zang and P. D. Bieniasz (2001). "HIV-1 and Ebola virus encode small peptide motifs that recruit Tsg101 to sites of particle assembly to facilitate egress." *Nat Med* **7**(12): 1313-1319.
- Martin, S., A. I. Chiramel, M. L. Schmidt, Y. C. Chen, N. Whitt, A. Watt, E. C. Dunham, K. Shifflett, S. Traeger, A. Leske, E. Buehler, C. Martellaro, J. Brandt, L. Wendt, A. Muller, S. Peitsch, S. M. Best, J. Stech, S. Finke, A. Romer-Oberdorfer, A. Groseth, H. Feldmann and T. Hoenen (2018). "A genome-wide siRNA screen identifies a druggable host pathway essential for the Ebola virus life cycle." *Genome Med* **10**(1): 58.
- Marzi, A., T. Gramberg, G. Simmons, P. Moller, A. J. Rennekamp, M. Krumbiegel, M. Geier, J. Eisemann, N. Turza, B. Saunier, A. Steinkasserer, S. Becker, P. Bates, H. Hofmann and S. Pohlmann (2004). "DC-SIGN and DC-SIGNR interact with the glycoprotein of Marburg virus and the S protein of severe acute respiratory syndrome coronavirus." *J Virol* **78**(21): 12090-12095.

- Mateo, M., S. P. Reid, L. W. Leung, C. F. Basler and V. E. Volchkov (2010). "Ebola virus VP24 binding to karyopherins is required for inhibition of interferon signaling." *J Virol* **84**(2): 1169-1175.
- Mehedi, M., D. Falzarano, J. Seebach, X. Hu, M. S. Carpenter, H. J. Schnittler and H. Feldmann (2011). "A new Ebola virus nonstructural glycoprotein expressed through RNA editing." *J Virol* **85**(11): 5406-5414.
- Meignin, C. and I. Davis (2008). "UAP56 RNA helicase is required for axis specification and cytoplasmic mRNA localization in *Drosophila*." *Dev Biol* **315**(1): 89-98.
- Merritt, W. M., M. Bar-Eli and A. K. Sood (2010). "The dicey role of Dicer: implications for RNAi therapy." *Cancer Res* **70**(7): 2571-2574.
- Messaoudi, I., G. K. Amarasinghe and C. F. Basler (2015). "Filovirus pathogenesis and immune evasion: insights from Ebola virus and Marburg virus." *Nat Rev Microbiol* **13**(11): 663-676.
- Miller, E. H., G. Obernosterer, M. Raaben, A. S. Herbert, M. S. Deffieu, A. Krishnan, E. Ndungo, R. G. Sandesara, J. E. Carette, A. I. Kuehne, G. Ruthel, S. R. Pfeffer, J. M. Dye, S. P. Whelan, T. R. Brummelkamp and K. Chandran (2012). "Ebola virus entry requires the host-programmed recognition of an intracellular receptor." *EMBO J* **31**(8): 1947-1960.
- Miranda, M. E., T. G. Ksiazek, T. J. Retuya, A. S. Khan, A. Sanchez, C. F. Fulhorst, P. E. Rollin, A. B. Calaor, D. L. Manalo, M. C. Roces, M. M. Dayrit and C. J. Peters (1999). "Epidemiology of Ebola (subtype Reston) virus in the Philippines, 1996." *J Infect Dis* **179** **Suppl 1**: S115-119.
- Miranda, M. E., Y. Yoshikawa, D. L. Manalo, A. B. Calaor, N. L. Miranda, F. Cho, T. Ikegami and T. G. Ksiazek (2002). "Chronological and spatial analysis of the 1996 Ebola Reston virus outbreak in a monkey breeding facility in the Philippines." *Exp Anim* **51**(2): 173-179.
- Misasi, J., K. Chandran, J. Y. Yang, B. Considine, C. M. Filone, M. Cote, N. Sullivan, G. Fabozzi, L. Hensley and J. Cunningham (2012). "Filoviruses require endosomal cysteine proteases for entry but exhibit distinct protease preferences." *J Virol* **86**(6): 3284-3292.
- Miyake, T., C. M. Farley, B. E. Neubauer, T. P. Beddow, T. Hoenen and D. A. Engel (2020). "Ebola Virus Inclusion Body Formation and RNA Synthesis Are Controlled by a Novel Domain of Nucleoprotein Interacting with VP35." *J Virol* **94**(16).
- Mohan, G. S., W. Li, L. Ye, R. W. Compans and C. Yang (2012). "Antigenic subversion: a novel mechanism of host immune evasion by Ebola virus." *PLoS Pathog* **8**(12): e1003065.

- Moller-Tank, S. and W. Maury (2015). "Ebola virus entry: a curious and complex series of events." PLoS Pathog **11**(4): e1004731.
- Momose, F., C. F. Basler, R. E. O'Neill, A. Iwamatsu, P. Palese and K. Nagata (2001). "Cellular splicing factor RAF-2p48/NPI-5/BAT1/UAP56 interacts with the influenza virus nucleoprotein and enhances viral RNA synthesis." J Virol **75**(4): 1899-1908.
- Morris, A. K., Z. Wang, A. L. Ivey, Y. Xie, P. S. Hill, K. L. Schey and Y. Ren (2020). "Cellular mRNA export factor UAP56 recognizes nucleic acid binding site of influenza virus NP protein." Biochem Biophys Res Commun **525**(2): 259-264.
- Morwitzer, M. J., S. R. Tritsch, L. H. Cazares, M. D. Ward, J. E. Nuss, S. Bavari and S. P. Reid (2019). "Identification of RUVBL1 and RUVBL2 as Novel Cellular Interactors of the Ebola Virus Nucleoprotein." Viruses **11**(4).
- Muhlberger, E. (2007). "Filovirus replication and transcription." Future Virol **2**(2): 205-215.
- Muhlberger, E., B. Lotfering, H. D. Klenk and S. Becker (1998). "Three of the four nucleocapsid proteins of Marburg virus, NP, VP35, and L, are sufficient to mediate replication and transcription of Marburg virus-specific monocistronic minigenomes." J Virol **72**(11): 8756-8764.
- Muhlberger, E., S. Trommer, C. Funke, V. Volchkov, H. D. Klenk and S. Becker (1996). "Termini of all mRNA species of Marburg virus: sequence and secondary structure." Virology **223**(2): 376-380.
- Muhlberger, E., M. Weik, V. E. Volchkov, H. D. Klenk and S. Becker (1999). "Comparison of the transcription and replication strategies of marburg virus and Ebola virus by using artificial replication systems." J Virol **73**(3): 2333-2342.
- Mullis, K. B. (1990). "The unusual origin of the polymerase chain reaction." Sci Am **262**(4): 56-61, 64-55.
- Nanbo, A., M. Imai, S. Watanabe, T. Noda, K. Takahashi, G. Neumann, P. Halfmann and Y. Kawaoka (2010). "Ebola virus is internalized into host cells via macropinocytosis in a viral glycoprotein-dependent manner." PLoS Pathog **6**(9): e1001121.
- Nelson, E. V., J. R. Pacheco, A. J. Hume, T. N. Cressey, L. R. Deflube, J. B. Ruedas, J. H. Connor, H. Ebihara and E. Muhlberger (2017). "An RNA polymerase II-driven Ebola virus minigenome system as an advanced tool for antiviral drug screening." Antiviral Res **146**: 21-27.

- Neumann, G., H. Feldmann, S. Watanabe, I. Lukashevich and Y. Kawaoka (2002). "Reverse genetics demonstrates that proteolytic processing of the Ebola virus glycoprotein is not essential for replication in cell culture." J Virol **76**(1): 406-410.
- Noda, T., H. Ebihara, Y. Muramoto, K. Fujii, A. Takada, H. Sagara, J. H. Kim, H. Kida, H. Feldmann and Y. Kawaoka (2006). "Assembly and budding of Ebolavirus." PLoS Pathog **2**(9): e99.
- Noda, T., P. Halfmann, H. Sagara and Y. Kawaoka (2007). "Regions in Ebola virus VP24 that are important for nucleocapsid formation." J Infect Dis **196 Suppl 2**: S247-250.
- Nott, A., H. Le Hir and M. J. Moore (2004). "Splicing enhances translation in mammalian cells: an additional function of the exon junction complex." Genes Dev **18**(2): 210-222.
- Nott, A., S. H. Meislin and M. J. Moore (2003). "A quantitative analysis of intron effects on mammalian gene expression." RNA **9**(5): 607-617.
- Olival, K. J. and D. T. Hayman (2014). "Filoviruses in bats: current knowledge and future directions." Viruses **6**(4): 1759-1788.
- Ortiz-Riano, E., N. Ngo, S. Devito, D. Eggink, J. Munger, M. L. Shaw, J. C. de la Torre and L. Martinez-Sobrido (2014). "Inhibition of arenavirus by A3, a pyrimidine biosynthesis inhibitor." J Virol **88**(2): 878-889.
- Panchal, R. G., G. Ruthel, T. A. Kenny, G. H. Kallstrom, D. Lane, S. S. Badie, L. Li, S. Bavari and M. J. Aman (2003). "In vivo oligomerization and raft localization of Ebola virus protein VP40 during vesicular budding." Proc Natl Acad Sci U S A **100**(26): 15936-15941.
- Pattyn, S., G. van der Groen, W. Jacob, P. Piot and G. Courteille (1977). "Isolation of Marburg-like virus from a case of haemorrhagic fever in Zaire." Lancet **1**(8011): 573-574.
- Pecot, C. V., G. A. Calin, R. L. Coleman, G. Lopez-Berestein and A. K. Sood (2011). "RNA interference in the clinic: challenges and future directions." Nat Rev Cancer **11**(1): 59-67.
- Pleat, M. L., C. DeMarino, B. Lepene, M. J. Aman and F. Kashanchi (2017). "The Role of Exosomal VP40 in Ebola Virus Disease." DNA Cell Biol **36**(4): 243-248.
- Pourrut, X., A. Delicat, P. E. Rollin, T. G. Ksiazek, J. P. Gonzalez and E. M. Leroy (2007). "Spatial and temporal patterns of Zaire ebolavirus antibody prevalence in the possible reservoir bat species." J Infect Dis **196 Suppl 2**: S176-183.
- Pringle (1991). "The order Mononegavirales." Arch Virol **117**(1-2): 137-140.

- Prins, K. C., J. M. Binning, R. S. Shabman, D. W. Leung, G. K. Amarasinghe and C. F. Basler (2010). "Basic residues within the ebolavirus VP35 protein are required for its viral polymerase cofactor function." J Virol **84**(20): 10581-10591.
- Prins, K. C., W. B. Cardenas and C. F. Basler (2009). "Ebola virus protein VP35 impairs the function of interferon regulatory factor-activating kinases IKKepsilon and TBK-1." J Virol **83**(7): 3069-3077.
- Read, E. K. and P. Digard (2010). "Individual influenza A virus mRNAs show differential dependence on cellular NXF1/TAP for their nuclear export." J Gen Virol **91**(Pt 5): 1290-1301.
- Reed, R. and H. Cheng (2005). "TREX, SR proteins and export of mRNA." Curr Opin Cell Biol **17**(3): 269-273.
- Reichert, V. L., H. Le Hir, M. S. Jurica and M. J. Moore (2002). "5' exon interactions within the human spliceosome establish a framework for exon junction complex structure and assembly." Genes Dev **16**(21): 2778-2791.
- Richards, G. A., S. Murphy, R. Jobson, M. Mer, C. Zinman, R. Taylor, R. Swanepoel, A. Duse, G. Sharp, I. C. De La Rey and C. Kassianides (2000). "Unexpected Ebola virus in a tertiary setting: clinical and epidemiologic aspects." Crit Care Med **28**(1): 240-244.
- Rojas, M., D. M. Monsalve, Y. Pacheco, Y. Acosta-Ampudia, C. Ramirez-Santana, A. A. Ansari, M. E. Gershwin and J. M. Anaya (2020). "Ebola virus disease: An emerging and re-emerging viral threat." J Autoimmun **106**: 102375.
- Rowe, A. K., J. Bertolli, A. S. Khan, R. Mukunu, J. J. Muyembe-Tamfum, D. Bressler, A. J. Williams, C. J. Peters, L. Rodriguez, H. Feldmann, S. T. Nichol, P. E. Rollin and T. G. Ksiazek (1999). "Clinical, virologic, and immunologic follow-up of convalescent Ebola hemorrhagic fever patients and their household contacts, Kikwit, Democratic Republic of the Congo. Commission de Lutte contre les Epidemies a Kikwit." J Infect Dis **179** **Suppl 1**: S28-35.
- Ryan, K. J. and S. R. Wentz (2000). "The nuclear pore complex: a protein machine bridging the nucleus and cytoplasm." Curr Opin Cell Biol **12**(3): 361-371.
- Sadek, J. and G. S. Read (2016). "The Splicing History of an mRNA Affects Its Level of Translation and Sensitivity to Cleavage by the Virion Host Shutoff Endonuclease during Herpes Simplex Virus Infections." J Virol **90**(23): 10844-10856.

- Saeed, M. F., A. A. Kolokoltsov, T. Albrecht and R. A. Davey (2010). "Cellular entry of ebola virus involves uptake by a macropinocytosis-like mechanism and subsequent trafficking through early and late endosomes." PLoS Pathog **6**(9): e1001110.
- Saez, A., S. Weiss, K. Nowak, V. Lapeyre, F. Zimmermann, A. Dux, H. S. Kuhl, M. Kaba, S. Regnaut, K. Merkel, A. Sachse, U. Thiesen, L. Villanyi, C. Boesch, P. W. Dabrowski, A. Radonic, A. Nitsche, S. A. Leendertz, S. Petterson, S. Becker, V. Kraehling, E. Couacy-Hymann, C. Akoua-Koffi, N. Weber, L. Schaade, J. Fahr, M. Borchert, J. F. Gogarten, S. Calvignac-Spencer and F. H. Leendertz (2015). "Investigating the zoonotic origin of the West African Ebola epidemic." EMBO Mol Med **7**(1): 17-23.
- Sanchez, A., M. P. Kiley, B. P. Holloway and D. D. Auperin (1993). "Sequence analysis of the Ebola virus genome: organization, genetic elements, and comparison with the genome of Marburg virus." Virus Res **29**(3): 215-240.
- Sanchez, A., S. G. Trappier, B. W. Mahy, C. J. Peters and S. T. Nichol (1996). "The virion glycoproteins of Ebola viruses are encoded in two reading frames and are expressed through transcriptional editing." Proc Natl Acad Sci U S A **93**(8): 3602-3607.
- Sanchez, A., Z. Y. Yang, L. Xu, G. J. Nabel, T. Crews and C. J. Peters (1998). "Biochemical analysis of the secreted and virion glycoproteins of Ebola virus." J Virol **72**(8): 6442-6447.
- Sanger, F. and A. R. Coulson (1975). "A rapid method for determining sequences in DNA by primed synthesis with DNA polymerase." J Mol Biol **94**(3): 441-448.
- Satterly, N., P. L. Tsai, J. van Deursen, D. R. Nussenzveig, Y. Wang, P. A. Faria, A. Levay, D. E. Levy and B. M. Fontoura (2007). "Influenza virus targets the mRNA export machinery and the nuclear pore complex." Proc Natl Acad Sci U S A **104**(6): 1853-1858.
- Schmidt, K. M., M. Schumann, J. Olejnik, V. Kraehling and E. Muhlberger (2011). "Recombinant Marburg virus expressing EGFP allows rapid screening of virus growth and real-time visualization of virus spread." J Infect Dis **204** Suppl 3: S861-870.
- Schmidt, M. L. and T. Hoenen (2017). "Characterization of the catalytic center of the Ebola virus L polymerase." PLoS Negl Trop Dis **11**(10): e0005996.
- Schuh, A. J., B. R. Amman, M. E. Jones, T. K. Sealy, L. S. Uebelhoer, J. R. Spengler, B. E. Martin, J. A. Coleman-McCray, S. T. Nichol and J. S. Towner (2017). "Modelling filovirus maintenance in nature by experimental transmission of Marburg virus between Egyptian rousette bats." Nat Commun **8**: 14446.
- Scott, J. T., F. R. Sesay, T. A. Massaquoi, B. R. Idriss, F. Sahr and M. G. Semple (2016). "Post-Ebola Syndrome, Sierra Leone." Emerg Infect Dis **22**(4): 641-646.

- Shabman, R. S., T. Hoenen, A. Groseth, O. Jabado, J. M. Binning, G. K. Amarasinghe, H. Feldmann and C. F. Basler (2013). "An upstream open reading frame modulates ebola virus polymerase translation and virus replication." *PLoS Pathog* **9**(1): e1003147.
- Shen, H., X. Zheng, J. Shen, L. Zhang, R. Zhao and M. R. Green (2008). "Distinct activities of the DExD/H-box splicing factor hUAP56 facilitate stepwise assembly of the spliceosome." *Genes Dev* **22**(13): 1796-1803.
- Sigoillot, F. D., J. A. Berkowski, S. M. Sigoillot, D. H. Kotsis and H. I. Guy (2003). "Cell cycle-dependent regulation of pyrimidine biosynthesis." *J Biol Chem* **278**(5): 3403-3409.
- Sigoillot, F. D., D. H. Kotsis, V. Serre, S. M. Sigoillot, D. R. Evans and H. I. Guy (2005). "Nuclear localization and mitogen-activated protein kinase phosphorylation of the multifunctional protein CAD." *J Biol Chem* **280**(27): 25611-25620.
- Sureau, P. H. (1989). "Firsthand clinical observations of hemorrhagic manifestations in Ebola hemorrhagic fever in Zaire." *Rev Infect Dis* **11 Suppl 4**: S790-793.
- Takada, A., C. Robison, H. Goto, A. Sanchez, K. G. Murti, M. A. Whitt and Y. Kawaoka (1997). "A system for functional analysis of Ebola virus glycoprotein." *Proc Natl Acad Sci U S A* **94**(26): 14764-14769.
- Takamatsu, Y., V. Krahling, L. Kolesnikova, S. Halwe, C. Lier, S. Baumeister, T. Noda, N. Biedenkopf and S. Becker (2020). "Serine-Arginine Protein Kinase 1 Regulates Ebola Virus Transcription." *mBio* **11**(1).
- Timmins, J., G. Schoehn, C. Kohlhaas, H. D. Klenk, R. W. Ruigrok and W. Weissenhorn (2003). "Oligomerization and polymerization of the filovirus matrix protein VP40." *Virology* **312**(2): 359-368.
- Timmins, J., S. Scianimanico, G. Schoehn and W. Weissenhorn (2001). "Vesicular release of ebola virus matrix protein VP40." *Virology* **283**(1): 1-6.
- Towbin, H., T. Staehelin and J. Gordon (1979). "Electrophoretic transfer of proteins from polyacrylamide gels to nitrocellulose sheets: procedure and some applications." *Proc Natl Acad Sci U S A* **76**(9): 4350-4354.
- Towner, J. S., B. R. Amman, T. K. Sealy, S. A. Carroll, J. A. Comer, A. Kemp, R. Swanepoel, C. D. Paddock, S. Balinandi, M. L. Khristova, P. B. Formenty, C. G. Albarino, D. M. Miller, Z. D. Reed, J. T. Kayiwa, J. N. Mills, D. L. Cannon, P. W. Greer, E. Byaruhanga, E. C. Farnon, P. Atimnedi, S. Okware, E. Katongole-Mbidde, R. Downing, J. W. Tappero, S. R. Zaki, T. G. Ksiazek, S. T. Nichol and P. E. Rollin (2009). "Isolation of genetically diverse Marburg viruses from Egyptian fruit bats." *PLoS Pathog* **5**(7): e1000536.

- Towner, J. S., M. L. Khristova, T. K. Sealy, M. J. Vincent, B. R. Erickson, D. A. Bawiec, A. L. Hartman, J. A. Comer, S. R. Zaki, U. Stroher, F. Gomes da Silva, F. del Castillo, P. E. Rollin, T. G. Ksiazek and S. T. Nichol (2006). "Marburgvirus genomics and association with a large hemorrhagic fever outbreak in Angola." *J Virol* **80**(13): 6497-6516.
- Towner, J. S., T. K. Sealy, M. L. Khristova, C. G. Albarino, S. Conlan, S. A. Reeder, P. L. Quan, W. I. Lipkin, R. Downing, J. W. Tappero, S. Okware, J. Lutwama, B. Bakamutumaho, J. Kayiwa, J. A. Comer, P. E. Rollin, T. G. Ksiazek and S. T. Nichol (2008). "Newly discovered ebola virus associated with hemorrhagic fever outbreak in Uganda." *PLoS Pathog* **4**(11): e1000212.
- Trunschke, M., D. Conrad, S. Enterlein, J. Olejnik, K. Brauburger and E. Muhlberger (2013). "The L-VP35 and L-L interaction domains reside in the amino terminus of the Ebola virus L protein and are potential targets for antivirals." *Virology* **441**(2): 135-145.
- Tunnicliffe, R. B., G. M. Hautbergue, P. Kalra, B. R. Jackson, A. Whitehouse, S. A. Wilson and A. P. Golovanov (2011). "Structural basis for the recognition of cellular mRNA export factor REF by herpes viral proteins HSV-1 ICP27 and HVS ORF57." *PLoS Pathog* **7**(1): e1001244.
- Tunnicliffe, R. B., G. M. Hautbergue, S. A. Wilson, P. Kalra and A. P. Golovanov (2014). "Competitive and cooperative interactions mediate RNA transfer from herpesvirus saimiri ORF57 to the mammalian export adaptor ALYREF." *PLoS Pathog* **10**(2): e1003907.
- Uebelhoer, L. S., C. G. Albarino, L. K. McMullan, A. K. Chakrabarti, J. P. Vincent, S. T. Nichol and J. S. Towner (2014). "High-throughput, luciferase-based reverse genetics systems for identifying inhibitors of Marburg and Ebola viruses." *Antiviral Res* **106**: 86-94.
- Valkov, E., J. C. Dean, D. Jani, S. I. Kuhlmann and M. Stewart (2012). "Structural basis for the assembly and disassembly of mRNA nuclear export complexes." *Biochim Biophys Acta* **1819**(6): 578-592.
- Vermeulen, A., L. Behlen, A. Reynolds, A. Wolfson, W. S. Marshall, J. Karpilow and A. Khvorova (2005). "The contributions of dsRNA structure to Dicer specificity and efficiency." *RNA* **11**(5): 674-682.
- Viphakone, N., G. M. Hautbergue, M. Walsh, C. T. Chang, A. Holland, E. G. Folco, R. Reed and S. A. Wilson (2012). "TREX exposes the RNA-binding domain of Nxf1 to enable mRNA export." *Nat Commun* **3**: 1006.

- Viphakone, N., I. Sudbery, L. Griffith, C. G. Heath, D. Sims and S. A. Wilson (2019). "Co-transcriptional Loading of RNA Export Factors Shapes the Human Transcriptome." Mol Cell **75**(2): 310-323 e318.
- Volchkova, V. A., H. D. Klenk and V. E. Volchkov (1999). "Delta-peptide is the carboxy-terminal cleavage fragment of the nonstructural small glycoprotein sGP of Ebola virus." Virology **265**(1): 164-171.
- Watanabe, S., T. Noda, P. Halfmann, L. Jasenosky and Y. Kawaoka (2007). "Ebola virus (EBOV) VP24 inhibits transcription and replication of the EBOV genome." J Infect Dis **196 Suppl 2**: S284-290.
- Watanabe, S., T. Noda and Y. Kawaoka (2006). "Functional mapping of the nucleoprotein of Ebola virus." J Virol **80**(8): 3743-3751.
- Watanabe, S., A. Takada, T. Watanabe, H. Ito, H. Kida and Y. Kawaoka (2000). "Functional importance of the coiled-coil of the Ebola virus glycoprotein." J Virol **74**(21): 10194-10201.
- Watanabe, S., T. Watanabe, T. Noda, A. Takada, H. Feldmann, L. D. Jasenosky and Y. Kawaoka (2004). "Production of novel ebola virus-like particles from cDNAs: an alternative to ebola virus generation by reverse genetics." J Virol **78**(2): 999-1005.
- Watt, A., F. Moukambi, L. Banadyga, A. Groseth, J. Callison, A. Herwig, H. Ebihara, H. Feldmann and T. Hoenen (2014). "A novel life cycle modeling system for Ebola virus shows a genome length-dependent role of VP24 in virus infectivity." J Virol **88**(18): 10511-10524.
- Weiss, B. and C. C. Richardson (1967). "Enzymatic breakage and joining of deoxyribonucleic acid, I. Repair of single-strand breaks in DNA by an enzyme system from *Escherichia coli* infected with T4 bacteriophage." Proc Natl Acad Sci U S A **57**(4): 1021-1028.
- Weissenhorn, W., L. J. Calder, S. A. Wharton, J. J. Skehel and D. C. Wiley (1998). "The central structural feature of the membrane fusion protein subunit from the Ebola virus glycoprotein is a long triple-stranded coiled coil." Proc Natl Acad Sci U S A **95**(11): 6032-6036.
- Wendt, L., J. Brandt, B. S. Bodmer, S. Reiche, M. L. Schmidt, S. Traeger and T. Hoenen (2020). "The Ebola Virus Nucleoprotein Recruits the Nuclear RNA Export Factor NXF1 into Inclusion Bodies to Facilitate Viral Protein Expression." Cells **9**(1).
- Whelan, S. P., J. N. Barr and G. W. Wertz (2004). "Transcription and replication of nonsegmented negative-strand RNA viruses." Curr Top Microbiol Immunol **283**: 61-119.

- White, J. M., S. E. Delos, M. Brecher and K. Schornberg (2008). "Structures and mechanisms of viral membrane fusion proteins: multiple variations on a common theme." Crit Rev Biochem Mol Biol **43**(3): 189-219.
- Wiegand, H. L., G. A. Coburn, Y. Zeng, Y. Kang, H. P. Bogerd and B. R. Cullen (2002). "Formation of Tap/NXT1 heterodimers activates Tap-dependent nuclear mRNA export by enhancing recruitment to nuclear pore complexes." Mol Cell Biol **22**(1): 245-256.
- Wisskirchen, C., T. H. Ludersdorfer, D. A. Muller, E. Moritz and J. Pavlovic (2011). "The cellular RNA helicase UAP56 is required for prevention of double-stranded RNA formation during influenza A virus infection." J Virol **85**(17): 8646-8655.
- Xiong, R., L. Zhang, S. Li, Y. Sun, M. Ding, Y. Wang, Y. Zhao, Y. Wu, W. Shang, X. Jiang, J. Shan, Z. Shen, Y. Tong, L. Xu, Y. Chen, Y. Liu, G. Zou, D. Lavillete, Z. Zhao, R. Wang, L. Zhu, G. Xiao, K. Lan, H. Li and K. Xu (2020). "Novel and potent inhibitors targeting DHODH are broad-spectrum antivirals against RNA viruses including newly-emerged coronavirus SARS-CoV-2." Protein Cell **11**(10): 723-739.
- Yamaoka, S. and H. Ebihara (2021). "Pathogenicity and Virulence of Ebolaviruses with Species- and Variant-specificity." Virulence **12**(1): 885-901.
- Yang, C. C., E. Y. Huang, H. C. Li, P. Y. Su and C. Shih (2014). "Nuclear export of human hepatitis B virus core protein and pregenomic RNA depends on the cellular NXF1-p15 machinery." PLoS One **9**(10): e106683.
- Yasuda, J., M. Nakao, Y. Kawaoka and H. Shida (2003). "Nedd4 regulates egress of Ebola virus-like particles from host cells." J Virol **77**(18): 9987-9992.
- Yatherajam, G., W. Huang and S. J. Flint (2011). "Export of adenoviral late mRNA from the nucleus requires the Nxf1/Tap export receptor." J Virol **85**(4): 1429-1438.
- Zhang, K., L. Miorin, T. Makio, I. Dehghan, S. Gao, Y. Xie, H. Zhong, M. Esparza, T. Kehrer, A. Kumar, T. C. Hobman, C. Ptak, B. Gao, J. D. Minna, Z. Chen, A. Garcia-Sastre, Y. Ren, R. W. Wozniak and B. M. A. Fontoura (2021). "Nsp1 protein of SARS-CoV-2 disrupts the mRNA export machinery to inhibit host gene expression." Sci Adv **7**(6).
- Zhang, W., A. W. Lohman, Y. Zhuravlova, X. Lu, M. D. Wiens, H. Hoi, S. Yaganoglu, M. A. Mohr, E. N. Kitova, J. S. Klassen, P. Pantazis, R. J. Thompson and R. E. Campbell (2017). "Optogenetic control with a photocleavable protein, PhoCl." Nat Methods **14**(4): 391-394.
- Zhou, Y., J. M. Su, C. E. Samuel and D. Ma (2019). "Measles Virus Forms Inclusion Bodies with Properties of Liquid Organelles." J Virol **93**(21).

Zolotukhin, A. S., W. Tan, J. Bear, S. Smulevitch and B. K. Felber (2002). "U2AF participates in the binding of TAP (NXF1) to mRNA." J Biol Chem **277**(6): 3935-3942.

8 Appendix

8.1 Curriculum vitae

Persönliche Daten

Name	Janine Brandt
Geburtsdatum	12.10.1990
Geburtsort	Weimar
Nationalität	Deutsch

Akademischer Werdegang

2018-Heute	Promotion
Institution	Universität Greifswald
Betreuung	Friedrich-Loeffler-Institut Institut für molekulare Virologie und Zellbiologie (IMVZ) Labor für Molekularbiologie der Filoviren Dr. Thomas Hoenen/ Prof. Dr. Dr. h.c. Thomas C. Mettenleiter
Thema	Functional analysis of the molecular interactions between ebolaviruses and host proteins
2015-2018	Master of Science
Institution	Rheinische Friedrich-Wilhelms-Universität Bonn
Studiengang	Mikrobiologie
Betreuung der Abschlussarbeit	Friedrich-Loeffler-Institut Labor für Molekularbiologie der Filoviren Dr. Thomas Hoenen
Thema	Analysis of the nuclear localization of the Filovirus matrix protein VP40

2014-2015	Auslandsaufenthalt
Land	Australien
2013-2014	Auslandsaufenthalt
Land	Neuseeland
2010-2013	Bachelor of Science
Institution	Friedrich-Schiller-Universität Jena
Studiengang	Ernährungswissenschaften
Betreuung der Abschlussarbeit	Institut für Ernährungsmedizin Dr. René Thierbach
Thema	Mögliche Rolle der Glykogen-Synthase-Kinase 3 als stoffwechselabhängiger, molekularer Schalter in der Kanzergenese
2009-2010	Staatsexamen
Institution	Friedrich-Schiller-Universität Jena
Studiengang	Pharmazie
2001-2009	Allgemeine Hochschulreife
Institution	ab 2006 Humboldt-Gymnasium Weimar Sophiengymnasium Weimer

8.2 Publications

Bodmer, B. S., J. Greßler, M. L. Schmidt, J. Holzerland, **J. Brandt**, S. Braun, A. Groseth and T. Hoenen (2020). "Differences in Viral RNA Synthesis but Not Budding or Entry Contribute to the In Vitro Attenuation of Reston Virus Compared to Ebola Virus." *Microorganisms*. 2020 Aug 11;8 (8):1215

Brandt, J., L. Wendt, B. S. Bodmer, T. C. Mettenleiter and T. Hoenen (2020). "The Cellular Protein CAD is Recruited into Ebola Virus Inclusion Bodies by the Nucleoprotein NP to Facilitate Genome Replication and Transcription." *Cells* 2020, 9, 1126

Wendt, L., **J. Brandt**, B. S. Bodmer, S. Reiche, M. L. Schmidt, S. Traeger, and T. Hoenen (2020). "The Ebola Virus Nucleoprotein Recruits the Nuclear RNA Export Factor NXF1 into Inclusion Bodies to Facilitate Viral Protein Expression." *Cells* 2020, 9, 187

Kämper, L., L. Zierke, M. L. Schmidt, A. Müller, L. Wendt, **J. Brandt**, E. Hartmann, S. Braun, J. Holzerland, A. Groseth, T. Hoenen (2019). "Assessment of the function and intergenus-compatibility of Ebola and Lloviu virus proteins." *J Gen Virol* 2019 May;100 (5):760-772

Brandt, J., L. Wendt and T. Hoenen (2018). "Structure and function of the Ebola virus matrix protein VP40." *future medicine*.

Martin, S., A. I. Chiramel, M. L. Schmidt, Y. C. Chen, N. Whitt, A. Watt, E. C. Dunham, K. Shifflett, S. Traeger, A. Leske, E. Buehler, C. Martellaro, **J. Brandt**, L. Wendt, A. Muller, S. Peitsch, S. M. Best, J. Stech, S. Finke, A. Romer-Oberdorfer, A. Groseth, H. Feldmann and T. Hoenen (2018). "A genome-wide siRNA screen identifies a druggable host pathway essential for the Ebola virus life cycle." *Genome Med* 10(1): 58.

8.3 Scientific presentations

- 2019** 18. Workshop “Cell Biology of Viral Infections” der Gesellschaft für Virologie (GfV) in Schöntal
- Poster Mapping the interactions of the filovirus matrix protein VP40 with nucleocapsids using chimeric tetracistronic transcription- and replication-competent virus-like particles
Brandt J. and Hoenen T.
- 2019** FLI Junior Scientist Symposium in Jena
- Poster Characterizing interactions of the filovirus matrix protein VP40 and nucleocapsids with chimeric tetracistronic transcription- and replication-competent virus-like particles
Brandt J. and Hoenen T.
- 2019** 29. jährlichen Konferenz der Gesellschaft für Virologie (GfV) in Düsseldorf
- Vortrag Analysis of the influence of the host factors NXF1 and CAD on the ebolavirus life cycle
Brandt J. and Hoenen T.
- 2018** 17. Workshop “Cell Biology of Viral Infections” der Gesellschaft für Virologie (GfV) in Schöntal
- Vortrag Molecular analysis of the functional interactions between ebolaviruses and the host proteins CAD, UAP56 and NXF1
Brandt J. and Hoenen T.
- 2018** FLI Junior Scientist Symposium auf der Insel Riems
- Spotlight-Vortrag und Poster Analysis of the nuclear localization of the filovirus matrix protein
Brandt J. and Hoenen T.

8.4 Acknowledgment

Here I would like to express my gratitude to all of those who gave me the possibility to complete this thesis.

First of all, I would like to thank **Dr. Thomas Hoenen** for the possibility and trust to work in this host-factor interaction project. I am most grateful for his outstanding scientific support, his consistent encouragement and his great patience at all times. Furthermore, I am deeply grateful for his valuable guidance and the instructive discussions we had throughout this thesis.

My special thanks also go to **Prof. Dr. Dr. h.c. Thomas C. Mettenleiter** for the opportunity to write my doctoral thesis at the Friedrich-Loeffler-Institut and for his friendly and supportive supervision.

I also would like to express my thanks to the German Research Association (**DFG**) for their financial support.

Further I would like to thank **Lisa Wendt** for the creative cooperation in this project and the inspiring scientific discussions we had.

I am most grateful to **Marie-Luisa Schmidt, Andreas Müller, Josephine Greßler, Stefanie Peitsch, Katrin Giesow** and **Cathleen Klement** who always had valuable advices and gave me answers to all my questions in technical and experimental problems and with whom I had a nice time during working together in the Lab.

In addition, I want to thank all the members and former members of the working group Arenavirus biology and most of all **Dr. Allison Groseth** for their great support during my project, the valuable advices during our Lab Meetings and help with the protein alignment.

I additionally thank **Dr. Thomas Hoenen** and **Dr. Bianca S. Bodmer** for carrying out the infection experiments as well as **Dr. Allison Groseth** and **Dr. Sandra Diederich** for technical assistance with the BSL4 work.

I would like to thank **Prof. Dr. Stefan Finke** and his working group for their support with the confocal microscope.

My thanks also go to **Dr. Barbara Klupp** and her working group for provision of the NPC antibody.

Special thanks also go to **Dr. Bianca S. Bodmer**, **Linus Bostedt** and **Justina Rath** for their great support during the experimental work and writing of this thesis. I always enjoy spending time with you and having scientific and non-scientific discussions.

This thesis wouldn't be done without the support of my **family** and I am more than grateful that I can always count on you. Most of all I want to thank my dad, my brother and my sister for always being there for me, even in the last three years, which was a tough time for all of us. I also thank my grandma, who always believed in me. I am more than sad that you will not see the completion of this work, but I know that you would be proud of me.

Finally, I like to thank **Alex** for his great patience and his personal support throughout the last years and without whom this thesis would never have been completed. I am most thankful for the good and bad times we go through together.

8.5 Eigenständigkeitserklärung

Hiermit erkläre ich, dass diese Arbeit bisher von mir weder an der Mathematisch-Naturwissenschaftlichen Fakultät der Universität Greifswald noch einer anderen wissenschaftlichen Einrichtung zum Zwecke der Promotion eingereicht wurde.

Ferner erkläre ich, dass ich diese Arbeit selbstständig verfasst und keine anderen als die darin angegebenen Hilfsmittel und Hilfen benutzt und keine Textabschnitte eines Dritten ohne Kennzeichnung übernommen habe.

.....
Greifswald, April 2021

Janine Brandt